Exploring the Formation of Metal Melaminates by Deprotonating Melamine in Solid-State Reactions and Investigating Melamine and Cyanuric Acid as Potential Precursors for Carbodiimide Synthesis

Dissertation

der Mathematisch-Naturwissenschaftlichen Fakultät

der Eberhard Karls Universität Tübingen

zur Erlangung des Grades eines

Doktors der Naturwissenschaften

(Dr. rer. nat.)

vorgelegt von

M. Sc. Elaheh Bayat

aus Zandschan, Iran

Tübingen

2025

Gedruckt mit Genehmigung der Mathematisch-Naturwissenschaftlichen Fakultät der Eberhard Karls Universität Tübingen.

Tag der mündlichen Qualifikation:	04.08.2025
Dekan:	Prof. Dr. Thilo Stehle
1. Berichterstatter/-in:	Prof. Dr. Hans-Jürgen Meyer
2. Berichterstatter/-in:	Prof. Dr. Eberhard Schweda

Acknowledgments

First, I would like to thank my supervisor, Prof. Dr. Hans-Jürgen Meyer, who kindly welcomed me to his esteemed research group and trusted me as an international student. His assistance has allowed me to gain knowledge in an interesting area of solid-state chemistry. His ideas and comments have been invaluable throughout my doctorate journey. I could not be more grateful for the mentorship he provided and for his professional supervision. Also, I sincerely appreciate the opportunities and support he has provided for my personal and academic growth. Moreover, I am grateful to my second mentor, Prof. Dr. Doris Kunz, for her support. I want to express my sincere gratitude to Prof. Dr. Eberhard Schweda for agreeing to be my second reviewer.

Secondly, I am particularly grateful to Dr. Markus Ströbele for his invaluable advice and support, especially in solving and refining crystal structures, and for sharing his scientific knowledge. I would also like to sincerely thank Prof. Dr. Thomas Jüstel and Dr. David Enseling for their help with photoluminescence measurements and for fostering a highly productive collaboration. Additionally, I would like to thank Prof. Dr. Scott Kroeker for his assistance with the solid-state NMR measurement and Dr. Jaroslav Valenta for his cooperation with magnetic measurement. Thank you to Dr. Jochen Glaser for his helpful advice on magnetic measurements.

I am deeply thankful to be part of an incredible research group supported by past and present colleagues. Their encouragement and the memorable moments we've shared have been truly invaluable. I want to extend special thanks to Patrick Schmidt, Florian Pachel, Fabian Grahlow, Albert Schwarz, Jan Beitlberger, Catharina Brand, Melena Groß, Paula Kallenbach, Dr. Manuel Löber, and Dr. Olexandr Kysliak for their support and collaboration.

Lastly, I would like to thank my parents and siblings for always being there for me. I am especially grateful to my wonderful sisters, Ilnaz, Elham, and Sohaila, and my brother, Alireza, whose encouragement to apply abroad for my PhD and constant support along the way meant so much to me. Above all, I wish to thank my dear boyfriend, Alex, for his unwavering encouragement and support throughout these years.

To my family

Table of Contents

Abbreviations

DFT	Density Functional Theory
NMR	Nuclear Magnetic Resonance
PXRD	Powder X-ray Diffraction
SC-XRD	Single-Crystal X-ray Diffraction
TGA	Thermogravimetric Analysis
DSC	Differential Scanning Calorimetry
DTA	Differential Thermal Analysis
IR	Infrared
s-triazine	Symmetrical Triazine
s-heptazine	Symmetrical Heptazine
MOF	Metal-Organic Frameworks
SHG	Second-Harmonic Generation
THF	Tetrahydrofuran
SSM	Solid-State Metathesis
RE	Rare-Earth
ELF	Electron Localization Function
CIF	Crystallographic Information File
DSC	Differential Scanning Calorimetry
PL	Photoluminescence
UV	Ultraviolet Radiation
LED	Light-Emitting Diode

Symbols

K	Kelvin
C	Celsius
°	Degree
Pm	Picometer
ns	Nanosecond
µs	Microsecond
GPA	Gigapascal
χ_{mol}	Magnetic susceptibility per mole
Y_{ab}	Young's modulus in the ab-plane
Y_c	Young's modulus along the c-axis
μ_{eff}	Effective magnetic moment
μ_B	Bohr magneton
θ_p	Curie temperature
χ_0	Temperature-independent susceptibility
eV	Electron volt
m^3/mol	Cubic meters per mole

Summary

Melamine and its condensation products, such as melam, melem, and melon, have gained significant attention in recent decades due to their structural versatility and potential applications as flame retardants and adhesives. This dissertation explores the thermal behavior and reactivity of melamine in the presence of various metal chlorides and a metal hydride at different temperatures. This research opens a new door in the coordination chemistry between metals and melamine, melam, and melem, introducing their potential applications as luminescent and sensor materials.

The first proposed method for synthesizing metal melaminates is a solid-state reaction in which melamine reacts with metal chlorides such as CuCl, $SbCl_3$, and $InCl_3$ in a silica ampule under controlled conditions. This work introduces tricopper melaminate ($Cu_3(C_3N_6H_3)$), which is the first study of three times deprotonated melamine. This compound is forming channels along the c-axis and has Cu(I)-Cu(I) bonding. Antimony melaminates were also obtained through a similar approach, revealing the stepwise deprotonation of melamine at different temperatures, which ultimately led to the formation of a layered structure of doubly deprotonated antimony melaminate. Additionally, the indium-melaminate compound displayed a novel supramolecular structure, which proves that melamine can be four times deprotonated and shows a new coordination system.

The second synthesis route for melaminates involved reacting melamine with metal hydrides. This approach was inspired by the alternative synthesis of $Cu_3(C_3N_6H_3)$ via the trimerization of hydrogen cyanamide. Specifically, $Cu_3(C_3N_6H_3)$ was successfully synthesized from $NaHCN_2$ and CuCl via a trimerization mechanism. In this process, $NaHCN_2$ and $KHCN_2$ are intermediates in the reaction between the respective metal hydride and melamine. Consequently, the reaction of KH with melamine led to the formation of two new intermediates of potassium melaminate compounds, $K(C_3N_6H_5)$ and $K_2(C_4N_7H_3)$.

Further studies on the reaction of melamine with transition metal chlorides ($MnCl_2$, $FeCl_2$, $CoCl_2$) at high temperatures than 350 ˚C led to the formation of Mn-, Fe-, and Co-coordinated melem and melam compounds.

Finally, the synthesis of metal carbodiimides was investigated by decomposing melaminates and metal cyanurates. This approach successfully produced indium carbodiimide from indium melaminate and lanthanum carbodiimide from lanthanum cyanurate. The reaction of cyanuric acid with metal chlorides and sodium hydroxide is also introduced as an alternative solid-state synthesis method for metal carbodiimides, leading to the discovery of $La_2(CN_2)_3$, which has been a missing rare-earth carbodiimide for two decades.

Zusammenfassung

Melamin und seine Kondensationsprodukte wie Melam, Melem und Melon haben in den letzten Jahrzehnten aufgrund ihrer strukturellen Vielseitigkeit und potenziellen Anwendungen als Flammschutzmittel und Klebstoffe große Aufmerksamkeit erlangt. Diese Dissertation untersucht das thermische Verhalten und die Reaktivität von Melamin in Gegenwart verschiedener Metallchloride und eines Metallhydrids bei unterschiedlichen Temperaturen. Diese Forschung eröffnet ein neues Feld in der Koordinationschemie von Metallen mit Melamin, Melam und Melem und zeigt deren potenzielle Anwendungen als lumineszierende und sensorische Materialien auf.

Die erste vorgeschlagene Methode zur Synthese von Metall-Melaminaten ist eine Festkörperreaktion, bei der Melamin mit Metallchloriden wie CuCl, $SbCl_3$ und $InCl_3$ in einer Glasampulle unter kontrollierten Bedingungen reagiert. In dieser Arbeit wird Trikupfer-Melaminat ($Cu_3(C_3N_6H_3)$) vorgestellt, die erste Studie über dreifach deprotoniertes Melamin. Diese Verbindung bildet Kanäle entlang der c-Achse und weist Cu(I)-Cu(I)-Bindungen auf. Antimon-Melaminate wurden ebenfalls durch einen ähnlichen Ansatz erhalten, der die schrittweise Deprotonierung von Melamin bei unterschiedlichen Temperaturen aufzeigt, was letztlich zur Bildung einer geschichteten Struktur von doppelt deprotoniertem Antimon-Melaminat führte. Darüber hinaus zeigte die Indium-Melaminat-Verbindung eine neuartige supramolekulare Struktur, die beweist, dass Melamin vierfach deprotoniert werden kann und ein neues Koordinationssystem aufweist.

Der zweite Syntheseweg für Melaminate bestand in der Reaktion von Melamin mit Metallhydriden. Dieser Ansatz wurde von der alternativen Synthese von $Cu_3(C_3N_6H_3)$ durch die Trimerisierung von Hydrogencyanamid inspiriert. Insbesondere wurde $Cu_3(C_3N_6H_3)$ erfolgreich aus $NaHCN_2$ und CuCl über einen Trimerisierungsmechanismus synthetisiert. In diesem Prozess fungieren $NaHCN_2$ und $KHCN_2$ als Zwischenprodukte in der Reaktion zwischen dem jeweiligen Metallhydrid und Melamin. Infolgedessen führte die Reaktion von KH mit Melamin zur Bildung zweier neuer Zwischenprodukte von Kalium-Melaminat-Verbindungen, $K(C_3N_6H_5)$ und $K_2(C_4N_7H_3)$.

Weitere Untersuchungen zur Reaktion von Melamin mit Übergangsmetallchloriden ($MnCl_2$, $FeCl_2$, $CoCl_2$) bei Temperaturen über 350 ˚C führten zur Bildung von Mn-, Fe- und Co-koordinierter Melem- und Melam-Verbindungen.

Schließlich wurde die Synthese von Metall-Carbodiimiden durch die Zersetzung von Melaminaten und Metall-Cyanuraten untersucht. Dieser Ansatz führte erfolgreich zur Herstellung von Indium-Carbodiimid aus Indium-Melaminat und Lanthan-Carbodiimid aus Lanthan-Cyanurat. Die Reaktion von Cyanursäure mit Metallchloriden und Natriumhydroxid erwies sich ebenfalls als alternative Festkörpersynthesemethode für Metall-Carbodiimide und führte zur Entdeckung von $La_2(CN_2)_3$, einem fehlenden Seltenerd-Carbodiimid, das seit zwei Jahrzehnten nicht nachgewiesen werden konnte.

Publications

Publication 1:

Tricopper melaminate, a metal-organic framework containing dehydrogenated melamine and Cu–Cu bonding

Paula Kallenbach, Elaheh Bayat, Markus Ströbele, Carl P Romao, Hans-Jürgen Meyer

Inorg. Chem. 2021, 60, 16303–16307

Publication 2:

High-Yield Synthesis Route, Post-Synthesis Treatment, and Insights into the Photoluminescence and Magnetic Properties of Tricopper(I) Melaminate $Cu_3(C_3N_6H_3)$

Elaheh Bayat, Markus Ströbele, Mojtaba Abbasi, Scott Kroeker, Jaroslav Valenta, David Enseling, Thomas Jüstel, Hans-Jürgen Meyer

Inorg. Chem. 2024, 63, 19053–19062

Publication 3:

Unraveling the Synthesis of $SbCl(C_3N_6H_4)$: A Layered Metal-Melaminate Obtained through Deprotonation of Melamine with Antimony(III) Chloride

Elaheh Bayat, Markus Ströbele, and Hans-Jürgen Meyer

Chemistry 2023, 5, 1465-1476

Publication 4:

Thermal deprotonation and condensation of melamine in the presence of indium(III) chloride

Elaheh Bayat, Markus Ströbele, David Enseling, Thomas Jüstel, Hans-Jürgen Meyer

Dalton Trans. 2024, 53, 10912-10918

Publication 5:

A Systematic Study of the Solid-State Pathway from Melamine via Melaminate to Carbodiimide under Evolution of Hydrogen

Markus Ströbele, Elaheh Bayat, Hans-Jürgen Meyer

Inorg. Chem. 2024, 63, 16565–16572

Publication 6:

$MnCl_2(C_6N_{10}H_6)$: Insights into a Luminescent Transition Metal-Melem Complex

Elaheh Bayat, Markus Ströbele, David Enseling, Thomas Jüstel, Hans-Jürgen Meyer

Molecules 2024, 29, 5598

Publication 7:

$La_2(CN_2)_3$ – the missing link of rare-earth carbodiimides, prepared through an efficient synthetic route and its Ce^{3+} activated photoluminescence

Philipp Schneiderhan, Elaheh Bayat, Markus Ströbele, David Enseling, Thomas Jüstel, and H.-Jürgen Meyer

Dalton Trans. 2025, 54, 4909–4917

Personal Contribution

Publication 1:

The initial synthesis and investigation of the $Cu_3(C_3N_6H_3)$ crystals were carried out by Paula Kallenbach. Supervision, funding acquisition, and manuscript review and writing were conducted by Prof. Hans-Jürgen Meyer. The crystal structure refinement and graphics were performed by Dr. Markus Ströbele, and Dr. Carl P. Romao conducted the electronic and structural property calculations using density functional theory (DFT). My contribution was participating in the review process of this paper. I have tried to prepare a large batch of the sample (or reproduce it) rather than just a few crystals to facilitate optical reflection measurements and compare the experimentally determined band-gap with the DFT-calculated value.

Publication 2:

Personal Contribution

Conceptualization, supervision, funding acquisition, and manuscript review and editing were conducted by Prof. Hans-Jürgen Meyer. I performed the synthesis, sample preparation, X-ray studies, data interpretation, and manuscript writing. Dr. Markus Ströbele handled the X-ray diffraction refinement and modeling. Dr.Jaroslav Valenta performed the magnetic measurements. The solid-state NMR studies were conducted by Mojtaba Abbasi and Prof. Scott Kroeker. Dr. David Enseling and Prof. Thomas Jüstel conducted the photoluminescence spectroscopy measurements and contributed to reviewing the manuscript.

Publication 3:

Conceptualization, supervision, funding acquisition, and manuscript review and editing were conducted by Prof. Hans-Jürgen Meyer. I performed the synthesis, crystallization, PXRD, DSC, IR spectroscopy, interpretation of each, and writing the manuscript. Dr. Markus Ströbele carried out the SC-XRD structure solutions.

Publication 4:

This publication was performed under the guidance of Prof. Hans-Jürgen Meyer, who managed the conceptualization, supervision, funding acquisition, and manuscript review and editing. I performed the synthesis, Crystallization, PXRD, SC-XRD, and IR spectroscopy, and prepared the manuscript draft. Dr. Markus Ströbele carried out the X-ray diffraction refinements and structure solutions. Dr. David Enseling and Prof. Thomas Jüstel performed the photoluminescence spectroscopy measurements and assisted in data interpretation and manuscript editing.

Publication 5:

The conception, supervision, funding acquisition, and manuscript review and editing were led by Prof. Hans-Jürgen Meyer. Dr. Markus Ströbele carried out X-ray diffraction, modeling, synthesis, and sample preparation. I contributed to the manuscript by synthesizing, interpreting, writing, creating the artwork, and organizing the final preparation of the manuscript.

Publication 6:

Conceptualization, supervision, funding acquisition, and manuscript review and editing were managed by Prof. Hans-Jürgen Meyer. I have done the synthesis, TGA (thermogravimetric analysis), DTA (differential thermal analysis), PXRD (powder X-ray diffraction), IR spectroscopy, manuscript writing, and interpretations. Dr. Markus Ströbele carried out the structure refinements**.** Dr. David Enseling and Prof. Thomas Jüstel were responsible for the photoluminescence(PL) spectroscopy measurements and contributed to the interpretation of PL results and the review of the manuscript.

Publication 7:

Prof. Hans-Jürgen Meyer led the conceptualization, supervision, funding acquisition, manuscript writing, review, and editing. Philipp Schneiderhana carried out the synthesis, PXRD, IR spectroscopy, and TGA and contributed to the writing and editing of the manuscript. I have contributed to manuscript writing, preparation, and experimental analysis. Dr. Markus Ströbele conducted the X-ray diffraction refinements and structure solutions. Prof. Thomas Jüstel and Dr. David Enseling performed the photoluminescence spectroscopy and contributed to manuscript editing.

1. **Introduction**

1.1 Introduction to Triazine and Heptazine Heterocycles

The presence of the heteroatom (N, S, O) in the structure of aromatic carbon rings, such as benzene (C_6H_6), forms a new class of organic chemistry named heterocyclic compounds.[1] The simplest and most similar hetero-analogue of benzene is pyridine (C_6H_5N), as N^+ and C are isoelectronic. The benzene-like structures, where one, two, three, or four carbon atoms are replaced by nitrogen atoms, are systematically known as azines, diazines, triazines, and tetrazines.[2, 3]

Azines show distinct reactivity due to their electron deficiency within the heterocyclic system. As more nitrogen atoms are introduced in aromatic rings (diazines, triazines, heptazine), the ring becomes less basic and less nucleophilic.[4] Triazine ($C_3H_3N_3$) was first synthesized in 1895 with a low yield of only 10%.[1] This process was later optimized, achieving a 55-60% yield by reacting hydrogen cyanide with hydrogen chloride.[1] The thermal and oxidative stability of systems containing C-N bonds like s-triazine and s-heptazine are much higher than heterocycles containing C-C, C-H, or N-N bonds since the difference in electronegativity of N and C can lead to high bond dissociation energy, increasing their resistance to degradation.[5] The 1,3,5-triazine molecule is the parent structure for many important triazines, such as cyanuric acid, cyanuric chloride, melamine, ammelide, ammeline, etc, as listed in Table 1 below.

Table 1. Important 1,3,5-triazine derivatives and their chemical structures.[1, 6]

Name	IUPAC name	Chemical Formula
Cyanuric Chloride	2,4,6-Trichloro-1,3,5-triazine	$C_3N_3Cl_3$
Cyanuric Acid	1,3,5-Triazinane-2,4,6-trione	$C_3N_3O_3H_3$
Melamine	1,3,5-Triazine-2,4,6-triamine	$C_3H_6N_6$
Ammeline	4,6-Diamino-1,3,5-triazin-2-ol	$C_3H_5N_5O$
Ammelide	6-Amino-1,3,5-triazine-2,4-diol	$C_3H_4N_4O_2$
Acetoguanamine	6-Methyl-1,3,5-triazine-2,4-diamine	$C_4H_7N_5$

Heptazine (Tri-s-heptazine, $C_6N_7H_3$) was introduced by Pauling and Sturdivant as the building block for melon or hydromelonic acid ($C_9H_3N_{13}$) and cyameluric acid ($C_6N_7O_3H_3$).[7] The existence of the heptazine nucleus was only proposed by quantum mechanical calculations and later verified by X-ray diffraction structural data.

Afterward, the molecular structure of 2,5,8-triamino-*s*-heptazine (melem) and poly(aminoimino)heptazine (melon) was established as condensation products of melamine.[8]

1,3,5-Triazines ($C_3H_3N_3$) and tri-s-heptazine ($C_6H_3N_7$) are also known as the cyanuric nucleus and cyameluric nucleus, respectively. Triazine is composed of only one ring of alternating N and C atoms, while the heptazine ring comprises three fused rings.[9] It is important to note that both s-triazine and s-heptazine represent uncommon cases of heterocycles since they contain neither C-C nor C-H bonds. Consequently, they can be classified inconsistently as organic or inorganic materials.

The reactivity of different triazines and heptazines with various functional groups is a fascinating aspect of heterocyclic chemistry, but it is beyond the scope of this work to elaborate on all their reactions and reactivities. Instead, in the next sections, we will shortly discuss the structures and reactivities of melamine, melem, and cyanuric acid, which are closely related to our research.

1.2 Melamine and its Condensation Products

Melamine (1,3,5-triazine-2,4,6-triamine) was first synthesized almost a century ago (1934) by Liebig from the reaction of ammonium chloride (NH_4Cl) with potassium thiocyanate (KSCN).[10] Later on, several researchers proposed additional synthetic methods with various sources like thiourea ($SC(NH_2)_2$), guanidine carbonate ($C_3H_{12}N_6O_3$), cyanamide (CH_2N_2), and dicyandiamide ($C_2H_4N_4$).[6, 10-13] Today, urea serves as the main precursor for the synthesis of melamine. As a result, the production has increased to millions of tons per year, which makes this material widely available.

Melamine has a monoclinic crystal structure with a space group of $P2_1/a$.[14] The units are staggered with respect to one another in such a way that N–H···H bonds are formed.[15] The NH_2 group itself is basic and acts as a proton acceptor or participates in hydrogen bonding. Melamine also contains three sp^2 nitrogen atoms with lone pair electrons and can act either as hydrogen-bond donors or coordination sites. The structure of melamine can exist in various tautomeric forms. Two hypothetical isomers

are isomelmaine and melamine, which are commonly discussed in numerous studies.[16, 17] These features make melamine an ideal scaffold for constructing supramolecular assemblies.

The condensation cascade of melamine starts at around 360 °C[18] (340 °C)[19] to melam ($C_6H_9N_{11}$), and then at roughly 400 °C[18] (380 °C)[19], it converts into melem ($C_6H_6N_{10}$). When heated further, melon and, consequently, carbon nitride (C_3N_4) material are formed.[20] All these C/H/N scaffolds were named and presented for the first time by Liebig from elemental analysis[21], and the respective crystal structures were identified later. May first suggested the synthesis of melam and described the degradation process in which melamine is thermally decomposed into cyanamide at a temperature ranging from 300 to 320 °C.[18] Cyanamide then condenses into melamine and then melam, and finally melem by eliminating two ammonia molecules.

Melam ($C_6H_9N_{11}$) is formed by the dimerization of melamine and the release of one equivalent ammonia. In other words, the two amino groups of the triazine ring in melamine are linked together by bridging the imide group, featuring a torsion angle of 11˚ to 14˚ between the two triazine rings.[19] The pure phase of melam is only achieved by controlling the reaction conditions in autoclave reactions, such as elevated ammonia pressure.[22] However, melam is commonly found with melem ($C_6H_6N_{10}$), which is formed at slightly above temperature. Therefore, melam is accounted as a reactive intermediate that mostly exists in the form of various melamine-melem[23] or melam-melem[22, 24] adducts. Melem was introduced by Klason.[20, 25] The crystal structure of a melem is composed of two types of stacked layers tilted at an angle of approximately 40°.[26, 27] The planar melem molecules formed containing the heptazine unit ($C_6H_3N_9$) have 327 pm interlayer spacing.[26, 27]

The final product of this condensation cascade is melon, which is a pale to bright yellow powder. Melon doesn’t describe a single compound; rather, its composition depends on the degree of polymerization, which is controlled by conditions like temperature and pressure.[28, 29] Two different structural models of melon have been proposed. The first model consists of three nuclei attached by imide bridges in a cyclic arrangement, while the second model features the building blocks arranged in infinite linear chains.[9] Melon has a band gap of ~2.7 eV [30], which can be attributed to its

extended conjugated π-system along the imide-bridged heptazine strands. Therefore, it has applications as a photocatalyst in water splitting or pollutant degradation.[8, 31]

The significance of melamine condensation products, such as melon, lies in their early association with the research aimed at discovering materials harder than diamond; however, later, it was known as C_3N_4. A wide range of synthetic methods has been employed to synthesize these materials. Many of them have yielded structures with imide-bridged heptazine chains or nitrogen-linked heptazine rings, which resemble an extended cyclic melon model. Most efforts have resulted either in amorphous powders of undefined compositions or in nitrogen-doped carbon thin films. Although there have been challenges to crystallinity, these findings highlight the potential of straightforward precursor-based routes for carbon nitride synthesis.

1.3 Other Reactions of Melamine and Melem

Aside from the condensation cascade reactions of melamine, melamine is itself a weak base, which enables it to form various salts with organic and inorganic acids such as cyanurate, picrate, and perchlorate.[12] Melamine undergoes hydrolysis in mineral acids and finally transforms into cyanuric acid.[11, 12] In less acidic media, melamine is typically protonated to form melaminium ions[32], which has been previously investigated by IR studies.[33, 34] Melamine can also be considered an intriguing building block for crystal engineering and the construction of metal-organic frameworks (MOFs) due to its three nitrogen atoms within the ring, which serve as potential coordination sites.

In most studies on the coordination of melamine, only the inner nitrogen atom of melamine is activated as a coordination site.[35] The possible reason might be the availability of hydrogen in melamine for hydrogen bonding, the steric hindrance between the adjacent amine groups, and the rigidity of the heterocycles.[35] In 1999, the first complex of metal-melamine was introduced as $[Cu(C_3H_6N_6)(\mu\text{-}OCH_3)(ONO_2)(HOCH_3)]_2$ and was synthesized by reacting diacetylmelamine and $Cu(NO_3)_2{\cdot}3H_2O$ in methanol.[36] Another example of coordinated melamine to silver ($Ag(C_3N_6H_6)_2ClO_4$)[37], which was synthesized by slowly diffusing a methanol solution of

$Ag(C_5H_5N)_2ClO_4$ into an aqueous solution of melamine.[37] Additionally, melamine can also react with $AgNO_3$ and form $[Ag(C_3H_6N_6)]NO_3$[38], or polymer of $[Ag_2(C_3N_6H_6)(CH_3CO_2)(NO_3)]_n$[39]. The reaction of melamine with some copper-containing reagents yields products with new coordination motif sites, such as the reaction of melamine and aluminum isopropoxide with copper halides (CuCl, CuBr) in water with autoclave, which yields $Cu_2Br_2(C_3H_6N_6)_n$ and $Cu_3Cl_3(C_3H_6N_6)_n$. Reacting mercury(I, II) with melamine in hydrothermal conditions also produces some of these metal-attached-melamine compounds. The study of such reactions started in 2004 by reacting melamine and mercury(II) chloride in water and methanol, resulting in needle crystals of $[MelH^+HgCl_3^-](C_3H_6N_6)$[40]. In 2023, two melamine-based mercury halides of $(C_3N_6H_7)(C_3N_6H_6)HgCl_3$, and $(C_3N_6H_7)_3HgCl_5$ were introduced as second-harmonic generation SHG materials.[41] Later, our group also discovered $HgCl_2(C_3N_6H_6)$, and $(C_3N_6H_7)ZnCl_3(C_3N_6H_6)$ as SHG material from the reaction of respective metal chloride and melamine in water.[42, 43]

Melamine can also be a major precursor to produce polymers and resins when reacting with formaldehyde and aldehydes and therefore have properties such as flame retardants, and adhesives.[10, 44-46] Melamine-cyanuric acid complex is also presented by Wang for the first time.[47] This study has been further developed as more functional materials such as supramolecular aggregates of gels and hydrogels[48]. These two-dimensional supramolecular assemblies of hydrogen-bonded melamine and cyanuric acid are used as flame retardants.[44, 49]

The reactivity of melem or melamine at higher temperatures, where it transforms into melem with its NH_2 groups, is another important aspect of s-heptazine chemistry. Since melem is insoluble in water and other solvents and has low reactivity, this area of study remains relatively unexplored.[50] Several melemium salts can be obtained from treating melem with mineral acids such as $C_6N_7(NH_2)_3 \cdot H_3PO_4$, $H_2C_6N_7(NH_2)_3SO_4 \cdot 2H_2O$, $HC_6N_7(NH_2)_3ClO_4 \cdot C_6N_7(NH_2)_3$.[51-53] The reaction of melem in aqueous suspension of metal nitrates such as $Zn(NO_3)_2$, $Cu(NO_3)_2$, $Co(NO_3)_2$, and $Ni(NO_3)_2$ has been studied recently by Xu et al.[54] Furthermore, the reaction of metal halides with melem introduced an interesting isotypic series of $M_6X_{12}(C_3N_6H_6)_4$ (M = Ca, Sr, Ba, Pb; X=Br, I) compounds.[55]

1.4 Melaminates

Melamine can undergo both protonation and deprotonation, which affects its chemical behavior and applications. It can accept protons to form cationic derivatives. The initial protonation results in mono, and further protonation results in di-protonated melamine.[56] Deprotonation of melamine involves the removal of one or even more hydrogens from melamine's amine groups. It is challenging but important, both from the chemical and application points of view. Deprotonating melamine more than once is difficult, but in this case, success has been achieved with stronger bases such as guanidine, where two deprotonations are possible. In the research done by Dronskowski, strontium guanidinate $SrC(NH)_3$, the first compound featuring a deprotonated guanidine unit, was successfully synthesized using strontium and guanidine in liquid ammonia.[57] So, if it is possible with guanidine, it can also be possible to deprotonate melamine.

To summarize the previous research on the area of melaminates: Two compounds, potassium melaminate with ammonia salt $KC_3N_6H_5{\cdot}nNH_3$ and tripotassium melaminate $K_3C_3N_6H_3$, were proposed as melaminates almost 100 years ago by Frankin.[58] However, these compounds were obtained as amorphous phases, and their compositions were only derived from elemental analysis. Later, in research done by Dronskowski, reactions of elemental potassium, sodium, and rubidium with melamine in liquid ammonia yielded crystals of adducts of potassium and rubidium as $KC_3N_6H_5{\cdot}NH_3$, $RbC_3N_6H_5{\cdot}½NH_3$, and amorphous $NaC_3N_6H_5{\cdot}NH_3$, under ammonothermal condition.[59] In a different approach, the fixation of triruthenium clusters on melamine has also offered the activation of two NH_2 groups of melamine.[60] In this study, which was conducted in 1997, melamine was reacted with $[Ru_3(CO)_{12}]$ in THF and led to the formation of monometallated, two bimetallated isomeric derivatives.[60] However, the trimetallated derivative was not detected, likely due to structural constraints and steric hindrance.[60] Many other studies received attention as polymeric complexes of melamine, one of which claimed the three times deprotonated melamine in the polymeric structures of melamine with di-butyl magnesium.[61] However, no crystallographic data proves this structure.

1.5 An Overview of Cyanuric Acid

Cyanuric acid (1,3,5-triazin-2,4,6-trione) with the formula of $(CNOH)_3$ is a white crystalline solid, prepared for the first time in 1776 by Scheele from the pyrolysis of uric acid ($C_5H_4N_4O_3$).[1] In 1875, Liebig and Wöhler synthesized and analyzed this compound, although they assigned a wrong molecular formula. Later, in 1875, Drescher found its correct formula.[1] The key feature of cyanuric acid is the s-triazine ring, which, as mentioned before, is formed through the trimerization of cyanate groups (−OCN).[16] In other words, hydrolysis of melamine ($C_3N_6H_6$) or cyanuric chloride ($C_3N_3Cl_3$) ultimately produces cyanuric acid.[11, 12] However, industrial production of cyanuric acid is from urea.[62]

Cyanuric acid exists in two forms: the keto form (isocyanuric acid) exists in solids, and the enol form is dominant in the solution.[63] Solid cyanuric acid does not undergo melting; rather, it sublimates, transitioning directly from a solid to a gaseous state.[63] The crystal structure of cyanuric acid features planar sheets with N–H–O hydrogen bonds.[64] Short, consistent C-O bond lengths indicate the prevalence of the keto tautomer, which is also supported by IR data.[64]

1.6 Metal Cyanurates

Cyanuric acid has three hydroxyl groups (-OH). These groups of cyanuric acid are weakly acidic due to the resonance stabilization of the conjugated base. The negative charge is delocalized over the oxygen and nitrogen atoms. The step-wise deprotonation of cyanuric acid occurs at pK_a values of 6.88, 11.40, and 13.5, respectively.[65, 66] This characteristic plays a crucial role in industrial applications, particularly in metal complexation and the formation of cyanurate salts.

Cyanurate salts can be classified as monosubstituted ($H_2C_3N_3O_3$), disubstituted ($HC_3N_3O_3$), and trisubstituted ($C_3N_3O_3$), along with mixed variations. However, mono- and disubstituted salts are the most common salts.[16] The first evidence for this classification emerged when mercury(II) acetate ($Hg(CH_3COO)_2$) reacted with sodium cyanurate or cyanuric acid and produced two different mercury cyanurates.[16] Typically,

cyanurate salts are synthesized by treating cyanuric acid with excess alkali, such as NaOH.[16, 67] Other metal cyanurates can be obtained through various synthetic routes, including precipitation reactions between cyanuric acid and metal hydroxides or the use of existing metal cyanurates as precursors.[67, 68] Numerous metal cyanurates have been synthesized using these methods. Some notable examples include $Na_2[HC_3N_3O_3]\cdot H_2O$, $Na_3C_3N_3O_3$[67], $K_2[HC_3N_3O_3]$[16], $Li(H_2C_3N_30_3)$[68], and etc. Furthermore, the crystal structure of some of the known metal cyanurates varies only in anionic composition as mixed cyanurates contain a different number of hydroxides or water. Therefore, the amount of pH alters the kind of metal cyanurate salt. Solid-state reactions between potassium cyanate K(OCN) and some metal chlorides, which have been developed by our group, are also methods to get water-free cyanurates such as $Ca_3(O_3C_3N_3)_2$ (CCY), $Sr_3(O_3C_3N_3)_2$ (SCY), $Eu_3(O_3C_3N_3)_2$ (ECY), and $Ba_3(O_3C_3N_3)_2$, of which CCY and SCY have shown strong SHG properties.[69, 70]

Metal cyanurates are important due to their potential to act as a ligand and design new materials with specific properties. The thermal decomposition of metal cyanurates can also link to carbodiimide chemistry.

1.7 Metal Carbodiimides

Metal carbodiimides or cyanamides are part of inorganic chemistry, which is shown with the general formula of $M_x(NCN)_y$. The $[NCN]^{2-}$ can exist in two forms, metal cyanamides ($N{\equiv}C\text{-}N^{2-}$) and metal carbodiimides ($^{-}N{=}C{=}N^{-}$).[71] The synthesis of metal carbodiimides dates back to 1994 when reacting calcium carbide (CaC_2) with nitrogen gas (N_2) at approximately 1,000°C produced calcium carbodiimide ($Ca(CN_2)$).[72] This commercial method, known as the Frank-Caro method, was followed by a large interest in producing other metal carbodiimides.[72] Most of the metal carbodiimides have been developed through solid-state reaction (SSM) using lithium carbodiimide (Li_2CN_2) as starting material, which enables the production of metal carbodiimides at lower temperatures (740°C to 850°C). Examples carbodiimides are $Mg(CN_2)$, $Sr(CN_2)$, $Ba(CN_2)$[73], $Mn(CN_2)$[74], $Cr_2(CN_2)_3$[75], $Zr(CN_2)_2$[76] and $Hf(CN_2)_2$[76], $Sc_2(CN_2)_3$,[77] $Sn(CN_2)$[78], and many other rare-earth carbodiimides[79, 80]. Many RE carbodiimides are prepared from metal halide and $Li_2(CN_2)$ in solid-state metathesis (SSM) reactions. It is worth

mentioning that, in some cases, the starting material of $Zn(CN_2)$[81] has been alternatively used.

Some transition metal carbodiimides can be synthesized using aqueous solution-based methods. This process involves reacting metal salts, such as chlorides, sulfates, acetates, and nitrates with cyanamide (H_2CN_2) in an ammonia solution (NH_3OH). For instance, $Zn(CN_2)$ can be synthesized by the reaction of $ZnSO_4$ with $Na_2(CN_2)$ in an aqueous solution.[81] Moreover, $Co(CN_2)$[82], $Ni(CN_2)$[82], $Cu(CN_2)$[83], and $Cd(CN_2)$[84] can be prepared by treating their respective metal chlorides with cyanamide and ammonia. Precipitation of $Ag_2(CN_2)$ occurs also by mixing silver nitrate ($AgNO_3$) and cyanamide in an ammonia solution.[85] Similarly, several p-block metal carbodiimides, such as $Pb(CN_2)$ can be obtained by reacting lead(II) acetate ($Pb(CH_3COO)_2$) with cyanamide and ammonia solution[86]. $Tl_2(CN_2)$ was prepared in a solution of thallium carbonate (Tl_2CO_3) and sodium carbodiimide $Na_2(CN_2)$.[87] $In_{2.24}(CN_2)$ can be also synthesized in a SSM reaction of indium(III) bromide (InBr) and sodium cyanide (NaCN)[88], or from a decomposition of $(NH_4)[(InCl_2)_3(C_{12}N_{20}H_8)]\cdot\frac{2}{3}[InCl_3(NH_3)]$ at around 700 ˚C[89]. Recently, a novel aqueous solution-based method followed by pyrolysis produced high-purity calcium cyanamide,[90] based on Seifer's earlier work.[16] The process involves reacting cyanuric chloride with metal chlorides and sodium hydroxide in water to produce cyanurate salts, which are then pyrolyzed to obtain the target carbodiimides. In this work, we will also use this synthetic method to investigate the possibility of an unknown carbodiimide.

2. Objective of This Thesis

The search for melaminate compounds and investigations by a few researchers to deprotonate melamine in liquid ammonia[59] attracted our attention to this field of chemistry. We aimed to open a new door to the chemistry of melamine using a solid-state route, not only to benefit from an easier synthetic route but also to obtain ammonia free structures that would be regarded to behave more stable under ambient conditions and had not been reported before. Deprotonated melamine can have the unique feature of acting as a linker between metal complexes or metal organic frameworks and can build supramolecular structures. Furthermore, melamine is widely available and exhibits interesting thermal condensation behavior. The thermal condensation of melamine at higher temperatures into melam, melem, and melon is accompanied by the release of ammonia. However, the presence of another reactant, such as NH_4Cl, can alter the reaction pathway, leading to the formation of melaminium chloride with a protonated melamine ion. This led us to investigate the reactions of melamine at different temperatures in the presence of metal chlorides in a solid-state route.

The first melaminate compound from the reaction of CuCl and melamine emerged as $Cu_3(C_3N_6H_3)$[91, 92], a deprotonated melamine MOF-like structure with very specific features, such as Cu-Cu bonding and channels along the c-axis. This study motivated us to explore various metal chlorides with melamine under different solid-state conditions and to analyze the obtained products. The deprotonation of melamine was indeed successful in some of these reactions, such as in the case of antimony melaminate, which demonstrated that deprotonation of melamine can occur stepwise.[93] Later, the reaction of indium chloride with melamine led to a porphyrin-like supramolecular structure, each structure exhibiting very interesting features.[89]

Next, we aimed to synthesize melaminates via alternative routes. This was inspired by the synthesis of $Cu_3(C_3N_6H_3)$ from $NaHCN_2$ and CuCl. $NaHCN_2$ was reported to be synthesized via the reaction of NaH with melamine. Similarly, we discovered two new potassium melaminates ($K(C_3N_6H_5)$, $K_2(C_4N_7H_3)$) by reacting KH with melamine. Ultimately, we could report three different routes for synthesizing certain metal melaminates, such as reacting melamine with metal chlorides, reacting with halides, and finally, trimerization of hydrogen cyanamide.

Finally, we also investigated the thermal behavior of melaminates, such as indium melaminate, and explored that indium carbodiimide can be obtained. The use of triazines to synthesize carbodiimides had previously been suggested, whether from melamine or cyanuric acid. However, we aimed to synthesize the missing rare-earth carbodiimides. We were able to successfully obtain lanthanum carbodiimide ($La_2(CN_2)_3$) through the decomposition of lanthanum cyanurates in various steps.

3. Summary of Main Results

3.1 (Publ. 1)

This study investigates the reaction of melamine in the presence of copper(I) chloride, yielding the tricopper melaminate ($Cu_3(C_3N_6H_3)$). The dehydrogenated melamine compound was obtained via a solid-state reaction between CuCl and melamine under an argon atmosphere at 275 °C.[92] Kallenbach obtained a small number of hexagonal brownish crystals using an equivalent amount of CuCl with two equivalents of melamine in a closed ampule at 400 °C.[91] Crystals of $Cu_3(C_3N_6H_3)$ were first produced with a 27 % yield, along with melaminium chloride ($C_3H_7N_6Cl$), elemental copper(Cu), and unreacted melamine.[91]

The crystal structure of $Cu_3(C_3N_6H_3)$ was refined through SC-XRD analysis. It has a hexagonal centrosymmetric structure with a space group of *P*6/*mcc* (*a* = 1205.42(5) pm, *c* = 616.00(3) pm). The asymmetric unit of the crystal structure comprises one copper atom, one carbon atom, and two NH groups. An interesting aspect of this compound is that the melaminate ion $(C_3N_6H_3)^{3-}$ (Figure 1a) is structurally and charge-wise very similar to the cyanurate ion.[70, 94-96] Another interesting feature is the presence of Cu–Cu dumbbells (Figure 1b) connecting two melaminate ions into planar layers, as well as forming a twisted ladder-like structure. In this arrangement, Cu_2 pairs connect two layers of the structure along the stacking direction of the *c*-axis. The distance between Cu atoms within a single planar layer is 248.7(1) pm, while the distance between adjacent Cu_2 dumbbells is 319.7(2) pm. Both values are smaller than the sum of the van der Waals radii (392 pm) and can thus indicate a cuprophilic d^{10}–d^{10} interaction.[97]

The arrangement of six melaminate ions around a six-fold rotation axis creates pores within the structure. These pores are aligned along the *c*-axis and are framed by six hydrogen atoms of the melaminate ions, with H-to-H diameters measuring 732.5(7) pm (Figure 2).

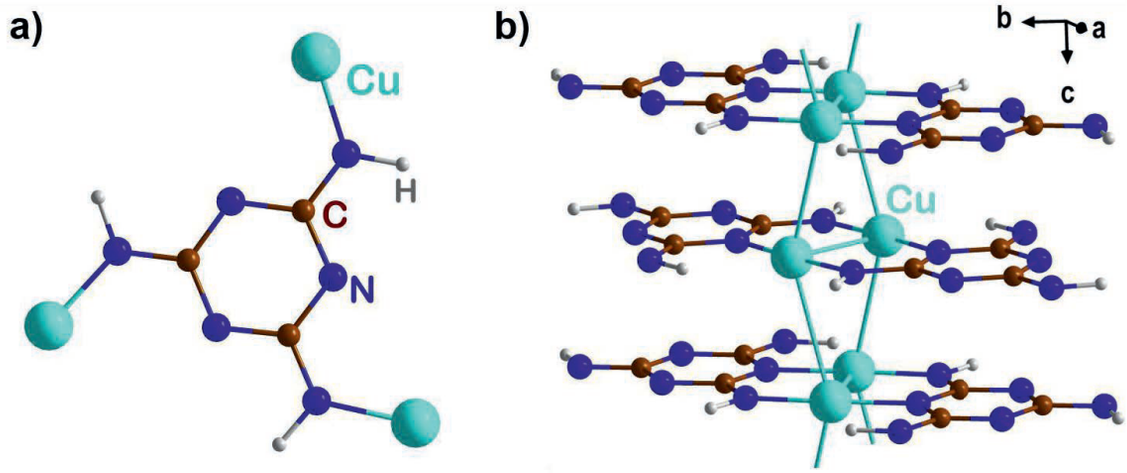

Figure 1. a) $Cu_3(C_3N_6H_3)$ with the melaminate ion obtained by replacing three hydrogens with copper atoms. **b)** structure of twisted ladder $Cu_3(C_3N_6H_3)$ combined with Cu_2 dumbbells.

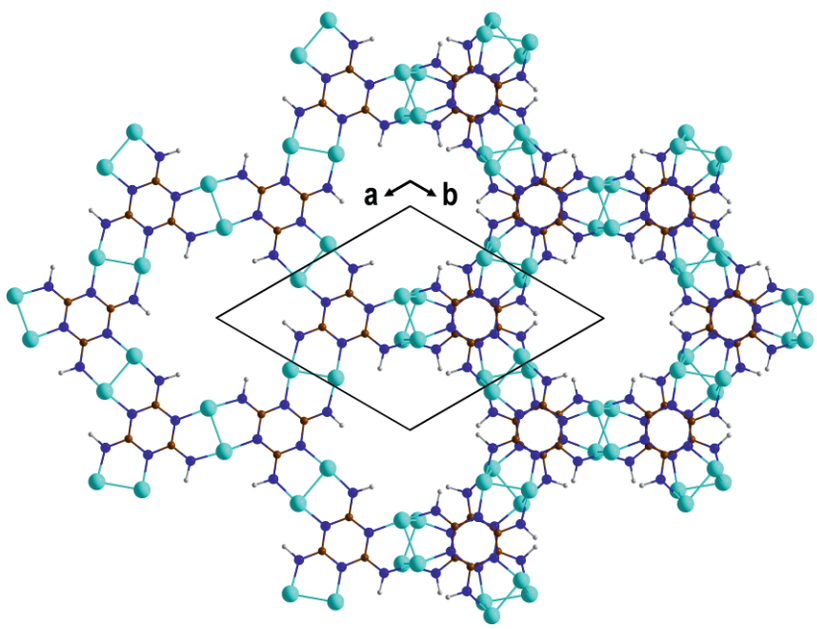

Figure 2. The stacking behavior of $Cu_3(C_3N_6H_3)$ in the *ab* plane is shown, with two layers on the right and one layer on the left.

The calculated electron localization function (ELF) of $Cu_3(C_3N_6H_3)$ has also been studied to demonstrate the different types of chemical bonds present in this material. Within the triazine rings, covalent bonding between C and N atoms can be seen by the presence of local maxima in the ELF at the midpoint of the bonds (Figure 3a). The very high values of the ELF around the H atoms (≈ 1) are the expected

behavior (hydrogen atoms have only one electron, which is localized in the 1s orbital). The presence of a nodal plane in the ELF between Cu and N demonstrates that the Cu–N bonds are ionic. The ELF around the Cu atoms shows some polarization towards each other, with the electrons lying between the Cu atoms being highly delocalized, indicating a metallic Cu–Cu interaction. Figure 3b shows the interlayer interactions. There is no sign of any electronic interactions between the triazine rings, suggesting that their stacking is driven by van der Waals forces.

Elastic tensor calculations in terms of the directional Young's modulus (Y) show that layers along the *ab* plane have a strong boded framework (Y_{ab} = 95 GPa) and directional bonding along *c* has weaker interlayer interactions (Y_c = 35 GPa). Since the ionic and dispersive interactions between the layers cannot produce such a spike in stiffness, this further confirms the presence of directional Cu–Cu bonding along the c-axis.

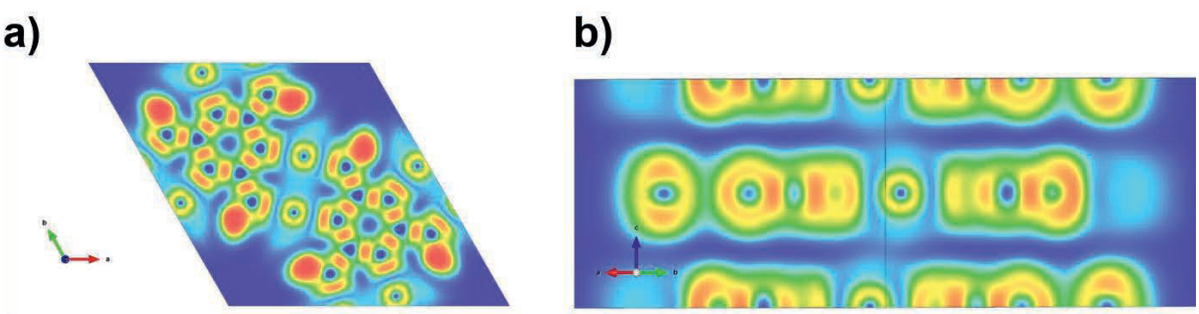

Figure 3. a) calculated ELF in ab plane **b)** and along c axis to show interlayer interactions. (color scale ranging from 1(red) to 0 (blue)

The calculated electronic band structure of $Cu_3(C_3N_6H_3)$, as shown in Figure 4a, indicates that the material behaves as a semiconductor. The calculated band gap is on the order of 2 eV, which is slightly smaller than the experimentally determined value of 2.7 eV obtained through optical reflection measurement (Figure 4b). The bands near the Fermi level exhibited a combination of N p and Cu d character which is suggesting a degree of hybridization between these orbitals. The channels in the $Cu_3(C_3N_6H_3)$ structure offer application as a sensor material when small molecules can be

incorporated. The full potential of $Cu_3(C_3N_6H_3)$ and similar compounds remains to be fully explored.

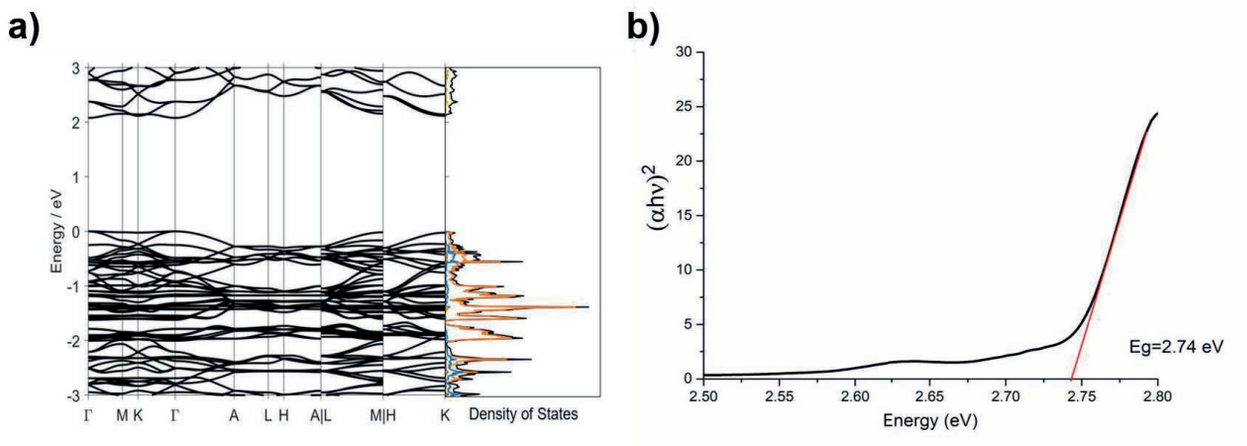

Figure 4. a) Electronic band structure of $Cu_3(C_3N_6H_3)$ and electron density of state on the right side. **b)** Optical reflection measurement

3.2 (Publ. 2)

There were several challenges in the previous route of $Cu_3(C_3N_6H_3)$ synthesis since two by-products of $Cu_3Cl_3(C_3N_6H_6)$ and $Cu_2Cl_2(C_3N_6H_6)$ compete with the pure phase of $Cu_3(C_3N_6H_3)$. The successful synthesis is highly dependent on pressure, argon flow, and diameter of reaction tube. Therefore, we needed a large-scale and high-yield synthesis, aiming to minimize by-products and enhance reproducibility. The reaction of the (1:1) stoichiometric ratio of CuCl and sodium hydrogen cyanamide $NaHCN_2$ was introduced as an alternative route to produce $Cu_3(C_3N_6H_3)$ via cyclotrimerization of $(HNCN)^-$ ions eq (1).[98]

$$3CuCl + 3\ NaHCN_2 \rightarrow Cu_3(C_3N_6H_3) + 3NaCl \qquad \text{eq (1)}$$

Differential thermoanalytic studies (DTA) with a heating and cooling rate of 2 °C min^{-1} in the range from 25 to 450 ˚C (Figure 1) were done to find the exact temperature of the reaction. The reaction for synthesizing $Cu_3(C_3N_6H_3)$ has been chosen to be exactly at 200 ˚C, slightly above the exothermic peak attributed to the formation of this compound (Figure 5). This temperature was kept for 45 hours for a complete reaction. There are no exothermic or endothermic peaks above 200 ˚C, suggesting good stability of $Cu_3(C_3N_6H_3)$. Additionally, TGA studies show that decomposition of $Cu_3(C_3N_6H_3)$ shows a slow onset, starting at temperatures above 300˚C. However, the decomposition remains almost negligible until 450 ˚C. In the final stage, the $Cu_3(C_3N_6H_3)$ decomposed into CuCN and elemental copper.

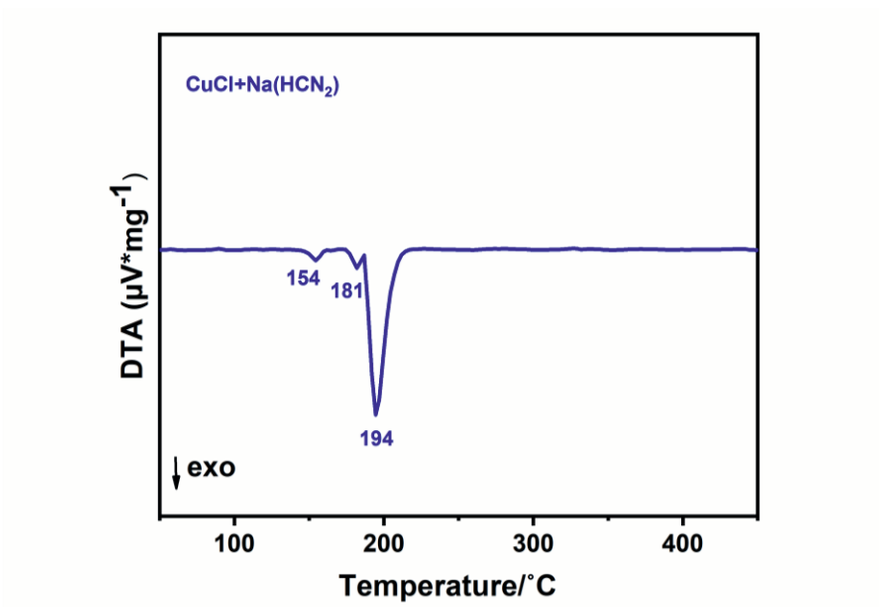

Figure 5. DTA of the reaction of CuCl and $NaHCN_2$.

Figure 6 presents the powder XRD pattern of the synthesized $Cu_3(C_3N_6H_3)$ with NaCl. To remove the metathesis salt (NaCl), the sample was washed with absolute methanol. A detailed comparison in Figure 6a and c highlights the differences between the calculated CIF derived from crystallographic data and PXRD measured. The intensity ratio of reflections at 2θ values of 8.46 and 16.98, corresponding to miller indices 100 and 200, respectively, deviates from those observed at the measured crystal. Notably, this ratio changes after washing with methanol (Figure 6b). Furthermore, a distinctive shift in reflections along the c-axis (002 reflections at 2θ = 28.92) is observed, along with some slight shifts in some smaller reflections. These differences cannot be solely ascribed to temperature measurement variations in single-crystal and powder XRD measurements or the orientation of particles in the sample.

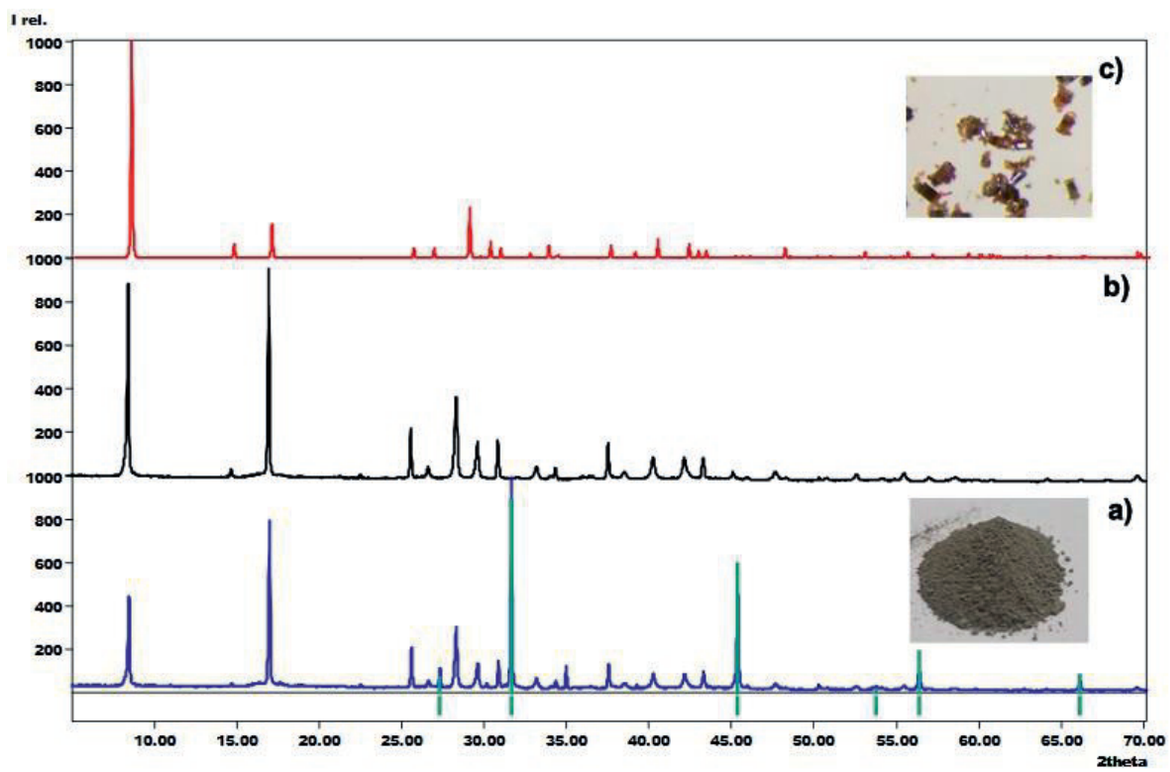

Figure 6. PXRD of **a)** synthesized $Cu_3(C_3N_6H_3)$ with metastasis salt with the sample color, **b)** sample washed with methanol, **c)** calculated pattern form SC-XRD measurement, with crystals color.

As discussed before, channels can accommodate any host molecule with a size smaller than 2r = 733.8 pm. Additionally, the presence of six hydrogen atoms per channel in each layer promotes the hydrogen bonding and stabilizes the host molecules. Therefore, the difference in the intensities of reflections may be attributed

to the presence of a host molecule (e.g., melamine, cyanamide derivatives) filling the channels in the crystal structure, while the shift and broadening in some peaks may be ascribed to particle defects. Sequential solvent exchange (methanol, acetonitrile, THF, pentane) and vacuum drying (260 °C, 4 weeks) can remove some of these guest molecules, yielding a stable, brown powder. The XRD pattern obtained from treated $Cu_3(C_3N_6H_3)$ in Figure 7d compares well with the calculated pattern from single-crystal refinement (Figure 7e).

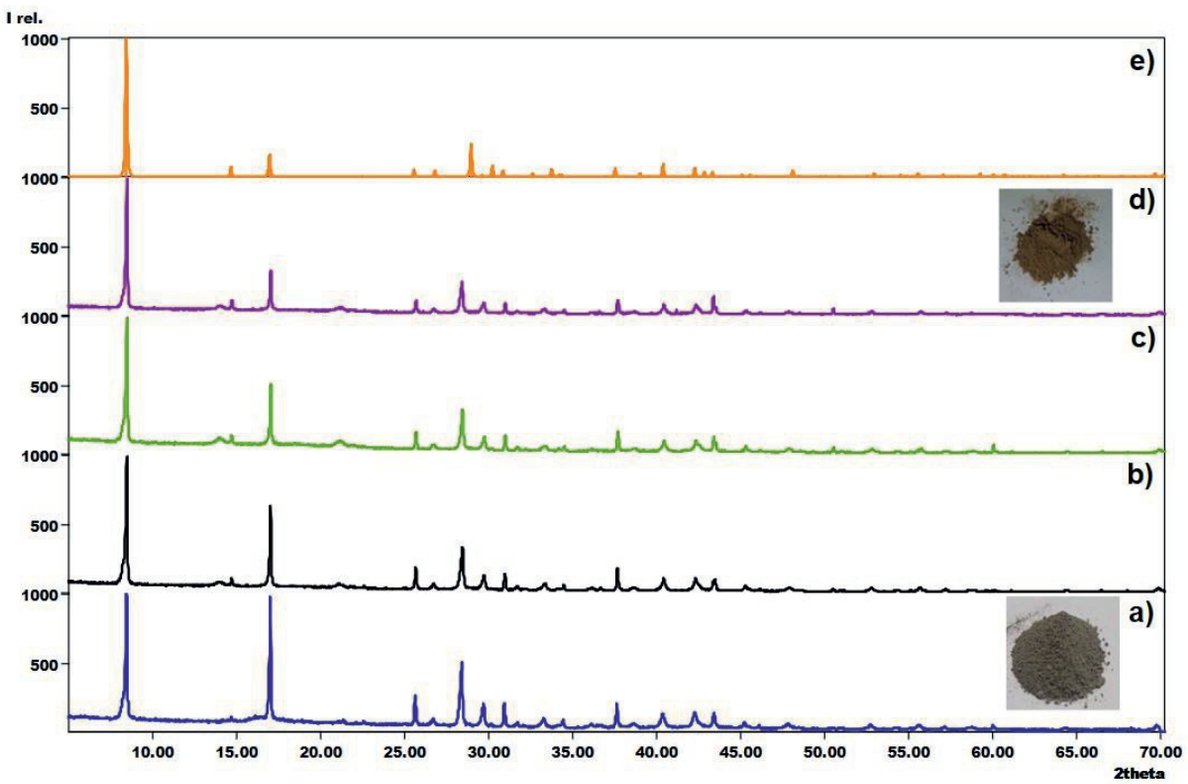

Figure 7. PXRD pattern of **a)** synthesized $Cu_3(C_3N_6H_3)$ washed with various solvents, **b)** washed sample vacuum dried under 260˚ C for 24 h, **c)** for 48 h, d) for 4 weeks **e)** calculated pattern form SC-XRD measurement.

Due to the six-fold rotation axis in the middle of the channels, any guest molecule, either cyanimide of dicyandiamide, will probably adapt a six-membered ring arrangement for the host; therefore, in the modeling with diamond graphics, we have placed melamine inside the channels and in between the channels to see the differences in XRD. Interestingly, the ratio of reflections changed and gave us the reason behind this discrepancy of experimental XRD and calculated CIF file of $Cu_3(C_3N_6H_3)$. Additionally, solid-state ^{13}C and ^{1}H NMR suggest that disordered melamine is a potential candidate for being trapped within the channels. However, IR

studies didn't show any evidence regarding the host molecule but could confirm the structure of $Cu_3(C_3N_6H_3)$. The band between 3000–3500 cm^{-1} corresponds to the N–H stretching vibration, and N–H bending vibration appears at 1537 cm^{-1}**,** while the N–H wagging deformation is at 752 cm^{-1}. Moreover, bands at 1450, 1251, and 642 cm^{-1} are linked to different vibrational modes of the melaminate ring.

We have also conducted photoluminescence studies on $Cu_3(C_3N_6H_3)$. Interestingly, the treated $Cu_3(C_3N_6H_3)$ (with nearly empty channels) is not luminescent. In contrast, the untreated sample (comprising the host molecules) exhibits a green-yellow emission color upon excitation with UV radiation. This suggests that host-guest interactions contribute to the observed emission, a phenomenon known as guest-induced luminescence.[99] This study confirms the potential of this functional material for application as a luminescent MOF-based sensor.[100]

In the data from PL spectra of synthesized $Cu_3(C_3N_6H_3)$, the excitation spectrum shows a distinct peak at 420 nm, while the corresponding emission spectrum exhibits a peak at 560 nm (Figure 8). The obtained broad emission band at 560 nm is consistent with the observed green-yellow light. The decay curve suggests that the luminescence dynamics of the synthesized $Cu_3(C_3N_6H_3)$ exhibit an almost mono-exponential and rather fast emission decay, as indicated by the calculated decay time of 14.5 µs.

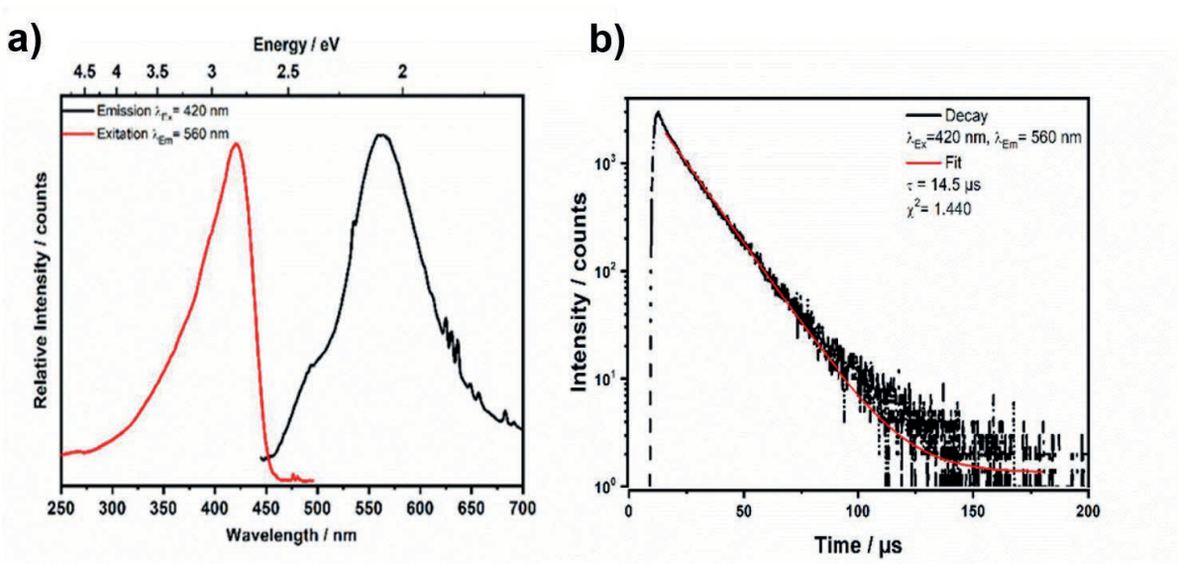

Figure 8. a) Excitation and emission spectrum of $Cu_3(C_3N_6H_3)$ at 77 ˚C and **b)** the decay curve.

Magnetic studies of $Cu_3(C_3N_6H_3)$ were carefully done due to the low signal intensity of the sample. Temperature-dependent magnetic susceptibility measurements (χ_{mol}) (2–300 K) show a paramagnetic response to the magnetic field (Figure 9). The molar susceptibility data were also fitted using a modified Curie-Weiss equation[101], giving paramagnetic Curie temperature (θ_p) of –0.48(3) K and an effective magnetic moment (μ_{eff}) of 0.262 μB (equivalent to 0.034 unpaired electrons) and a temperature-independent susceptibility (χ_o) of 7.91×10^{-9} m^3/mol. The magnetism of copper is defined by its electron configuration, and a saturated 3d shell usually has diamagnetism. Ligand interaction in Cu(I) complexes may disrupt the electron configuration, adding to the number of unpaired electrons and inducing paramagnetism. The Cu_2 dumbbells in $Cu_3(C_3N_6H_3)$ are connected in a twisted ladder structure along the c-axis, distorting the d^{10} configuration, which can also contribute to its paramagnetism.

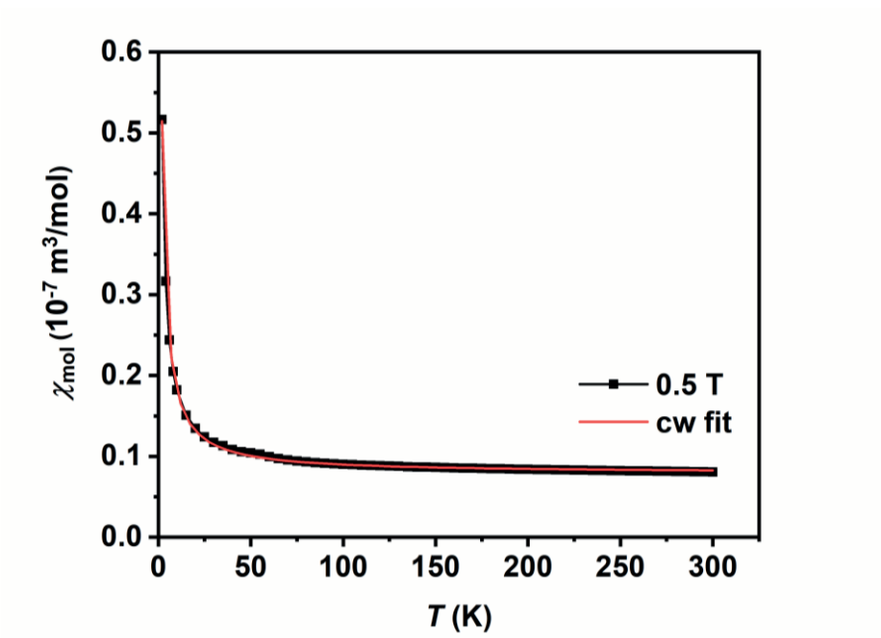

Figure 9. The measured magnetic susceptibility of $Cu_3(C_3N_6H_3)$, showing the variation of χ_{mol} with temperature, accompanied by the fitted red curve.

3.3 (Publ. 3)

In this section, a new set of melaminate compounds with antimony were introduced. This work has a similar synthetic route as $Cu_3(C_3N_6H_3)$ from melamine and CuCl. As can be seen in Figure 10, the step-wise deprotonation of melamine via a solid-state route gave us three different compounds and provided insight into the mechanism of these kinds of reactions. Compounds **(1)** and **(2)** are mono-deprotonated melamine, and compound **(3)** is double-deprotonated melamine.[93]

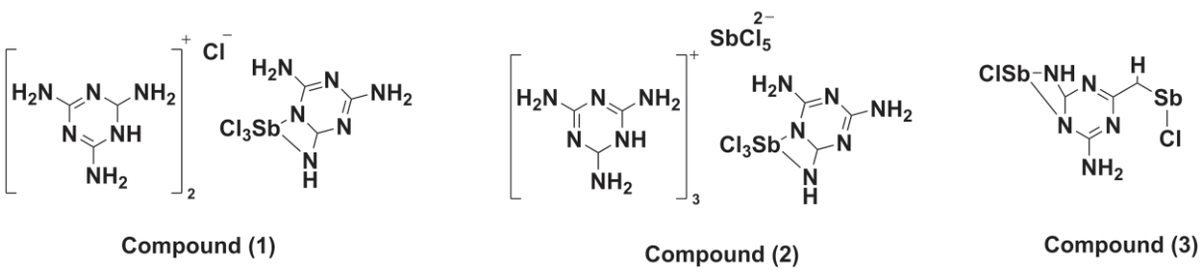

Figure 10. Three deprotonated melamine compounds synthesized in the presence of $SbCl_3$ at various conditions.

The compound **(1)** was obtained from a ratio of 1:4 at 200 °C. It has been crystalized in a triclinic system in with space group of $P\bar{1}$. The crystal structure of **(1)** consists of two protonated melamine ions, one deprotonated melamine, a single chloride ion, and $SbCl_3$ forming $SbCl_4(C_3N_6H_5)(C_3N_6H_7)_2$ **(1)**. The crystal structure consists of three unique layers arranged sequentially along the *b*-axis. The antimony center is attached to an exocyclic nitrogen atom of the melaminate ion via Sb-N4 (204.7(3) pm) and Sb-N1 (253.6(3) pm). A single Cl^- ion in the structure is connected via hydrogen bonding (Figure 11).

The crystal structure of **(2)** consists of three protonated melaminium ions and one deprotonated melamine, an $(SbCl_5)^{2-}$ ion, and an $SbCl_3$ unit, forming $(SbCl_4)_2(C_3N_6H_5)(C_3N_6H_7)_3$, as shown in Figure 12. Antimony in $SbCl_3$ is linked to the melaminate ion $(C_3H_5N_6)^-$ via Sb-N4 (204.4(6) pm) and a weaker interaction via Sb-N1 (256.1(3) pm). It crystallizes in the monoclinic $P2_1/c$ space group, and similarly, the crystal structure features a layered arrangement and hydrogen bridging within layers. This compound was synthesized at 200 ˚C with a 1:2 molar ratio of $SbCl_3$ to melamine. The arrangement of stacked layers in compound **(1)** and **(2)** is primarily influenced by

the tendency for the nitrogen atom in the triazine ring of one layer to alternate with a carbon atom in the triazine ring of the adjacent layer, which is a behavior similar to copper melaminate $Cu_3(C_3N_6H_3)$ compound. Thus, these compounds possibly have π-π between C_3N_3 rings.

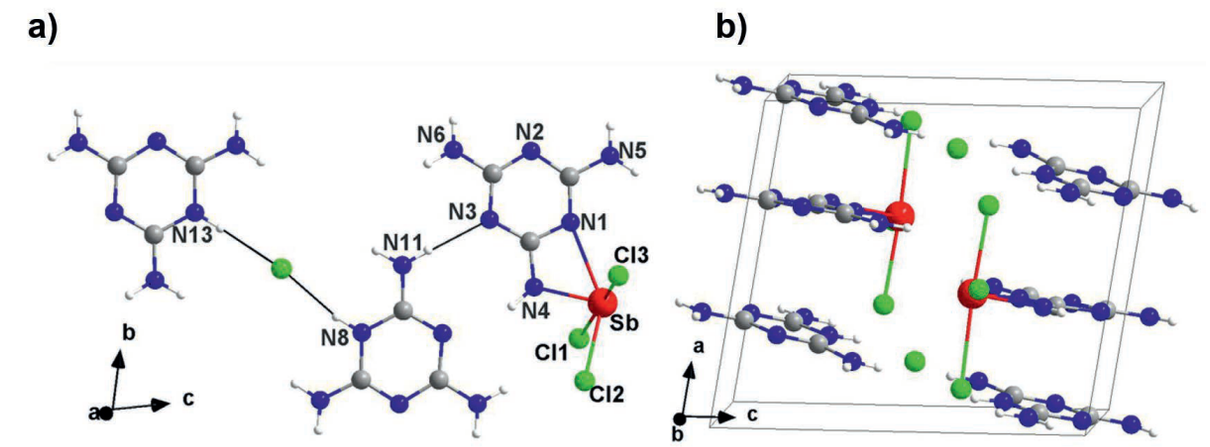

Figure 11. a) the structure of **(1)** as $SbCl_4(C_3N_6H_5)(C_3N_6H_7)_2$, and **b)** a perspective view of the unit cell of **(1)** along the *b*-axis (N: blue, C: gray, H: white, Cl: green, Sb: red).

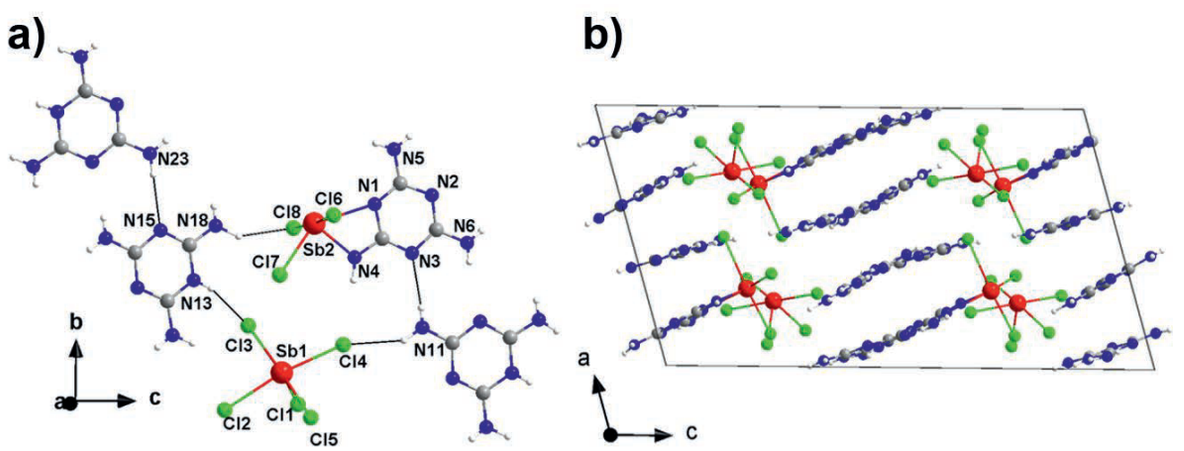

Figure 12. a) Structure of **(2)** as $(SbCl_4)_2(C_3N_6H_5)(C_3N_6H_7)_3$ projected on the *bc*-plane, and **b)** a perspective view along the *b*-axis (N: blue, C: gray, H: white, Cl: green, Sb: red).

The crystal structure of **(3)** consists of the melaminate ion $(C_3N_6H_4)^{2-}$ and $(SbCl)^{2+}$ forming $SbCl(C_3N_6H_4)$. It crystallizes in the monoclinic $P2_1/n$ space group. Unlike the two previous structures, this structure adopts an infinite chain arrangement as a result of the bridging connectivity of the divalent melaminate anion, as depicted in

Figure 13, SbCl (d_{Sb-Cl} = 254.9 pm) is linked through exocyclic nitrogen atoms of two melaminate ions, forming Sb-N4 (204.4(6) pm) and Sb-N6 (208.6 pm) interactions, along with a weaker interaction via Sb-N2 (241.5(1) pm). This compound was obtained at a higher temperature (250-280 ˚C) from both 1:2 and 1:4 molar ratios of $SbCl_3$ to Melamine

Unlike the two previously mentioned structures (**1**,**2**), that show layered arrangement and possibly π-π interaction between C_3N_3 units, the centroid-to-centroid distance of C_3N_3 rings in compound **(3)** is 560-590 pm which is an indication of no π-π interaction between the layers.

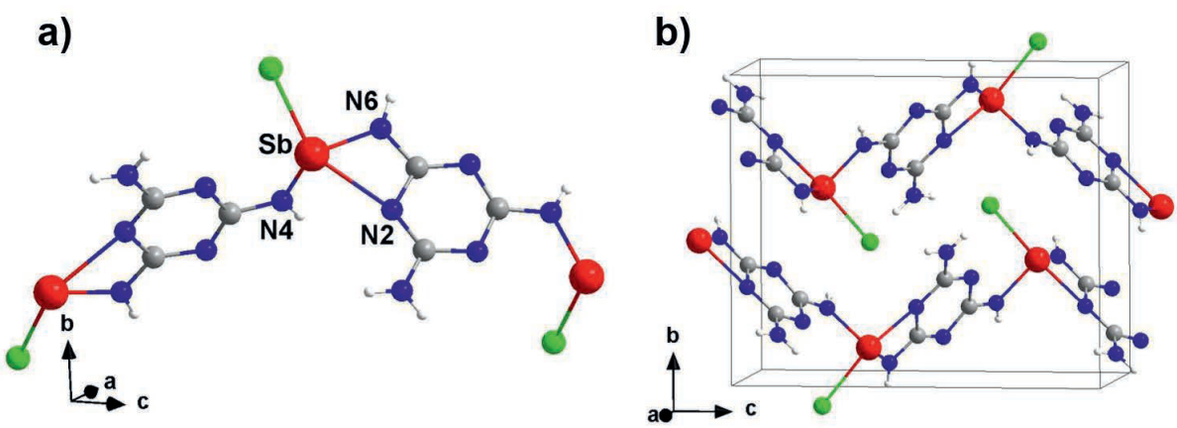

Figure 13. a) Structure of **(3)** and **b)** a perspective view of the unit cell almost along the *a*-axis (N: blue, C: gray, H: white, Cl: green, Sb: red).

Additionally, the IR spectroscopy confirms the presence of both protonated and deprotonated melamine species in these compounds. DSC analysis is a helpful tool combined with XRD to reveal a sequence of exothermic and endothermic events corresponding to the formation and decomposition of each product and intermediates. The reaction mechanism is also predicted to be similar to tricopper melaminate with the release of HCl or, in other words, melaminium chloride, which here is present in the crystal structure of **(1)** rather than being a side phase of the reaction. In contrast to our previous work on $Cu_3(C_3N_6H_3)$, the antimony melaminate compounds couldn't be deprotonated three times, and further heating to higher temperatures led to the formation of an amorphous glass-like phase. This study demonstrates the possibility of using $SbCl_3$ to synthesize metal-melaminates, which can validate our previous route for the development of metal melaminate compounds. However, the probable obstacles to obtaining three times deprotonation of melamine are high reactivity and condensation behavior of melamine at the required temperature.

3.4 (Publ. 4)

Similar to the earlier route, in this research, the solid-state reaction (SSM) of melamine with indium(III) chloride ($InCl_3$) is investigated. The reaction yields a novel supramolecular and porphyrin-like assembly of deprotonated melamine. SSM reaction between 1.2 molar ratio of $InCl_3$ and 1 molar of melamine was conducted at 250 ˚ C to yield the $(NH_4)[(InCl_2)_3(C_{12}N_{20}H_8)]\cdot\frac{2}{3}[InCl_3(NH_3)]$ compound.[89] The side phase of the reaction was characterized as $(NH_4)_2[InCl_5(NH_3)]$ and $(NH_4)_3InCl_6$, which were sublimed on the top of the ampule. These compounds were characterized using single-crystal X-ray diffraction to determine the crystal structure and powder X-ray diffraction to study the phase purity.

The crystal structure of indium melaminate ($(NH_4)[(InCl_2)_3(C_{12}N_{20}H_8)]\cdot\frac{2}{3}[InCl_3(NH_3)]$) was solved and refined with a transparent yellow single crystal based on X-ray diffraction data in the cubic space group *I* $\bar{4}$3*d*. This novel compound features either four deprotonated melamine units or two melam units in a supramolecular assembly, having $[C_{12}N_{20}H_8]^{4-}$ anion interconnected in the structure via N–In–N bonding. As shown in Figure 14a, the central indium atom is linked via dative bonding to the inner nitrogen atoms **(1)** of melam or melamine within the ring-shaped molecule. The other two terminal nitrogen atoms **(2)** are completely deprotonated, interconnecting melamine units and also forming N-In bonding. Similarly, the nitrogen atom **(3)** undergoes complete deprotonation, forming N-C and N-In bonds.

The indium(II) ions within the $[(InCl_2)(InCl_2)_{4/2}(C_{12}N_{20}H_8)]^-$ fragments are coordinated in two distinct octahedral configurations. One type is located at the center of $[C_{12}N_{20}H_8]^{4-}$, while the remaining four indium atoms surround the $[C_{12}N_{20}H_8]^{4-}$ centres and act as a bridge to connect other units, as shown in Figure 14b. Moreover, In–N bond lengths vary from 204.2(2) pm to 228.1(6) pm. The ammonium ions and $[InCl_3(NH_3)]$ molecules in the structure of $(NH_4)[(InCl_2)_3(C_{12}N_{20}H_8)]\cdot\frac{2}{3}[InCl_3(NH_3)]$ are situated in the voids of the described structure, as shown in Figure 15.

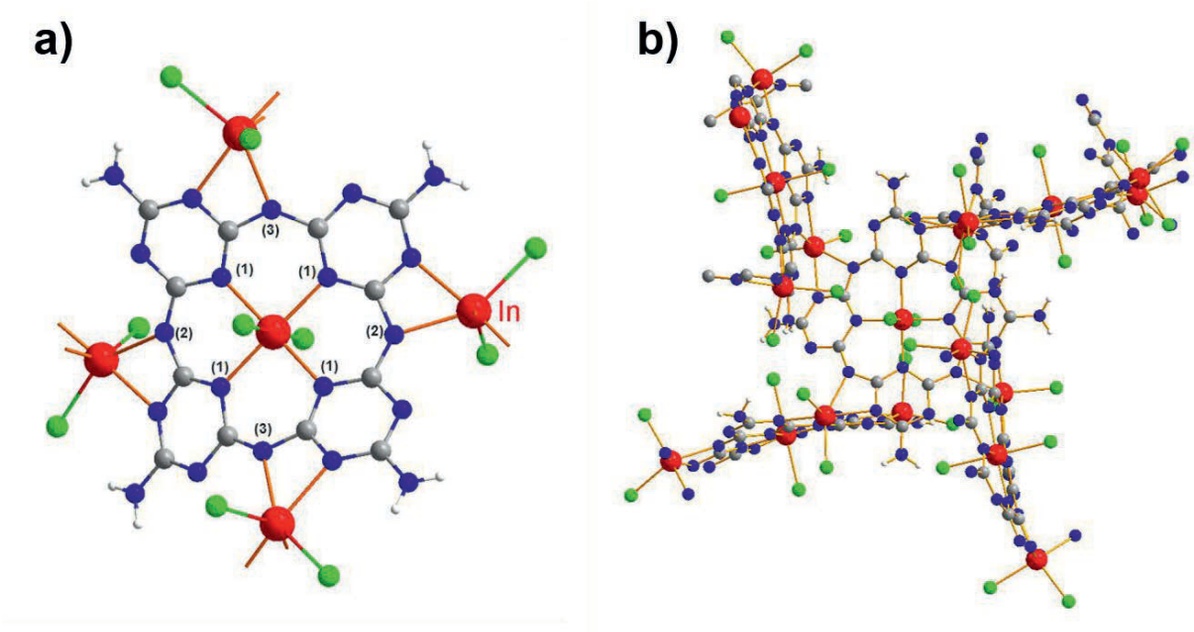

Figure 14. a) Connectivity of $[C_{12}N_{20}H_8]^{4-}$ ion with indium(III) ion, b) tilted connectivity of $[C_{12}N_{20}H_8]^{4-}$ units via -N-In-N- bonds (In is red, Cl green, C grey, N blue).

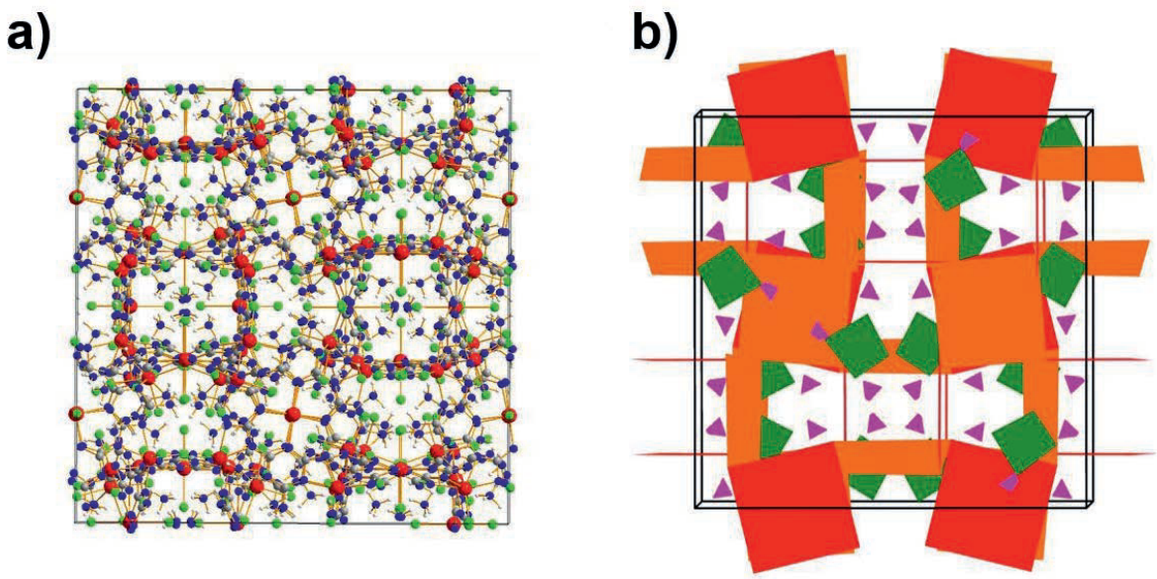

Figure 15. a) content of unit cell of $(NH_4)[(InCl_2)_3(C_{12}N_{20}H_8)]\cdot\frac{2}{3}[InCl_3(NH_3)]$, **b)** schematic polyhedral drawing of structure showing position of NH_4^+ in violet and $[InCl_3(NH_3)]$ molecules in green.

The thermal stability of this compound has also been studied with TGA analysis. The decomposition starts at around 413 ˚C and continues until 700 ˚C, until the compound is finally converted into indium carbodiimide $(In_{2.24}(NCN)_3)$[102]. This compound is also stable at ambient conditions.

The solid-state luminescence of the synthesized material was investigated at ambient temperature (Figure 16). The emission spectra depicted two broad bands at 380 and 530 nm, while the corresponding excitation bands are at 350 and 460 nm, respectively. The 530 nm emission causes greenish luminescence. To further analyse the photoluminescence behaviour, decay curves of the emission spectra excited at 350 nm were recorded. The decay curves indicated emission lifetimes of 604 µs and 325 µs for the emission bands at 358 nm and 530 nm, respectively. Given that the decay times of ligand-to-metal charge transfers (LMCT) fall within the microsecond range and ligand-centered processes like π–π* transitions fall into the nanosecond range, the luminescence of this compound can be attributed to either LMCT or metal-centred transitions.

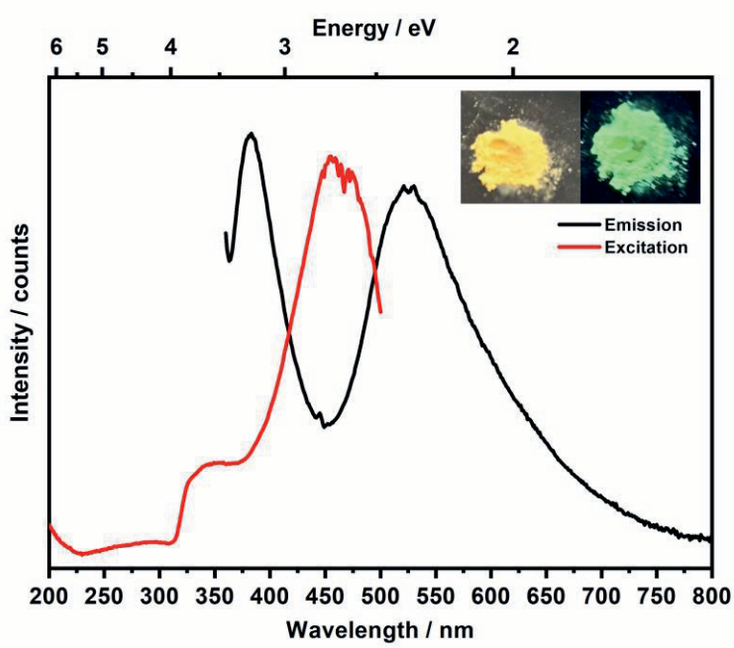

Figure 16. Photoluminescence spectrum of $((NH_4)[(InCl_2)_3(C_{12}N_{20}H_8)]\cdot\frac{2}{3}[InCl_3(NH_3)])$ at ambient temperature. The excitation spectrum was recorded at 535 nm, and the emission at 350 nm. (The inset displays the yellow crystalline powder and its green luminescence under UV light.)

3.5 (Publ. 5)

This study explores an alternative solid-state route for the synthesis of melaminate compounds. First, the reaction between KH and melamine in the 6:1 ratio was analyzed using DSC analysis.[103] Thermal analyses are powerful tools for the study of sequences of reactions and their intermediates.[104] Therefore, the DSC analysis of the reaction of NaH and LiH with melamine was separately analyzed. However, the DSC results revealed a tight reaction sequence in NaH and a sharp exothermic peak in LiH reactions. Therefore, we decided to investigate the deprotonation sequence of KH with melamine. Additionally, this study also introduces a new synthesis route for carbodiimides such as $Li_2(CN_2)$ and $K_2(CN_2)$. Unlike the traditional method of reacting metal nitrides (Li_3N) with excess melamine, this new approach employs a stochiometric amount of metal hydrides and melamine.

In the DSC plot (Figure 17), one endothermic effect and six exothermic peaks are observed. To identify each phase following an exothermic peak, parallel reactions were conducted in fused silica ampules or Schlenk tubes to obtain either pure PXRD patterns or single crystals for structural identification. DSC studies show that this new pathway for synthesizing carbodiimides results in a much less exothermic reaction compared to the old route. (–350 kJ/mol compared to –500 kJ/mol).

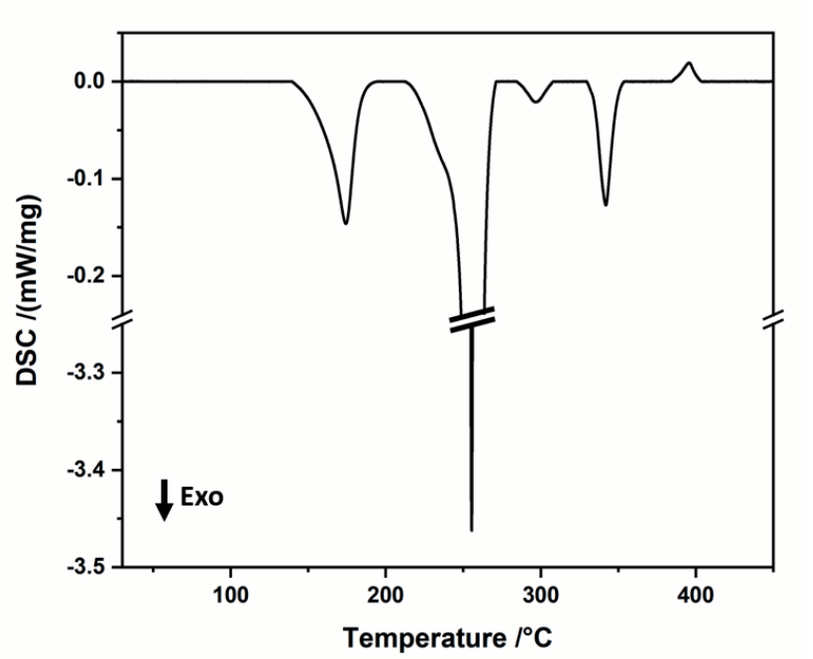

Figure 17. DSC plot of the reaction 6 KH + $C_3N_6H_6$ → 3 $K_2(CN_2)$ + 6 H_2 with a heating rate of 2 °/min.

The first and second exothermic peaks at 170 °C and 175 °C correspond to the formation of new potassium melaminate ($K(C_3N_6H_5)$) and potassium cyanomelaminate ($K_2(C_4N_7H_3)$), respectively. Around 230 °C, $K_2(C_4N_7H_3)$ decomposes, forming the previously known $KHCN_2$[105], and then transforming into $K_5H(CN_2)_3$[106] at 250 °C. The monoclinic *α*-$K_2(CN_2)$ is formed at approximately 270 °C, and the weak exothermic effect at 400 °C is attributed to the formation of the tetragonal *β*-$K_2(CN_2)$ phase. Furthermore, the exothermic peak at around 300 °C is also attributed to the formation of $K_5(CN_2)_2H$[107], however, the pure phase of this compound can be obtained by a 7:1 ratio of KH to melamine.

Before this study, previous research in the K-H-(NCN) system was mostly conducted in liquid ammonia, and several compounds were already characterized, such as $K_5H(CN_2)_3$[106], $KHCN_2$[108], and $K_5(CN_2)_2H$[107]. In each of these compounds, hydrogen has a different role and is represented differently. In $K_5H(CN_2)_3$, hydrogen acts as a proton, while in $K_5H(CN_2)_3$, it exists as a hydride, and in $KHCN_2$, hydrogen acts as a protonic imide. The ($K_5H(CN_2)_3$) compound was prepared by the reaction of melamine and KNH_2 at approximately 320 ˚C or form $KHCN_2$ and potassium.[106] Meanwhile, the $K_5(CN_2)_2H$ compound, in which hydrogen acts as a hydride, is formed from the reaction of $K(NH_2)$ and carbon in an autoclave at 650 °C.[107] $KHCN_2$ can be prepared via the reaction of KNH_2 and melamine in liquid ammonia.[108] *α*-$K_2(CN_2)$ is prepared in liquid ammonia from the reaction of $KH(CN_2)$ and KNH_2.[105] Herein, only three of the compounds that appeared in the DSC study are newly identified, and therefore, their crystal structures are discussed here in detail.

$K(C_3N_6H_5)$, known as monopotassium melaminate, was synthesized by reacting 75 mg of KH with 214.41 mg of melamine in a fused silica ampule at 225 °C for 40 hours. The crystal structure consists of the $(C_3N_3)(NH_2)_2(NH^-)$ monoanion, together with two distinct melaminate ions and two crystallographically different potassium ions, each coordinated by six neighboring nitrogen atoms in a distorted trigonal-prismatic fashion with distances of 280 and 301 pm (Figure 18). The unit cell contains 16 melaminate ions forming the orthorhombic structure of $K(C_3N_6H_5)$ with a space group of *Pbcn*.

By reacting 75 mg of KH with 147.4 mg of melamine at 240 ˚C for 60 h in a sealed silica tube, $K_2(C_4N_7H_3)$ can be obtained. The formation of the cyano group can be explained by the decomposition of melamine at higher temperatures to cyanamide and dicyandiamide. The crystal structure contains mono-cyanomelaminate anions coordinated by two crystallographically distinct potassium cations (Figure 19a) and forms orthorhombic *Pmc*2_1. As can be seen in Figure 19b, the structure forms a layered arrangement of $(C_4N_7H_3)^{2-}$ anions in the bc-plane, with potassium ions positioned above and below the layers. In cyanomelaminate, the (NCN) group is disordered alongside the NH group, resulting in the neighboring K2 being distributed into two crystallographic positions.

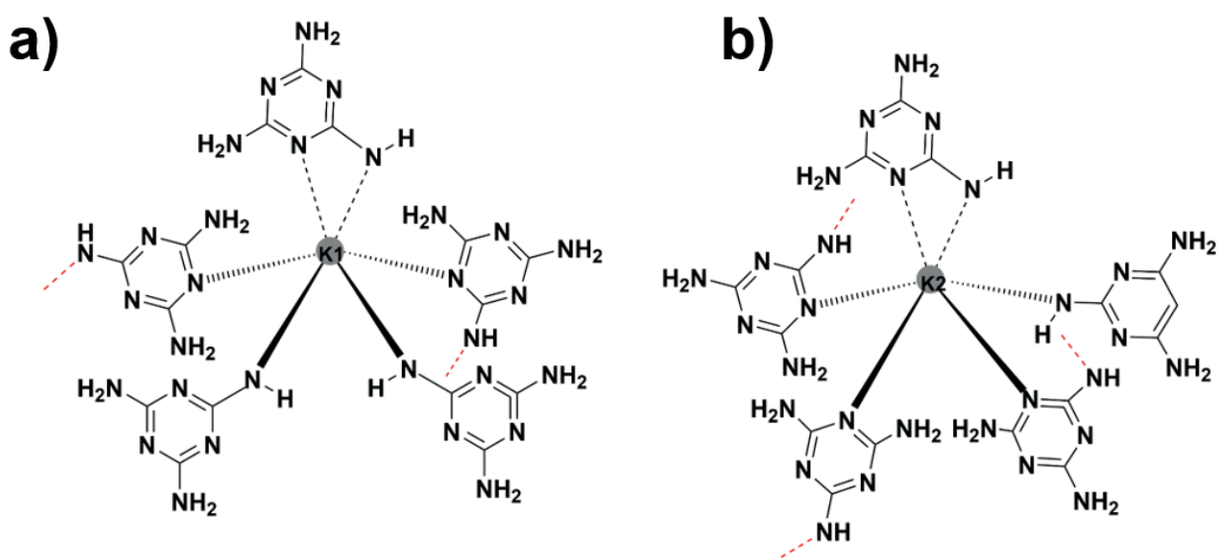

Figure 18. Two crystallographically different K ions in $K(C_3N_6H_5)$.

The new modification of β-$K_2(CN_2)$ is also obtained in the Schlenk tube with 150 mg KH and 78.6 mg melamine at 450 ˚C for 2 h. The tetragonal $K_2(CN_2)$ crystallizes in $I4_1/a$ space group and is sensitive to moist air. The crystal structure features two types of $(NCN)^{2-}$ ions: fully symmetric ($d_{N2–C2-N3}$ = 124.9(2) pm) and nearly symmetric ($d_{N1–C1-N2}$ = 121.4(3) pm and 121.9(3) pm), both classified as carbodiimides. The fully symmetric carbodiimide is coordinated by twelve potassium ions in a double-square-antiprismatic arrangement (Figure 20a), while the second type is positioned around these columns, as shown in Figure 20b. Additional channels are also formed in this structure (Figure 21), which are occupied by disordered potassium ions (K3 and K4).

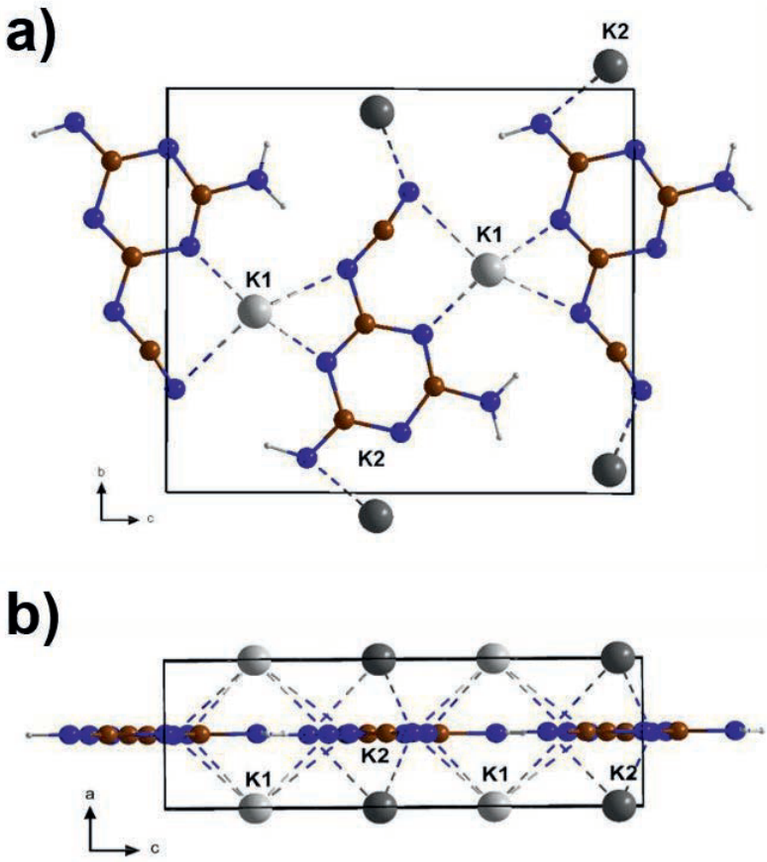

Figure 19. Two views of the $K_2(C_4N_7H_3)$ unit cell.

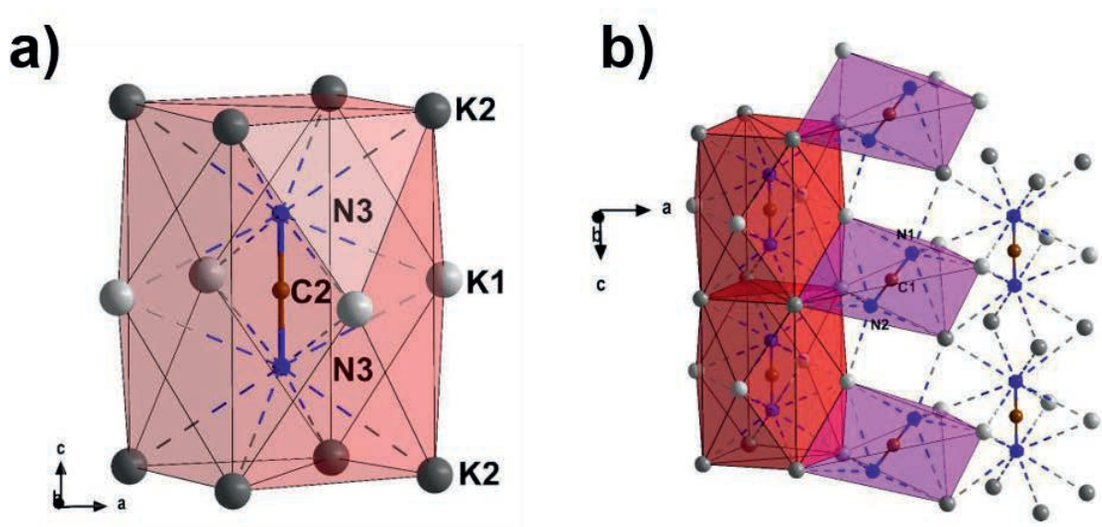

Figure 20. Coordination environments of two types of $(NCN)^{2-}$ ions in the structure of β-$K_2(CN_2)$: **a)** coordination by twelve potassium ions, **b)** violet polyhedral depicts coordination by six potassium ions.

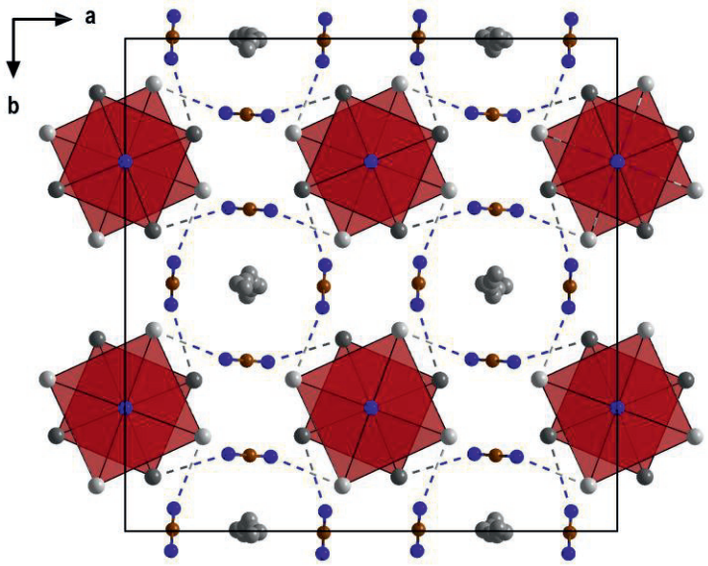

Figure 21. Unit cell of tetragonal β-$K_2(CN_2)$ showing disordered potassium atoms (K: grey, C: red, N: blue).

Besides the given results, the reaction of 6 MH (M: Li, Na, K) with 1 melamine involves the transfer of positive and negative charges, leading to the release of equal numbers of molecular hydrogen (H_2) alongside the formation of $M_2(CN_2)$. This reaction eq (2) can be compared to the typical reaction of hydrogen generation in $LiBH_4$-$LiNH_2$ composite[109-111] eq (3) materials. In both reactions, hydridic and protic hydrogens combine in favor of hydrogen generation. Although the reactions are not currently reversible, catalytic hydrogenation may provide a potential route for hydrogen absorption and the reformation of precursors (melamine and KH) in the future. Both reactions offer a significant amount of hydrogen and offer hydrogen storage capacities

$$6\ MH + C_3N_3(NH_2)_3 \rightarrow 3\ M_2(CN_2) + 6\ H_2\uparrow \quad (M: Li, Na, K) \qquad \text{eq (2)}$$

$$LiBH_4 + 2\ LiNH_2 + \rightarrow Li_3(BN_2) + 4\ H_2\uparrow \qquad \text{eq (3)}$$

3.6 (Publ. 6)

This study investigates the reactivity of melamine at elevated temperatures in the presence of some transition metal chlorides, such as $MnCl_2$, $FeCl_2$, and $CoCl_2$, to introduce three new compounds of $MnCl_2(C_6N_{10}H_6)$, $FeCl_2(C_6N_{11}H_9)$, and $CoCl_2(C_6N_{11}H_9)$ (eq (4-6)).[112] The main purpose is to investigate the reactivity of melam and melem as intermediate phases of melamine condensation and discover the new coordination chemistry of these units. Due to the insolubility of melem and melam in most organic solvents, solid-state (SSM) reactions were used.

$$MnCl_2 + 2\ C_3N_6H_6 \rightarrow MnCl_2(C_6N_{10}H_6) + 2\ NH_3 \qquad \text{eq (4)}$$

$$FeCl_2 + 2\ C_3N_6H_6 \rightarrow FeCl_2(C_6N_{11}H_9) + NH_3 \qquad \text{eq (5)}$$

$$CoCl_2 + 2\ C_3N_6H_6 \rightarrow CoCl_2(C_6N_{11}H_9) + NH_3 \qquad \text{eq (6)}$$

All crystalline compounds were prepared in a 6 cm silica ampule (inner diameter) with a molar ratio of 1:2 of metal chloride and melamine at around 400 ˚C for 100 h. The XRD obtained from the reaction of metal chlorides and melamine at 400 ˚C in a closed ampule was in a good agreement with the calculated pattern from single crystal; however, with a high background. This can be attributed to either the existence of an amorphous phase or the fluorescence effect of respective metals. To purify the $MnCl_2(C_6N_{10}H_6)$ compound, a double chamber ampule was used to separate these phases with a temperature gradient. The pure $MnCl_2(C_6N_{10}H_6)$ stays on the hot side of the ampule, while melamine and ammonium chloride were on the cooler side.

$MnCl_2(C_6N_{10}H_6)$, $FeCl_2(C_6N_{11}H_9)$, and $CoCl_2(C_6N_{11}H_9)$ all crystallize in monoclinic system, with space groups of *I*2/*a*, and *P*2$_1$/*c*, respectively. As can be seen in Figure 22, $MnCl_{4/4}$ chains (along a-axis) are connected to melem units to create a layered structure. The interesting aspect is that melem is coordinated with manganese via inner nitrogen atoms (N1), and melam units are positioned between $MnCl_{4/4}$ layers. In $CoCl_2(C_6N_{11}H_9)$ and $FeCl_2(C_6N_{11}H_9)$, metal chloride is coordinated via N1 and N7 to a melam unit (Figure 23). $CoCl_2(C_6N_{11}H_9)$ crystals were obtained under similar conditions and exhibited a similar PXRD pattern to $FeCl_2(C_6N_{11}H_9)$, suggesting isotypic structures.

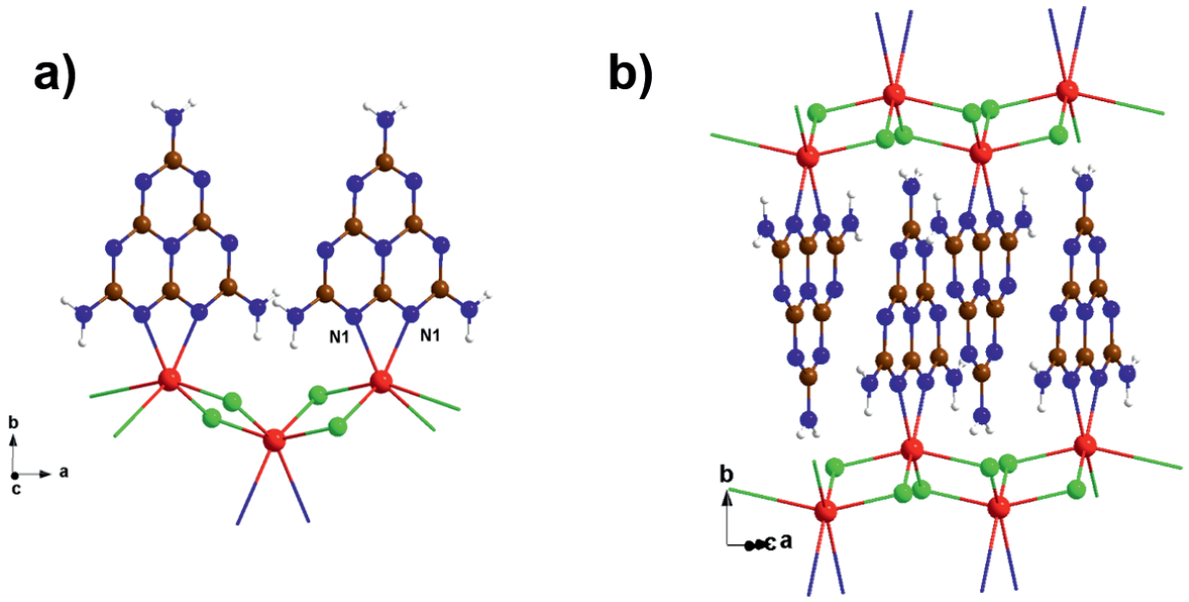

Figure 22. A perspective representation of the crystal structure of $MnCl_2(C_6N_{10}H_6)$ **a**) in the *ab*-plane and **b**) the stacking along the *b*-axis (N: blue, C: brown, H: white, Cl: green, and Mn: red).

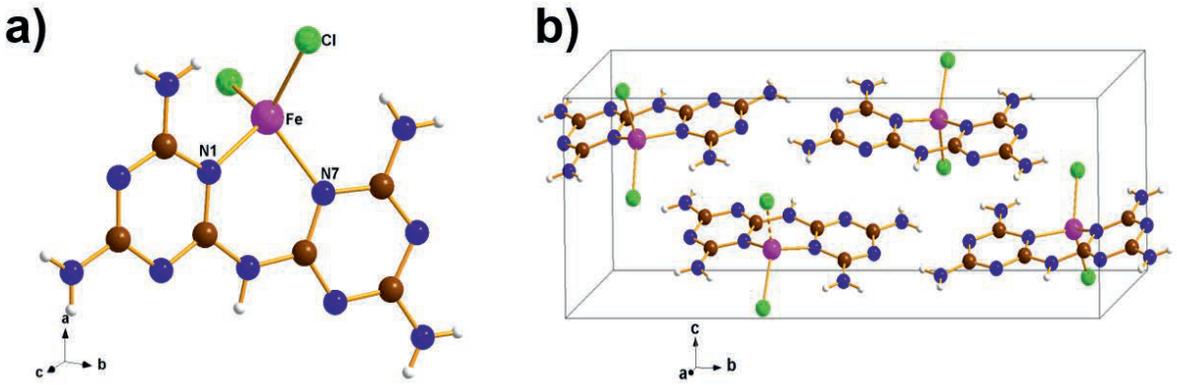

Figure 23. Section of the crystal structure of $FeCl_2(C_6N_{11}H_9)$ projected on **a)** *bc*-plane and **b)** the unit cell content of the structure. axis (N: blue, C: brown, H: white, Cl: green, and Fe: purple).

DSC, combined with XRD analysis, revealed that the exothermic peak at 370 ˚C results in the formation of the $MnCl_2(C_6N_{10}H_6)$ phase. Additionally, the two other endothermic and exothermic peaks at 300 ˚C and 306 ˚C, respectively, lead to two unidentified intermediate phases. The stability of $MnCl_2(C_6N_{10}H_6)$ was also studied by TGA and XRD analysis. The weight loss at 700 ˚C is related to the decomposition of

the $MnCl_2(C_6N_{10}H_6)$ to manganese carbodiimide ($Mn(CN_2)$), and at 900 ˚C, the manganese carbide Mn_7C_3 (ICSD 69534) is formed.

In the rest of the study, the primary focus is on the photoluminescence properties of $MnCl_2(C_6N_{10}H_6)$, as it is the first luminescent transition metal-melem compound. Generally, the PL of Mn^{2+} is attributed to 3d-3d transitions. However, the local coordination of the ion and overall crystal structure of the respective inorganic material also affects the PL behavior. The 3d-3d transition has spin and Laporte forbidden character, so the luminescent materials containing Mn^{2+} have a weak absorption line. Mn^{2+} luminophores are therefore sensitized by a coactivator,[113, 114] a band-to-band transition of a host,[115] or ligand-centered transitions[116].

Photoluminescence studies of $MnCl_2(C_6N_{10}H_6)$ show similar results as Mn(II) complexes. The broad emission band that appears at 620 nm is attributed to the spin-forbidden $^4T_{1g}(G) \rightarrow {}^6A_{1g}({}^6S)$ transition (Figure 24).[116-118]. The emitted color is orange to red, which is in agreement with the emission band. The strong excitation band at 325 nm originates from coordination ligand melam, which enhances Mn^{2+} luminescence. However, small excitation bands are also observed between 350-500 nm (Figure 24), which are associated with Mn^{2+}-centered transitions from the ground state term $^6A_{1g}$ to the excited state terms $4T_{1g}$, $4T_{2g}$, $4A_{1g}$, and ^4E_g.[119]

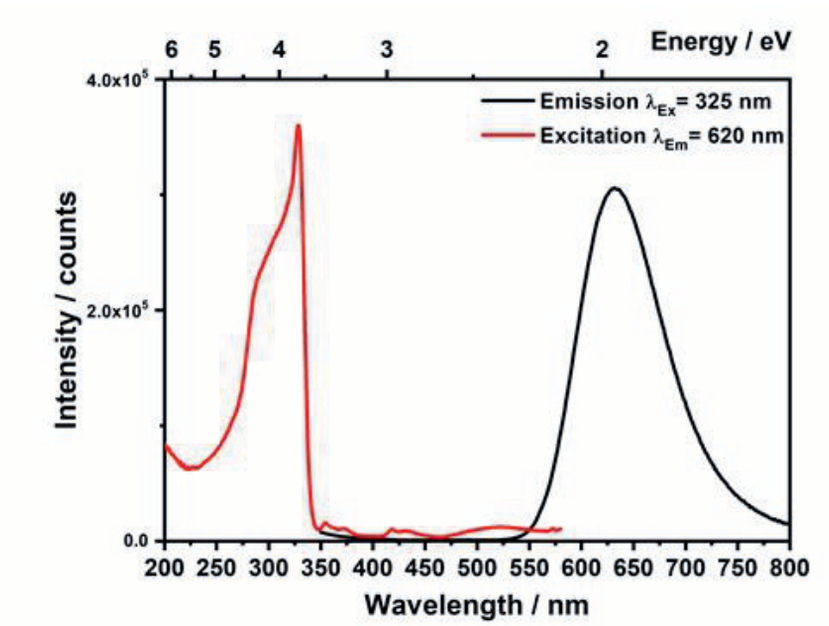

Figure 24. Photoluminescence spectra of $MnCl_2(C_6N_{10}H_6)$ in the solid-state at room temperature.

3.7 (Publ. 7)

In the previous synthesis of metal carbodiimides such as $Li_2(CN_2)$, melamine was used as a precursor and reacted with either a metal nitride (Li_3N)[106] or a metal hydride (LiH)[103]. This preparation route, combined with a new synthetic method for highly pure calcium carbodiimide[72] and the proposition of Seifer[16], inspired us to produce missing rare earth carbodiimide $La_2(CN_2)_3$ from its cyanurate salts. In the first step, cyanuric acid and sodium hydroxide were reacted with metal chloride to prepare the cyanurate salts, and subsequently, the decomposition of metal cyanurates led to the formation of metal carbodiimide. As mentioned in the introduction section, the pH value plays a crucial role in synthesizing different cyanurate salts since it influences the stabilization of various deprotonated forms of cyanuric acid. Two salts of lanthanum cyanurates, $La(HC_3N_3O_3)(H_2C_3N_3O_3)(H_2O)_3$ **(1),** eq (7), and $La(H_2C_3N_3O_3)_2(OH)(H_2O)_4{\cdot}H_2O$ **(2)** were obtained using the same amount of the precursors (69.5 mg cyanuric acid, 100 mg lanthanum(III) chloride, 32.2 mg sodium hydroxide) but different amounts of water (10 ml vs 40 ml). [120]

The thermal decomposition of **(1)** is investigated with TGA combined with DTA. As shown in Figure 25, the compound **(1)** undergoes three-step decomposition at 187 ˚C (–12.04% mass loss) eq (8), 450 ˚C (–28.38%) eq (9), and 737 ˚C (–14.82%) eq (10) corresponding to loss of water, decomposition to $La(C_3N_3O_3)$, formation of $La_2(CN_2)_3$ by the release of carbon dioxide, respectively.

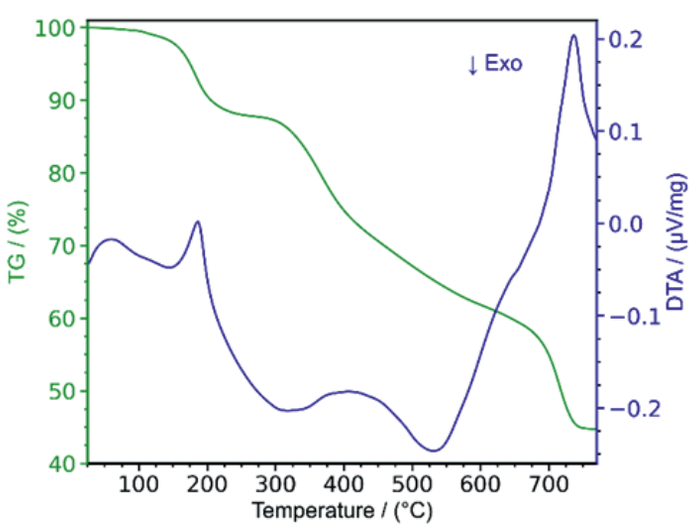

Figure 25. Thermogravimetric analysis (TGA) combined with differential thermal analysis (DTA) of $La(HC_3N_3O_3)(H_2C_3N_3O_3)(H_2O)_3$ **(1)**.

$LaCl_3 + 2\ (HOCN)_3 + 3\ NaOH \rightarrow La(H_2O_3C_3N_3)(HO_3C_3N_3)(H_2O)_3\downarrow + 3\ NaCl$ eq (7)

$2\ La(HC_3N_3O_3)(H_2C_3N_3O_3)(H_2O)_3 \rightarrow 2\ La(HC_3N_3O_3)(H_2C_3N_3O_3) + 6\ H_2O\uparrow$ eq (8)

$2\ La(HC_3N_3O_3)(H_2C_3N_3O_3) \rightarrow 2\ La(C_3N_3O_3) + 2\ H_3C_3N_3O_3\uparrow$ eq (9)

$2\ La(C_3N_3O_3) \rightarrow La_2(CN_2)_3 + 3\ CO_2\uparrow$ eq (10)

The crystal system of new lanthanum cyanurates **(1)** and **(2)** is monoclinic ($P2_1/c$) and triclinic ($P\ \bar{1}$), respectively. The crystal structure of **(1)** is shown in Figure 26. and depicts a lanthanum surrounded by five cyanurate ions (mono and divalent) and three coordinated water molecules. The other compound **(2)** consists of monovalent cyanurate anions, a bridging hydroxide, and four water molecules (Figure 26. b).

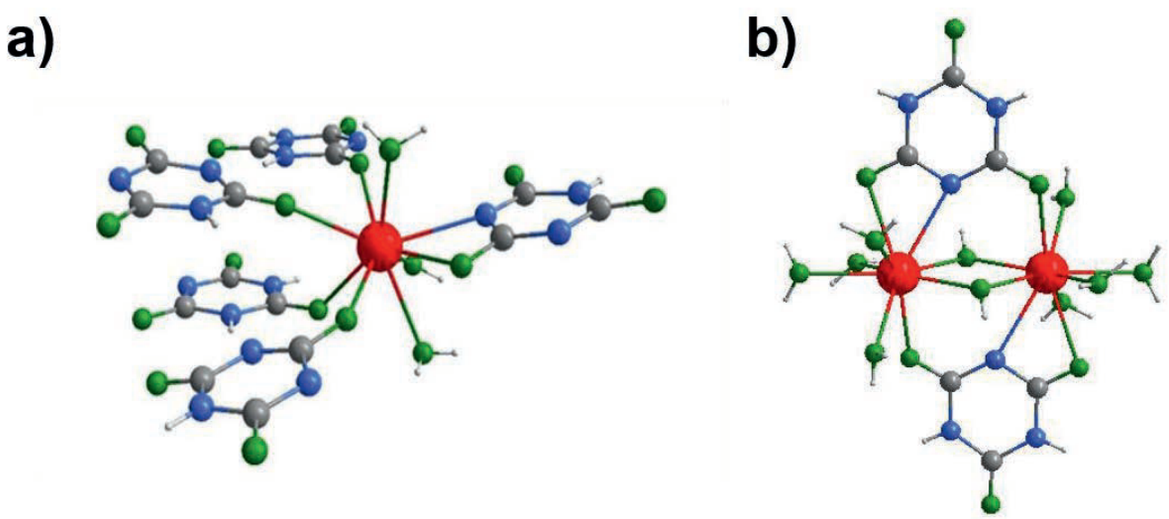

Figure 26. **a)** The coordination environment of the La^{3+} in the structure of **(1)** and **b) (2)** (gray: C, blue: N, green: O, red: La, white: H).

The crystal structure of $La_2(CN_2)_3$ was obtained from PXRD Rietveld refinement and is reported to crystallize in a monoclinic crystal system with *I*2/*a* space group. As shown in Figure 27, the crystal structure of $La_2(CN_2)_3$ is composed of two crystallographically different carbodiimide ions and one type of lanthanum with a coordination number of eight. The coordination environment of La^{3+} in $La_2(CN_2)_3$ is represented by a dodecahedron. The carbodiimide character of $La_2(CN_2)_3$ is also confirmed by asymmetric stretching vibrations (ν_{as}) at 2029 and 1929 cm^{-1}, and bending vibrations (δ) are observed at 685, 660, and 621 cm^{-1}.

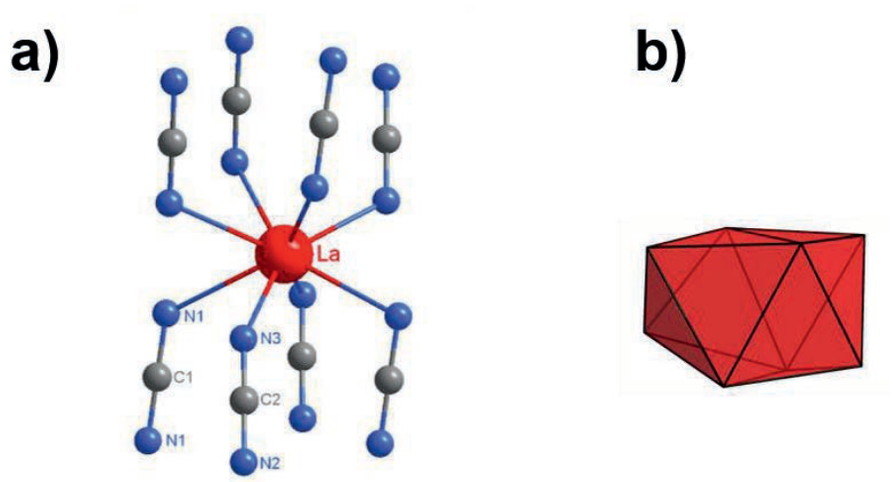

Figure 27. a) The environment of lanthanum with two crystallographically distinct $[N=C=N]^{2-}$ ions **b)** dodecahedron representing the coordination environment of La^{3+} in the structure of $La_2(CN_2)_3$.

Binary rare-earth carbodiimides exhibit three distinct types of structures. Those containing smaller rare-earth ions, such as RE = Sc[77], Yb, Tm, and Lu[79, 121], typically crystallize in the trigonal rhombohedral space group $R\bar{3}c$ ($Z = 6$), whereas compounds with RE = Y and Ce–Er (except Pm) adopt a monoclinic structure with space group of $C2/m$ ($Z = 2$). In the former, the coordination number (CN) is six[79], while in the latter, it is seven.[79, 121, 122] Here, $La_2(CN_2)_3$ exhibits a coordination number of eight and is considered the largest lanthanide when comparing the general trend of coordination patterns with the molar volumes (V/Z) of all rare-earth carbodiimides (Figure 28).

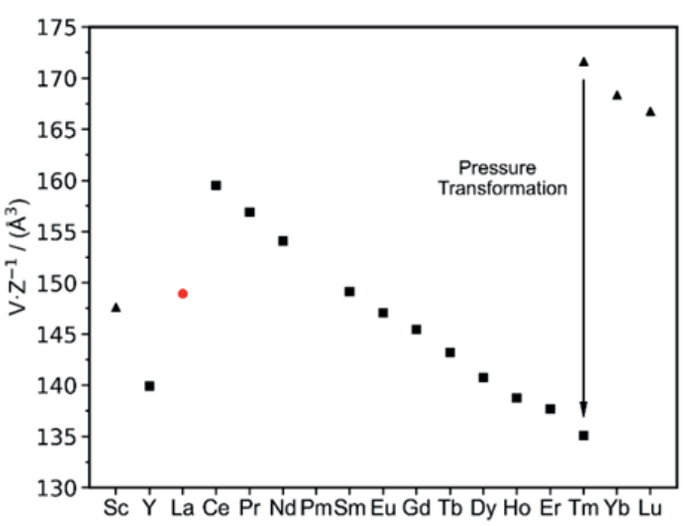

Figure 28. The molar volume (V/Z) of rare-earth carbodiimides, $La_2(CN_2)_3$, varies based on their crystal structures.

The study also investigates the photoluminescence (PL) spectrum of Ce^{3+} (5% w.r.t La) doped $La_2(CN_2)_3$ for its viability in luminescent screen applications. Ce^{3+} is a very good emitter with established uses in LED phosphors, scintillators, and UV lamps.[123-127]. Its luminescence is attributable to interconfigurational transitions, where the excitation transfers the electron from the $[Xe]4f^1$ to the $[Xe]5d^1$ state. Emission occurs on relaxation, leading to two broad bands from spin-orbit splitting ($^2F_{5/2}$ and $^2F_{7/2}$). The energy needed for this transition depends on the crystal field splitting of the 5d levels, which are under the influence of the surrounding anions and centroid shift.

As shown in Figure 29, the PL spectrum of $La_2(CN_2)_3:Ce^{3+}$ shows two broad emission maxima at 450 nm and 500 nm upon 400 nm excitation, with a low Stokes shift of 2800 cm^{-1}, indicating small relaxation. The band gap between $[Xe]4f^1$ and $[Xe]5d^1$ configuration is under the influence of crystal field strength or chemical environment such as ligand type, symmetry, and metal-to-ligand distance. Therefore, the change of location of Ce^{3+} in different crystallographic positions can change the PL spectra**.** $La_2(CN_2)_3:Ce^{3+}$ is blue-shifted with respect to $Gd_2(CN_2)_3:Ce^{3+}$ and $Y_2(CN_2)_3:Ce^{3+}$, which emited at ~575 nm, due to a weaker crystal field from longer metal-to-ligand distances.[80, 128] Low-temperature decay measurements show a single exponential decay curve with a 26 ns decay time at 77 K, demonstrating its promise as a blue-emitting luminescent material or scintillator.

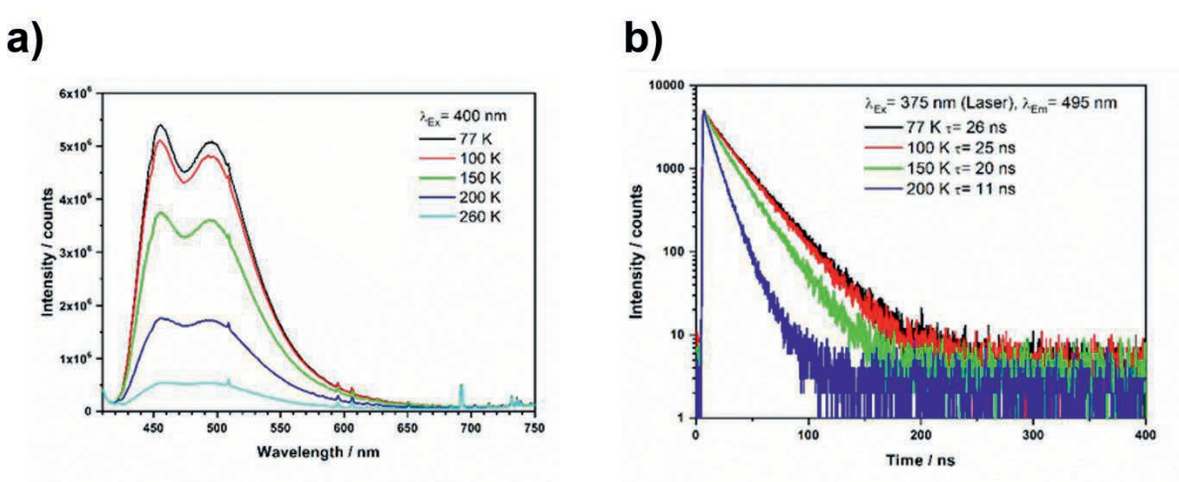

Figure 29. **a)** Emission spectra at several temperatures and **b)** decay curve upon 375 nm excitation of $La_2(CN_2)_3:Ce^{3+}$(5%).

4. Conclusion and outlook

This dissertation, titled "Exploring the Formation of Metal Melaminates by Deprotonating Melamine in Solid-State Reactions and Investigating Melamine and Cyanuric Acid as Potential Precursors for Carbodiimide Synthesis," presents new synthetic approaches for some metal melaminates and metal carbodiimides. The primary objective was to investigate whether melamine, as a widely available weak base, could be effectively deprotonated. Previous studies on the deprotonation of melamine[59] and even a stronger base such as guanidine[57] were done in pressure liquefied ammonia, and the formation of the strontium guanidinate inspired this investigation. Furthermore, the reaction of condensation products of melamine, such as melam and melem with metal chlorides, have also been studied.

The core of this research lies in three different ways introduced for deprotonation of melamine in solid-state route. First, the solid-state reaction between various metal chlorides (CuCl, $SbCl_3$, and $InCl_3$) and melamine is introduced. Deprotonation of melamine with metal chlorides acting as a lewis acids yielded several deprotonated compounds.[89, 92, 93] Second, metal hydrides such as KH reacted with melamine and hydrogen was released during the reaction. Potassium melaminate $K(C_3N_6H_5)$ and potassium cyanomelaminate $K_2(C_4N_7H_3)$ are two melaminates obtained in this route.[103] Third route is via cyclotrimerization of $(HCN_2)^-$ that enabled us to successfully reproduced the $Cu_3(C_3N_6H_3)$ compound from the reaction of $NaHCN_2$ and CuCl in solid-state.[98]

Deprotonated melamine can act as a ligand to form layered structures to metal organic frameworks or even supramolecular structures, all of which present interesting properties. For instance, $Cu_3(C_3N_6H_3)$ was shown to behave as a semiconductor and has potential applications in gas sensing.[92] Moreover, guest-induced luminescence observed in this compound indicates promising sensor applications.[98] The reaction of KH with melamine additionally suggests potential applications in hydrogen storage.[103] Furthermore, our group's investigation of mercury melaminates with second-harmonic generation (SHG) activity further points to potential applications of melaminates.[42, 43] The photoluminescence properties of indium melaminate and $MnCl_2(C_6N_{10}H_6)$[112] further confirm the optical potential of this class of compounds. However, the potential of melaminate acting as a ligand for compounds is highly promising and can introduce

further sets of properties depending on the type of metal centers involved in the structure.

In terms of carbodiimide synthesis, the decomposition of indium melaminates yielded $In_{2.24}(NCN)_3$, or the reaction of melamine with metal hydrides (KH, LiH, NaH) yielded metal carbodiimides such as $Li_2(CN_2)$, and $Na_2(CN_2)$, and two different modifications of $K_2(CN_2)$.[103] This way, we have improved the synthetic route for $Li_2(CN_2)$, which is a main precursor for preparation of other metal carbodiimides in SSM reactions. The previous route, which was the reaction of Li_3N with melamine, has a higher enthalpy of reaction and requires an excess amount of melamine and a more controlled condition. There are also various routes of synthesizing metal carbodiimides in solid-state or solution-based chemistry. However, some of the rare earth metal carbodiimides, such as $La_2(CN_2)_3$[120], were not obtained from previously suggested routes because the $LaCl(CN_2)$[129] was formed as a stable phase. Investigating the new synthetic route of decomposing metal cyanurates to carbodiimides yielded this undiscovered rare earth carbodiimide, $La_2(CN_2)_3$, with a new coordination number of eight. Furthermore, the successful doping of $La_2(CN_2)_3$ with Ce^{3+} for blue emission highlights a pathway for application as luminescent materials and scintillators.[120]

In conclusion, the solid-state chemistry of melamine and its derivatives of melam, melem, and cyanuric acid offers a broad and interesting range of new compounds that seem to be partly unexplored. Metal melaminates open a new chapter in melamine chemistry, enabling us to study the formation and functionalities of novel layered, porous, and supramolecular materials. Metal cyanurates also demonstrate significant potential, especially for SHG-active materials. Overall, melaminates and the condensation products of melamine and carbodiimide chemistry contribute to a broader understanding of s-triazines. Future work can further expand these findings toward the design of new functional materials and MOFs using melamine-based ligands, as well as by investigating the potential of underexplored metal carbodiimides.

5. References

1. A. R. R. Katritzky, Charles W. (Charles Wayne) *Comprehensive Heterocyclic Chemistry*, Oxford [Oxfordshire]; New York : Pergamon Press, 1984.
2. L. A. Paquette, *Principles of modern heterocyclic chemistry*, W . A. Benjamin New York, 1968.
3. J. A. Joule, Keith Mills, *Heterocyclic chemistry*, CRC Press, 5th edn., 2020.
4. T. L. Gilchrist, *Heterocyclic Chemistry*, Harlow, Essex, England: Longman, 3rd edn., 1997.
5. E. Kroke and M. Schwarz, *Coord. Chem. Rev.*, 2004, **248**, 493-532.
6. A. Schwarzer, T. Saplinova and E. Kroke, *Coord. Chem. Rev.*, 2013, **257**, 2032-2062.
7. P. Linus and J. H. Sturdivant, *PNAS USA*, 1937, **23**, 615-620.
8. F. K. Kessler, Y. Zheng, D. Schwarz, C. Merschjann, W. Schnick, X. Wang and M. J. Bojdys, *Nat. Rev. Mater.*, 2017, **2**, 1-17.
9. F. K. Kessler, Ph.D. Thesis, Ludwig Maximilian University of Munich, 2019.
10. B. Bann, Miller, S. A, *Chem. Rev.*, 1958, **58**, 131-172.
11. B. V. Lotsch, Doctoral dissertation, Ludwig Maximilian University of Munich, 2006.
12. G. M. Crews, W. Ripperger, D. B. Kersebohm, T. Güthner and B. Mertschenk, *Ullmann's Encycl. Ind. Chem.*, 2000.
13. A. Kawasaki and Y. Ogata, *Tetrahedron*, 1966, **22**, 1267-1274.
14. A. Cousson, B. Nicolai and F. Fillaux, *Acta Crystallogr. E.*, 2005, **61**, o222-o224.
15. E. Hughes, *J. Am. Chem. Soc.*, 1941, **63**, 1737-1752.
16. G. Seifer, *Russ. J. Coord. Chem.*, 2002, **28**, 301-324.
17. M. Dewar and L. Paoloni, *Trans. Faraday Soc.*, 1957, **53**, 261-271.
18. H. May, *J. Appl. Chem.*, 1959, **9**, 340-344.
19. B. V. Lotsch and W. Schnick, *Chem. Eur. J.*, 2007, **13**, 4956-4968.
20. P. Klason, *J. prakt. Chem*, 1886, **33**, 285-289.
21. J. Liebig, *Ann. Phys. Chem.*, 1835, **110**, 570-613.
22. E. Wirnhier, M. B. Mesch, J. Senker and W. Schnick, *Chem. Eur. J.*, 2013, **19**, 2041-2049.
23. A. Sattler, S. Pagano, M. Zeuner, A. Zurawski, D. Gunzelmann, J. Senker, K. Müller-Buschbaum and W. Schnick, *Chem. Eur. J.*, 2009, **15**, 13161-13170.
24. F. K. Kessler, A. M. Burow, G. Savasci, T. Rosenthal, P. Schultz, E. Wirnhier, O. Oeckler, C. Ochsenfeld and W. Schnick, *Chem. Eur. J.*, 2019, **25**, 8415-8424.
25. P. Klason, *J. prakt. Chem*, 1886, **33**, 116-132.
26. A. Sattler and W. Schnick, *Z. Anorg. Allg. Chem.*, 2006, **632**, 238-242.
27. B. Jürgens, E. Irran, J. Senker, P. Kroll, H. Müller and W. Schnick, *J. Am. Chem. Soc.*, 2003, **125**, 10288-10300.
28. V. W.-h. Lau, M. B. Mesch, V. Duppel, V. Blum, J. r. Senker and B. V. Lotsch, *J. Am. Chem. Soc.*, 2015, **137**, 1064-1072.
29. T. Komatsu, *Macromol. Chem. Phys.*, 2001, **202**, 19-25.
30. X. Wang, K. Maeda, A. Thomas, K. Takanabe, G. Xin, J. M. Carlsson, K. Domen and M. Antonietti, *Nat. Mater.*, 2009, **8**, 76-80.
31. Y. Wang, X. Wang and M. Antonietti, *Angew. Chem.*, 2012, **124**, 70-92.
32. L. Vella-Zarb, D. Braga, A. Guy Orpen and U. Baisch, *CrystEngComm*, 2014, **16**.
33. N. E. Mircescu, M. Oltean, V. Chiş and N. Leopold, *Vibr. Spectrosc.*, 2012, **62**, 165-171.
34. W. J. Jones and W. Orville-Thomas, *Trans. Faraday Soc.*, 1959, **55**, 203-210.
35. L. Zhang, J. Zhang, Z. J. Li, J. K. Cheng, P. X. Yin and Y. G. Yao, *Inorg. Chem.*, 2007, **46**, 5838-5840.

36. D. M. L. Goodgame, I. Hussain, A. J. P. White and D. J. Williams, *Dalton Trans.*, 1999, 2899-2900.
37. H. Zhu, Z. Yu, X. You, H. Hu and X. Huang, *J. Chem. Crystallogr.*, **1999**, **29**, 239-242.
38. K. Sivashankar, A. Ranganathan, V. Pedireddi and C. Rao, *J. Mol. Struct.*, 2001, **559**, 41-48.
39. A. Baraka, H. Hatem, M. S. El-Geundi, H. Tantawy, K. Karaghiosoff, M. Gobara, A. Elbeih, M. Shoaib, M. A. Elsayed and M. M. Kotb, *J. Solid State Chem.*, **2019**, **274**, 168-175.
40. P. Nockemann and G. Meyer, *Z. Anorg. Allg. Chem.*, 2004, **630**, 2571-2572.
41. Z. Bai, J. Lee, H. Kim, C. L. Hu and K. M. Ok, *Small*, 2023, **19**, 2301756.
42. M. Groß, P. Schmidt, C. P. Romao and H.-J. Meyer, unpublished work.
43. M. Groß, P. Schmidt, C. P. Romao, D. Enseling, T. Jüstelc, M. Brytskyi, S. Kroeker and H.-J. Meyer, unpublished work.
44. C. T. Seto and G. M. Whitesides, *J. Am. Chem. Soc.*, 1990, **112**, 6409-6411.
45. D. J. Merline, S. Vukusic and A. A. Abdala, *Polym. J.*, 2013, **45**, 413-419.
46. K. Bretterbauer and C. Schwarzinger, *Curr. Org. Synth..* 2012, **9**, 342-356.
47. Y. Wang, B. Wei and Q. Wang, *J. Cryst. Spectrosc. Res.*, 1990, **20**, 79-84.
48. B. Roy, P. Bairi and A. K. Nandi, *RSC Adv.*, 2014, **4**, 1708-1734.
49. H. Huang, K. Zhang, J. Jiang, J. Li and Y. Liu, *Polym. Int.*, 2017, **66**, 85-91.
50. P. Audebert, E. Kroke, C. Posern and S.-H. Lee, *Chem. Rev.*, 2021, **121**, 2515-2544.
51. A. Sattler, L. Seyfarth, J. Senker and W. Schnick, *Z. anorg. allg. Chem.*, 2005, **631**, 2545-2554.
52. A. Sattler and W. Schnick, *Z. Anorg. Allg. Chem.*, 2008, **634**, 457-460.
53. A. Sattler, Doctoral degree, Ludwig Maximilian University of Munich, 2010.
54. H. Meng, P. Meng, Z. Liu, J. McMurtrie and J. Xu, *Inorg. Chem.*, 2024, **63**, 6980-6987.
55. M. Ströbele, D. Enseling, T. Jüstel, M. Abbasi, S. Kroeker and H. J. Meyer, *Eur. J. Inorg. Chem.*, 2024, **27**, e202400434.
56. G. J. Perpétuo and J. Janczak, *Acta Crystallogr. C.*, 2006, **62**, o372-o375.
57. R. Missong, J. George, A. Houben, M. Hoelzel and R. Dronskowski, *Angew. Chem. Int. Ed.*, 2015, **54**, 12171-12175.
58. E. C. Franklin, *J. Am. Chem. Soc.*, 1922, **44**, 486-509.
59. A. L. Görne, T. Scholz, D. Kobertz and R. Dronskowski, *Inorg. Chem.*, 2021, **60**, 15069-15077.
60. R. Dorta, H. Stoeckli-Evans, U. Bodensieck and G. Süss-Fink, *J. Organomet. Chem.*, **1998**, **553**, 307-315.
61. K. Pareek, R. Rohan and H. Cheng, *RSC Adv.*, 2015, **5**, 10886-10891.
62. K. Huthmacher and D. Most, *Ullmann's Encycl. Ind. Chem.*, 2000.
63. J. A. Wojtowicz, *J. Swim. Pool Spa Ind.*, 2001, **4**, 9-16.
64. E. Wiebenga, *J. Am. Chem. Soc.*, 1952, **74**, 6156-6157.
65. W. M. Haynes, *CRC Handbook of Chemistry and Physic*, CRC press, CRC Press LLC, Boca Raton95th Edition, 95th edn., 2016.
66. P. Gross and H. A. Höppe, *Z. Anorg. Allg. Chem.*, 2017, **643**, 1692-1703.
67. P. Gross and H. A. Höppe, *Z. Anorg. Allg. Chem.*, 2019, **645**, 257-266.
68. X. Hao, M. Luo, C. Lin, D. Lin, L. Cao and N. Ye, *Dalton Trans.*, 2019, **48**, 12296-12302.
69. M. Kalmutzki, M. Stroebele, F. Wackenhut, A. J. Meixner and H. J. Meyer, *Angew. Chem. Int. Ed.*, 2014, **53**, 14260-14263.

70. M. Kalmutzki, M. Ströbele, F. Wackenhut, A. J. Meixner and H. J. Meyer, *Inorg. Chem.*, 2014, **53**, 12540-12545.
71. B. Jia, D. Sun, W. Zhao and F. Huang, *J. Energy Chem.*, 2021, **61**, 347-367.
72. M. Kastens and W. McBurney, *Ind. Eng. Chem.*, 1951, **43**, 1020-1033.
73. U. Berger and W. Schnick, *J. Alloys Compd.*, 1994, **206**, 179-184.
74. X. Liu, M. Krott, P. Müller, C. Hu, H. Lueken and R. Dronskowski, *Inorg. Chem.*, 2005, **44**, 3001-3003.
75. X. Tang, H. Xiang, X. Liu, M. Speldrich and R. Dronskowski, *Angew. Chem. Int. Ed*, 2010, **49**, 4738-4742.
76. K. Dolabdjian, A. Kobald, C. P. Romao and H.-J. Meyer, *Dalton Trans.*, 2018, **47**, 10249-10255.
77. P. Kallenbach, M. Ströbele and H. J. Meyer, *Z. Anorg. Allg. Chem.*, 2020, **646**, 1281-1284.
78. M. Löber, K. Dolabdjian, M. Ströbele, C. P. Romao and H.-J. r. Meyer, *Inorg. Chem.*, 2019, **58**, 7845-7851.
79. M. Neukirch, S. Tragl and H.-J. Meyer, *Inorg. Chem.*, 2006, **45**, 8188-8193.
80. J. Glaser, L. Unverfehrt, H. Bettentrup, G. Heymann, H. Huppertz, T. Jüstel and H.-J. r. Meyer, *Inorg. Chem.*, 2008, **47**, 10455-10460.
81. M. Becker and M. Jansen, *Acta Crystallogr. C.*, 2001, **57**, 347-348.
82. M. Krott, X. Liu, B. P. Fokwa, M. Speldrich, H. Lueken and R. Dronskowski, *Inorg. Chem.*, 2007, **46**, 2204-2207.
83. X. Liu, M. A. Wankeu, H. Lueken and R. Dronskowski, *Z. Naturforsch. B.*, 2005, **60**, 593-596.
84. G. Baldinozzi, B. Malinowska, M. Rakib and G. Durand, *J. Mater. Chem.*, 2002, **12**, 268-272.
85. M. Becker, J. Nuss and M. Jansen, *Z. Naturforsch. B.*, 2000, **55**, 383-385.
86. X. Liu, A. Decker, D. Schmitz and R. Dronskowski, *Z. Anorg. Allg. Chem.*, 2000, **626**, 103-105.
87. L. Stork, X. Liu, B. P. Fokwa and R. Dronskowski, *Z. Anorg. Allg. Chem.*, 2007, **633**, 1339-1342.
88. R. Dronskowski, *Z. Naturforsch. B.*, 1995, **50**, 1245-1251.
89. E. Bayat, M. Ströbele, D. Enseling, T. Jüstel and H. J. Meyer, *Dalton Trans.*, 2024.
90. A. Klimek, J. Yount, D. Wozniak, M. Zeller and D. G. Piercey, *Inorg. Chem.*, 2023, **62**, 16280-16282.
91. P. Kallenbach, Master dissertation, Eberhard Karls Universität Tübingen, 2021.
92. P. Kallenbach, E. Bayat, M. Ströbele, C. P. Romao and H.-J. Meyer, *Inorg. Chem.*, 2021, **60**, 16303-16307.
93. E. Bayat, M. Ströbele and H.-J. Meyer, *Chemistry*, 2023, **5**, 1465-1476.
94. M. Kalmutzki, M. Ströbele, D. Enseling, T. Jüstel and H.-J. Meyer, *Eur. J. Inorg. Chem.*, 2015, **2015**, 134-140.
95. M. Kalmutzki, M. Ströbele, H. F. Bettinger and H.-J. Meyer, *Eur. J. Inorg. Chem..* 2014, **2014**, 2536-2543.
96. M. Kalmutzki, M. Ströbele and H.-J. Meyer, *Dalton Trans.*, 2013, **42**, 12934-12939.
97. N. S. Harisomayajula, S. Makovetskyi and Y. C. Tsai, *Chem. Eur. J.*, 2019, **25**, 8936-8954.
98. E. Bayat, M. Ströbele, M. Abbasi, S. Kroeker, J. Valenta, D. Enseling, T. Jüstel and H.-J. Meyer, *Inorg. Chem.*, 2024, **63**, 19053-19062.
99. M. D. Allendorf, C. A. Bauer, R. Bhakta and R. Houk, *Chem. Soc. Rev.*, 2009, **38**, 1330-1352.

100. Z. Hu, B. J. Deibert and J. Li, *Chem. Soc. Rev.*, 2014, **43**, 5815-5840.
101. S. Mugiraneza and A. M. Hallas, *Commun. Phys.*, 2022, **5**, 95.
102. R. Dronskowski, *Z. Naturforsch. B.*, 1995, **50**, 1245-1251.
103. M. Ströbele, E. Bayat and H.-J. Meyer, *Inorg. Chem.*, 2024, DOI: 10.1021/acs.inorgchem.4c02996.
104. M. Ströbele and H.-J. Meyer, *Dalton Trans.*, 2019, **48**, 1547-1561.
105. M. Becker and M. Jansen, *Solid State Sci.*, 2000, **2**, 711-715.
106. M. Becker, M. Jansen, A. Lieb, W. Milius and W. Schnick, *Z. Anorg. Allg. Chem.*, 1998, **624**, 113-118.
107. R. Niewa, P. Höhn, R. Kniep, A. Weiske and H. Jacobs, *Z. Kristallogr. New Cryst.* , 2001, **216**, 357-358.
108. W. Schnick and H. Huppertz, *Z. Anorg. Allg. Chem.*, 1995, **621**, 1703-1707.
109. H. W. Langmi, G. S. McGrady, R. Newhouse and E. Rönnebro, *Int. J. Hydrogen Energy.*, 2012, **37**, 6694-6699.
110. J. P. Singer, M. S. Meyer, R. M. Speer Jr, J. E. Fischer and F. E. Pinkerton, *J. Phys. Chem. C.*, 2009, **113**, 18927-18934.
111. G. P. Meisner, M. L. Scullin, M. P. Balogh, F. E. Pinkerton and M. S. Meyer, *J. Phys. Chem. B.*, 2006, **110**, 4186-4192.
112. E. Bayat, M. Ströbele, D. Enseling, T. Jüstel and H.-J. Meyer, *Molecules*, 2024, **29**, 5598.
113. B. C. G. G. Blasse *Luminescent Materials*, Springer: Berlin, Heidelberg, Germany, New York, U.S.A.,, 1994.
114. V. Singh, G. Sivaramaiah, J. Rao, N. Singh, A. K. Srivastava, H. Jirimali, J. Li, H. Gao, R. S. Kumaran and P. K. Singh, *J. Electron. Mater.*, 2016, **45**, 2776-2783.
115. A. A. Bol and A. Meijerink, *J. Phys. Chem. B*, 2001, **105**, 10197-10202.
116. Z. Yan, N. Li, L. Wang, Z. Yu, M. Li, J. Zhang, X. Li, K. Yang, G. Gao and L. Wang, *J. Phys. Chem. C*, 2020, **124**, 23317-23323.
117. C. Duan, A. Delsing and H. Hintzen, *Chem. Mat.*, 2009, **21**, 1010-1016.
118. M. Bortoluzzi, V. Ferraro and J. Castro, *Dalton Trans.*, 2021, **50**, 3132-3136.
119. B. C. G. G. Blasse, *Luminescent Materials, 1st ed*, Springer, New York, United States, 1994.
120. P. Schneiderhan, E. Bayat, M. Ströbele, D. Enseling, T. Jüstel and H. J. Meyer, *Dalton Trans.*, 2025.
121. O. Reckeweg, T. Schleid and F. J. DiSalvo, *Z. Naturforsch. B.*, 2007, **62**, 658-662.
122. D. Dutczak, M. Ströbele, D. Enseling, T. Jüstel and H. J. Meyer, *Eur. J. Inorg. Chem.*, 2016, **2016**, 4011-4016.
123. A. Žukauskas, M. Shur and R. Gaska, *Introduction to solid-state lighting*, John Wiley & Sons, 2002.
124. P. Dorenbos, *J. Lumin.*, 2002, **99**, 283-299.
125. Z. Xia and A. Meijerink, *Chem. Soc. Rev.*, 2017, **46**, 275-299.
126. A. C. Berends, M. A. van de Haar and M. R. Krames, *Chem. Rev.*, 2020, **120**, 13461-13479.
127. S. Wang, Z. Song and Q. Liu, *J. Mater. Chem. C.*, 2023, **11**, 48-96.
128. Y.-C. Wu, T.-M. Chen, C.-H. Chiu and C.-N. Mo, *J. Electrochem. Soc.*, 2010, **157**, J342.
129. R. Srinivasan, J. Glaser, S. Tragl and H. J. Meyer, *Z. Anorg. Allg. Chem.*, 2005, **631**, 479-483.

5. Publications

Publication 1

Tricopper Melaminate, a Metal–Organic Framework Containing Dehydrogenated Melamine and Cu–Cu Bonding

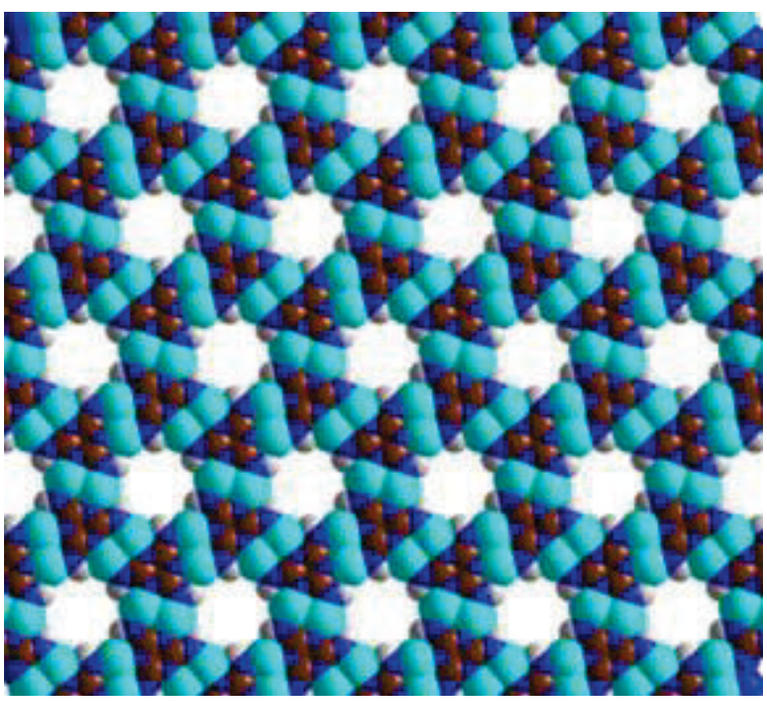

https://doi.org/10.1021/acs.inorgchem.1c02748

Reprinted with permission from

Inorg. Chem. 2021, 60, 21, 16303–16307

Inorganic Chemistry

pubs.acs.org/IC Article

Tricopper Melaminate, a Metal−Organic Framework Containing Dehydrogenated Melamine and Cu−Cu Bonding

Paula Kallenbach, Elaheh Bayat, Markus Ströbele, Carl P. Romao, and Hans-Jürgen Meyer*

Cite This: *Inorg. Chem.* 2021, 60, 16303−16307 Read Online

ACCESS | Metrics & More | Article Recommendations | Supporting Information

ABSTRACT: Crystals of $Cu_3(C_3N_6H_3)$ are formed by a solid-state reaction of CuCl with melamine to form a layered framework structure with open pores running along the hexagonal axis direction of the *P6/mcc* structure. The compound contains the hitherto unknown $(C_3N_6H_3)^{3-}$ ion, assigned as melaminate. Bonding interactions within and between Cu−Cu dumbbells, which connect melaminate ions into layers, are analyzed by density functional theory calculations of the electron localization function and directional Young's modulus. Band structure calculations reveal the material to be a semiconductor with a band gap on the order of 2 eV.

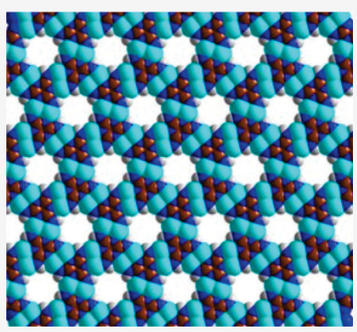

INTRODUCTION

The discovery of melamine ($C_3N_6H_6$, or 1,3,5-triazine-2,4,6-triamine) dates back to the work of Liebig in 1834.[1] Since then, a remarkable number of derivative compounds, including supramolecular assemblies, flame-retardant materials, and melamine formaldehyde resins, have emerged, even as materials used in our daily life.[2−26] Thermal treatment of melamine leads to condensation reactions, forming melam ($C_6N_{10}H_6$) and melem ($C_6N_{11}H_9$) with increasing temperature, with release of ammonia.[27,28] The course of the thermal conversation reactions of melamine has been shown to depend on a subtle interplay of reaction conditions with respect to temperature, pressure, and the specific reaction rate.[28,29]

Thermally induced reactions of melamine involve the formation of compounds which include sizable assemblies of 1,3,5-triazine moieties; the involvement of other reactants into such a reaction can have a significant effect on the reaction pathway. For example, the presence of NH_4Cl leads to the formation of melaminium chloride with a protonated melamine ion in $(C_3N_6H_7)Cl$.[30]

Our exploration of the reactions of melamine with metal halides has established the existence of the melaminate anion, $(C_3N_3(NH)_3)^{3-}$. As a first example we present herein the novel compound $Cu_3(C_3N_3(NH)_3)$ whose composition and structure are related to the recently discovered family of metal cyanurates,[31−33] which have been established by means of solid-state metathesis reactions. Cyanurates such as $Ca_3(C_3N_3O_3)_2$ (CCY) show remarkable SHG (second-harmonic-generation) properties,[34−36] and their discovery has triggered significant research efforts in the field.

RESULTS AND DISCUSSION

$Cu_3(C_3N_6H_3)$ was synthesized by a solid-state reaction of CuCl with melamine under flowing argon at 275 °C. $Cu_3(C_3N_6H_3)$ forms hexagonal brownish, rod-shaped crystals and powder along with melaminium chloride as a white sublimate (eq 1):

$$3CuCl + 4C_3N_6H_6 \rightleftharpoons Cu_3(C_3N_6H_3) + 3(C_3N_6H_7)Cl \quad (1)$$

A recorded powder X-ray diffraction pattern (XRD) evidenced the new compound in estimated 80% yield based on copper. The crystal structure of $Cu_3(C_3N_6H_3)$ was refined by single-crystal XRD, revealing the centrosymmetric space group *P6/mcc* (a = 1205.42(5) pm, c = 616.00(3) pm). Only one copper, one carbon, and two NH groups are contained in the asymmetric unit of the crystal structure. The crystal structure includes two interesting features: the novel melaminate ion and the presence of Cu−Cu bonding.

$Cu_3(C_3N_3(NH)_3)$ with the melaminate ion $(C_3N_3(NH)_3)^{3-}$ can be simply derived from melamine (Figure 1) by substitution of three hydrogens by copper atoms (Figure 2, left). The melaminate ion and the cyanurate ion can be seen as analogues with respect to their structures and total charge.

Received: July 15, 2021
Published: October 19, 2021

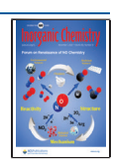

https://doi.org/10.1021/acs.inorgchem.1c02145
Inorg. Chem. 2021, 60, 16303−16307

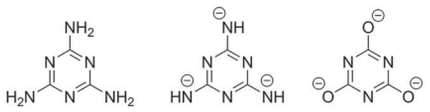

Figure 1. Structural formula of melamine ($C_3N_3(NH_2)_3$, left) compared to the $(C_3N_3(NH)_3)^{3-}$ ion (center) in $Cu_3(C_3N_3(NH)_3)$, and the cyanurate ion $(C_3N_3O_3)^{3-}$ adapted from the structure of $Ca_3(C_3N_3O_3)_2$ (right).

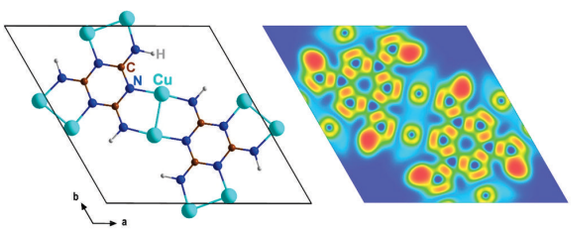

Figure 2. A layer section of the structure of $Cu_3(C_3N_3(NH)_3)$, showing Cu_2 dumbbells, connecting melaminate ions into layers (left) and the calculated ELF shown on a color scale ranging from 1 (red) to 0 (blue) (right).

Copper atoms in the structure form Cu−Cu dumbbells with short Cu−Cu distances (248.7(1) pm), which are emphasized in Figure 2 (left). Each pair of copper atoms connects two melaminate ions into planar layers. The Cu_2 dumbbells can be envisioned to be further connected with other Cu_2 pairs along the stacking direction (*c*) to generate the motif of a twisted-ladder structure, as shown in Figure 3 (left). Distances between copper atoms of adjacent Cu_2 dumbbells (d_{Cu-Cu} = 319.7(2) pm) are slightly longer than the separation between layers in the structure (308.0(2) pm). Cu−Cu separations shorter than the sum of the van der Waals radii (approximately 392 pm) have been previously considered as cuprophilic $d^{10}-d^{10}$ interactions.[37−43] The bonding characteristics between copper atoms were analyzed using the electron localization function (ELF), as shown in Figures 2 and 3 (right) and described below.

The overall crystal structure of $Cu_3(C_3N_3(NH)_3)$ is composed of melaminate rings arranged in layers with hexagonal symmetry, interconnected by Cu_2 dumbbells, as shown in Figure 4. All atoms are situated in mirror planes (m_z) of the structure. Layers are stacked in an AB type hexagonal

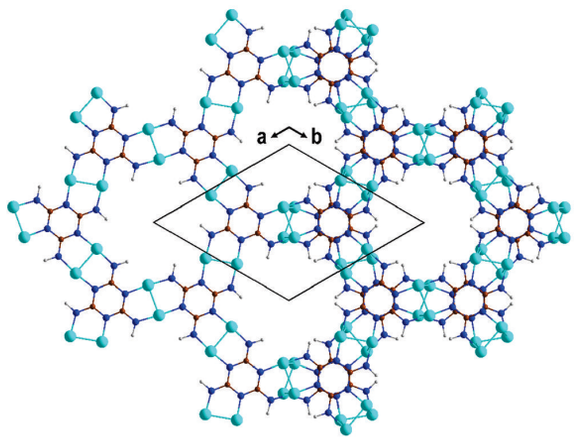

Figure 4. Crystal structure projection of $Cu_3(C_3N_3(NH)_3)$ on the hexagonal *ab* plane, emphasizing the stacking behavior, with two layers on the right side and one layer on the left side of the drawing. Pores run along the stacking (*c*) direction.

fashion in which the triazine rings of melaminate are stacked on top of each other with a slight twist relative to each other. This structural pattern is displayed with a single-layer and a double-layer arrangement in Figure 4. A similar type of stacking behavior of twisted melaminate rings has been a characteristic feature in the structures of metal cyanurates $M_3(C_3N_3O_3)$ (M = Ca, Sr, Ba, Eu).[31,33,44] The stacking of melaminate rings with N positions located above and below C positions (and vice versa) could be influenced by weak electrostatic interactions between layers, as is seen in h-BN, for example.[45]

The arrangement of six melaminate ions around a 6-fold rotation axis generates pores in the structure of $Cu_3(C_3N_6H_3)$ running parallel to the *c* axis. These pores are framed by six hydrogen atoms (per layer) of melaminate ions with H to H diameters of 732.5(7) pm. Therefore, the structure can be considered to be a nanoporous metal−organic framework (MOF).

The electronic and structural properties of $Cu_3(C_3N_6H_3)$ were investigated using density functional theory (DFT) using the Abinit software package (example input files are available as part of the Supporting Information).[46−50] A plane-wave basis set, the Perdew−Burke−Ernzerhof exchange−correlation

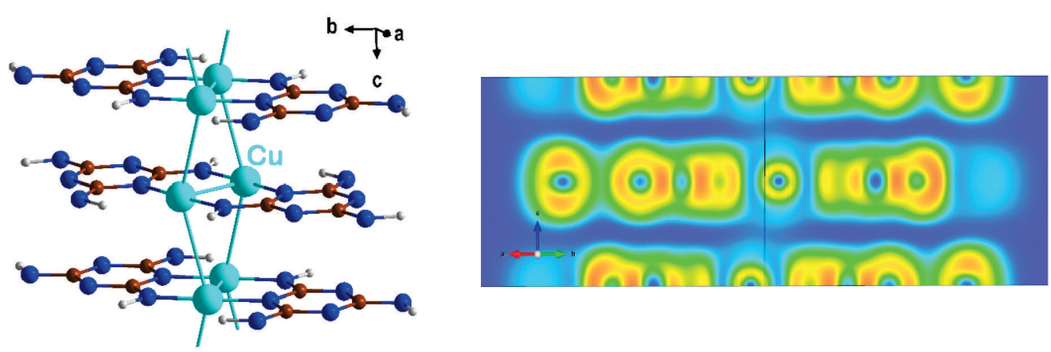

Figure 3. Section of the structure of $Cu_3(C_3N_3(NH)_3)$, showing Cu_2 dumbbells combined into a twisted ladder structure (left) and the calculated ELF in a plane including the Cu and C atoms of the top and bottom layers.

https://doi.org/10.1021/acs.inorgchem.1c02145
Inorg. Chem. 2021, 60, 16303−16307

functional, and the vdw-DFT-D2 dispersion correction were used. Structural relaxation was performed prior to the calculation of properties. The calculated electron localization function (ELF) of $Cu_3(C_3N_6H_3)$, shown in Figures 2 and 3, beautifully demonstrates the various types of chemical bonds present in this material. Within the melaminate rings, covalent bonding between C and N atoms can be seen by the presence of local maxima in the ELF at the midpoint of the bonds. The very high values of the ELF around the H atoms (~1) follow the expected behavior for organic materials.[51] The presence of a nodal plane in the ELF between Cu and N demonstrates that the Cu−N bonds are ionic, with a local maximum of the ELF from N to Cu indicating a polarization of the N electron density toward Cu. The ELF around the Cu atoms shows some polarization toward each other, with the electrons lying between the Cu atoms being highly delocalized, indicating a metallic Cu−Cu interaction (i.e., a sharing of electrons without clearly defined orbital hybridization as is seen in covalent bonds). Figure 3 shows the interlayer interactions in terms of the ELF. There is no sign of any electronic interactions between the triazine rings, indicating that their stacking is driven primarily by van der Waals forces. Between the Cu atoms, there is some evidence of delocalized electrons, potentially indicating weak interlayer Cu−Cu metallic bonding.

The strength and directionality of the interlayer interactions was studied further by calculation of the elastic tensor (Figure 5).

$$c = \begin{pmatrix} 136 & 74.6 & 1.12 & 0 & 0 & 0 \\ 74.6 & 136 & 1.12 & 0 & 0 & 0 \\ 1.12 & 1.12 & 34.8 & 0 & 0 & 0 \\ 0 & 0 & 0 & 0.69 & 0 & 0 \\ 0 & 0 & 0 & 0 & 0.69 & 0 \\ 0 & 0 & 0 & 0 & 0 & 30.7 \end{pmatrix} \times \text{GPa}.$$

Figure 5. Elastic tensor of $Cu_3(C_3N_6H_3)$ in Voigt notation.

The elastic anisotropy is visualized in Figure 6 in terms of the directional Young's modulus (Y). In the ab plane, Y has a value of 95 GPa, indicating that the layers form a strongly bonded framework. Along c, Y has a value of 35 GPa, which falls off steeply with any deviation away from the c axis. This elastic behavior evidences directional bonding along c;[52] dispersive and/or ionic interactions between layers are insufficient to produce such a spike in stiffness.[53,54] Therefore, we can conclude that Cu−Cu bonding is present along c, making $Cu_3(C_3N_6H_3)$ a three-dimensional framework material.

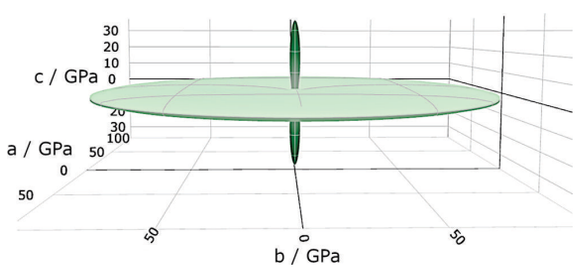

Figure 6. Perspective projection of the calculated directional Young's modulus of $Cu_3(C_3N_6H_3)$ with a view approximately along the a axis (c vertically).

Interestingly, the Poisson ratio is also nearly zero for uniaxial stresses along c.

The calculated electronic band structure of $Cu_3(C_3N_6H_3)$ is shown in Figure 7. The material is predicted to be a semiconductor with a band gap on the order of 2 eV, slightly smaller than the experimental value of 2.7 eV obtained from optical reflection measurement (Figure S1). The bands near the Fermi level have a mixture of Cu d and N p character, indicating some hybridization between those orbitals.

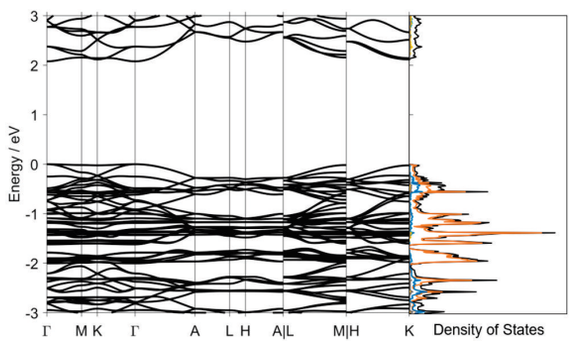

Figure 7. Electronic band structure of $Cu_3(C_3N_6H_3)$, with the electronic density of states shown at right (Cu, orange; N, blue; C, yellow; H, gray; total, black). Special points in and paths through the Brillouin zone were chosen following ref 55.

CONCLUSION

The new $Cu_3(C_3N_3(NH)_3)$ (tricopper-1,3,5-triazine-2,4,6-triimide) is formed by the solid-state reaction of a metal halide with melamine at moderate temperature; it represents the first compound with a melaminate ion. The synthesis of $Cu_3(C_3N_3(NH)_3)$ from CuCl and melamine is based on HCl elimination with formation of melaminium chloride as a sublimate.

$Cu_3(C_3N_3(NH)_3)$ crystallizes with a layered framework structure including metallically bonded Cu_2 dumbbells. According to our studies, more compounds with melaminate anions can be expected to be developed.

The full potential of $Cu_3(C_3N_3(NH)_3)$ and related compounds has yet to be determined. The close structural relationship of $Cu_3(C_3N_3(NH)_3)$ to the metal cyanurates (CCY, SCY) suggests the potential for SHG applications once a noncentrosymmetric structure is found. $Cu_3(C_3N_3(NH)_3)$ is a metal−organic framework with small one-dimensional channels, and therefore, incorporation of small molecules into channels of the structure may be considered, as can employment as a sensor material. Electronic structure calculations and experimental studies suggest $Cu_3(C_3N_3(NH)_3)$ to be a semiconductor with a band gap on the order of 2−3 eV.

ASSOCIATED CONTENT

Supporting Information

The Supporting Information is available free of charge at https://pubs.acs.org/doi/10.1021/acs.inorgchem.1c02145.

Input files for the Abinit software (ZIP)

Crystal data and structure refinement for $Cu_3(C_3N_6H_3)$, atomic coordinates and equivalent isotropic displacement parameters (pm^2) for $Cu_3(C_3N_6H_3)$, Tauc plot of

https://doi.org/10.1021/acs.inorgchem.1c02145
Inorg. Chem. 2021, 60, 16303−16307

a UV−vis reflectance measurement of $Cu_3(C_3N_6H_3)$, and PXRD pattern of $Cu_3(C_3N_6H_3)$ (PDF)

Accession Codes

CCDC 2063421 contains the supplementary crystallographic data for this paper. These data can be obtained free of charge via www.ccdc.cam.ac.uk/data_request/cif, or by emailing data_request@ccdc.cam.ac.uk, or by contacting The Cambridge Crystallographic Data Centre, 12 Union Road, Cambridge CB2 1EZ, UK; fax: +44 1223 336033.

AUTHOR INFORMATION

Corresponding Author

Hans-Jürgen Meyer − *Section for Solid State and Theoretical Inorganic Chemistry Institute of Inorganic Chemistry, Eberhard Karls Universität Tübingen, 72076 Tübingen, Germany;* orcid.org/0000-0003-2450-4011; Email: juergen.meyer@uni-tuebingen.de

Authors

Paula Kallenbach − *Section for Solid State and Theoretical Inorganic Chemistry Institute of Inorganic Chemistry, Eberhard Karls Universität Tübingen, 72076 Tübingen, Germany*

Elaheh Bayat − *Section for Solid State and Theoretical Inorganic Chemistry Institute of Inorganic Chemistry, Eberhard Karls Universität Tübingen, 72076 Tübingen, Germany*

Markus Ströbele − *Section for Solid State and Theoretical Inorganic Chemistry Institute of Inorganic Chemistry, Eberhard Karls Universität Tübingen, 72076 Tübingen, Germany;* orcid.org/0000-0002-5147-5677

Carl P. Romao − *Section for Solid State and Theoretical Inorganic Chemistry Institute of Inorganic Chemistry, Eberhard Karls Universität Tübingen, 72076 Tübingen, Germany;* orcid.org/0000-0002-5519-2519

Complete contact information is available at: https://pubs.acs.org/10.1021/acs.inorgchem.1c02145

Notes

The authors declare no competing financial interest.

ACKNOWLEDGMENTS

Support by the state of Baden-Württemberg through bwHPC and the German Research Foundation (DFG) through grant no. INST 40/575-1 FUGG (JUSTUS 2 cluster) is gratefully acknowledged. We thank Benjamin Junker and Peter Janoschek (both Univ. Tübingen) for performing the reflectance measurement.

REFERENCES

(1) Liebig, J. Über einige Stickstoff - Verbindungen. *Ann. Pharm.* **1834**, *10*, 1−47.

(2) Binder, W. H.; Dunky, M.; Jahromi, S. *Kirk-Othmer Encyclopedia of Chemical Technology*; Wiley: 2005. .

(3) Binder, W. H.; Dunky, M. *Encyclopedia of Polymer Science and Technology*; Wiley: 2004. .

(4) Weil, E. D.; Levchik, S. V. Flame retardants in commercial use or development for textiles. *J. Fire Sci.* **2008**, *26*, 243−281.

(5) Tan, Y. L.; Sun, L.; Shao, S. C.; Fu, J. P.; Peng, Z. H. Synthesis and characterization of melamine halogen acid salts and its application as flame retardant. *Adv. Mater. Res.* **2013**, *750*, 1087−1090.

(6) Zhang, L.; Zhang, J.; Li, Z.-J.; Cheng, J.-K.; Yin, P.-X.; Yao, Y.-G. New Coordination Motifs of Melamine Directed by N−H···X (X = Cl or Br) Hydrogen Bonds. *Inorg. Chem.* **2007**, *46*, 5838−5840.

(7) Zerkowski, J. A.; Seto, C. T.; Whitesides, G. M. Solid-state structures of rosette and crinkled tape motifs derived from the cyanuric acid melamine lattice. *J. Am. Chem. Soc.* **1992**, *114*, 5473−5475.

(8) Zerkowski, J. A.; Seto, C. T.; Wierda, D. A.; Whitesides, G. M. The design of organic structures in the solid state: hydrogen-bonded molecular "tapes". *J. Am. Chem. Soc.* **1990**, *112*, 9025−9026.

(9) Zerkowski, J. A.; MacDonald, J. C.; Seto, C. T.; Wierda, D. A.; Whitesides, G. M. Design of Organic Structures in the Solid State: Molecular Tapes Based on the Network of Hydrogen Bonds Present in the Cyanuric Acid•Melamine Complex. *J. Am. Chem. Soc.* **1994**, *116*, 2382−2391.

(10) Zerkowski, J. A.; Whitesides, G. M. Steric Control of secondary, solid-state architecture in 1:1 complexes of melamines and barbiturates that crystallize as crinkled tapes. *J. Am. Chem. Soc.* **1994**, *116*, 4298−4304.

(11) Mathias, J. P.; Simanek, E. E.; Zerkowski, J. A.; Seto, C. T.; Whitesides, G. M. Structural Preferences of Hydrogen-Bonded Networks in Organic Solution - the Cyclic $CA_3•M_3$ "Rosette". *J. Am. Chem. Soc.* **1994**, *116*, 4316−4325.

(12) Whitesides, G. M.; Simanek, E. E.; Mathias, J. P.; Seto, C. T.; Chin, D.; Mammen, M.; Gordon, D. M. Noncovalent Synthesis: Using Physical-Organic Chemistry To Make Aggregates. *Acc. Chem. Res.* **1995**, *28*, 37−44.

(13) Sivashankar, K.; Ranganathan, A.; Pedireddi, V. R.; Rao, C. N. R. Novel supramolecular organizations in melamine complexes with 4,4′-bipyridyl and silver nitrate. *J. Mol. Struct.* **2001**, *559*, 41−48.

(14) Ranganathan, A.; Pedireddi, V. R.; Rao, C. N. R. Hydrothermal Synthesis of Organic Channel Structures: 1:1 Hydrogen-Bonded Adducts of Melamine with Cyanuric and Trithiocyanuric Acids. *J. Am. Chem. Soc.* **1999**, *121*, 1752−1753.

(15) Timmerman, P.; Prins, L. J. Noncovalent Synthesis of Melamine−Cyanuric/Barbituric Acid Derived Nanostructures: Regio- and Stereoselection. *Eur. J. Org. Chem.* **2001**, *2001*, 3191−3205.

(16) Zhang, X.-L.; Ye, B.-H.; Chen, X.-M. Infinite water chains trapped in an organic framework constructed from melamine with 1, 5-naphthalenedisulfonic acid via hydrogen bonds. *Cryst. Growth Des.* **2005**, *5*, 1609−1616.

(17) Li, X.-H.; Yang, S.-Z.; Xiang, W.-D.; Shi, Q. A novel porous supramolecular complex constructed by the co-crystallization of melamine and sulfate via hydrogen bonds and aromatic π-π interaction. *Struct. Chem.* **2007**, *18*, 661−666.

(18) Vella-Zarb, L.; Braga, D.; Orpen, A. G.; Baisch, U. The influence of hydrogen bonding on the planar arrangement of melamine in crystal structures of its solvates, cocrystals and salts. *CrystEngComm* **2014**, *16*, 8147−8159.

(19) Li, P.; Arman, H. D.; Wang, H.; Weng, L.; Alfooty, K.; Angawi, R. F.; Chen, B. Solvent Dependent Structures of Melamine: Porous or Nonporous? *Cryst. Growth Des.* **2015**, *15*, 1871−1875.

(20) Janczak, J. Supramolecular solid-state architecture formed by co-crystallization of melamine and phenylacetic acid. *J. Mol. Struct.* **2020**, *1207*, 127833.

(21) Janczak, J. Supramolecular solid-state architectures formed by co-crystallization of melamine and 2-, 3-and 4-chlorophenylacetic acids. *J. Mol. Struct.* **2016**, *1125*, 493−502.

(22) Castiñeiras, A.; García-Santos, I.; González-Pérez, J. M.; Bauzá, A.; Zaręba, J. K.; Niclós-Gutiérrez, J.; Torres, R.; Vílchez, E.; Frontera, A. Multicomponent Supramolecular Assemblies of Melamine and α-Hydroxycarboxylic Acids: Understanding the Hydrogen Bonding Patterns and Their Physicochemical Consequences. *Cryst. Growth Des.* **2018**, *18*, 6786−6800.

(23) Oh, H.; Kim, D.; Kim, D.; Park, I.-H.; Jung, O.-S. 2D Porous Organic Templates via Cocrystallization of Melamine with Disulfonic Acids: Adsorption of Various Alcohols in SCSC Mode. *Cryst. Growth Des.* **2020**, *20*, 7027−7033.

(24) Yang, H.; Song, L.; Tai, Q.; Wang, X.; Yu, B.; Yuan, Y.; Hu, Y.; Yuen, R. K. Comparative study on the flame retarded efficiency of melamine phosphate, melamine phosphite and melamine hypophosphite on poly (butylene succinate) composites. *Polym. Degrad. Stab.* **2014**, *105*, 248−256.
(25) Feng, Y.; Yao, J. Design of melamine sponge-based three-dimensional porous materials toward applications. *Ind. Eng. Chem. Res.* **2018**, *57*, 7322−7330.
(26) Schartel, B.; Weiß, A.; Mohr, F.; Kleemeier, M.; Hartwig, A.; Braun, U. Flame retarded epoxy resins by adding layered silicate in combination with the conventional protection-layer-building flame retardants melamine borate and ammonium polyphosphate. *J. Appl. Polym. Sci.* **2010**, *118*, 1134−1143.
(27) Ono, S.; Inoue, Y.; Watanabe, N.; Yoshimura, T.; Morita, H.; Shiroishi, A.; Takakura, M.; Shimasaki, C. pH-Dependent elution behaviour of meleme in high-performance cation-exchange chromatography. *J. Chromatogr. A* **1996**, *752*, 287−290.
(28) Lotsch, B. V.; Schnick, W. New Light on an Old Story: Formation of Melam during Thermal Condensation of Melamine. *Chem. - Eur. J.* **2007**, *13*, 4956−4968.
(29) Gal'perin, V. A.; Finkel'shtein, A. I.; Gavrilova, N. K. Synthesis of melam from melamine. *Russ. J. Org. Chem.* **1971**, *7*, 2431.
(30) Jing, H.; Ströbele, M.; Weisser, M.; Meyer, H.-J. Die Kristallstruktur von wasserfreiem Melaminiumchlorid. *Z. Anorg. Allg. Chem.* **2003**, *629*, 368−370.
(31) Kalmutzki, M.; Ströbele, M.; Bettinger, H. F.; Meyer, H.-J. Development of Metal Cyanurates: The Example of Barium Cyanurate (BCY). *Eur. J. Inorg. Chem.* **2014**, *2014*, 2536−2543.
(32) Kalmutzki, M.; Ströbele, M.; Meyer, H. J. From cyanate to cyanurate: cyclotrimerization reactions towards the novel family of metal cyanurates. *Dalton Trans.* **2013**, *42*, 12934−12939.
(33) Kalmutzki, M.; Ströbele, M.; Enseling, D.; Jüstel, T.; Meyer, H.-J. Synthesis, Structure, and Luminescence of Rare Earth Cyanurates. *Eur. J. Inorg. Chem.* **2015**, *2015*, 134−140.
(34) Kalmutzki, M.; Ströbele, M.; Wackenhut, F.; Meixner, A. J.; Meyer, H.-J. Synthesis, Structure, and Frequency-Doubling Effect of Calcium Cyanurate. *Angew. Chem., Int. Ed.* **2014**, *53*, 14260−14263.
(35) Kalmutzki, M.; Wang, X.; Meixner, A. J.; Meyer, H.-J. Second harmonic generation properties of $Ca_3(O_3C_3N_3)_2$-$Sr_3(O_3C_3N_3)_2$ solid solutions. *Cryst. Res. Technol.* **2016**, *51*, 460−465.
(36) Kalmutzki, M. J.; Dolabdjian, K.; Wichtner, N.; Ströbele, M.; Berthold, C.; Meyer, H.-J. Formation, structure, and frequency-doubling effect of a modification of strontium cyanurate (α-SCY). *Inorg. Chem.* **2017**, *56*, 3357−3362.
(37) Harisomayajula, N. V. S.; Makovetskyi, S.; Tsai, Y.-C. Cuprophilic Interactions in and between Molecular Entities. *Chem. - Eur. J.* **2019**, *25*, 8936−8954.
(38) Batsanov, S. S. Van der Waals Radii of Elements. *Inorg. Mater.* **2001**, *37*, 871−885.
(39) Batsanov, S. S. Thermodynamic determination of van der Waals radii of metals. *J. Mol. Struct.* **2011**, *990*, 63−66.
(40) Batsanov, S. S.; Batsanov, A. S. Intermolecular Forces. In *Introduction to Structural Chemistry*; Springer Netherlands: 2012; pp 227−274. .
(41) Hu, S.-Z.; Zhou, Z.-H.; Robertson, B. E. Consistent approaches to van der Waals radii for the metallic elements. *Z. Kristallogr.* **2009**, *224*, 375−383.
(42) Hietsoi, O.; Filatov, A. S.; Dubceac, C.; Petrukhina, M. A. Structural diversity and photoluminescence of copper (I) carboxylates: from discrete complexes to infinite metal-based wires and helices. *Coord. Chem. Rev.* **2015**, *295*, 125−138.
(43) Liddle, S. T. *Molecular Metal-Metal Bonds*; Wiley Online Library: 2015.
(44) Kalmutzki, M.; Ströbele, M.; Meyer, H.-J. From cyanate to cyanurate: cyclotrimerization reactions towards the novel family of metal cyanurates. *Dalton Trans.* **2013**, *42*, 12934−12939.
(45) Hod, O. Graphite and Hexagonal Boron-Nitride have the Same Interlayer Distance. Why? *J. Chem. Theory Comput.* **2012**, *8*, 1360−1369.
(46) Monkhorst, H. J.; Pack, J. D. Special points for Brillouin-zone integrations. *Phys. Rev. B* **1976**, *13*, 5188−5192.
(47) Hamann, D. R.; Wu, X.; Rabe, K. M.; Vanderbilt, D. Metric tensor formulation of strain in density-functional perturbation theory. *Phys. Rev. B: Condens. Matter Mater. Phys.* **2005**, *71*, 035117.
(48) Bottin, F.; Leroux, S.; Knyazev, A.; Zérah, G. Large-scale ab initio calculations based on three levels of parallelization. *Comput. Mater. Sci.* **2008**, *42*, 329−336.
(49) Van Troeye, B.; Torrent, M.; Gonze, X. Interatomic force constants including the DFT-D dispersion contribution. *Phys. Rev. B: Condens. Matter Mater. Phys.* **2016**, *93*, 144304.
(50) Gonze, X.; Amadon, B.; Antonius, G.; Arnardi, F.; Baguet, L.; Beuken, J.-M.; Bieder, J.; Bottin, F.; Bouchet, J.; Bousquet, E.; Brouwer, N.; Bruneval, F.; Brunin, G.; Cavignac, T.; Charraud, J.-B.; Chen, W.; Côté, M.; Cottenier, S.; Denier, J.; Geneste, G.; Ghosez, P.; Giantomassi, M.; Gillet, Y.; Gingras, O.; Hamann, D. R.; Hautier, G.; He, X.; Helbig, N.; Holzwarth, N.; Jia, Y.; Jollet, F.; Lafargue-Dit-Hauret, W.; Lejaeghere, K.; Marques, M. A. L.; Martin, A.; Martins, C.; Miranda, H. P. C.; Naccarato, F.; Persson, K.; Petretto, G.; Planes, V.; Pouillon, Y.; Prokhorenko, S.; Ricci, F.; Rignanese, G.-M.; Romero, A. H.; Schmitt, M. M.; Torrent, M.; van Setten, M. J.; Van Troeye, B.; Verstraete, M. J.; Zérah, G.; Zwanziger, J. W. The Abinitproject: Impact, environment and recent developments. *Comput. Phys. Commun.* **2020**, *248*, 107042.
(51) Savin, A.; Nesper, R.; Wengert, S.; Fässler, T. F. ELF: The electron localization function. *Angew. Chem., Int. Ed. Engl.* **1997**, *36*, 1808−1832.
(52) Ortiz, A. U.; Boutin, A.; Fuchs, A. H.; Coudert, F.-X. Anisotropic Elastic Properties of Flexible Metal-Organic Frameworks: How Soft are Soft Porous Crystals? *Phys. Rev. Lett.* **2012**, *109*, 195502.
(53) Bosak, A.; Serrano, J.; Krisch, M.; Watanabe, K.; Taniguchi, T.; Kanda, H. Elasticity of hexagonal boron nitride: Inelastic x-ray scattering measurements. *Phys. Rev. B: Condens. Matter Mater. Phys.* **2006**, *73*, 041402.
(54) Gauster, W. B.; Fritz, I. J. Pressure and temperature dependences of the elastic constants of compression-annealed pyrolytic graphite. *J. Appl. Phys.* **1974**, *45*, 3309−3314.
(55) Hinuma, Y.; Pizzi, G.; Kumagai, Y.; Oba, F.; Tanaka, I. Band structure diagram paths based on crystallography. *Comput. Mater. Sci.* **2017**, *128*, 140−184.

https://doi.org/10.1021/acs.inorgchem.1c02145
Inorg. Chem. 2021, 60, 16303−16307

Tricopper Melaminate, a Metal–Organic Framework Containing Dehydrogenated Melamine and Cu–Cu Bonding

Paula Kallenbach, Elahe Bayat, Markus Ströbele, Carl P. Romao, and Hans-Jürgen Meyer*

P. Kallenbach, Elaheh Bayat, Dr. M. Ströbele, Dr. C. P. Romao, Prof. Dr. H.-J. Meyer
Section for Solid State and Theoretical Inorganic Chemistry
Institute of Inorganic Chemistry
Eberhard Karls Universität Tübingen
Auf der Morgenstelle 18, 72076 Tübingen (Germany)
E-mail: juergen.meyer@uni-tuebingen.de

Table of Contents

Table S1. Crystal data and structure refinement for $Cu_3(C_3N_6H_3)$.

CCDC Identification code	2063421
Empirical formula	C3 H3 Cu3 N6
Formula weight	313.73
Temperature	100.0(1) K
Wavelength	154.184 pm
Crystal system	Hexagonal
Space group	P*6/mcc*
Unit cell dimensions	a = 1205.42(5) pm
	b = 1205.42(5) pm
	c = 616.00(3) pm
Volume	0.77515(7) nm^3
Z	4
Density (calculated)	2.688 g/cm^3
Absorption coefficient	9.144 mm^{-1}
F(000)	600
Crystal size	0.042 x 0.035 x 0.024 mm^3
Theta range for data collection	4.235 to 80.032°.
Index ranges	$-14 \leq h \leq 12$, $-14 \leq k \leq 15$, $-7 \leq l \leq 7$
Reflections collected	17353
Independent reflections	313 [R(int) = 0.0557]
Completeness to theta = 67.684°	100.0 %
Absorption correction	Gaussian
Max. and min. transmission	0.855 and 0.766
Refinement method	Full-matrix least-squares on F^2
Data / restraints / parameters	313 / 0 / 28
Goodness-of-fit on F^2	1.070
Final R indices [$I > 2\sigma(I)$]	R1 = 0.0319, wR2 = 0.0850
R indices (all data)	R1 = 0.0329, wR2 = 0.0863
Largest diff. peak and hole	0.719 and -0.400 $e.Å^{-3}$

Table S2. Atomic coordinates (x 10^4) and equivalent isotropic displacement parameters (pm^2x 10^{-1}) for $Cu_3(C_3N_6H_3)$. U(eq) is defined as one third of the trace of the orthogonalized U^{ij} tensor.

	x	y	z	U(eq)
Cu(1)	410(1)	4236(1)	½	34(1)
N(1)	6479(3)	2108(3)	½	34(1)
N(2)	8679(3)	2949(3)	½	34(1)
C(1)	7680(3)	3133(3)	½	28(1)

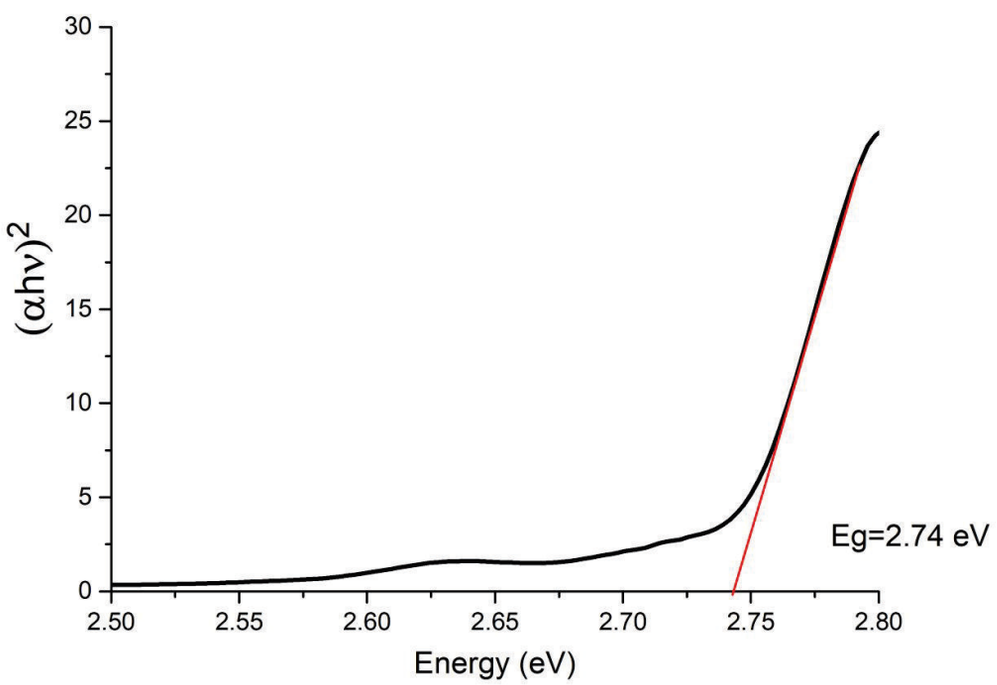

Figure S1. Tauc plot of a UV-Vis reflectance measurement of $Cu_3(C_3N_6H_3)$ indicating a direct band gap of 2.74 eV. α corresponds to the absorption coefficient, h is planck's constant and ν is the frequency.

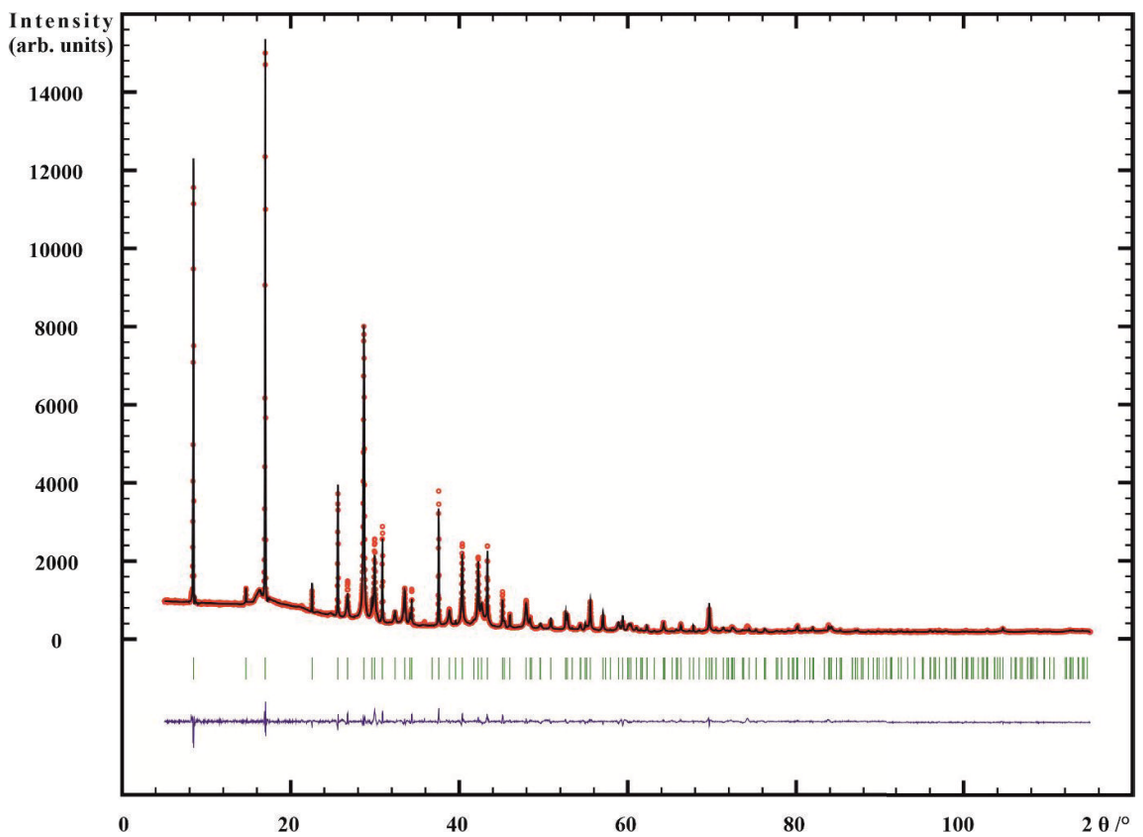

Figure S2. PXRD pattern of $Cu_3(C_3N_6H_3)$ recorded in air. Red circles: measured data points, black line: calculated pattern, green strokes: bragg positions, blue line: difference curve.

Publication 2

High-Yield Synthesis Route, Post-Synthesis Treatment, and Insights into the Photoluminescence and Magnetic Properties of Tricopper(I) Melaminate $Cu_3(C_3N_6H_3)$

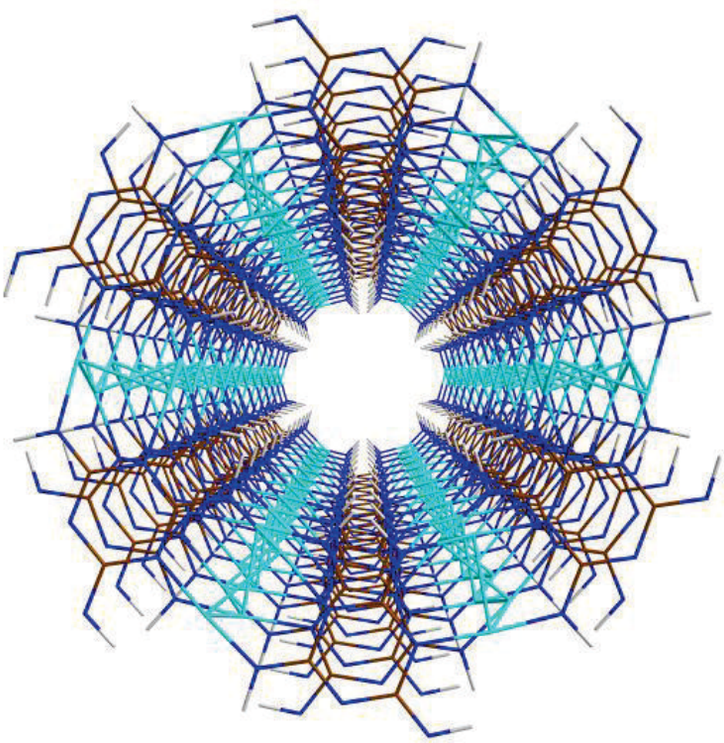

https://doi.org/10.1021/acs.inorgchem.4c01658

Reprinted with permission from

Inorg. Chem. 2024, 63, 41, 19053–19062

Inorganic Chemistry

pubs.acs.org/IC Article

High-Yield Synthesis Route, Post-Synthesis Treatment, and Insights into the Photoluminescence and Magnetic Properties of Tricopper(I) Melaminate $Cu_3(C_3N_6H_3)$

Elaheh Bayat, Markus Ströbele, Mojtaba Abbasi, Scott Kroeker, Jaroslav Valenta, David Enseling, Thomas Jüstel, and Hans-Jürgen Meyer*

Cite This: *Inorg. Chem.* 2024, 63, 19053−19062 Read Online

ACCESS | Metrics & More | Article Recommendations | Supporting Information

ABSTRACT: A novel and more efficient synthesis of $Cu_3(C_3N_6H_3)$ is presented through a salt-metathesis reaction using copper(I) chloride and sodium hydrogen cyanamide. This synthesis yields a melaminate trianion through the cyclotrimerization of $(HNCN)^-$ ions, offering an alternative route to the deprotonation of melamine for synthesizing melaminate. The reaction is analyzed via differential thermal analysis. After the unconventional formation of this MOF-like structure by solid-state reaction, this material still requires treatment via solvent exchange and vacuum drying due to the presence of a host molecule inside the channels of the structure. The process and the impact of the treatment of $Cu_3(C_3N_6H_3)$ on its XRD pattern are thoroughly discussed. Additionally, results from stability, NMR and infrared spectroscopy, and thermogravimetric analysis. Finally, photoluminescence and magnetic studies are conducted to evaluate their potential as a functional material.

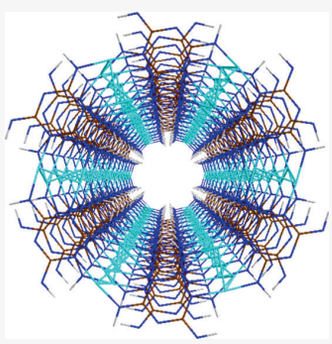

1. INTRODUCTION

The compound 2,4,6-triamino-1,3,5-triazine, widely known as melamine, is today commercially synthesized from urea.[1−3] However, in 1943, the only commercially feasible method for its production was the trimerization of cyanamide or using dicyandiamide as a precursor.[4,5] In this process, crystalline cyanamide or dicyandiamide was placed in an organic solvent at 190−250 °C under atmospheric pressure, and melamine was produced in 95% purity with 5% contamination of deamination products.[4] Melamine is mostly insoluble in common organic solvents, making the study of its reactions more challenging.[6] Despite the capability of melamine to form extended hydrogen networks, this compound can act as a poor ligand, especially in an aqueous medium.[7−9] Up to now, several metal complexes with melamine have been investigated to study the coordination chemistry of melamine.[7−13] However, dealing with melamine in solid-state reactions facilitates the study of this material as a ligand and provides an opportunity to explore its applications.

The first layered metal melaminate metal−organic framework, $Cu_3(C_3N_6H_3)$, was reported in our previous research,[14] which represented an initial understanding of the structure of three-times deprotonated melamine as a ligand for copper metallic centers. However, the synthetic method reported in our previous work with melamine (eq 1) cannot be well reproduced since a successful synthesis depends on various factors such as pressure, the flow of argon, and the diameter of the reaction tube or the vessel.[18,19] In our previous investigation of the synthetic route, we discovered that two byproducts, $Cu_2Cl_2(C_3N_6H_6)$ (eq 2) and $Cu_3Cl_3(C_3N_6H_6)$ (eq 3),[13] compete with the pure phase of $Cu_3(C_3N_6H_3)$.[14] In fact, this issue arises from the early sublimation of melamine (at various pressures) before reaching the reaction temperature of 275 °C.[15,16] In other words, the amount of melamine available for reacting with copper chloride is continually changing due to the degree of sublimation of melamine.

$$3CuCl + 4C_3N_6H_6 \rightleftharpoons Cu_3(C_3N_6H_3) + 3(C_3N_6H_7)Cl \quad (1)$$

$$2CuCl + C_3N_6H_6 \rightleftharpoons Cu_2Cl_2(C_3N_6H_6) \quad (2)$$

$$3CuCl + C_3N_6H_6 \rightleftharpoons Cu_3Cl_3(C_3N_6H_6) \quad (3)$$

In our previous research, $Cu_3(C_3N_6H_3)$ was crystallized into brown hexagonal rods. Single crystal measurement uncovered that the structure of copper-melaminate is characterized by its twisted ladder structure of Cu−Cu dumbbells and six melaminates arranged to create a layered framework with pores running along the hexagonal *c*-axis direction (Figure 1).

Received: April 23, 2024
Revised: August 23, 2024
Accepted: September 19, 2024
Published: September 30, 2024

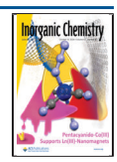

https://doi.org/10.1021/acs.inorgchem.4c01658
Inorg. Chem. 2024, 63, 19053−19062

This substance behaves as a semiconductor and exhibits a band gap of 2 eV.[14]

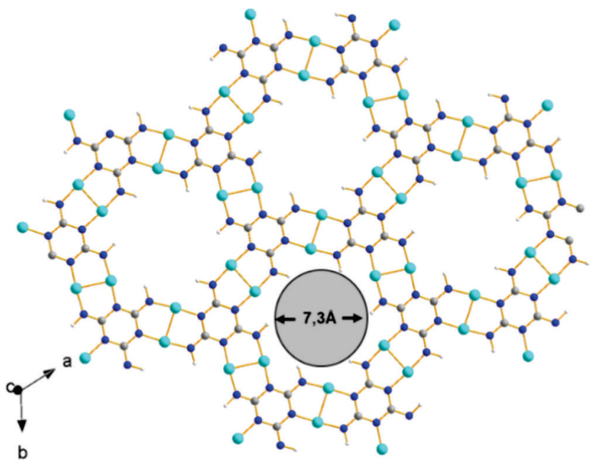

Figure 1. Single layer of $Cu_3(C_3N_6H_3)$ with channel size (hydrogen-to-hydrogen distance). Copper atoms are shown in light blue, nitrogen blue, carbon gray, and hydrogen white.

One challenge in the synthesis of MOFs for commercialization is scaling up their production (>1 g)[17−19] while maintaining good crystallinity. To further explore the potential of $Cu_3(C_3N_6H_3)$, this critical aspect needs to be addressed. First, a large-scale and high-yield synthesis approach should be introduced to enable us to produce a significant quantity of $Cu_3(C_3N_6H_3)$. Then, the XRD patterns of powders obtained from large-scale synthesis have been compared with the calculated ones from the measured single crystal.

Our present work demonstrates that simpler and more efficient solid-state metathesis reactions can be used to synthesize tricopper-melaminate via the cyclotrimerization of hydrogen cyanamide $(HNCN)^-$, as has been previously demonstrated for the synthesis of metal-cyanurates via cyclotrimerization of cyanates $(OCN)^-$. Overall, in this study, we have successfully tackled the challenge of achieving a high yield and good reproducibility by using a novel synthesis route for $Cu_3(C_3N_6H_3)$.[20−22] We also discuss the methodology employed for treating $Cu_3(C_3N_6H_3)$. Furthermore, stability, IR, and NMR studies, along with an exploration of its magnetic properties and photoluminescence have been carried out to further discover the potential of this material.

2. RESULTS AND DISCUSSION

2.1. Synthesis and Structure. The number of compounds containing deprotonated melamine is very small, as even the deprotonation of a weak base is challenging. However, our study, combined with previous research in this area,[14] shows that there are various approaches to achieving these kinds of compounds. Two compounds, sodium melaminate $Na(C_3N_6H_5)\cdot nNH_3$ and tripotassium melaminate $K_3(C_3N_6H_3)$, were proposed for the first time to be melaminates by Schnick.[23] These compounds were obtained as amorphous phases, and their compositions were only derived from elemental analysis. Later, attempts to deprotonate melamine in liquid ammonia have yielded a class of materials known as melaminate adducts with ammonia, such as rubidium $(Rb(C_3N_6H_5)\cdot 1/2NH_3)$ and potassium $(K(C_3N_6H_5)\cdot NH_3)$, as investigated by Dronskowski.[24] In our previous paper, we were also able to deprotonate melamine three times with copper chloride (CuCl) in a solid-state synthesis (eq 1), which allowed us to further study the effects of other metal halides such as antimony chloride $(SbCl_3)$ and achieve the three deprotonated compounds of $SbCl_4(C_9N_{18}H_{19})$, $SbCl_4(C_6N_{12}H_{13})_2$, and $SbCl(C_3N_6H_4)$.[25] Herein, we propose a new method to obtain melaminates.

Deprotonation of melamine can be logically achieved by a strong base such as liquid ammonia.[24] Therefore, we studied the effect of bases such as NaH and $NaNH_2$ in the deprotonation of melamine in the solid state. Reacting either of these compounds with melamine gave us different intermediates, $Na_5H(CN_2)_3$[26] and $Na(HCN_2)$, providing us with the idea of achieving the melaminate anion through the cyclotrimerization of $(HNCN)^-$ ions (Figure 2). This resulted in a higher yield (>90% w.r.t. Cu) of the previously reported $Cu_3(C_3N_6H_3)$ eq 4.[14]

$$3CuCl + 3Na(HCN_2) \rightleftharpoons Cu_3(C_3N_6H_3) + 3NaCl \quad (4)$$

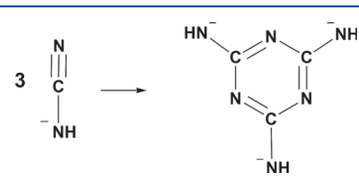

Figure 2. Cyclotrimerization of $HNCN^-$ to give $(C_3N_6H_3)^{3-}$.

This new strategy, along with the fundamental concept that cyanamide trimerization yields the melaminate unit, introduces a new approach to synthesizing melaminate structures. The layered structure of $Cu_3(C_3N_6H_3)$ has been reported to be hexagonal with the space group of *P6/mcc* (a = 1205.42(5) pm, c = 616.00(3) pm) in our previous work.[14] The crystal structure refinement obtained from these brown crystals suggests that the channels within the crystal were empty with no discernible residue of electron density present. The channels within the layered crystal structure of $Cu_3(C_3N_6H_3)$ are schematically shown in Figure 3a,b.

2.2. Thermoanalytic Studies. The reaction of the (1:1) stoichiometric ratio of CuCl and $Na(HCN_2)$ was conducted using differential thermoanalytic (DTA) studies with a heating and cooling rate of 2 °C min^{-1} in the range from 25 to 450 °C (Figure 4). There are three distinct exothermic peaks, each representing a specific reaction between the reactants. Each peak was studied by stopping the reaction at each temperature and studying the X-ray diffraction (XRD) taken from each experiment.[27] The peak at 194 °C corresponds to the formation of $Cu_3(C_3N_6H_3)$. The reaction for synthesizing $Cu_3(C_3N_6H_3)$ has been chosen to be exactly at 200 °C, slightly above the exothermic peak attributed to the formation of this compound, and kept for 45 h for a complete reaction. Notably, there are no additional exothermic or endothermic peaks observed upon heating to 450 °C, suggesting the good stability of $Cu_3(C_3N_6H_3)$ at higher temperatures. However, the thermal stability has been further investigated through a TGA test conducted on as-synthesized $Cu_3(C_3N_6H_3)$ (**1**), and the results are explained in the stability section. The small exothermic peaks observed at 154 and 180 °C are attributed to the formation of intermediate and unidentified phases (Figure S1). Unfortunately, despite many efforts, crystallizing

https://doi.org/10.1021/acs.inorgchem.4c01658
Inorg. Chem. 2024, 63, 19053−19062

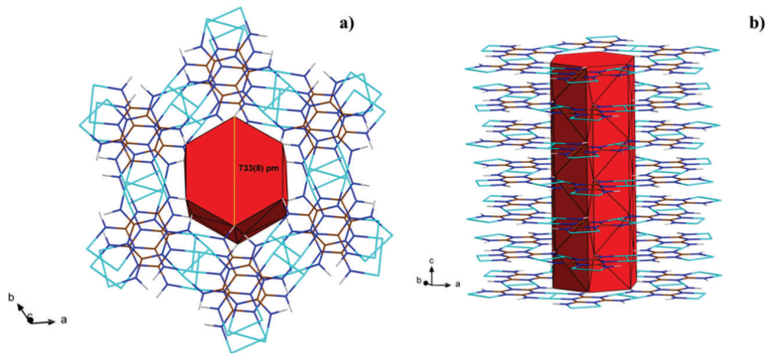

Figure 3. (a) Shape and diameter of channels in $Cu_3(C_3N_6H_3)$ (top view); (b) channels in the multilayer view (side view).

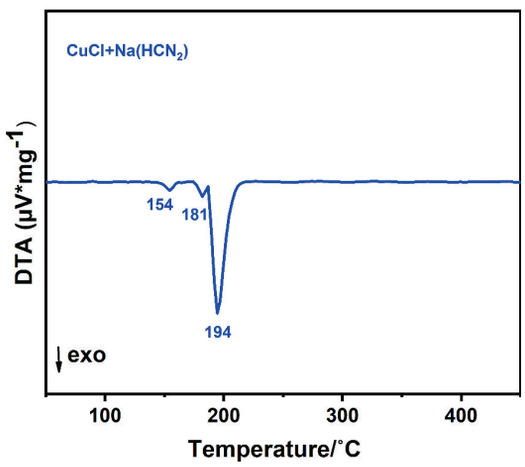

Figure 4. DTA of the reaction of CuCl and $Na(HCN_2)$ in a stoichiometric ratio of 1:1.

and resolving these intermediate phases from XRD data was not successful.

2.3. X-ray Powder Diffraction. Figure 5a displays the powder XRD pattern of the as-synthesized $Cu_3(C_3N_6H_3)$ (sample **1**) with NaCl as the metathesis salt. The sample was washed with absolute methanol to remove NaCl (sample **2**). A closer look at Figure 5a,b shows the differences between the calculated CIF from crystallographic data (Figure 5c). The intensity ratio of peaks at 2θ values of 8.46° and 16.98°, corresponding to Miller indices 100 and 200, respectively, differs from the measured crystal, while this ratio already changes by washing the sample with methanol (sample **2**) (Figure 5b). In addition, there is an obvious shift in the peaks along the *c*-axis (002 reflections at 2θ = 28.92°) and some subtle shifts in some smaller peaks. These differences cannot be solely ascribed to variations in measurement temperature between single-crystal and powder measurements or the orientation of particles in the sample. The difference in the intensities may be attributed to the presence of a host molecule filling the channels in the crystal structure, while the shift and broadening in some peaks may be attributed to particle defects. As can be seen in Figure 3a, channels can accommodate any host molecule smaller than $2r$ = 733.8 pm (hydrogen-to-hydrogen distance in the pores). Moreover, hydrogen bonding is favored by the presence of six hydrogen atoms per layer in each channel[14] which can stabilize host molecules.

It is important to note that since the reaction occurred in the solid state, we did not expect any solvent to be trapped in the pores. However, the presence of an organic side phase resulting from the decomposition of $Na(HCN_2)$, such as cyanamide, dicyandiamide, guanidine, or melamine, cannot be excluded. Therefore, various methods, including vacuum heating (Figure 6a–e), solvent exchange, sonication, and chemical treatment, were used to treat $Cu_3(C_3N_6H_3)$. The best treatment method was to wash the powder in sequential steps with solvents, starting with methanol, followed by acetonitrile, acetone, tetrahydrofuran (THF), and finally the less polar solvent pentane, and keeping the sample under vacuum at 260 °C for 4 weeks. This temperature was carefully chosen because at higher temperatures some of the product decomposed with the formation of elemental copper. The XRD pattern obtained from treated $Cu_3(C_3N_6H_3)$ (sample **3**) in Figure 6d compares relatively well with the calculated pattern from single-crystal refinement which is shown in Figure 6e. Interestingly, the as-synthesized sample (**1**) shows an olive-green color (Figure 6a), but after treatment under vacuum, the powder changes to a brown color (Figure 6d), resembling the color of the empty-channeled crystals (Figure 5c) obtained through the original melamine synthetic route.

We recall that there had been no significant residual electron density in the original structure refinement of $Cu_3(C_3N_6H_3)$.[14] However, in bulk production, the host molecule in channels of the herein prepared sample (eq 4) could accommodate any molecule in the size of smaller than 700 pm such as melamine ($2r$ = 640 pm) or fragments thereof, originating from the heating of $Na(HCN_2)$.

The impact a guest molecule would have on the (calculated) X-ray pattern was modeled with the Diamond[28] graphics program. In any case, the 6-fold rotation axis in the center of channels of the structure will induce a six-membered ring arrangement for a single host atom. This prompted us to consider a fraction of a disordered melamine molecule (Figure 7) in our model. The presence of (disordered) melamine molecules changed the intensity ratio, mainly of calculated XRD peaks at 2θ values of 8.46° and 16.98°. This model was solely used to demonstrate how the presence of a host molecule, like melamine, within the channels or between layers can alter the intensity of XRD peaks. The calculated XRD powder pattern of this model is given in Figure S2 for comparison with our experimental patterns. These patterns can give an insight into the main reason behind discrepancies between the XRD pattern of bulk $Cu_3(C_3N_6H_3)$ with that of the refined crystal structure with empty channels.

https://doi.org/10.1021/acs.inorgchem.4c01658
Inorg. Chem. 2024, 63, 19053−19062

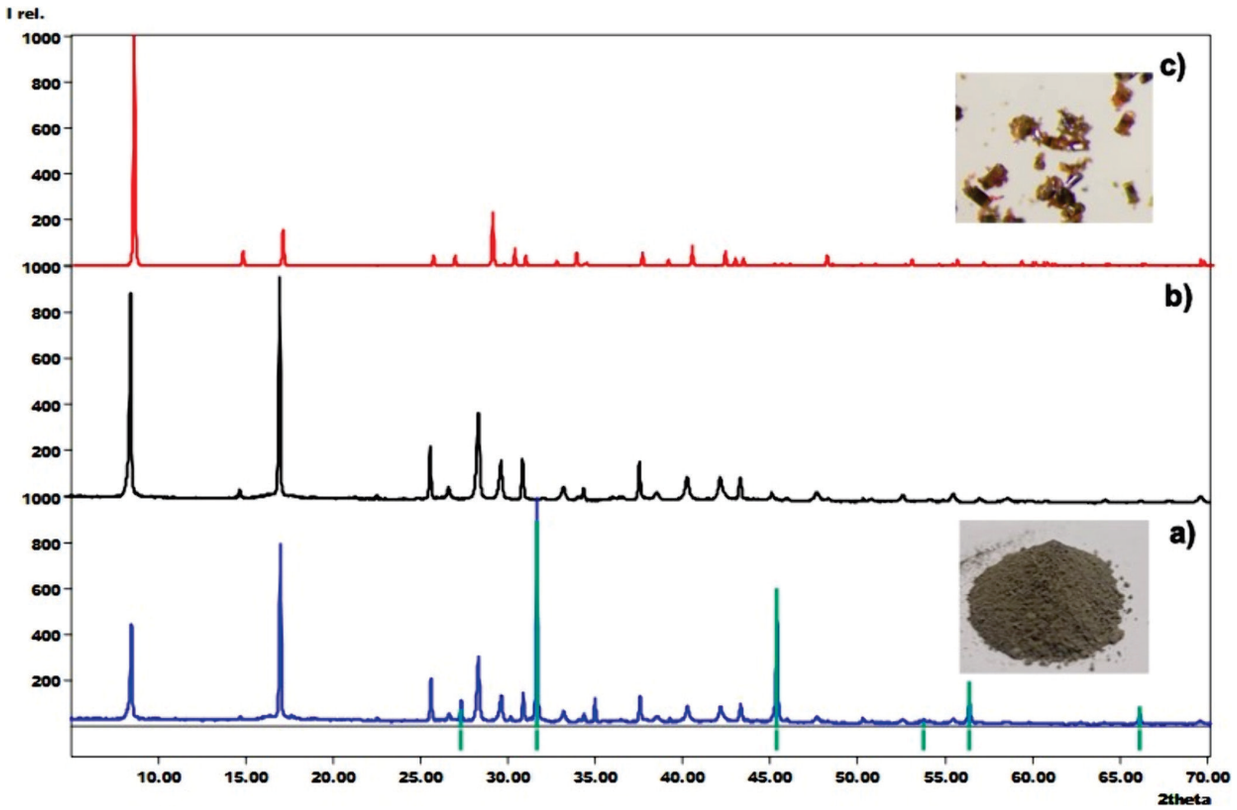

Figure 5. (a) XRD pattern of the as-synthesized $Cu_3(C_3N_6H_3)$ (sample **1**) with NaCl as metathesis salt; (b) XRD pattern of the washed sample with methanol (sample **2**); and (c) calculated pattern based on the single-crystal measurement of $Cu_3(C_3N_6H_3)$ (CCDC code: 2063421). The insets show brown crystalline powder of the "empty" (c), and olive-green powder of the as-synthesized $Cu_3(C_3N_6H_3)$ (sample **1**) (a) compound. (Green lines represent positions of Bragg reflections for NaCl).

2.4. Solid-State NMR Studies. Nuclear magnetic resonance (NMR) spectroscopy was performed to assist in identifying the pore occupants. Due to its paramagnetic character (vide infra), signals from the $Cu_3(C_3N_6H_3)$ framework are not observed, due to rapid relaxation, anisotropic electron−nuclear dipolar coupling, or large contact shifts. While such NMR signals can be measured under some circumstances,[29,30] the experiments and parameters were chosen to bias against detection and selectively highlight signals from species in the channels.

^{13}C cross-polarization (CP) magic-angle spinning (MAS) NMR of the as-synthesized $Cu_3(C_3N_6H_3)$ (**1**) reveals a single peak at 167 ppm (Figure 8a), corresponding to what is observed for pure melamine (Figure 8c). Whereas melamine has three magnetically inequivalent carbons producing two distinct peaks Figure 8,[31] the peak width observed for (**1**) is broad enough to encompass both signals, suggesting that melamine in the $Cu_3(C_3N_6H_3)$ channels is somewhat disordered. The ^{13}C CPMAS NMR spectrum of the $Cu_3(C_3N_6H_3)$ sample after washing with methanol and vacuum-drying (**2**) is very similar (Figure 8b), confirming that melamine remains in the channels. While NMR is not especially reliable for comparing absolute intensities between different samples, it may be noted that the signal intensities for (**1**) and (**2**) are comparable under identical acquisition conditions, while that of the pure melamine is greater by several orders of magnitude, implying that the amount of melamine included in the $Cu_3(C_3N_6H_3)$ channels is relatively small.

^1H MAS NMR spectra of the $Cu_3(C_3N_6H_3)$ samples (**1**,**2**) yield a single prominent peak at 4.8 ppm (Figure 8a,b), confirming the similarity of these materials. In solution, melamine appears at 5.94 ppm in ^1H NMR spectra[32]; however, in the solid state, two peaks of approximately equal intensity are observed at 8.2 and 4.2 ppm (Figure 8c), reflecting the chemical inequivalency of these hydrogens in a crystalline phase. Since the mean value of these peaks (6.2 ppm) is very near the solution value, it is likely that amine rotation is responsible for their coalescence into a single signal. The observation of a single peak in the $Cu_3(C_3N_6H_3)$ samples rather than the two peaks found for pure melamine implies that the molecules are disordered within the $Cu_3(C_3N_6H_3)$ pores. Such disorder could be dynamic on the NMR time scale, as in the solution phase, but likely restricted and anisotropic within the confinement of the channel, giving rise to a peak that is slightly shifted from the expected value of 6 ppm, as documented for adsorbates in MOFs.[33] Alternatively, the near alignment of the single peak at 4.8 ppm with the 4.2 ppm peak of pure melamine may imply that hydrogen bonding of the proton observed at 8.2 ppm with the paramagnetic framework renders it spectroscopically silent. In either case, the close correspondence of the observed ^1H and ^{13}C NMR peaks in the $Cu_3(C_3N_6H_3)$ samples with the melamine signals is

https://doi.org/10.1021/acs.inorgchem.4c01658
Inorg. Chem. 2024, 63, 19053−19062

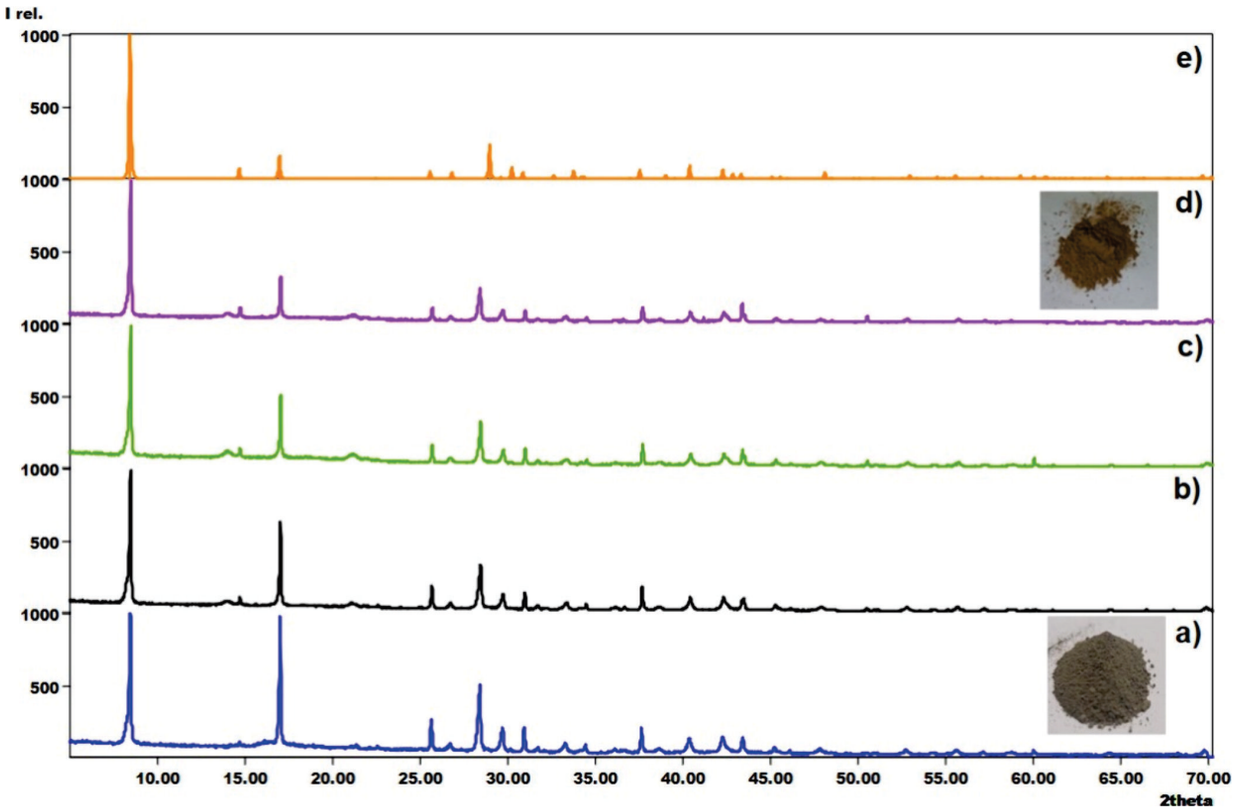

Figure 6. (a) As-synthesized $Cu_3(C_3N_6H_3)$ sample sequentially washed with methanol (sample **1**), then with acetonitrile, acetone, tetrahydrofuran (THF), and pentane; (b) washed sample dried under vacuum at 260 °C for 24 h; (c) washed sample dried under vacuum at 260 °C for 48 h; (d) washed sample dried under vacuum at 260 °C for 4 weeks (sample (**3**)); (e) calculated pattern from the single-crystal measurement of $Cu_3(C_3N_6H_3)$ (CCDC code: 2063421).

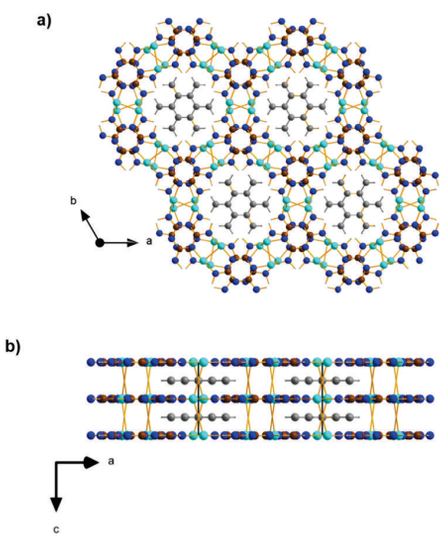

Figure 7. Structure of three-layer sequences of $Cu_3(C_3N_6H_3)$ shown in two projections, (a) and (b), modeled with disordered melamine (two orientations only) molecules (gray) in-between channels.

strong evidence that melamine remains occluded in the channels.

^{23}Na MAS NMR spectra of (**1**) and (**2**) were acquired under identical conditions to estimate the relative sodium content in the samples as a result of the NaCl metathesis salt (Figure S3). The as-prepared sample yields a very strong signal at 7.1 ppm, which can be assigned to NaCl, whereas the methanol-washed sample, before (not shown) and after vacuum-drying, contains a barely detectable NaCl signal. Caveats about the precision of spin-counting in NMR notwithstanding, it is clear that washing with methanol is quite effective at removing the NaCl.

2.5. Infrared Spectroscopy (IR). The Fourier-transform infrared spectroscopy (FTIR) analyses of two different samples of as-synthesized (**1**) and treated $Cu_3(C_3N_6H_3)$ (**3**) were conducted and compared with the IR spectrum of $Na(HCN_2)$ and melamine (Figure 9). This effort aimed to enhance our understanding of the structural properties and characterization of the synthesized material. In both $Cu_3(C_3N_6H_3)$ samples (**1**,**3**), the IR spectrum shows a single band between 3000 and 3500 cm^{-1}, which can be attributed to the stretching vibration of the N−H group. The N−H bending vibration is also evident at 1537 cm^{-1}, while the presence of a band at 752 cm^{-1} indicates the N−H wagging deformation.[34,35] Additional peaks at around 1450, 1251, and 642 cm^{-1} are assigned to the semicircle stretch of the ring, the aromatic ring stretch of the ring, and the bending of the ring of melaminate, respectively.[25,34,36] The strong multiple bands at around 2100−2200 cm^{-1}, observed in $Na(HCN_2)$, can be attributed to the stretching vibration of C≡N in cyanamides,[37,38] which

https://doi.org/10.1021/acs.inorgchem.4c01658
Inorg. Chem. 2024, 63, 19053−19062

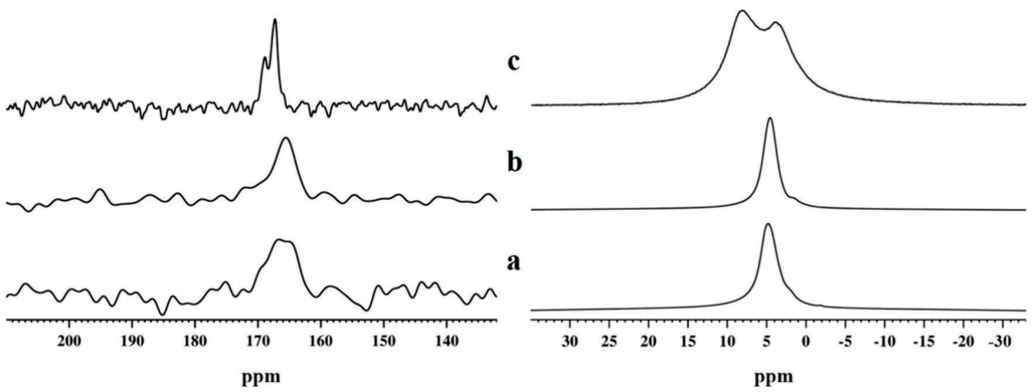

Figure 8. ^{13}C CPMAS (left traces) and ^{1}H MAS NMR (right traces) spectra of (a) as-synthesized $Cu_3(C_3N_6H_3)$ (**1**); (b) $Cu_3(C_3N_6H_3)$ after washing with methanol and vacuum-drying, (**2**), and (c) melamine.

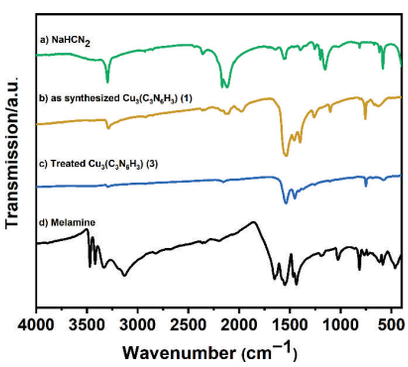

Figure 9. IR comparison of $Cu_3(C_3N_6H_3)$ (sample **1**) and treated $Cu_3(C_3N_6H_3)$ (sample **3**) with that of $Na(HCN_2)$ and melamine.

is also present in different samples of $Cu_3(C_3N_6H_3)$. This can be attributed to the small amount of unreacted precursor, which is minimized during the washing process.

To investigate the presence of host molecules in the channels, a comparative analysis of the IR patterns of as-synthesized $Cu_3(C_3N_6H_3)$ (sample **1**) and treated $Cu_3(C_3N_6H_3)$ (sample **3**) with melamine is essential. As can be seen in Figure 9, the as-synthesized sample (sample **1**) and melamine have similarities in the region 1438−1470 cm^{-1}. Despite these similarities, the presence of melamine or other molecules inside the channels could not be confirmed by IR, likely due to the small amount of trapped molecules.

2.6. Stability and Surface Area of the $Cu_3(C_3N_6H_3)$. The stability of as-synthesized $Cu_3(C_3N_6H_3)$ (sample **1**) was investigated through TGA analysis, as depicted in Figure S4. The decomposition of $Cu_3(C_3N_6H_3)$ shows a slow onset, starting at temperatures above 300 °C. The decomposition remains almost negligible until 450 °C is reached. This observation suggests that the formation of elemental copper is likely above 300 °C, especially with a longer reaction time at or above this temperature. The decomposition of $Cu_3(C_3N_6H_3)$ results in the formation of CuCN and elemental copper. Furthermore, treated $Cu_3(C_3N_6H_3)$ (sample **3**) is also stable in air and can be handled outside of the glovebox. The stability of the as-synthesized $Cu_3(C_3N_6H_3)$ (sample **1**) was also checked in various polar and nonpolar solvents, including THF, MeCN, ethanol, acetone, pentene, pyridine, water, DMF, DMSO, and toluene. While XRD measurements show that the crystal structure of $Cu_3(C_3N_6H_3)$ is stable, the intensity of peaks is changing with every solvent, which might indicate that the pore's occupancy is constantly changing (Figure S5), and it is plausible that any of these solvents could be trapped in the unoccupied channels of $Cu_3(C_3N_6H_3)$.

The BET surface area of the sample slightly increased from 12.7156 m^2/g before removing the host molecule to 13.2103 m^2/g after treatment, indicating an improvement in surface area accessibility. However, these values are relatively small, and several factors could contribute to this observation, such as pore blocking or collapse or the surface chemistry of this material. The total pore volume (0.049748 cm^3/g) indicates the presence of mesopores (2−50 nm). Average pore widths and diameters from BET and BJH analyses confirm the predominance of mesopores with average sizes around 15 nm and pore diameters between 4.9 and 7.1 nm.

2.7. Photoluminescence (PL) Spectroscopy. Copper compounds are known to exhibit interesting optical properties, while the specific ligands can influence the electronic structure of the complex.[13,39,40] However, in this study, the treated $Cu_3(C_3N_6H_3)$ (sample **3**) is not luminescent (Figure S6), rather a sample just comprising the host molecules (sample **2**) shows a green-yellow emission color upon excitation with UV radiation. This means that the host−guest interactions, such as hydrogen bonding and π-stacking of the host molecule with melaminates, could contribute to the emission which is a phenomenon called guest-induced luminescence.[41] This study confirms the potential of this functional material for application as a luminescent MOF-based sensor.[42]

PL spectra were recorded to understand the nature of the yellow light emitted from as-synthesized $Cu_3(C_3N_6H_3)$ (sample **2**) under excitation with UV radiation. In the data presented (Figure 10a), the excitation spectrum shows a distinct peak at 420 nm (23,800 cm^{-1}), while the corresponding emission spectrum exhibits a peak at 560 nm (17,900 cm^{-1}). The obtained broad emission band at 560 nm is in line with the observed green-yellow light. The temperature dependence of the emission spectra (Figure 10b) can be rationalized by considering the structural changes that occur with temperature increases. Conversely, as the temperature increases to 500 K, thermal effects may disrupt the interaction of guest molecules to the $Cu_3(C_3N_6H_3)$ structure (due to thermal expansion), leading to a decrease in luminescence intensity and thus thermally induced quenching of the photoluminescence.

https://doi.org/10.1021/acs.inorgchem.4c01658
Inorg. Chem. 2024, 63, 19053−19062

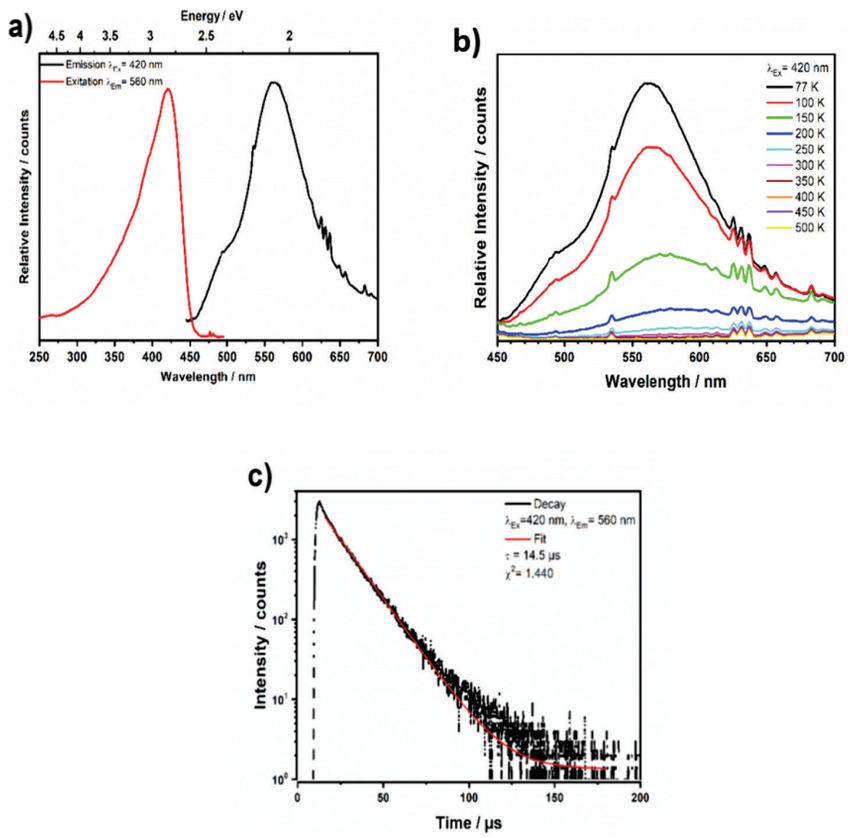

Figure 10. (a) Excitation and emission spectrum of $Cu_3(C_3N_6H_3)$ (**2**) at 77 °C; (b) temperature-dependent emission spectra of $Cu_3(C_3N_6H_3)$ between 77 and 500 K, (the artifacts at around 630 nm are remnants of the excitation lamp spectrum due to the application of an imperfect correction function); (c) decay curve after 420 nm excitation monitored at 560 nm.

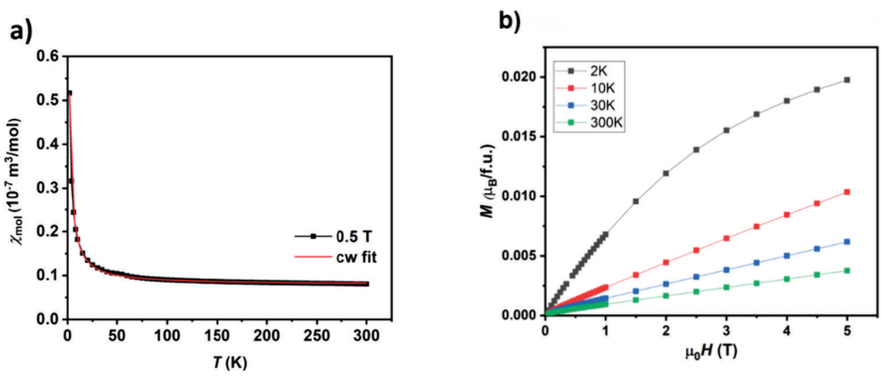

Figure 11. (a) Temperature dependence of χ_{mol} along with fitted red curve, (b) magnetization at various temperatures for $Cu_3(C_3N_6H_3)$.

The decay curve in Figure 10c suggests that the luminescence dynamics of the as-synthesized $Cu_3(C_3N_6H_3)$ (sample **2**) exhibits an almost monoexponential and rather fast emission decay, as indicated by the calculated decay time of 14.5 μs.

2.8. Magnetic Studies. The magnetic measurements were performed in detail regarding the low signal of the sample. The diamagnetic contribution caused by the sample holder, glue, and capsule was subtracted. Other diamagnetic contribution was observed during measurement which was calculated to the value ~3.10^{-9} m^3/mol and interpreted as core diamagnetism. The temperature-dependent (2−300 K) magnetic susceptibility of $Cu_3(C_3N_6H_3)$ (**2**) is shown in Figure 11a in the form of χ versus T plots. The curves are typical for paramagnetic response to the magnetic field.[43] The molar susceptibility data are fitted by the modified Curie−Weiss equation. Assuming a modified Curie−Weiss type equation, $\chi(T) = K\mu_s^2/(T - \theta_P) + \chi_0$, it can be calculated that the paramagnetic Curie temperature (θ_P) is−0.48(3) K and an effective magnetic moment (μ_{eff}) is 0.262 μ_B, which is equivalent to 0.034 electrons, and temperature-independent susceptibility is χ_0 = 7.91 × 10^{-9} m^3/mol. Figure 11b also shows magnetization as a

https://doi.org/10.1021/acs.inorgchem.4c01658
Inorg. Chem. 2024, 63, 19053−19062

function of the magnetic field at different temperatures and depicts a paramagnetic behavior at higher temperatures (T > 10 K), whereas at T = 2 K it appears to saturate slower than expected.

Copper exhibits both diamagnetic and Pauli paramagnetic contributions depending on its electron configuration. With a filled 3d shell and a half-filled outer shell, the cancellation of magnetic moments occurs, leading to a diamagnetic behavior. However, the presence of unpaired electrons results in Pauli paramagnetism.[44] Copper(I) compounds are typically diamagnetic, because the copper(I) ion has a fully filled $3d^{10}$ electron configuration with all electrons paired. However, in copper(I) complexes, ligands can cause a distortion in the electron structure, leading to an unpaired electron and paramagnetic behavior. The magnetic properties of copper-based MOFs are significantly influenced by the distance between the copper metal centers and the type of bridging ligand.[45] Furthermore, an extended conjugated network might make tunable conductivity and magnetic properties.[46] The formation of copper-to-copper bonding in the structure involves the interaction of two copper(I) ions in such a way that it disrupts the d^{10} electron configuration. This loss or redistribution of electrons could lead to unpaired electrons, inducing paramagnetic behavior. In $Cu_3(C_3N_6H_3)$, Cu_2 dumbbells in one layer are also in a twisted ladder manner connected to other Cu_2 dumbbells along the c-axis, which further contributes to the disruption of the d^{10} orbital and thus the paramagnetic property of this compound. Moreover, solid-state NMR studies of the $Cu_3(C_3N_6H_3)$ sample show that the ^1H T_1 relaxation is 367(7) ms for the as-prepared sample and 302(6) ms for the methanol-washed and vacuum-dried sample. In comparison with the 160 s T_1 estimated for pure melamine, these short T_1 values corroborate the paramagnetic character of $Cu_3(C_3N_6H_3)$.

3. CONCLUSIONS

As studied in our previous work, the compound known as tricopper(I) melaminate appears as a MOF exhibiting a unique semiconducting behavior and Cu−Cu bonding. In this study, we have presented a novel and more efficient and reproducible synthesis route for $Cu_3(C_3N_6H_3)$ through cyclotrimerization of $(HNCN)^-$ ions toward $(C_3N_6H_3)^{3-}$ in a salt-metathesis reaction using copper(I) chloride and sodium hydrogen cyanamide. This new synthesis method offers higher yield and scalability compared to those of the previous methods, addressing a critical aspect in the commercialization of this MOF.

A number of special properties of $Cu_3(C_3N_6H_3)$ are very interesting and worthy of further investigation.[14] The $Cu_3(C_3N_6H_3)$ is treated by washing the sample with various solvents and heating it to 280 °C in vacuum. Treated $Cu_3(C_3N_6H_3)$ (sample **3**) is stable in ambient air and can be heated to 300 °C without significant decomposition. Photoluminescence studies show a dependency of optical behavior on the presence of guest molecules trapped inside the channels or between the layers (guest-induced luminescence), qualifying $Cu_3(C_3N_6H_3)$ as a potential sensor material. Moreover, the paramagnetic behavior of $Cu_3(C_3N_6H_3)$ is attributed to a disrupted $[Ar]3d^{10}$ electronic configuration of copper ions in the ladders of Cu−Cu bonding. Overall, this comprehensive study offers valuable insights into the synthesis, treatment, and characterization of $Cu_3(C_3N_6H_3)$, paving the way for further exploration of its potential applications based on photoluminescence or electrical conductivity behavior.

4. EXPERIMENTAL SECTION

4.1. Material and Method. The starting materials, CuCl and $Na(HCN_2)$, were purchased from Thermo Fisher Scientific (99.999%) and Sigma-Aldrich (98%), respectively. Both materials were used without further purification. The reaction mixtures were prepared in a glovebox under an argon atmosphere, ensuring that moisture and oxygen levels were maintained below 1 ppm.

4.2. Synthesis of $Cu_3(C_3N_6H_3)$. Copper(I) chloride and $Na(HCN_2)$ in a stoichiometric ratio of 1:1 were mixed in an agate mortar under a dry atmosphere in a glovebox (total mass of 1 g). Silica tubes with 8 cm length, outer diameter of 10 mm, and inner diameter of 7 mm (handmade) were used as containers for the reaction and sealed under a vacuum. The product was obtained by heating the mixture to 200 °C in a Carbolite oven and maintaining this temperature for 45 h with a heating rate of 2 K min^{-1} and a cooling ramp of 0.5 K min^{-1}. The experimental theoretical yield of $Cu_3(C_3N_6H_3)$ is estimated >90%.

4.3. Scaling Up Synthesis. A 3 g portion of CuCl and 1.949 g of $Na(HCN_2)$ were mixed under similar conditions mentioned above. The powder was sealed into the silica tubes with 9 cm length, outer diameters of 16 mm (inner diameter of 13 mm) and heated to 200 °C in a Carbolite oven for 45 h.

4.4. Washing and Drying Procedure. The synthesized sample of $Cu_3(C_3N_6H_3)$ and NaCl was carefully washed several times with methanol to remove NaCl (theoretical yield from scale-up synthesis: 91.48%). Then, a 500 mg portion of the powder was transferred into a Schlenk tube and soaked in 30 mL of each solvent sequentially: acetonitrile, acetone, THF, and pentane. The powder was left in each solvent overnight. After each soaking period, the solvent was removed under vacuum before the next solvent was added under an argon atmosphere. After washing, the dried powder was transferred into a glass boat in the glovebox. The glass boat was then placed into a vacuum tube at 260 °C for 4 weeks.

4.5. X-ray Powder Diffraction. The XRD analysis of the $Cu_3(C_3N_6H_3)$ sample was conducted using a powder diffractometer (STOE Darmstadt, STADIP, Ge-monochromator) with Cu−Kα_1 (λ = 154.0598 pm) radiation, covering the 2θ range of 5−70 or 100°. To compare the obtained patterns with the crystal structure, the Match3! Software[47] was used.

4.6. Thermoanalytic Studies. The DTA measurements were carried out using a Netzsch Jupiter, STA 449 F3 device. Samples were fused into specially crafted silica containers and subjected to heating and cooling at a rate of 2 K/min, allowing analysis within the temperature range from ambient temperature to 600 °C.

4.7. Infrared Spectra. Infrared spectra were recorded using a VERTEX 70 FT-IR spectrometer in the range of 400−4000 cm^{-1} using KBr pellets of $Na(HCN_2)$ and $Cu_3(C_3N_6H_3)$. Samples were handled in a glovebox under an argon atmosphere.

4.8. Optical Measurements. Excitation and emission spectra of $Cu_3(C_3N_6H_3)$ powder samples were collected employing a fluorescence spectrometer, FLS920 (Edinburgh Instruments), which is equipped with a 450 W xenon discharge lamp (OSRAM) and a cryostat "MicrostatN" from Oxford Instruments serving as the sample chamber for atmospheric and temperature adjustments during measurements. A mirror optic was specifically utilized for the powder samples. Detection was carried out using a Hamamatsu R2658P single-photon-counting photomultiplier tube. All photoluminescence spectra were recorded with a spectral resolution of 1 nm, a dwell period of 0.5 s in 1 nm steps, and two repeats. The photoluminescence decay curve was measured using the same spectrometer and a 445 nm picosecond laser.

4.9. Magnetic Studies. Magnetic susceptibility measurements for $Cu_3(C_3N_6H_3)$ were conducted using a Quantum Design MPMS superconducting quantum interference device (SQUID) magnetometer within the temperature range from 1.8 to 300 K. The samples were affixed with diluted superglue (using acetone as the solvent) and

https://doi.org/10.1021/acs.inorgchem.4c01658
Inorg. Chem. 2024, 63, 19053−19062

subsequently dried under argon flow. The sample capsule was placed in a straw and holder for the MPMS device. To account for any interference, the slight diamagnetic signal from the capsule, holder, and remaining superglue was subtracted during the evaluation. The normalized data is presented relative to a magnetic field of 0.5T per mole.

4.10. Solid-State Nuclear Magnetic Resonance. All NMR spectra were acquired on a Bruker 500 Avance III (B_0 = 11.7 T) with a 2.5 mm triple-resonance MAS probe at ambient temperature. ^{1}H MAS NMR spectra were collected with a 30 kHz sample spinning rate by using a rotor-synchronized Hahn-echo pulse sequence. For the $Cu_3(C_3N_6H_3)$ samples, 512 transients were coadded with a 2 s recycle delay; for melamine (Thermo Scientific, 99% purity), the ^{1}H MAS NMR spectrum was acquired by coadding 64 transients with an 800 s recycle delay. Spin−lattice relaxation times were measured by using inversion recovery. $^{13}C\{^{1}H\}$ cross-polarization (CP) MAS NMR spectra of the $Cu_3(C_3N_6H_3)$ samples were acquired at 20 kHz spinning rates, with 4000 coadded transients separated by a 2 s recycle delay and an optimized contact time of 1.2 ms. For melamine, 60 transients were coadded with a recycle delay of 1000 s and an optimized contact time of 3.0 ms. ^{23}Na MAS NMR at a 15 kHz sample spinning rate was done using short (30°) polarization pulses to ensure uniform excitation, coadding 256 transients with a 15 s recycle delay. Sample masses differed by <1% to facilitate direct comparisons of absolute intensities. Chemical shifts are referenced to TMS (^{1}H and ^{13}C) and 0.1 M NaCl (^{23}Na).

■ ASSOCIATED CONTENT

Data Availability Statement

Data is contained within the article and Supporting Information.

Supporting Information

The Supporting Information is available free of charge at https://pubs.acs.org/doi/10.1021/acs.inorgchem.4c01658.

XRD pattern of compounds (Figures S1−S2−S5), ^{23}Na MAS NMR spectra, thermal gravimetric analysis, and temperature-dependent emission spectrum of $Cu_3(C_3N_6H_3)$ (PDF)

■ AUTHOR INFORMATION

Corresponding Author

Hans-Jürgen Meyer − *Section for Solid State and Theoretical Inorganic Chemistry, Institute of Inorganic Chemistry, Eberhard Karls Universität Tübingen, 72076 Tübingen, Germany;* orcid.org/0000-0003-2450-4011; Email: juergen.meyer@uni-tuebingen.de

Authors

Elaheh Bayat − *Section for Solid State and Theoretical Inorganic Chemistry, Institute of Inorganic Chemistry, Eberhard Karls Universität Tübingen, 72076 Tübingen, Germany*

Markus Ströbele − *Section for Solid State and Theoretical Inorganic Chemistry, Institute of Inorganic Chemistry, Eberhard Karls Universität Tübingen, 72076 Tübingen, Germany;* orcid.org/0000-0002-5147-5677

Mojtaba Abbasi − *Department of Chemistry, University of Manitoba, Winnipeg, Manitoba R3T 2N2, Canada*

Scott Kroeker − *Department of Chemistry, University of Manitoba, Winnipeg, Manitoba R3T 2N2, Canada;* orcid.org/0000-0003-1986-2797

Jaroslav Valenta − *Research Center for Materials Nanoarchitectonics (MANA), National Institute for Materials Science (NIMS), Ibaraki 305-0044, Japan;* orcid.org/0000-0002-2268-7187

David Enseling − *Department of Chemical Engineering, FH Münster University of Applied Sciences, 48565 Steinfurt, Germany*

Thomas Jüstel − *Department of Chemical Engineering, FH Münster University of Applied Sciences, 48565 Steinfurt, Germany*

Complete contact information is available at: https://pubs.acs.org/10.1021/acs.inorgchem.4c01658

Author Contributions

Conceptualization, supervision, funding acquisition, review and editing, H.-J. M.; synthesis, sample preparations, X-ray studies, IR, and writing, E.B.; X-ray diffraction and modeling, M.S.; magnetic measurement, J.V.; solid-state NMR section, M.A., and S.K., photoluminescence spectroscopy, T.J. and D.E. All authors have read and agreed to the published version of the manuscript.

Funding

This research is supported by the Deutsche Forschungsgemeinschaft (DFG) through grant ME 914/34-1.

Notes

The authors declare no competing financial interest.

■ ACKNOWLEDGMENTS

Funding by the Deutsche Forschungsgemeinschaft through grant ME 914/34-1 is gratefully acknowledged. We like to thank Prof. Takao Mori and Dr. Naohito Tsujii (National Institute for Materials Science (NIMS), Tsukuba, Japan) for magnetic measurements, Dr. Jochen Glaser (Univ. Tübingen) for fruitful discussions and suggestions, and Dr. Olexandr Kysliak (Univ. Tübingen) for his preparative support. S.K. acknowledges the Natural Sciences and Engineering Research Council (NSERC) of Canada and the Canada Foundation for Innovation (CFI) for generous support.

■ REFERENCES

(1) Crews, G. M.; Ripperger, W.; Kersebohm, D. B.; Güthner, T.; Mertschenk, B. Melamine and guanamines. In *Ullmann's Encyclopedia of Industrial Chemistry*; Wiley, 2000.

(2) Keßler, F. K. Structure and reactivity of s-triazine-based compounds in C/N/H chemistry. Doctoral dissertation; lmu, 2019.

(3) Klason, P. Über Melamverbindungen. *Journal für Praktische Chemie* **1886**, *33* (1), 285−289.

(4) Michaud, H.; Ortenburger, G.; Poschinger, W.; Rock, H.; Seeholzer, J. Method of preparing melamine from cyanamide and/or Dicyandiamide, U.S. Patent 4,069,383, 1978.

(5) Paden, J. H.; Mackay, J. S.*Greenwich, Conn. Preparation of Melamine*; A Corporation of Maine(patent): New York, N.Y., Serial No. 495,216, 1943.

(6) Chapman, R.; Averell, P.; Harris, R. Solubility of melamine in water. *Industrial & Engineering Chemistry* **1943**, *35* (2), 137−138.

(7) Zhu, H.; Yu, Z.; You, X.; Hu, H.; Huang, X. The crystal and molecular structure of bis (melamine) silver(I)perchlorate, Ag-$(C_3H_6N_6)$ $2ClO_4$. *Journal of chemical crystallography* **1999**, *29*, 239−242.

(8) Baraka, A.; Hatem, H.; El-Geundi, M. S.; Tantawy, H.; Karaghiosoff, K.; Gobara, M.; Elbeih, A.; Shoaib, M.; Elsayed, M. A.; Kotb, M. M. A new cationic silver(I)/melamine coordination polymer,$[Ag_2$ (melamine)$]_n^{2n+}$: Synthesis, characterization and potential use for aqueous contaminant anion exchange. *J. Solid State Chem.* **2019**, *274*, 168−175.

(9) Zhang, L.; Li, W.; Zhang, J.; Li, Z.-J.; Qin, Y.-Y.; Cheng, J.-K.; Yao, Y.-G. Antiferromagnetic interactions in melamine-bridged

trinuclear cobalt complex. *Inorg. Chem. Commun.* **2008**, *11* (3), 279−282.
(10) Dorta, R.; Stoeckli-Evans, H.; Bodensieck, U.; Süss-Fink, G. Fixation of triruthenium clusters on melamine: synthesis and structure of $[Ru_3(\mu_2\text{-}H)(CO)_9\ \{\mu_3,\ \eta_2\text{-}NHC_3N_3(NH_2)_2\}]$, cis-$[\{Ru_3\ (\mu_2\text{-}H)(CO)_9\}_2\ \{\mu_3,\ \eta_2\text{:}\ \mu_3,\ \eta_2\text{-}NHC_3N_3(NH_2)\}]$ and trans-$[\{Ru_3\ (\mu_2\text{-}H)(CO)_9\}_2\ \{\mu_3, \eta_2\text{:}\ \mu_3, \eta_2\text{-}NHC_3N_3(NH_2)\}]$. *Journal of organometallic chemistry* **1998**, *553* (1−2), 307−315.
(11) Wiles, A. B.; Bozzuto, D.; Cahill, C. L.; Pike, R. D. Copper (I) and (II) complexes of melamine. *Polyhedron* **2006**, *25* (3), 776−782.
(12) Goodgame, D. M.; Hussain, I.; White, A. J.; Williams, D. J. Synthesis and structure of a copper(II)melamine complex,$[Cu(C_3H_6N_6)(\mu\text{-}OCH_3)(ONO_2)(HOCH_3)]_2$, with direct Cu−melamine coordination. *J. Chem. Soc., Dalton Trans.* **1999**, *17*, 2899−2900.
(13) Zhang, L.; Zhang, J.; Li, Z.-J.; Cheng, J.-K.; Yin, P.-X.; Yao, Y.-G. New Coordination Motifs of Melamine Directed by N−H···X (X = Cl or Br) Hydrogen Bonds. *Inorganic chemistry* **2007**, *46* (15), 5838−5840.
(14) Kallenbach, P.; Bayat, E.; Ströbele, M.; Romao, C. P.; Meyer, H. J. Tricopper melaminate, a metal−organic framework containing dehydrogenated melamine and Cu−Cu bonding. *Inorg. Chem.* **2021**, *60* (21), 16303−16307.
(15) Ullah, S.; Bustam, M.; Nadeem, M.; Naz, M.; Tan, W.; Shariff, A. Synthesis and thermal degradation studies of melamine formaldehyde resins. *Sci. World J.* **2014**, *2014*, No. 940502.
(16) Hirt, R.; Steger, J.; Simard, G. Vapor pressure of 2, 4, 6-triamino-s-triazine (melamine). *J. Polym. Sci.* **1960**, *43* (142), 319−323.
(17) Ma, D.; Huang, X.; Zhang, Y.; Wang, L.; Wang, B. Metal-organic frameworks: Synthetic methods for industrial production. *Nano Research* **2023**, *16* (5), 7906−7925.
(18) Cheong, V. F.; Moh, P. Y. Recent advancement in metal−organic framework: synthesis, activation, functionalisation, and bulk production. *Mater. Sci. Technol.* **2018**, *34* (9), 1025−1045.
(19) Rubio-Martinez, M.; Avci-Camur, C.; Thornton, A. W.; Imaz, I.; Maspoch, D.; Hill, M. R. New synthetic routes towards MOF production at scale. *Chem. Soc. Rev.* **2017**, *46* (11), 3453−3480.
(20) Kalmutzki, M.; Stroebele, M.; Wackenhut, F.; Meixner, A. J.; Meyer, H.-J. Synthesis, Structure, and Frequency-Doubling Effect of Calcium Cyanurate. *Angew. Chem., Int. Ed.* **2014**, *53* (51), 14260−14263.
(21) Kalmutzki, M.; Wang, X.; Meixner, A. J.; Meyer, H.-J. Second harmonic generation properties of $Ca_3(O_3C_3N_3)_2$-$Sr_3(O_3C_3N_3)_2$ solid solutions. *Crystal Research and Technology* **2016**, *51* (8), 460−465.
(22) Kalmutzki, M.; Ströbele, M.; Wackenhut, F.; Meixner, A. J.; Meyer, H.-J. Synthesis and SHG properties of two new cyanurates: $Sr_3(O_3C_3N_3)_2$ (SCY) and $Eu_3(O_3C_3N_3)_2$ (ECY). *Inorganic chemistry* **2014**, *53* (23), 12540−12545.
(23) Schnick, W.; Huppertz, H. Darstellung, Kristallstruktur und Eigenschaften von Kaliumhydrogencyanamid. *Zeitschrift für anorganische und allgemeine Chemie* **1995**, *621* (10), 1703−1707.
(24) Görne, A. L.; Scholz, T.; Kobertz, D.; Dronskowski, R. Deprotonating Melamine to Gain Highly Interconnected Materials: Melaminate Salts of Potassium and Rubidium. *Inorg. Chem.* **2021**, *60* (20), 15069−15077.
(25) Bayat, E.; Ströbele, M.; Meyer, H.-J. Unraveling the Synthesis of $SbCl(C_3N_6H_4)$: A Metal-Melaminate Obtained through Deprotonation of Melamine with Antimony(III)Chloride. *Chemistry* **2023**, *5* (2), 1465−1476.
(26) Becker, M.; Jansen, M. Synthesis and Characterization of $Na_5H(CN_2)_3$. *Journal of Chemical Research, Synopses* **1998**, *2*, 86−87.
(27) Ströbele, M.; Mos, A.; Meyer, H.-J. Cluster harvesting by successive reduction of a metal halide with a nonconventional reduction agent: a benefit for the exploration of metal-rich halide systems. *Inorg. Chem.* **2013**, *52* (12), 6951−6956.
(28) Pennington, W. T. DIAMOND−visual crystal structure information system. *J. Appl. Crystallogr.* **1999**, *32* (5), 1028−1029.
(29) Michaelis, V. K.; Greer, B. J.; Aharen, T.; Greedan, J. E.; Kroeker, S. Determining electron spin-transfer mechanisms in paramagnetic Ba_2YMO_6 (M= Mo, Re, Ru) double perovskites by ^{89}Y and ^{137}Ba MAS NMR spectroscopy. *J. Phys. Chem. C* **2012**, *116* (44), 23646−23652.
(30) Levin, K.; Kroeker, S. Probing Jahn-Teller distortions in $Mn(acac)_3$ through paramagnetic interactions in solid-state MAS NMR. *Solid State Nucl. Magn. Reson.* **2019**, *101*, 101−109.
(31) Jürgens, B.; Irran, E.; Senker, J.; Kroll, P.; Müller, H.; Schnick, W. Melem (2, 5, 8-triamino-tri-s-triazine), an important intermediate during condensation of melamine rings to graphitic carbon nitride: Synthesis, structure determination by X-ray powder diffractometry, solid-state NMR, and theoretical studies. *J. Am. Chem. Soc.* **2003**, *125* (34), 10288−10300.
(32) Lachenmeier, D. W.; Humpfer, E.; Fang, F.; Schütz, B.; Dvortsak, P.; Sproll, C.; Spraul, M. NMR-spectroscopy for non-targeted screening and simultaneous quantification of health-relevant compounds in foods: the example of melamine. *Journal of agricultural and food chemistry* **2009**, *57* (16), 7194−7199.
(33) Nandy, A.; Forse, A. C.; Witherspoon, V. J.; Reimer, J. A. NMR spectroscopy reveals adsorbate binding sites in the metal−organic framework UiO-66 (Zr). *J. Phys. Chem. C* **2018**, *122* (15), 8295−8305.
(34) Lotsch, B. V.; Schnick, W. New light on an old story: formation of melam during thermal condensation of melamine. *Chemistry−A. European Journal* **2007**, *13* (17), 4956−4968.
(35) Wen, J.; Li, R.; Lu, R.; Yu, A. Photophysics and photocatalysis of melem: a spectroscopic reinvestigation. *Chem.−Asian J.* **2018**, *13* (8), 1060−1066.
(36) Kessler, F. K.; Schuhbeck, A. M.; Schnick, W. Melamium Thiocyanate Melam, a Melamium Salt with Disordered Anion Sites. *Zeitschrift für anorganische und allgemeine Chemie* **2019**, *645* (12), 840−847.
(37) Davies, M.; Jones, W. J. The infra-red spectrum and structure of cyanamide and dimethylcyanamide. *Trans. Faraday Soc.* **1958**, *54*, 1454−1463.
(38) Jürgens, B.; Höppe, H. A.; Schnick, W. Synthesis, crystal structure, vibrational spectroscopy, and thermal behaviour of lead dicyanamide $Pb[N(CN)_2]_2$. *Solid state sciences* **2002**, *4* (6), 821−825.
(39) Zhang, J.-P.; Lin, Y.-Y.; Huang, X.-C.; Chen, X.-M. Copper(I)1, 2, 4-triazolates and related complexes: studies of the solvothermal ligand reactions, network topologies, and photoluminescence properties. *J. Am. Chem. Soc.* **2005**, *127* (15), 5495−5506.
(40) Shimada, K.; Kobayashi, A.; Ono, Y.; Ohara, H.; Hasegawa, T.; Taketsugu, T.; Sakuda, E.; Akagi, S.; Kitamura, N.; Kato, M. Core-structure-dependent luminescence of thiolato-bridged copper(I)-cluster complexes. *J. Phys. Chem. C* **2016**, *120* (29), 16002−16011.
(41) Allendorf, M. D.; Bauer, C. A.; Bhakta, R.; Houk, R. Luminescent metal−organic frameworks. *Chem. Soc. Rev.* **2009**, *38* (5), 1330−1352.
(42) Hu, Z.; Deibert, B. J.; Li, J. Luminescent metal−organic frameworks for chemical sensing and explosive detection. *Chem. Soc. Rev.* **2014**, *43* (16), 5815−5840.
(43) Mugiraneza, S.; Hallas, A. M. Tutorial: a beginner's guide to interpreting magnetic susceptibility data with the Curie-Weiss law. *Commun. Phys.* **2022**, *5* (1), 95.
(44) Coey, J. M. *Magnetism and magnetic materials*; Cambridge University Press, 2010.
(45) Sengupta, A.; Datta, S.; Su, C.; Herng, T. S.; Ding, J.; Vittal, J. J.; Loh, K. P. Tunable electrical conductivity and magnetic property of the two dimensional metal organic framework $[Cu(TPyP)\text{-}Cu_2(O_2CCH_3)_4]$. *ACS Appl. Mater. Interfaces* **2016**, *8* (25), 16154−16159.
(46) Navas, C.; Turnbull, M. M.; Giogas, C.; Landee, C. P.; Zhang, W.; Pon, G.; Willett, R. Synthesis, structure and magnetic studies of copper(II) and copper(I)complexes of methylpyrazines. *Polyhedron* **1993**, *12* (9), 1019−1026.
(47) Putz, H. B. K. Match! —Phase Analysis Using Powder Diffraction. In *Version 3.15.x*; Crystal Impact: Bonn, Germany, 2023.

https://doi.org/10.1021/acs.inorgchem.4c01658
Inorg. Chem. 2024, 63, 19053−19062

Supporting Information

High-Yield Synthesis Route, Post-Synthesis Treatment, and Insights into the Photoluminescence and Magnetic Properties of Tricopper(I) Melaminate $Cu_3(C_3N_6H_3)$

Elaheh Bayat,[a] Markus Ströbele,[a] Mojtaba Abbasi,[b] Scott Kroeker,[b] Jaroslav Valenta,[c] David Enseling,[d] Thomas Jüstel,[d] and Hans-Jürgen Meyer*,[a]

[a] Section for Solid State and Theoretical, Inorganic Chemistry, Institute of Inorganic Chemistry, Eberhard Karls Universität Tübingen, Auf der Morgenstelle 18, 72076 Tübingen (Germany), E-mail: juergen.meyer@uni-tuebingen.de

[b] Department of Chemistry, University of Manitoba, Winnipeg, Manitoba, R3T 2N2, Canada.

[c] Research Center for Materials Nanoarchitectonics (MANA), National Institute for Materials Science (NIMS), 1-2-1 Sengen, Tsukuba, Ibaraki 305-0044, Japan.

[d] Department of Chemical Engineering, FH Münster University of Applied Sciences, Stegerwaldstraße 39, 48565 Steinfurt, Germany.

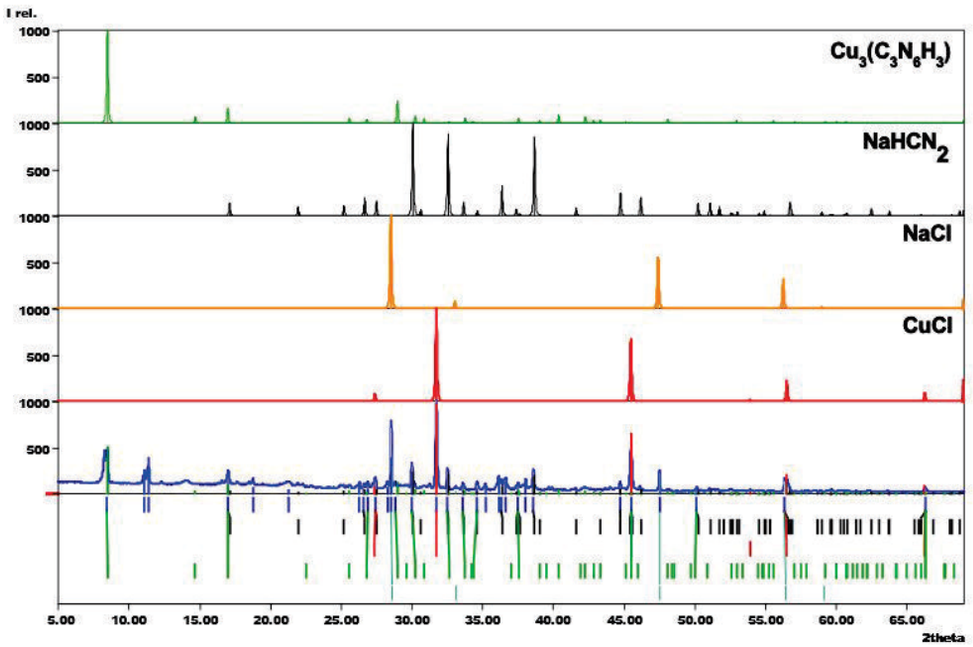

Figure S1. XRD pattern of the unknown intermediate phase (bottom) from the reaction of CuCl and $NaHCN_2$ at 150 °C.

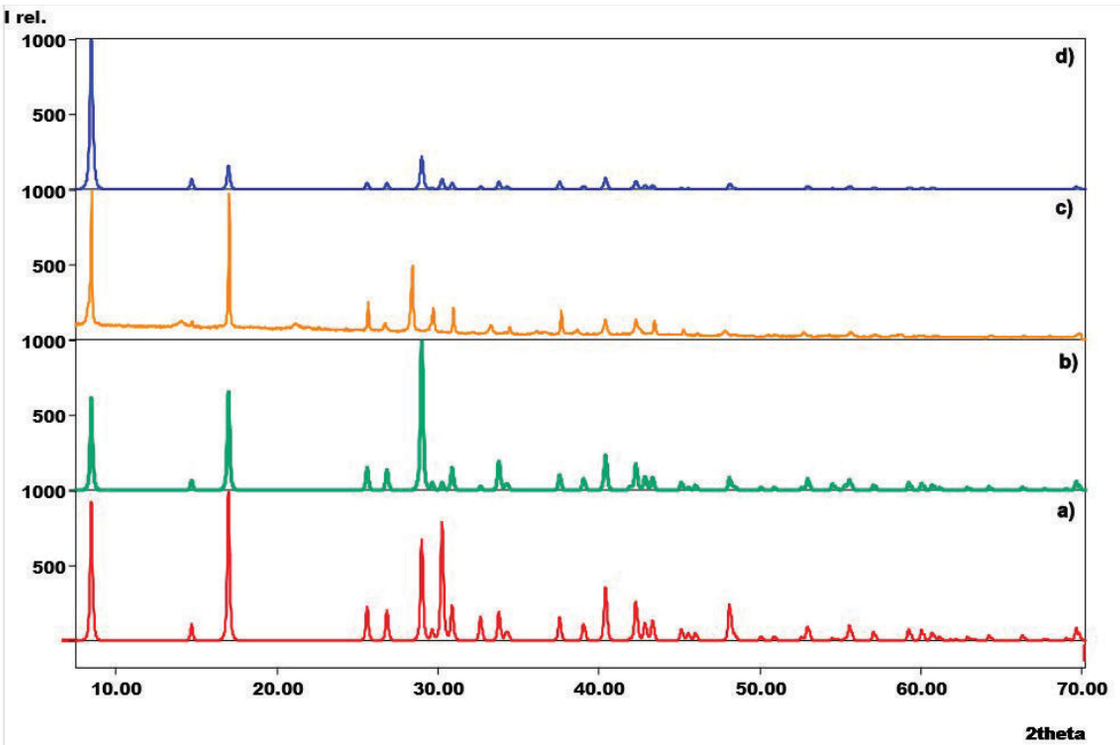

Figure S2. Calculated pattern from single crystal measurement of $Cu_3(C_3N_6H_3)$: **a)** with melamine in the channels; **b)** with melamine between the layers; c) experimental powder pattern of $Cu_3(C_3N_6H_3)$ (sample **2**) ; **(2) d)** with empty channels and layer distances (CCDC code: 2063421).

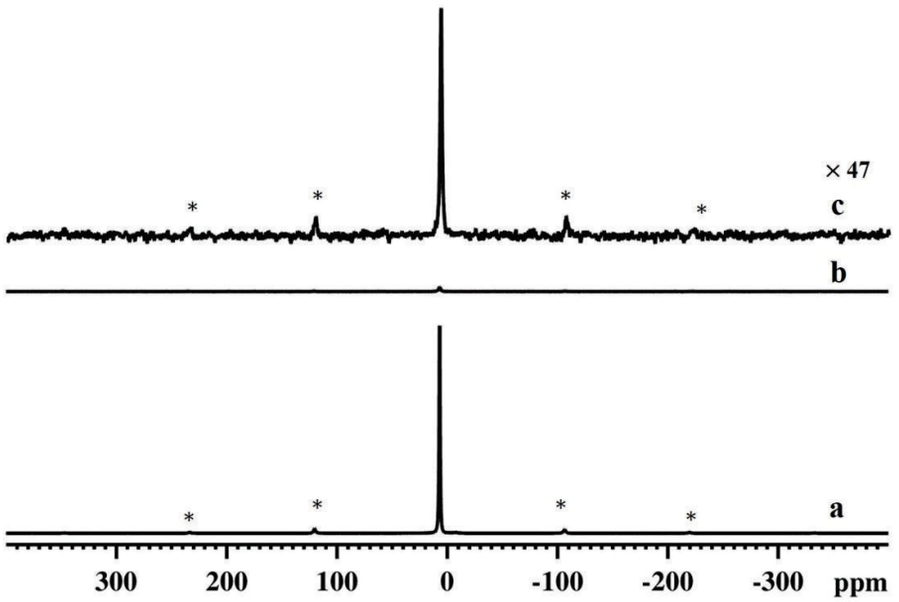

Figure S3. ^{23}Na MAS NMR spectra of (a) as-synthesized $Cu_3(C_3N_6H_3)$ (sample **1**), (b) the $Cu_3(C_3N_6H_3)$ sample after washing with methanol and vacuum-drying (sample **2**), (c) sample **2** with the vertical scale increased by a factor of X. Spinning sidebands are marked with asterisks.

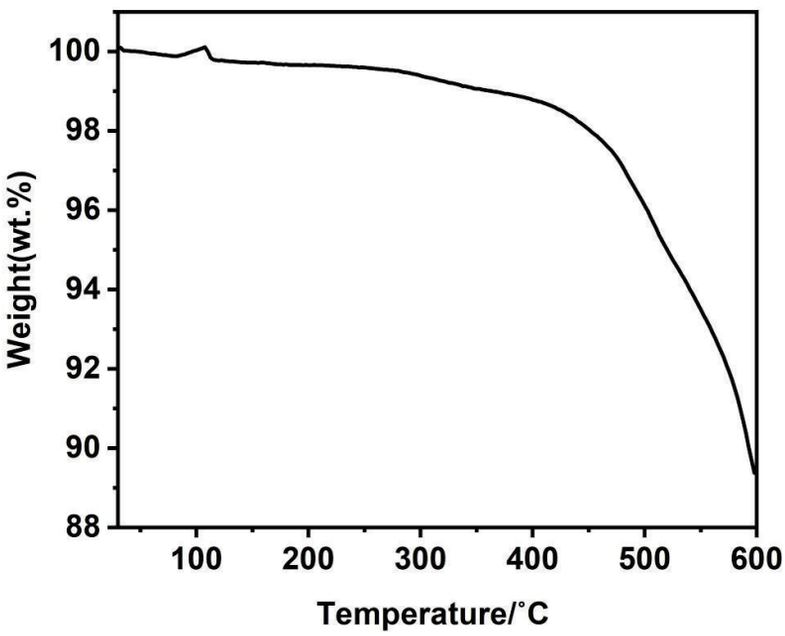

Figure S4. Thermal Gravimetric Analysis (TGA) of $Cu_3(C_3N_6H_3)$ (**1**).

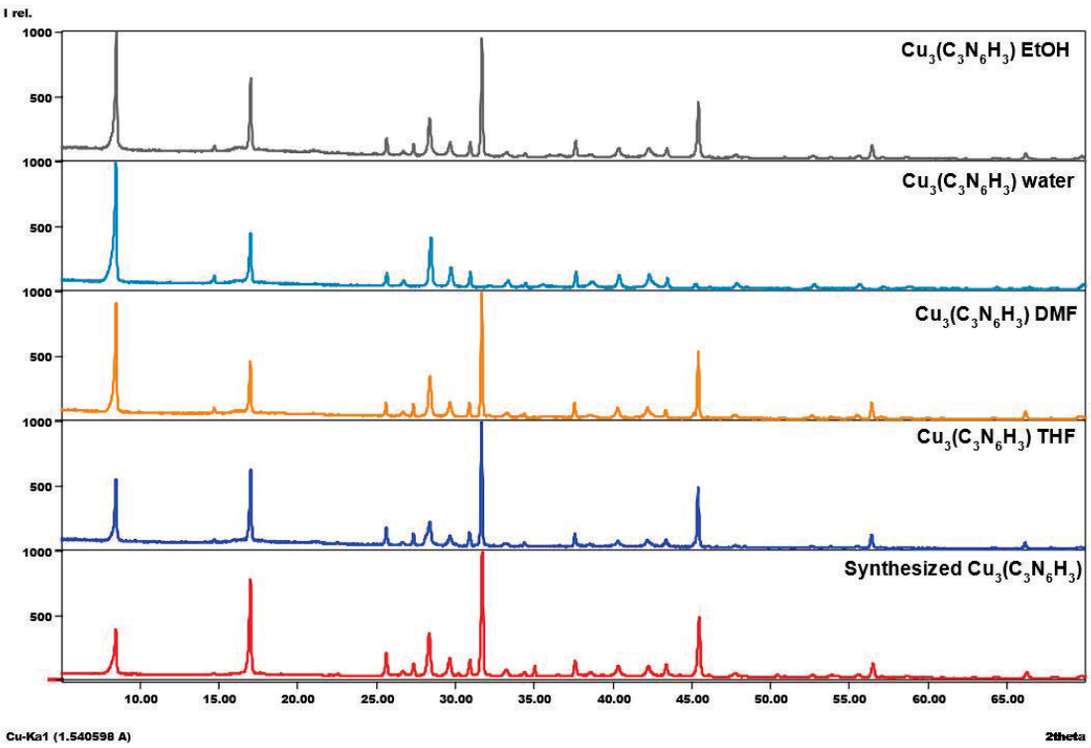

Figure S5. Comparsion of XRD pattern of the synthesized $Cu_3(C_3N_6H_3)$ washed with different solvents and then dried (under vaccum for 24h at 60˚C).

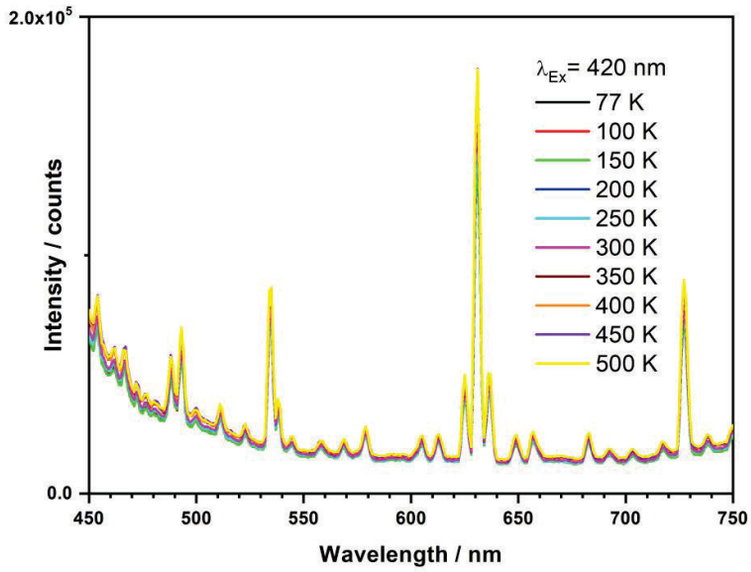

Figure S6. Temperature-dependent emission spectrum of $Cu_3(C_3N_6H_3)$ (**3**). The artifacts at around 630 nm and so on, are remnants of the excitation lamp spectrum due to the application of an imperfect correction function

Publication 3

Unraveling the Synthesis of $SbCl(C_3N_6H_4)$: A Metal-Melaminate Obtained through Deprotonation of Melamine with Antimony(III)Chloride

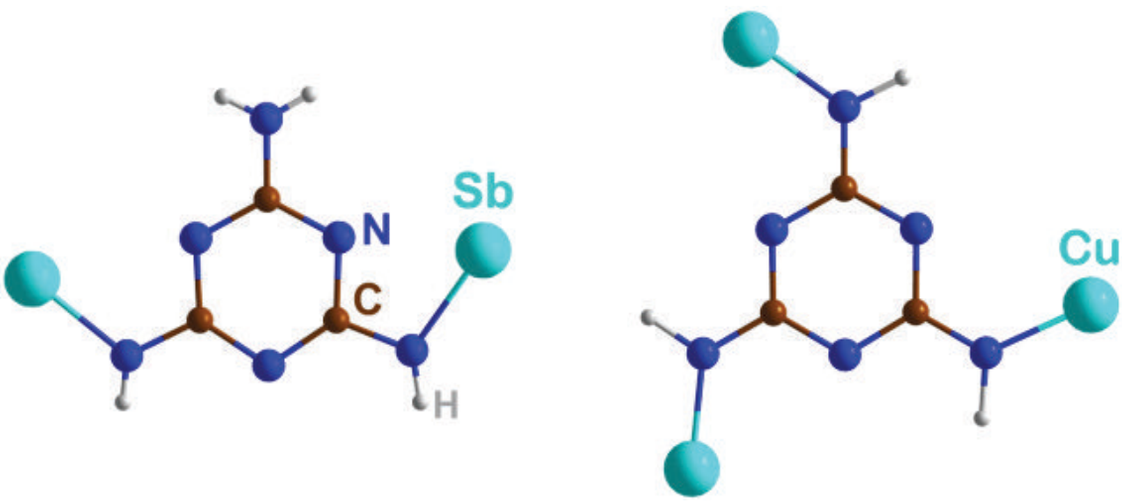

https://doi.org/10.3390/chemistry5020099

Reprinted with permission from

Chemistry ***2023****, 5, 1465-1476*

chemistry

MDPI

Article

Unraveling the Synthesis of $SbCl(C_3N_6H_4)$: A Metal-Melaminate Obtained through Deprotonation of Melamine with Antimony(III)Chloride

Elaheh Bayat, Markus Ströbele and Hans-Jürgen Meyer *

Section for Solid State and Theoretical Inorganic Chemistry, Institute of Inorganic Chemistry, University of Tübingen, Auf der Morgenstelle 18, 72076 Tübingen, Germany
* Correspondence: juergen.meyer@uni-tuebingen.de

Abstract: The discovery of melamine by Justus von Liebig was fundamental for the development of several fields of chemistry. The vast majority of compounds with melamine or melamine derivatives appear as adducts. Herein, we focus on the development of novel compounds containing anionic melamine species, namely the melaminates. For this purpose, we analyze the reaction of $SbCl_3$ with melamine by differential scanning calorimetry (DSC). The whole study includes the synthesis and characterization of three antimony compounds that are obtained during the deprotonation process of melamine to melaminate with the reaction sequence from $SbCl_4(C_9N_{18}H_{19})$ (**1**) via $(SbCl_4(C_6N_{12}H_{13}))_2$ (**2**) to $SbCl(C_3N_6H_4)$ (**3**). Compounds are characterized by single-crystal X-ray diffraction (SXRD), powder X-ray diffraction (PXRD), and infrared spectroscopy (IR). The results give an insight into the mechanism of deprotonation of melamine, with the replacement of one, two, or eventually three hydrogen atoms from the three amino groups of melamine. The structure of (**3**) suggests that metal melaminates are likely to form supramolecular structures or metal-organic frameworks (MOFs).

Keywords: melaminate; antimony; melamine; melaminium; deprotonation; crystal structures

Citation: Bayat, E.; Ströbele, M.; Meyer, H.-J. Unraveling the Synthesis of $SbCl(C_3N_6H_4)$: A Metal-Melaminate Obtained through Deprotonation of Melamine with Antimony(III)Chloride. *Chemistry* **2023**, *5*, 1465–1476. https://doi.org/10.3390/chemistry5020099

Academic Editors: Christoph Janiak, Sascha Rohn and Georg Manolikakes

Received: 4 May 2023
Revised: 12 June 2023
Accepted: 14 June 2023
Published: 20 June 2023

1. Introduction

In the 19th century, the foundation of amine-substituted s-triazine derivatives was laid for the first time by Liebig and Gmelin [1–3] with the synthesis of melamine, melam, melem and their condensation product called melon. Melamine (1,3,5-triazine-2,4,6-triamine) is the simplest and most intensively studied C/N/H compound synthesized from potassium thiocyanate and ammonium chloride for the first time (1834) by Liebig [1,4]. However, it can also be easily achieved with trimerization of cyanamide (CN_2H_2), while today, industrial productions take place from urea in tons [5–7]. Melamine has a relatively high-melting point for an organic compound and undergoes condensation reactions on heating. The condensation products melem, melam, and melon (Figure 1) of this ancestry compound have been studied extensively using various spectroscopy techniques [8,9]. For a long period, thermal condensation was not fully understood due to the chemical inertness and low solubility of these products [10]. In 1959, May conducted a study on the pyrolysis of melamine at temperatures between 200 °C and 500 °C [11]. Afterward, this process was investigated by several scientists, particularly by Schnick and Lotsch [12,13]. The temperature-programmed XRD (TPXRD) was used in the temperature range between 25 °C and 660 °C to clarify the exact temperatures of formation of condensed products, which shows that the sublimation temperature of melamine is approximately 360–370 °C at atmospheric pressure. However, TPXRD in semi-closed systems shows that the X-ray reflections of melamine disappear at 296 °C, and then melamine forms melam and melem, which are stable up to 379 °C [13]. Pure melem, which consists of internally hydrogen-

bonded heptazine molecules, can be obtained at 379 °C and is stable up to 500 °C. The polymeric carbon nitride material melon is also achieved with further heating [13].

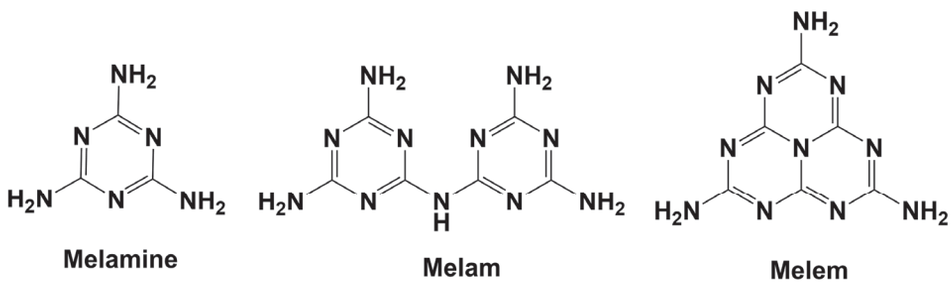

Figure 1. Molecular structures of melamine ($C_3N_6H_6$), melam ($C_6N_{11}H_9$) and melem ($C_6N_{10}H_6$).

In addition to the many applications melamine has, such as surface coating [14], flame redundancy [14–17], and heavy metal removal [18,19], it has some unique characteristics which make it a relevant research topic up to this day. The most important potential of melamine is its ability to create a metal-organic framework (MOF) [20] or porous-organic framework (POFs) [21] by the formation of metal melaminates.

Justus von Liebig's discovery of melamine was essential in the progress of C/N/H chemistry. Most melamine-containing compounds and their derivatives are found as adducts. Cationic C/N/H ions are present in various molecular compounds, including melamine, melam, and melem. These ions are formed by protonating the ring nitrogen atoms, which are more basic than the terminal amino groups. The most common cations are monoprotonated, but di- or trications have also been observed. More research into the chemistry of these substances led to the discovery of melaminium [22–26], melamium, and melemium salts. By far, the majority of salts were produced by melamine, including melaminium sulfate [27], melaminium nitrate, melaminium phosphates [16,28], melaminium chloride [29], organic slats of phthalates [30], benzoates, or citrates [31], and many inorganic salts containing complex anions [32,33]. On the other hand, a small number of melamium salts have been studied, such as melamium bromide and iodide [26]. Recently, melemium salts, namely melemium sulfate, triple protonated melemium methylsulfonate, and melemium perchlorate, are also discovered [34,35]. Melamine was also reported to coordinate with metal halides to form organic-inorganic hybrid copper halides such as $Cu_2Br_2(C_3N_6H_7)]_n$, $[Cu_3Cl_3(C_3N_6H_7)]_n$ [36], the silver complex $[Ag(C_3N_6H_6)(H_2O)(NO_3)]_n$, and the mercury compound $(C_3N_6H_7)(C_3N_6H_6)HgCl_3$ [37], which have biochemical applications and nonlinear optical properties [38,39].

Regarding the basic property of melamine, protonation is easy, and a great variety of such compounds, either theoretically or experimentally, have been investigated [25,26,40,41]. A new class of chemistry related to melaminates (deprotonated melamine) has received less attention until now; however, it is very important from either a chemistry or application perspective. The coordination behavior of molecules such as guanidine or melamine, capable of forming extended hydrogen bonds, can be changed by deprotonation [36,42]. Thus, it is a promising strategy for synthesizing interconnected supramolecular structures or MOFs. Despite the challenge which arises from the rigidity of its heterocyclic structure, the affinity of ring-N atoms to act as H-bond acceptors, and the steric hindrance of neighboring amino groups [35], the deprotonation of melamine seems to be plausible since guanidine (a stronger base) has already been deprotonated twice [43]. Franklin pioneered the work on anionic melaminate by synthesizing two compounds of $K(C_3N_6H_5)\cdot NH_3$ and $K_3(C_3N_6H_3)$ [44,45] in liquid ammonia. However, these compounds were only characterized using elemental analyses, and no crystallographic structure information was provided. Later, Dronskowski and coworkers confirmed the presence of the two ammonia adducts, $K(C_3N_6H_5)\cdot NH_3$ and $Rb(C_3N_6H_5)\cdot\frac{1}{2}NH_3$ by single-crystal X-ray diffraction. Ammonia-free $K_3(C_3N_6H_3)$ has been assigned by its characteristic infrared bands, being compared with

calculated bands from density-functional theory (DFT) [42]. There was no further research reported on these classes of compounds and their properties until the discovery and identification of the copper melaminate $Cu_3(C_3N_6H_3)$ with a layered framework structure by Meyer & coworkers [20].

In this work, the step-wise deprotonation of melamine in a solid state has been studied by thermal analysis. Herein, antimony (III) chloride is used for the deprotonation of melamine due to its low melting point of 73.4 °C [46]. The recorded reaction sequence shows three compounds that were prepared and later characterized by powder X-ray diffraction (PXRD), single-crystal diffraction, and IR measurements. The structure of $SbCl(C_3N_6H_4)$ suggests the potential of synthesizing interconnected supramolecular structures or metal-organic frameworks (MOFs).

2. Materials and Methods

2.1. Materials

The starting materials, melamine (2,4,6-triamino-1,3,5-triazine, purchased from Sigma-Aldrich, 99%), and antimony(III)chloride (Sigma-Aldrich, 99%), ammonium chloride (Sigma-Aldrich, 99.99%) were used without further purification. The reaction mixtures were prepared under an argon atmosphere in a glovebox with moisture and oxygen levels below 1 ppm and transferred into homemade silica tubing (inner diameter 13 mm and 7 mm) and sealed under vacuum. The reactions were carried out in Simon–Müller and Carbolite chamber furnaces.

2.1.1. Synthesis

Synthesis of $SbCl_4(C_9N_{18}H_{19})$ (1):

Precursors were pestled in an agate mortar with a 1:4 molar ratio of antimony(III)chloride and melamine. A mixture of antimony(III) chloride and melamine with a total mass of ≈200.0 mg was transferred into a homemade silica ampule and sealed therein under vacuum. The ampoule was placed into a Simon–Müller furnace and heated to 200 °C for 20 h with a heating rate of 2 °C/min and cooling ramp of 0.5 °C/min (Figure S1). The reaction produced a white color product crystallized on the top of the ampule (>90% yield w.r.t Sb). A temperature gradient seemed to play an essential role in the separation of the product (**1**).

The solubility of compound (**1**) has been investigated in acetonitrile, THF, DCM, ethanol, methanol, and water. The PXRD measurements showed the decomposition of this product to unknown phases.

Synthesis of $(SbCl_4(C_6N_{12}H_{13}))_2$ (2):

Similar to the previous preparation, the mixture of antimony (III)chloride and melamine was mixed in a 1:2 molar ratio (total mass of ≈200.0 mg) and heated to 200 °C for 20 h with a heating and cooling rate of 2 °C/min (Figure S1). The product was X-ray amorphous powder and contained transparent single crystals of (**2**) (10% w.r.t Sb).

Synthesis of $SbCl(C_3N_6H_4)$ (3):

The structure of (**3**) was obtained from both (1:2 and 1:4) ratios of antimony(III)chloride and melamine by heating the 1:2 ratio at 250 °C for 20 h, or by heating the 1:4 ratio at 280 °C for 20 h (Figure S1). The beige color product was isolated in 50% yield w.r.t Sb.

The solubility of compound (**3**) has been studied in many solvents. The powder was soaked for one hour in acetonitrile, THF, DMF, DCM, ethanol, methanol, water, and diluted acetic acid. Subsequent PXRD measurements were undertaken. The results showed that compound (**3**) remains stable in acetonitrile, THF, DMF, DCM, ethanol, and methanol. However, in water and DMSO, compound (**3**) decomposes and forms Sb_2O_3 and an unknown phase, respectively. The schematic synthesis of all three compounds is presented in Figure S1.

2.1.2. X-ray Powder Diffraction

The X-ray diffraction of prepared powders was recorded with a powder diffractometer (STOE Darmstadt, STADIP, Ge-monochromator) using Cu-$K_{\alpha 1}$ (λ = 1.540598 Å) radiation

in the range of $5 < 2\theta < 120°$. Match3! Software [47] was used to compare the patterns with patterns of the corresponding crystal structures.

2.1.3. Single-Crystal X-ray Diffraction

Single Crystals of (**1**), (**2**), and (**3**) were selected and placed on a single-crystal X-ray diffractometer (Rigaku XtaLab Synergy-S) with Cu-K_α radiation (λ = 1.54184 Å) and a mirror monochromator at 150 or 220 K. Crystal structures were solved by direct methods (SHELXT) [48], followed by full-matrix least-squares structure refinements (SHELXL-2014) [49]. The absorption correction of X-ray intensities was performed with numerical methods using the CrysAlisPro 1.171.41.92a software (Rigaku Oxford Diffraction). Hydrogen atoms were found in the difference map and refined therefrom isotropically.

2.1.4. Thermoanalytic Studies

Differential scanning calorimetry (DSC) was carried out using a DSC 204 F1 Phoenix (Fa. Netzsch, Selb, Germany). The starting materials were enclosed under Ar in a glovebox into gold-plated (5 µm) steel autoclaves with a volume of 100 µL (Bächler Feintech AG in Hölstein, Switzerland). The reactions of $SbCl_3$ with melamine were analyzed for different ratios between room temperature and 500 °C at a heating and cooling rate of 2 °C/min.

2.1.5. Infrared Spectra

The infrared (IR) spectra of samples were recorded with a Bruker VERTEX 70 FT-IR spectrometer within the spectra range of 400−4000 cm^{-1}. Tablets of KBr were used as a background.

3. Results and Discussion

3.1. Thermoanalytic Studies

Thermal analyses based on DSC and DTA have been shown to be highly insightful regarding the examination of reaction sequences [50,51] and for comprehensive studies of binary or ternary systems [52], especially when combined with PXRD studies. Following this method, the formation or decomposition of a crystalline species is usually indicated by a thermal event, and the newly formed species is characterized by X-ray diffraction techniques.

The differential scanning calorimetric (DSC) measurements of 1:2 and 1:4 molar mixtures of antimony chloride and melamine are shown in Figure 2, with heating and cooling rates of 2 °C/min. The DSC patterns display a small exothermic peak at around 70 °C, which can be attributed to the melting point of antimony(III)chloride. Figure 2a,b show multiple exothermic effects between 200 °C and 300 °C. The resolution of thermal events in this region is rather poor and cannot be significantly improved by changing the heating ramp. For example, we have explored different heating rates throughout. At lower heating rates, the signals were smeared out and were not as sharp as the signals shown in Figure 2a,b, so the resolution was worse. The presented heating rate is the optimized heating rate with respect to the signal-to-noise ratio. Moreover, the effects are slightly different for different ratios of starting materials, with lower reaction temperatures in the presence of more melamine.

Powder XRD patterns were recorded on samples obtained under conditions given in the DSC experiments, being interrupted at certain temperatures, especially in the temperature region between 200 °C and 280 °C. Compound (**1**) was already formed at 200 °C from a 1:4 ratio of starting materials, and compound (**2**) was observed in the XRD pattern from a 1:2 ratio at the same temperature. Compound (**3**) was identified at around 280 °C from a 1:4 ratio of starting materials or, alternatively, at 250 °C from a 1:2 ratio. The endothermic peaks at 370 °C indicate the melting/decomposition of (excess) melamine, which appears sharper for the 1:4 ratio due to the larger amount of melamine. This assignment is confirmed by a DSC of melamine (Figure S2), which shows a similar endothermic peak with a slight shift at 361 °C. At slightly higher temperatures, compound (**3**) is decomposed, which is followed by a strong exothermic peak at 400 °C and 417 °C for the 1:4 and a 1:2 ratio, respectively.

These intense exothermic peaks led to the formation of a phase with a yellow color (**4**) that looked glassy under the microscope. This was further studied by means of IR spectroscopy (see the relevant section).

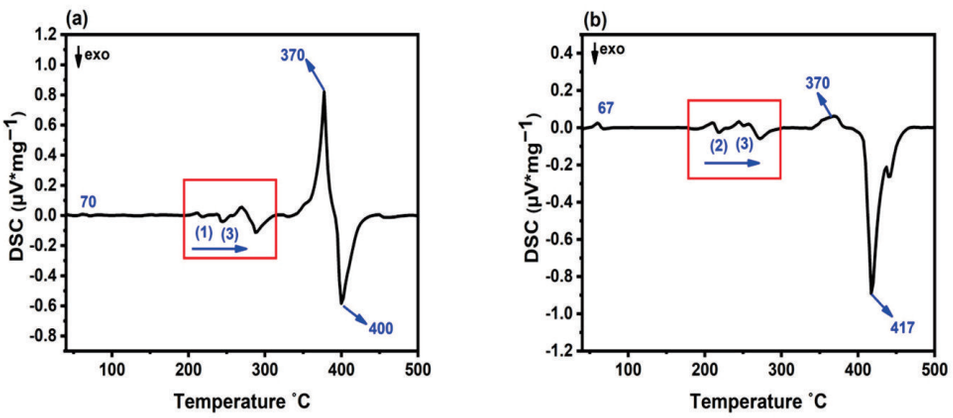

Figure 2. (**a**) DSC of the reaction of $SbCl_3$ and melamine in a ratio of 1:4, (**b**) DTA of the reaction of $SbCl_3$ and melamine in a ratio of 1:2.

From this study, we note that reactions in the given system proceed very quickly, almost simultaneously, making the assignment of compounds and their preparations challenging. This is due to the high reactivity of reaction partners.

3.2. Crystal Structures

Crystal structures of all three compounds (**1**), (**2**), and (**3**) were solved and refined based on single-crystal X-ray diffraction data with triclinic ($P\bar{1}$) and monoclinic ($P2_1/c$ and $P2_1/n$) space groups, respectively, with crystallographic details summarized in Table 1 and relevant distances given in Table 2. The asymmetric unit of each compound is shown in Figure S3.

The crystal structure of (**1**) is composed of one deprotonated melamine, two protonated melamine and a single chloride ion besides $SbCl_3$ to make up $SbCl_4(C_3N_6H_5)(C_3N_6H_7)_2$. The crystal structure contains a sequence of three distinct layers stacked on top of each other (along *b*); one of them is displayed in Figure 3. Stacking behavior is most common for melamine-based structures.

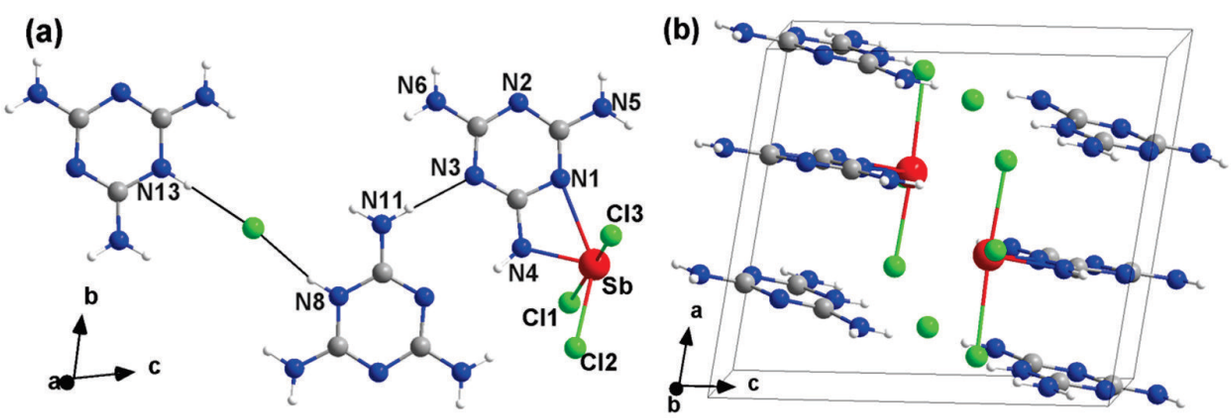

Figure 3. (**a**) Constituents of one layer in the structure of (**1**) as $SbCl_4(C_3N_6H_5)(C_3N_6H_7)_2$, and (**b**) a perspective view of the unit cell of (**1**) along the *b*-axis, with the color code: N: blue, C: gray, H: white, Cl: green, Sb: red).

Table 1. Crystallographic details of the crystal structure refinement of compounds (**1**), (**2**), and (**3**).

Compound	(1)	(2)	(3)
CCDC code	2201273	2210244	2213381
Formula weight	642.97	1033.67	281.32
Temperature/K	220.0(1)	150.0(1)	150.0(1)
Wavelength/Å	1.54184	1.54184	1.54184
Space group	$P\bar{1}$	$P2_1/c$	$P2_1/n$
a/Å	9.5878(5)	13.2780(2)	5.3562(2)
b/Å	10.5395(3)	10.6878(1)	10.5432(3)
c/Å	11.4338(5)	24.0953(2)	12.5618(4)
α/°	74.011(3)	90	90
β/°	79.122(4)	105.860(1)	93.710(3)
γ/°	85.602(3)	90	90
Volume/Å^3	1090.37(8)	3289.26(7)	707.90(4)
Z	2	4	4
R_{int}	0.0364	0.0485	0.0312
Goodness-of-fit on F^2	1.074	1.044	1.044
wR_2 (all data)	0.0660	0.0607	0.0267
wR_2	0.0643	0.0603	0.0264
Final R indices (all data)	0.0339	0.0251	0.0120
R_1	0.0278	0.0243	0.0110
$\theta_{Max.}$/°	4.365	3.460	5.483
$\theta_{Min.}$/°	66.585	66.583	70.067
μ/mm^{-1}	14.93	19.478	33.932
$\Delta\rho_{Max.}$/e·Å^{-3}	0.508	2.491	0.322
$\Delta\rho_{Min.}$/e·Å^{-3}	−0.593	−0.597	−0.451
Completeness/%	97.3	100	99.8

Table 2. Selected interatomic distances (pm) of compounds (**1**), (**2**), and (**3**).

Compound (1)			Compound (2)			Compound (3)		
Atom	**Atom**	**Length/pm**	**Atom**	**Atom**	**Length/pm**	**Atom**	**Atom**	**Length/pm**
Sb1	Cl1	276.5(8)	Sb1	Cl3	284.7(6)	Sb1	N2	241.5(1)
Sb1	N1	253.6(3)	Sb1	Cl4	260.6(0)	Sb1	N6	208.6(8)
Sb1	Cl2	247.0(0)	Sb1	Cl5	248.7(2)	Sb1	N4	204.4(6)
Sb1	Cl3	256.8(2)	Sb1	Cl1	240.2(1)	Sb1	Cl1	254.9(3)
Sb1	N4	204.7(3)	Sb2	N1	256.1(3)			
			Sb2	N4	204.7(3)			
			Sb2	Cl6	279.2(7)			
			Sb2	Cl7	247.2(8)			
			Sb2	Cl8	251.1(1)			

The $SbCl_3$ entity in the structure, with its lone pair, is well known from several crystal structures having average Sb-Cl distances of 260.1 pm [53]. The antimony is connected with an exocyclic nitrogen atom of the melaminate ion $(C_3H_5N_6)^-$ via Sb-N4 (204.7(3) pm) and an obviously weaker interaction via Sb-N1 (253.6(3) pm). The constituents in each layer in (**1**) are interconnected by a network of hydrogen bonds (Figure 3a). An isolated Cl^- ion in the structure is interconnected by hydrogen bridges at $d_{H\text{-}Cl}$ = 216.3 pm and 225.6 pm, consistent with the corresponding value in melaminium chloride $d_{H\text{-}Cl}$ = 239.7 pm [29].

The crystal structure of (**2**) comprises one deprotonated melamine, three protonated melaminium ions, an $SbCl_3$ unit and an $(SbCl_5)^{2-}$ ion to make up $(SbCl_4)_2(C_3N_6H_5)(C_3N_6H_7)_3$ displayed in Figure 4. The average Sb-Cl distances in $SbCl_3$ are 259.3 pm, and those of $SbCl_5$ are 262.1 pm and 257.8 pm, supporting the presence of Sb^{3+} throughout. Antimony in $SbCl_3$ is interconnected with the melaminate ion $(C_3H_5N_6)^-$ via Sb-N4 (204.4(6) pm) and an obviously

weaker interaction via Sb-N1 (256.1(3) pm). Again, the crystal structure features a layered arrangement and hydrogen bridging within layers.

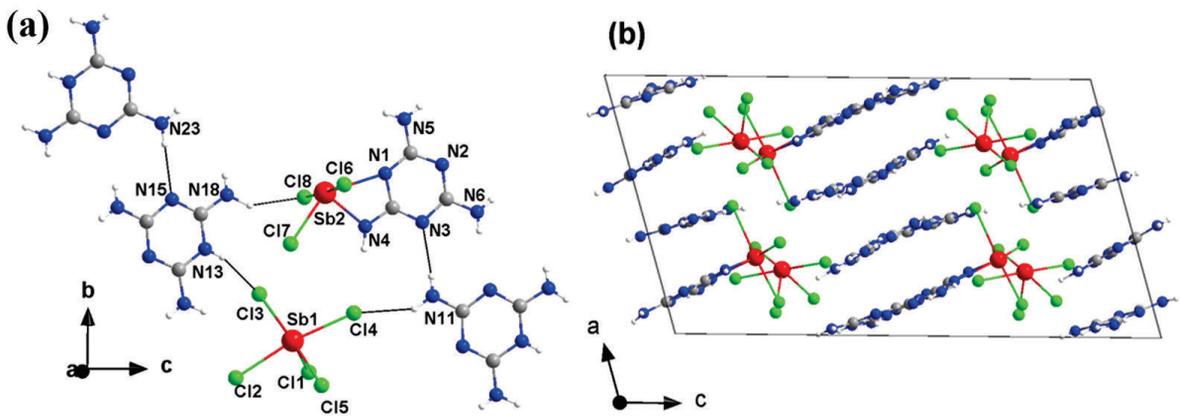

Figure 4. (**a**) Section of the crystal structure of (**2**) as $(SbCl_4)_2(C_3N_6H_5)(C_3N_6H_7)_3$ projected on the *bc*-plane, and (**b**) a perspective view along the *b*-axis with the color code: N: blue, C: gray, H: white, Cl: green, Sb: red).

The crystal structure of (**3**) features the presence of $(SbCl)^{2+}$ and the melaminate ion $(C_3N_6H_4)^{2-}$ in $SbCl(C_3N_6H_4)$. Unlike the two previous systems, this structure can be described as an infinite chain structure due to the bridging connectivity of the divalent melaminate anion, all shown in Figure 5. The $(SbCl)^{2+}$ ($d_{Sb\text{-}Cl}$ = 254.9(3) pm) is interconnected via exocyclic nitrogen atoms of two melaminate ions via Sb-N4 (204.4(6) pm) and Sb-N6 (208.6(8) pm) interactions and an obviously weaker interaction via Sb-N2 (241.5(1) pm).

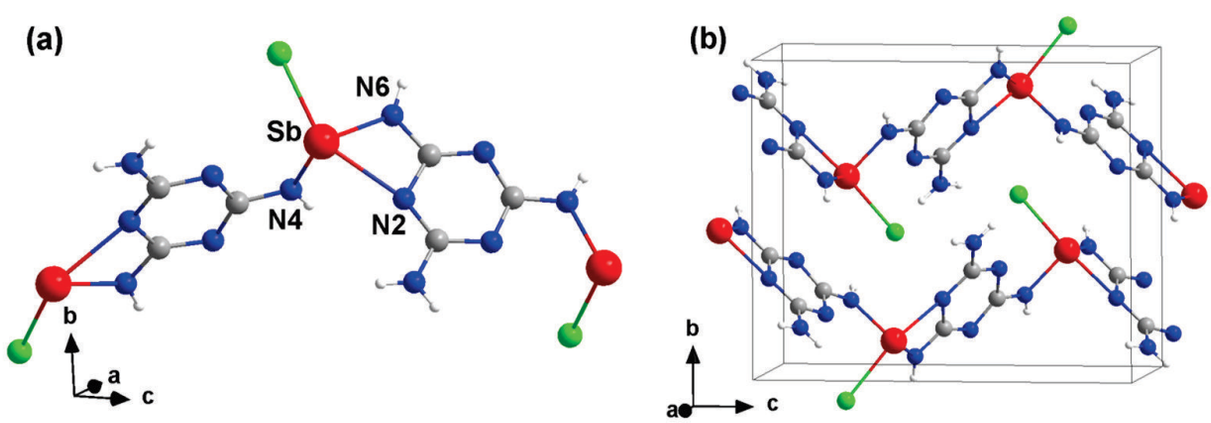

Figure 5. (**a**) Section of a chain section of the crystal structure of (**3**) and (**b**) a perspective view of the unit cell roughly along the *a*-axis with the color code: N: blue, C: gray, H: white, Cl: green, Sb: red.

The stacking sequences of layers are often dominated by the preference that the N atom of the triazine ring in one layer is alternating with a C atom of the triazine ring in the next layer, which is a characteristic feature in copper melaminate [20] and metal cyanurates as well [54,55]. This is achieved by rotating or shifting C_3N_3 units in adjacent layers relative to each other. However, this is not apparent in the structure of compounds (**1**–**3**). Layered arrangements of C_3N_3 units are quite clearly visible in compounds (**1**) and (**2**) but not in compound (**3**) (Figures S3–S6). Hence there is the possibility of π-π interactions between C_3N_3 units in (1) and (2). Such interactions can play a crucial role in the stabilization of parallel and antiparallel ring architectures in the crystal structure. The centroid-to-centroid

distance at which C_3N_3 rings may be considered representative of π-π stacking interactions is 360–390 pm in compounds (**1**) and (**2**). This distance increases to 560–590 pm in (**3**) which might present no π-π interactions between layers in this structure.

The range from 357–393 pm was previously reported for several compounds [38,56,57]; for example, in a zinc(II) complex containing melamine (392.8 pm) [56]. In many other studies of copper halide complexes (357.2–389.2 pm), we can see the stacking behavior of twisted melamine rings, which represents the π-π interactions [58].

3.3. X-ray Powder Diffraction and Infrared Spectroscopy

The reaction products were investigated by PXRD, and the XRD patterns of (**1**), and (**3**) are provided in Figures S7 and S8. Therein, the recorded data are compared with the calculated patterns obtained from the structure refinement based on single-crystal data. Compound (**2**) was obtained in low yield; therefore, no powder pattern of this intermediate could be recorded. This compound was always found in the presence of (**3**) or melamine at higher and lower temperatures, respectively. The powder pattern of compound (**3**) in Figure S8 shows some unidentified diffraction peaks.

3.4. Infrared Spectroscopy (IR)

The IR spectrum of (**1**), (**3**) and (**4**) has been compared to that of melamine and melaminium chloride, as presented in Figure 6. Table S1 lists the frequencies associated with each vibrational mode of these molecules, along with the corresponding bond assignments. Three IR absorption bands, indicative of the asymmetric and symmetric stretching of $-NH_2$ groups of melamine, can be found in the 3500–3300 cm^{-1} range of the melamine spectrum [29,59]. These vibrations can overlap with the $-NH^+$ in melaminium chloride, and due to coupling, the peak is broadened [60]. The characteristic bands of $-NH_2$ groups and $-NH^+$ are also seen in the spectrum of compound (**1**) at 3462, 3357, and 3433 cm^{-1}. We can see that the first peak (3462 cm^{-1}) in compound (**1**) is shifted to lower wavenumbers when compared to melamine. This shift may be due to the presence of protonated melamine units in (**1**). In fact, the presence of hydrogen bonding would shift $-NH_2$ IR bands to lower wavenumbers, as the hydrogen bond would weaken the NH_2 bond and lower its vibrational frequency [61]. However, due to coupling with the N-H $\cdots$ Cl stretching mode or the presence of heavier atoms (Cl, Sb) in compound (**1**), the second peak (3357 cm^{-1}) is shifted to slightly higher wavenumbers and also broadened [29]. Similarly, infrared spectra for compounds (**3**) and (**4**) indicate that the asymmetric and symmetric vibrations of $-NH_2$ overlap with those of $-NH^+$ in both compounds, as evidenced by the disappearance of the first peak (3471 cm^{-1} for melamine) and the broadening of the other two peaks. The bending mode bands for melaminium chloride and compound (**1**) are substantially higher than those for melamine (1652 cm^{-1}) at 1722, 1676, 1649 cm^{-1} and 1679, 1656, and 1612 cm^{-1}, respectively. This is explained by the fact that melaminium chloride and (**1**) have fewer intermolecular interactions than melamine. In compounds (**3**) and (**4**), bending modes are split into multiple bands, showing that $-NH_2$ groups in these compounds have different vibrational frequencies due to the presence of neighboring atoms and molecular interactions in these structures. The region below 1500 cm^{-1} is related to C-N, and C=N ring stretching modes, C-N side group stretching, N-H rocking, and triazine ring breath and bending vibrations, which are listed with detailed numbers in Table S1. The exact position of these peaks can depend on various factors, such as the substitution pattern of the triazine ring and the nature of the surrounding chemical environment, which agrees well with the slight shifts in each region for compounds (**1**), (**3**), and (**4**). The strong split-band at 800 cm^{-1}, which is brought on by the sextant-bend of both the triazine and heptazine rings, provides additional evidence that compound (**4**) is still either a heptazine- or triazine-based compound (IR cannot differentiate between triazine and heptazine) [13,22,62], whereas the yellow emission color of the compound under ultraviolet radiation rather indicates a heptazine based compound.

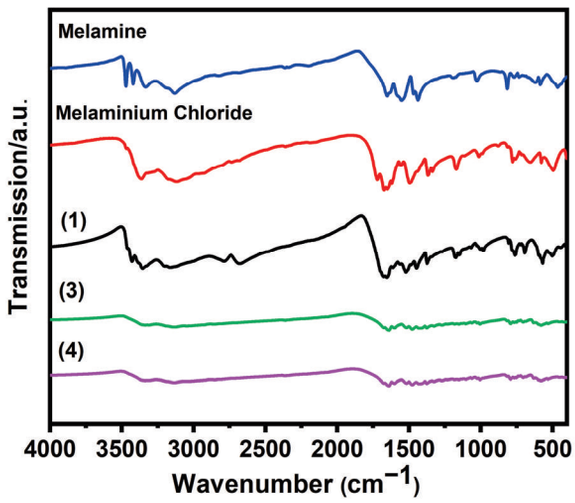

Figure 6. FTIR spectrum of melamine, melaminium chloride powder, compared with compounds (**1**), (**3**), (**4**).

4. Conclusions

The development of metal melaminates is just at its beginning. A preparative concept for the development of melaminates was recently established for $Cu_3(C_3H_3N_3)$ based on the reaction of CuCl with melamine. The same concept is employed in this study for the reaction of $SbCl_3$ with melamine. Thermal studies (DSC) reveal a narrow sequence of thermal events, or rather intertwining reactions that reveal new compounds, following the sequence (**1**), (**2**) and (**3**) with increasing temperature.

Indeed, the final product of the given reaction cascade is compound (**3**), observed via compounds (**1**) and (**2**). For a better description of the reaction sequence of compounds, we use the abbreviation *Mel* for melamine, with $Mel^{(n-)}$ for melaminate and $Mel^{(+)}$ for melaminium. The overall reaction representing the formation of compound (**3**) can be described as follows:

$$SbCl_3 + Mel \rightarrow SbCl Mel^{(2-)} + 2\,HCl\uparrow$$

The formation of HCl in this reaction can be equivalent to melaminium chloride ($Mel^{(+)}Cl$), which is, in fact, present in compound (**1**) but is lost at elevated temperatures through sublimation, which indeed has been reported as a side-phase for the corresponding reaction of CuCl and melamine [20]. This reaction scheme with metal halide and melamine is indeed a useful way to develop metal melaminates. However, reactions with melamine are intrinsically difficult due to the high reactivity and condensation behavior of melamine.

The reaction of $SbCl_3$ with excess melamine passes through some intermediate reaction stages with the formations of melamine derivatives (Mel^-, Mel^+) that are successively lost with increasing temperature from (**1**) to (**2**) and finally (**3**). Compound (**1**) is best described as $SbCl_4Mel^{(-)}(Mel^{(+)})_2$ containing three melamine species per antimony atom, and compound (**2**) is given as $(SbCl_4)_2Mel^{(-)}(Mel^{(+)})_3$ and contains only two melamine derivatives per antimony atom until only one melaminate is left in (**3**). The formation of the expectable compound $SbMel^{(3-)}$ is not observed.

Supplementary Materials: The following supporting information can be downloaded at: https://www.mdpi.com/article/10.3390/chemistry5020099/s1, Reference [29] is also cited in the supplementary materials.

Author Contributions: Conceptualization, supervision, funding acquisition, review and editing, H.-J.M.; Synthesis, PXRD and IR, writing, E.B.; X-ray diffraction refinements and structure solutions, M.S. All authors have read and agreed to the published version of the manuscript.

Funding: This research received no external funding.

Data Availability Statement: Data is contained within the article and Supplementary Materials.

Acknowledgments: A sincere thank you to Mike Healey Smith for his diligent English revisions and proofreading of this article.

Conflicts of Interest: The authors declare no conflict of interest.

References

1. Liebig, J. Über einige Stickstoff-Verbindungen. *Ann. Pharm. Fr.* **1834**, *10*, 1–47. [CrossRef]
2. Gmelin, L. Über einige Verbindungen des Melon's. *Ann. Pharm. Fr.* **1835**, *15*, 252–258. [CrossRef]
3. Liebig, J. Über die Constitution der Mellonverbindungen. *Justus Liebigs Ann. Chem.* **1855**, *95*, 257–282. [CrossRef]
4. Finkel'shtein, A.; Boitsov, E. The molecular structure of 1,3,5-triazine and its derivatives. *Russ. Chem. Rev.* **1962**, *31*, 712. [CrossRef]
5. Crews, G.M.; Ripperger, W.; Kersebohm, D.B.; Güthner, T.; Mertschenk, B. Melamine and guanamines. In *Ullmann's Encyclopedia of Industrial Chemistry*; Wiley: Weinheim, Germany, 2001. [CrossRef]
6. Keßler, F.K. Structure and Reactivity of S-Triazine-Based Compounds in C/N/H Chemistry. Ph.D. Thesis, Ludwig Maximilian University of Munich, Munich, Germany, 2019.
7. Klason, P. Über Melamverbindungen. *J. Prakt. Chem.* **1886**, *33*, 285–289. [CrossRef]
8. Finkel'shtein, A.I.; Spiridonova, N.Y.V. Chemical properties and molecular structure of derivatives of sym-heptazine [1,3,4,6,7,9,9b-heptaazaphenalene, tri-1,3,5-triazine]. *Russ. Chem. Rev.* **1964**, *33*, 400. [CrossRef]
9. Jürgens, B.; Irran, E.; Senker, J.; Kroll, P.; Müller, H.; Schnick, W. Melem (2,5,8-Triamino-tri-s-triazine), an Important Intermediate during Condensation of Melamine Rings to Graphitic Carbon Nitride: Synthesis, Structure Determination by X-ray Powder Diffractometry, Solid-State NMR, and Theoretical Studies. *J. Am. Chem. Soc.* **2003**, *125*, 10288–10300. [CrossRef]
10. Kroke, E.; Schwarz, M. Novel group 14 nitrides. *Coord. Chem. Rev.* **2004**, *248*, 493–532. [CrossRef]
11. May, H. Pyrolysis of melamine. *J. Appl. Chem.* **1959**, *9*, 340–344. [CrossRef]
12. Sattler, A.; Pagano, S.; Zeuner, M.; Zurawski, A.; Gunzelmann, D.; Senker, J.; Müller-Buschbaum, K.; Schnick, W. Melamine–melem adduct phases: Investigating the thermal condensation of melamine. *Chem.-Eur. J.* **2009**, *15*, 13161–13170. [CrossRef]
13. Lotsch, B.V.; Schnick, W. New light on an old story: Formation of melam during thermal condensation of melamine. *Chem.-Eur. J.* **2007**, *13*, 4956–4968. [CrossRef] [PubMed]
14. Weil, E.D. Fire-Protective and Flame-Retardant Coatings—A State-of-the-Art Review. *J. Fire Sci.* **2011**, *29*, 259–296. [CrossRef]
15. Schartel, B.; Weiß, A.; Mohr, F.; Kleemeier, M.; Hartwig, A.; Braun, U. Flame retarded epoxy resins by adding layered silicate in combination with the conventional protection-layer-building flame retardants melamine borate and ammonium polyphosphate. *J. Appl. Polym. Sci.* **2010**, *118*, 1134–1143. [CrossRef]
16. Yang, H.; Song, L.; Tai, Q.; Wang, X.; Yu, B.; Yuan, Y.; Hu, Y.; Yuen, R.K.K. Comparative study on the flame retarded efficiency of melamine phosphate, melamine phosphite and melamine hypophosphite on poly(butylene succinate) composites. *Polym. Degrad. Stab.* **2014**, *105*, 248–256. [CrossRef]
17. Weil, E.D.; Levchik, S.V. Flame Retardants in Commercial Use or Development for Textiles. *J. Fire Sci.* **2008**, *26*, 243–281. [CrossRef]
18. Yin, N.; Wang, K.; Xia, Y.a.; Li, Z. Novel melamine modified metal-organic frameworks for remarkably high removal of heavy metal Pb(II). *Desalination* **2018**, *430*, 120–127. [CrossRef]
19. Cao, Y.; Huang, J.; Li, Y.; Qiu, S.; Liu, J.; Khasanov, A.; Khan, M.A.; Young, D.P.; Peng, F.; Cao, D.; et al. One-pot melamine derived nitrogen doped magnetic carbon nanoadsorbents with enhanced chromium removal. *Carbon* **2016**, *109*, 640–649. [CrossRef]
20. Kallenbach, P.; Bayat, E.; Ströbele, M.; Romao, C.P.; Meyer, H.-J. Tricopper Melaminate, a Metal-Organic Framework Containing Dehydrogenated Melamine and Cu-Cu Bonding. *Inorg. Chem.* **2021**, *60*, 16303–16307. [CrossRef]
21. Pareek, K.; Rohan, R.; Cheng, H. Polymeric organo–magnesium complex for room temperature hydrogen physisorption. *RSC Adv.* **2015**, *5*, 10886–10891. [CrossRef]
22. Kessler, F.K.; Schuhbeck, A.M.; Schnick, W. Melamium Thiocyanate Melam, a Melamium Salt with Disordered Anion Sites. *Z. Anorg. Allg. Chem.* **2019**, *645*, 840–847. [CrossRef]
23. Sattler, A.; Schnick, W. Preparation and Structure of Melemium Melem Perchlorate $HC_6N_7(NH_2)_3ClO_4 \cdot C_6N_7(NH_2)_3$. *Z. Anorg. Allg. Chem.* **2008**, *634*, 457–460. [CrossRef]
24. Sattler, A.; Schnick, W. Melemium Hydrogensulfate $H_3C_6N_7(NH_2)_3(HSO_4)_3$—The First Triple Protonation of Melem. *Z. Anorg. Allg. Chem.* **2010**, *636*, 2589–2594. [CrossRef]
25. Vella-Zarb, L.; Braga, D.; Guy Orpen, A.; Baisch, U. The influence of hydrogen bonding on the planar arrangement of melamine in crystal structures of its solvates, cocrystals and salts. *CrystEngComm* **2014**, *16*, 8147–8159. [CrossRef]
26. Kessler, F.K.; Koller, T.J.; Schnick, W. Synthesis and Structure of Melamium Bromide $C_6N_{11}H_{10}Br$ and Melamium Iodide $C_6N_{11}H_{10}I$. *Z. Anorg. Allg. Chem.* **2018**, *644*, 186–192. [CrossRef]
27. Braml, J.; Perpétuo, G.J. Bis (melaminium) sulfate dihydrate. *Acta Crystallogr. Sect. C Cryst. Struct. Commun.* **2001**, *57*, 1431–1433. [CrossRef]
28. Volfkovi, S.I.; Feldmann, W.W.; Kozmina, M.L. Über Kondensierte Phosphate des Melamins. *Z. Anorg. Allg. Chem.* **1979**, *457*, 20–30. [CrossRef]
29. Janczak, J.; Perpétuo, G.J. Melaminium chloride hemihydrate. *Acta Crystallogr. Sect. C Cryst. Struct. Commun.* **2001**, *57*, 1120–1122. [CrossRef] [PubMed]

30. Janczak, J.; Perpétuo, G.J. Melaminium phthalate. *Acta Crystallogr. Sect. C Cryst. Struct. Commun.* **2001**, *57*, 123–125. [CrossRef]
31. Marchewka, M.; Pietraszko, A. Structure and spectra of melaminium citrate. *J. Phys. Chem. Solids* **2003**, *64*, 2169–2181. [CrossRef]
32. Colombo, A.; Menabue, L.; Motori, A.; Pellacani, G.C.; Porzio, W.; Sandrolini, F.; Willett, R. Crystal structure and spectroscopic, magnetic, and electrical properties of a copper (II) dimer, melaminium hexachlorodicuprate, exhibiting a new stacking interaction. *Inorg. Chem.* **1985**, *24*, 2900–2905. [CrossRef]
33. Kroenke, W.J.; Fackler, J.P., Jr.; Mazany, A.M. Structure and bonding of melaminium. beta-octamolybdate. *Inorg. Chem.* **1983**, *22*, 2412–2416. [CrossRef]
34. Sattler, A.; Seyfarth, L.; Senker, J.; Schnick, W. Synthesen, Kristallstrukturen und spektroskopische Eigenschaften des Melem-Adduktes $C_6N_7(NH_2)_3 \cdot H_3PO_4$ sowie der Melemium-Salze $(H_2C_6N_7(NH_2)_3)SO_4.2H_2O$ und $(HC_6N_7(NH_2)_3)ClO_4 \cdot H_2O$. *Z. Anorg. Allg. Chem.* **2005**, *631*, 2545–2554. [CrossRef]
35. Sattler, A.; Schönberger, S.; Schnick, W. Melemium Methylsulfonates $HC_6N_7(NH_2)3H_2C_6N_7(NH_2)_3(SO_3Me)_3 \cdot H_2O$ and $H_2C_6N_7(NH_2)_3(SO_3Me)_2 \cdot H_2O$. *Z. Anorg. Allg. Chem.* **2010**, *636*, 475–482. [CrossRef]
36. Zhang, L.; Zhang, J.; Li, Z.-J.; Cheng, J.-K.; Yin, P.-X.; Yao, Y.-G. New Coordination Motifs of Melamine Directed by N−H···X (X=Cl or Br) Hydrogen Bonds. *Inorg. Chem.* **2007**, *46*, 5838–5840. [CrossRef]
37. Rana, A.; Bera, M.; Chowdhuri, D.S.; Hazari, D.; Jana, S.K.; Zangrando, E.; Dalai, S. 3D Coordination Network of Ag(I) Ions with μ_3 -Bridging Melamine Ligands. *J. Inorg. Organomet. Polym. Mater.* **2012**, *22*, 360–368. [CrossRef]
38. Bai, Z.; Lee, J.; Kim, H.; Hu, C.L.; Ok, K.M. Unveiling the Superior Optical Properties of Novel Melamine-Based Nonlinear Optical Material with Strong Second-Harmonic Generation and Giant Optical Anisotropy. *Small*, 2023; *in press*. [CrossRef] [PubMed]
39. Liu, L.; Wu, Y.; Ma, L.; Fan, G.; Gao, W.; Wang, W.; Ma, X. A new melamine-based Cu(I) coordination polymer with an excellent photocatalytic activity, therapeutic and nursing effects on the blood glucose regulation. *J. Struct. Chem.* **2022**, *63*, 302–309. [CrossRef]
40. Braml, N.E.; Sattler, A.; Schnick, W. Formation of melamium adducts by pyrolysis of thiourea or melamine/NH_4Cl mixtures. *Chem.-Eur. J.* **2012**, *18*, 1811–1819. [CrossRef] [PubMed]
41. Mukherjee, S.; Ren, J. Gas-phase acid-base properties of melamine and cyanuric acid. *J. Am. Soc. Mass Spectrom.* **2010**, *21*, 1720–1729. [CrossRef]
42. Gorne, A.L.; Scholz, T.; Kobertz, D.; Dronskowski, R. Deprotonating Melamine to Gain Highly Interconnected Materials: Melaminate Salts of Potassium and Rubidium. *Inorg. Chem.* **2021**, *60*, 15069–15077. [CrossRef]
43. Gorne, A.L.; George, J.; van Leusen, J.; Duck, G.; Jacobs, P.; Chogondahalli Muniraju, N.K.; Dronskowski, R. Ammonothermal Synthesis, Crystal Structure, and Properties of the Ytterbium(II) and Ytterbium(III) Amides and the First Two Rare-Earth-Metal Guanidinates, $YbC(NH)_3$ and $Yb(CN_3H_4)_3$. *Inorg. Chem.* **2016**, *55*, 6161–6168. [CrossRef]
44. Franklin, E.C. The ammono carbonic acids. *J. Am. Chem. Soc.* **1922**, *44*, 486–509. [CrossRef]
45. Schnick, W.; Huppertz, H. Darstellung, Kristallstruktur und Eigenschaften von Kaliumhydrogencyanamid. *Z. Anorg. Allg. Chem.* **1995**, *621*, 1703–1707. [CrossRef]
46. Haynes, W.M. *CRC Handbook of Chemistry and Physic*, 95th ed.; CRC Press LLC: Boca Raton, FL, USA, 2016.
47. Putz, H.; Brandenburg, K. *Match!—Phase Analysis Using Powder Diffraction, Version 3.15.x*; Crystal Impact: Bonn, Germany, 2023.
48. Sheldrick, G.M. *SHELXS-97 and SHELXL-97, Program for Crystal Structure Solution and Refinement*; University of Göttingen: Göttingen, Germany, 1997.
49. Dolomanov, O.; Bourhis, L.; Gildea, R.; Howard, J.; Puschmann, H. OLEX2: A complete structure solution, refinement and analysis program. *J. Appl. Crystallogr.* **2009**, *42*, 339–341. [CrossRef]
50. Mos, A.; Castro, C.; Indris, S.; Ströbele, M.; Fink, R.F.; Meyer, H.-J. From WCl_6 to WCl_2: Properties of Intermediate Fe–W–Cl Phases. *Inorg. Chem.* **2015**, *54*, 9826–9832. [CrossRef]
51. Ströbele, M.; Mos, A.; Meyer, H.-J. Cluster harvesting by successive reduction of a metal halide with a nonconventional reduction agent: A benefit for the exploration of metal-rich halide systems. *Inorg. Chem.* **2013**, *52*, 6951–6956. [CrossRef] [PubMed]
52. Ströbele, M.; Meyer, H.-J. Pandora's box of binary tungsten iodides. *Dalton Trans.* **2019**, *48*, 1547–1561. [CrossRef]
53. Lizarazo-Jaimes, E.H.; Reis, P.G.; Bezerra, F.M.; Rodrigues, B.L.; Monte-Neto, R.L.; Melo, M.N.; Frezard, F.; Demicheli, C. Complexes of different nitrogen donor heterocyclic ligands with $SbCl_3$ and $PhSbCl_2$ as potential antileishmanial agents against Sb(III)-sensitive and -resistant parasites. *J. Inorg. Biochem.* **2014**, *132*, 30–36. [CrossRef]
54. Kalmutzki, M.; Ströbele, M.; Bettinger, H.F.; Meyer, H.-J. Development of Metal Cyanurates: The Example of Barium Cyanurate (BCY). *Eur. J. Inorg. Chem.* **2014**, *2014*, 2536–2543. [CrossRef]
55. Kalmutzki, M.; Ströbele, M.; Enseling, D.; Jüstel, T.; Meyer, H.-J. Synthesis, Structure, and Luminescence of Rare Earth Cyanurates. *Eur. J. Inorg. Chem.* **2015**, *2015*, 134–140. [CrossRef]
56. Salah, T.; Mhadhbi, N.; Ben Ahmed, A.; Hamdi, B.; Krayem, N.; Loukil, M.; Guesmi, A.; Khezami, L.; Houas, A.; Ben Hamadi, N. Physico-Chemical Characterization, DFT Modeling and Biological Activities of a New Zn(II) Complex Containing Melamine as a Template. *Crystals* **2023**, *13*, 746. [CrossRef]
57. Li, F.; Xu, H.; Xu, X.; Cang, H.; Xu, J.; Chen, S. Supramolecular salts assembled by melamine and two organic hydroxyl acids: Synthesis, structure, hydrogen bonds, and luminescent property. *CrystEngComm* **2021**, *23*, 2235–2248. [CrossRef]
58. Mitra, M.; Hossain, A.; Manna, P.; Choudhury, S.R.; Kaenket, S.; Helliwell, M.; Bauzá, A.; Frontera, A.; Mukhopadhyay, S. Melamine-mediated self-assembly of a Cu(II)–methylmalonate complex assisted by π+–π+ and anti-electrostatic H-bonding interactions. *J. Coord. Chem.* **2017**, *70*, 463–474. [CrossRef]

59. Araar, H.; Benounis, M.; Direm, A.; Touati, A.; Atailia, S.; Barhoumi, H.; Jaffrezic-Renault, N. A new thin film modified glassy carbon electrode based on melaminium chloride pentachlorocuprate (II) for selective determination of nitrate in water. *Mon. Chem.* **2019**, *150*, 1737–1744. [CrossRef]
60. Hesse, M.; Meier, H.; Zeeh, B. *Spektroskopische Methoden in der Organischen Chemie*; Georg Thieme: Stuttgart, Germany, 2005.
61. Pavia, D.L.; Lampman, G.M.; Kriz, G.S.; Vyvyan, J.A. *Introduction to Spectroscopy*; Cengage Learning: Boston, MA, USA, 2014; pp. 14–101.
62. Lotsch, B.V.; Döblinger, M.; Sehnert, J.; Seyfarth, L.; Senker, J.; Oeckler, O.; Schnick, W. Unmasking melon by a complementary approach employing electron diffraction, solid-state NMR spectroscopy, and theoretical calculations—Structural characterization of a carbon nitride polymer. *Chem.-Eur. J.* **2007**, *13*, 4969–4980. [CrossRef]

Supplementary data

Unraveling the Synthesis of $SbCl(C_3N_6H_3)$: A Metal-Melaminate Obtained through Deprotonation of Melamine with Antimony(III)Chloride

Elaheh Bayat, Markus Ströbele and Hans-Jürgen Meyer *

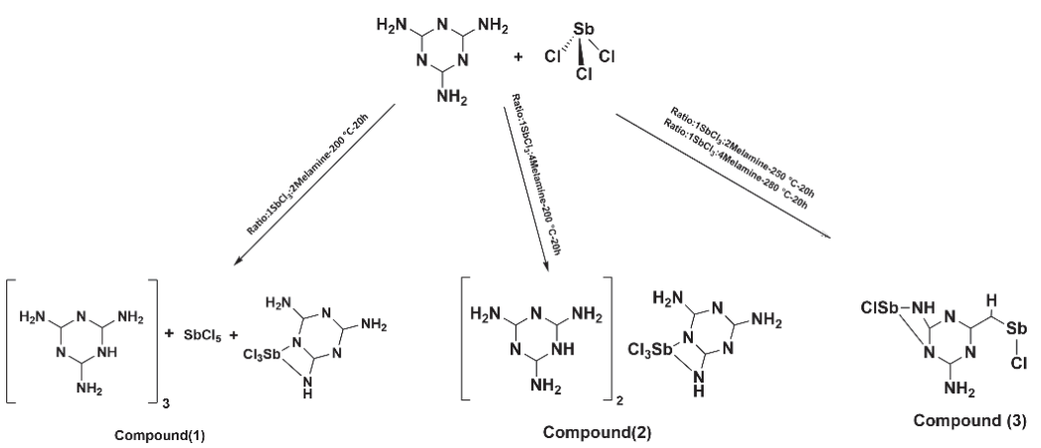

Figure S1: Schematic synthesis of three synthesized compounds ((1),(2),(3)).

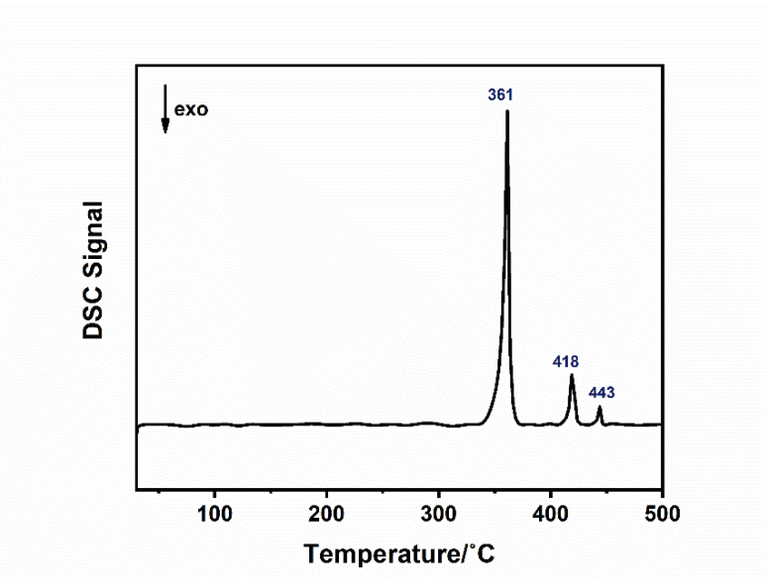

Figure S2: DSC pattern of pure Melamine.

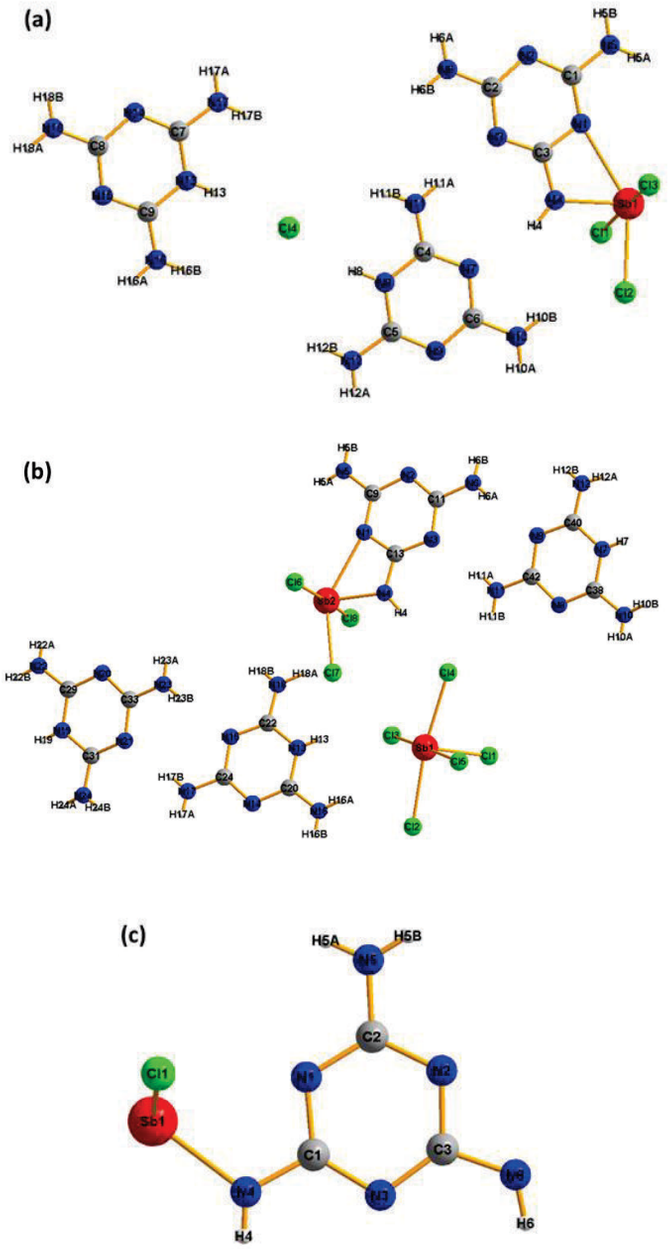

Figure S3: Asymmetric unit of compound a. **(1)**, b. **(2)**, c. **(3)**

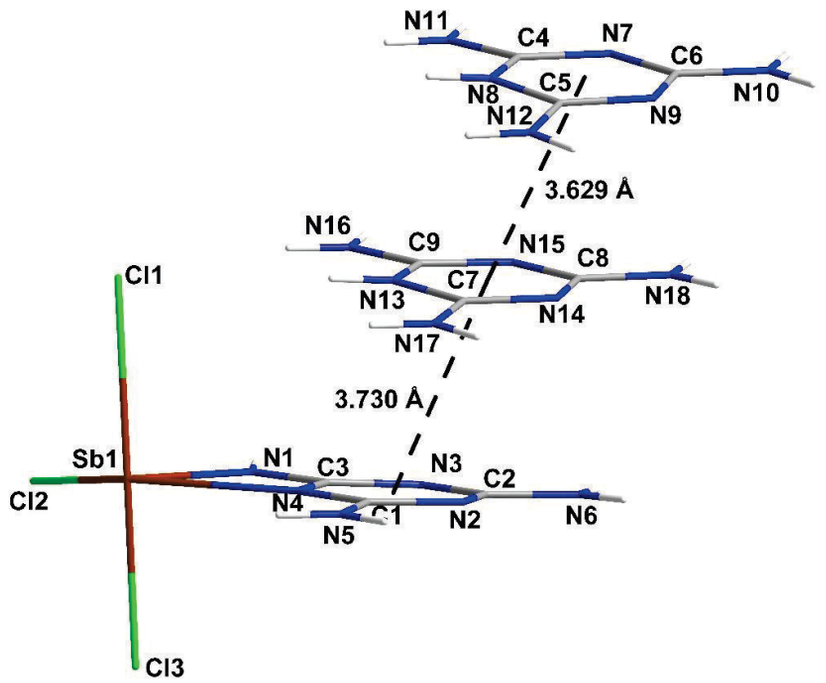

Figure S4: Stacking pattern of the C_3N_3 units in compound **(1)**.

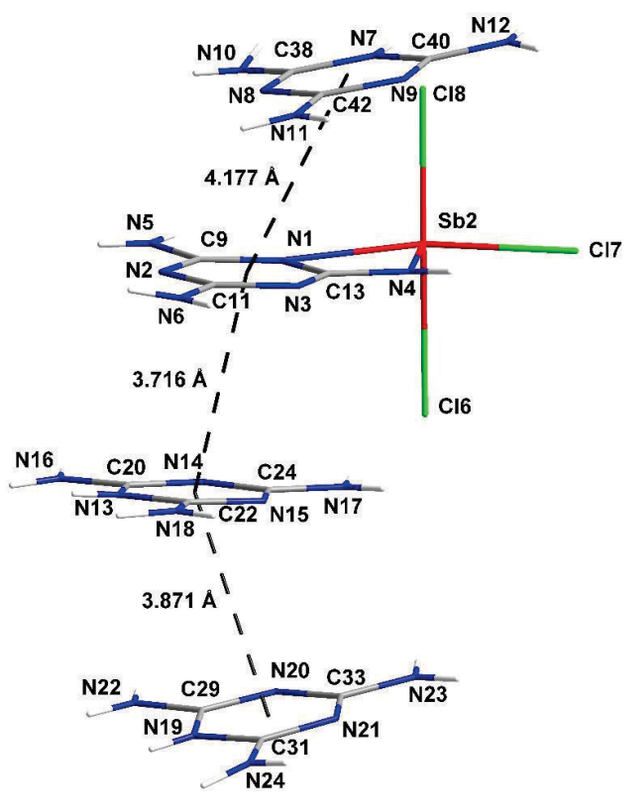

Figure S5: Stacking pattern of the C_3N_3 units in compound **(2)**.

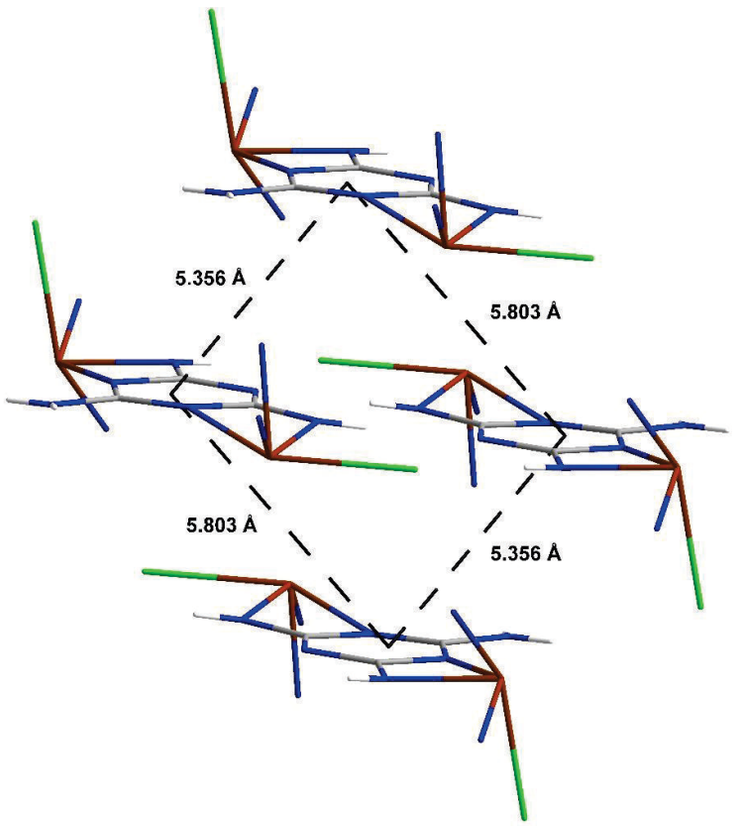

Figure S6: Stacking pattern of the C_3N_3 units in compound **(3)**.

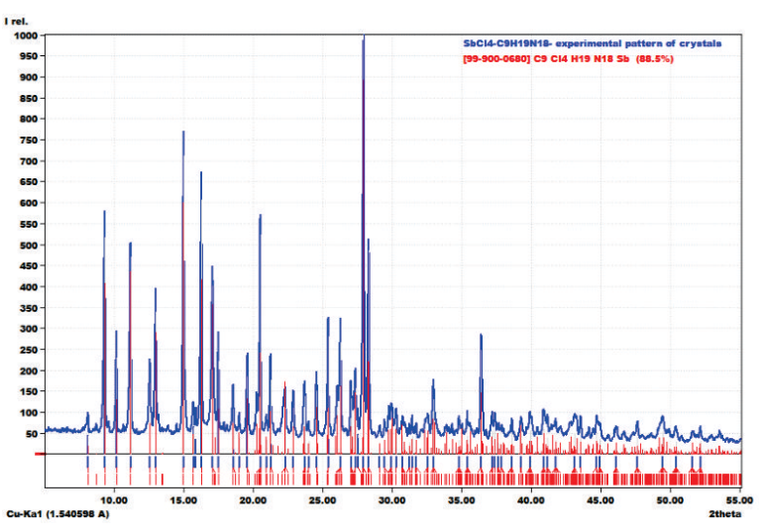

Figure S7: Comparison of the recorded powder pattern of **(1)** with the calculated pattern**.** Calculated (red) and recorded (blue)

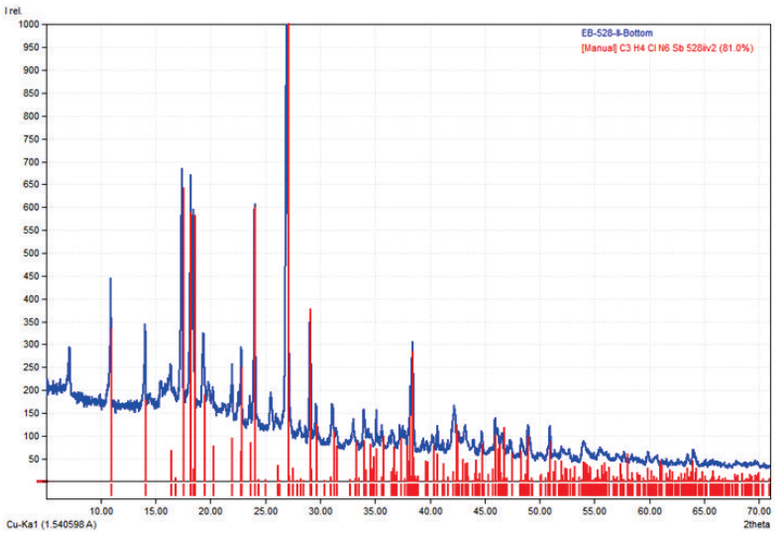

Figure S8: Comparison of the recorded powder pattern of **(3)** with the calculated pattern**.** Calculated (red) and recorded (blue)

Table S1. Assignment of recorded infrared wavenumbers (cm^{-1}) of obtained compounds compared to those of melamine [1], and melaminium chloride [2].

Melamine	Melaminium chloride[29]	Compound (1)	Compound (3)	Compound (4)	Tentative assignment
3471	3469	3462			NH_2 asym stretch
3421	3363	3433	3342	3332	NH_2 asym stretch
	3363	3370	3334		N-H... Cl stretch
3334		3357			NH_2 sym stretch
3180				3147	Combination tone: NH_2 bend+ side chain asym C-N stretch
		3203			N-H... N stretch
3132	3120	3157	3134		N-H... N stretch
		3116	3049		N-H... N stretch
	2945				N-H... N stretch
	2734	2785			Combination tone:
2677	2679	2680			NH_2 asym stretch side
2368	2356		2364	2370	chain out of plane C-N
2198	2175				bend
	1722				NH_2 bend
	1676	1679			NH_2 bend
1652	1649	1656	1639	1651	NH_2 bend
	1620	1612	1600		Side chain asym C-N
1554	1556	1565		1510	stretch
		1521	1515	1508	
1465					Ring semi-circle
	1492	1487	1479		stretch
1438	1452	1448	1375	1390	Side chain C-N breath
	1367	1373	1325	1350	Ring semi-circle
	1336				stretch
1193					

1172	1168	1172	1004		Ring semi-circle stretch+NH_2 rock
		1145			Ring semi-circle stretch
1022	1014				Ring breath
		979			triazine ring, in phase radial
815				802	Ring out of plane bend
769	779	759	792	781	Side chain out of plane bend +Ring-sextant out of plane bend
730					Side chain out of plane bend +Ring-sextant out of plane bend
		692	703		Ring breath and NH_2
	655				bend (out of plane)
626					NH_2 wag
586	578	568	580		Ring bend
464	495	501		472	Combination tone: NH_2 bend+NH_2 rock

Publication 4

Thermal deprotonation and condensation of melamine in the presence of indium(III) chloride

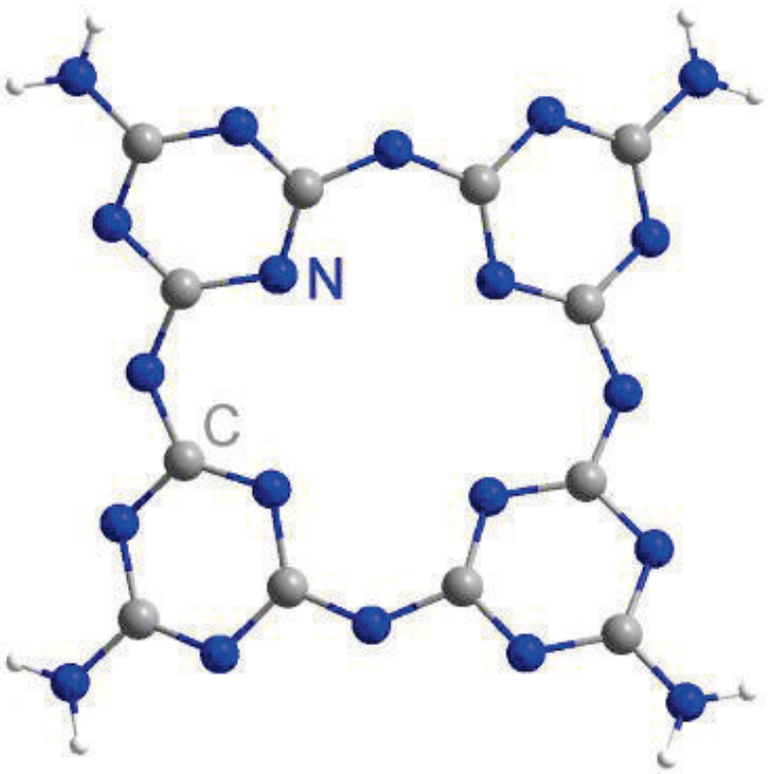

https://doi.org/10.1021/acs.inorgchem.4c01658

Reprinted with permission from

Inorg. Chem. 2024, 63, 41, 19053–19062

Dalton Transactions

ROYAL SOCIETY OF CHEMISTRY

PAPER

View Article Online
View Journal | View Issue

Cite this: *Dalton Trans.*, 2024, **53**, 10912

Thermal deprotonation and condensation of melamine in the presence of indium(III)chloride†

Elaheh Bayat,[a] Markus Ströbele,[a] David Enseling,[b] Thomas Jüstel[b] and H.-Jürgen Meyer*[a]

Received 8th April 2024,
Accepted 6th June 2024

DOI: 10.1039/d4dt01029a

rsc.li/dalton

The thermal condensation of melamine into molecules melam, melem, and the one-dimensional polymer melon has already been reported. An interesting question arises about the impact of other compounds being present in this process of thermal conversion. The solid-state reaction of $C_3N_6H_6$ with $InCl_3$ leads to a novel compound featuring deprotonated melam units in a supramolecular assembly, based on the $[C_{12}N_{20}H_8]^{4-}$ anion that is interconnected in the structure *via* N–In–N bonding. The reaction pathway of the formation of this compound is investigated by thermal analysis and the crystal structure of unique $(NH_4)[(InCl_2)_3(C_{12}N_{20}H_8)]\cdot\frac{2}{3}[InCl_3(NH_3)]$ is reported as well as its photoluminescence properties.

Introduction

Melamine, also known as 2,4,6-triamino-s-triazine, was first discovered by the German chemist Justus von Liebig in the 1830s.[1] Commercial manufacture of urea increased its widespread availability.[2–4] Later, in the early twentieth century, the recognition of its properties, particularly its thermal stability, contributed to a better understanding of the compound. Although Liebig and Gmelin[1,5] initially proposed the condensation product of melamine, known as heptazine compounds, only elemental analysis was performed during that period.[4,6,7]

The exact molecular structure of these compounds was later proposed by Linus Pauling about a century ago.[8] In the subsequent studies, conducted by various scientists,[9,10] the mechanism of the condensation reactions was explored, leading to the characterization of intermediates such as melam, melem, and melon formed during thermal treatment. B. Lotsch's investigations further disclosed that melem and melam could be obtained by heating melamine, cyanamide, dicyanamide, or ammonium cyanamide.[11] This implies that at slightly elevated temperatures, any of these precursors have the potential to transform into melamine. Moreover, the formation of melem was previously postulated by May,[12] who elucidated a decomposition process in which some melamine is decomposed to produce cyanamide at temperatures ranging from 300 to 320 °C. Following this, cyanamide condenses with melamine, giving rise to the formation of melam, and subsequently melem, by eliminating two ammonia molecules.[12]

Melem and melemium salts are famous for their potential as highly effective flame retardants,[13] excellent polymer compatibility, and their status as halogen-free compounds.[6] However, melem faces limitations in practical applications due to its insolubility and chemical stability.[6] Despite these challenges, melem can be dissolved in mineral acid solutions to isolate melemium salts such as melem-phosphoric acid adducts $C_6N_7(NH_2)_3\cdot H_3PO_4$,[14] melemium perchlorate $[HC_6N_7(NH_2)_3]ClO_4\cdot H_2O$,[14] melemium-melem perchlorate $HC_6N_7(NH_2)_3ClO_4\cdot C_6N_7(NH_2)_3$,[15] *etc.*

Recent investigations propose that the formation of melam is dependent on specific heating conditions, including temperature, pressure, and duration.[16,17] Furthermore, melam is only stable in a small temperature range. Notably, it is recognized as a minor by-product in the condensation of melamine to melem, observed under specific conditions.[17–19] The crystal structure of this intermediate has recently been characterized,[17,20] indicating its potential significance in the development of new compounds with applications extending beyond flame retardancy. Several groups of melam-based compounds have been identified, including melamium salts such as melamium perchlorate $(C_6N_{11}H_{11}(ClO_4)_2\cdot 2H_2O)$,[21] melamium bromide $(C_6N_{11}H_{10}Br)$,[3,22] melamium iodide $(C_6N_{11}H_{10}I)$,[22] and melamium chloride ammonium chloride $(C_6N_{11}H_{10}Cl_{0.5}NH_4Cl)$.[20] Additionally, melamium adduct compounds like melamium thiocyanate melamine $(C_6N_{11}H_{10}SCN\cdot 2C_3N_6H_6)$[23] and melamium thiocyanate melam (1 : 1) adduct $(C_6N_{11}H_{10}SCN\cdot C_6N_{11}H_9)$ have been discovered.[3] Our research group has also uncovered new sets of compounds

[a]*Section for Solid State and Theoretical Inorganic Chemistry, Institute of Inorganic Chemistry, University of Tübingen, Auf der Morgenstelle 18, 72076 Tübingen, Germany. E-mail: juergen.meyer@uni-tuebingen.de*
[b]*Department of Chemical Engineering, Münster University of Applied Science, Stegerwaldstraße 39, 48565 Steinfurt, Germany*

†Electronic supplementary information (ESI) available. CCDC 2333063. For ESI and crystallographic data in CIF or other electronic format see DOI: https://doi.org/10.1039/d4dt01029a

involving LiBr-melam, LiI-melam, CuX (Cl, Br, I)-melam, Cu_3Cl_2-melam, and Cu_3Cl_3-melam.[24] These compounds exhibit a distinctive feature where a metal halide is linked to inner nitrogen atoms in all structures. Furthermore, in the latter two structures, (Cu_3Cl_2-melam, and Cu_3Cl_3-melam), outer nitrogen atoms are also connected to metal halides. These findings introduce a new array of metal-containing melam compounds, suggesting potential applications across a wide spectrum of chemistry[25] and biochemistry.[26]

Exploring the realm of C/H/N chemistry, melamine, protonated melamine, and melaminate compounds present intriguing aspects.[27,28] Melamine exhibits the ability to coordinate with metal halides, forming compounds like $[Cu_3Cl_3(C_3N_6H_6)]_n$,[29] $[Cu_2Br_2(C_3N_6H_6)]_n$,[29] the silver complex $[Ag(C_3N_6H_6)(H_2O)(NO_3)]_n$,[30] $[Ag(C_3H_6N_6)]NO_3$,[31] and the mercury compound $(C_3N_6H_7)(C_3N_6H_6)HgCl_3$.[25] However, compounds involving deprotonated melamine are of heightened interest compared to these adducts. Noteworthy examples include $K(C_3N_6H_5)\cdot NH_3$, $Rb(C_3N_6H_5)\cdot\frac{1}{2}NH_3$,[32] $K_3(C_3N_6H_3)$,[33] $Cu_3(C_3N_6H_3)$,[27] $SbCl_4(C_9N_{18}H_{19})$, $(SbCl_4(C_6N_{12}H_{13}))_2$, and $SbCl(C_3N_6H_4)$.[28]

In this context, we present a new compound featuring melam units in a captivating supramolecular porphyrin-like design with indium chloride. We have investigated the solid-state synthesis, infrared (IR) spectroscopy, stability assessed through thermogravimetric analysis (TGA), stability in air, X-ray diffraction (XRD), crystal structure analysis, and photoluminescent properties of this compound. This exploration establishes an unprecedented avenue for the development of additional compounds that could hold significant applications. Additionally, it offers novel insights into the chemistry of melamine, and melam-based compounds, revealing their potential to be deprotonated and used as a ligand.

Results and discussion

The new compound $(NH_4)[(InCl_2)_3(C_{12}N_{20}H_8)]\cdot\frac{2}{3}[InCl_3(NH_3)]$ and the hitherto unknown side-phases of $(NH_4)_2[InCl_5(NH_3)]$, and $(NH_4)_3InCl_6$ are obtained on heating equimolar amounts of indium(III) chloride and melamine at 250 °C. The inner nitrogen (1) atoms of melam (shown in Scheme 1a) form connections with an indium atom in the center of the ring-shaped molecule (Scheme 1b). Two terminal nitrogen atoms (2) are completely deprotonated and interconnect two melam units and form N–In bonding displayed in Fig. 1, while the remaining nitrogen atom (3) undergoes complete deprotonation, forming N–In bonding instead. Alternatively, one can envision this structure as comprising four melaminate units (deprotonated four times), interconnected through nitrogen linkages, resembling a porphyrin-like assembly (Scheme 1b). The side phases sublimed off during the reaction and were removed from the main product. All crystal structures were refined by single-crystal X-ray refinement.

Crystal structure

The crystal structure of $(NH_4)[(InCl_2)_3(C_{12}N_{20}H_8)]\cdot\frac{2}{3}[InCl_3(NH_3)]$ was solved and refined with a transparent yellow single-crystal based on X-ray diffraction data in the cubic space group $I\bar{4}3d$ (Table 1). The characteristic motif in the structure is the molecular $[C_{12}N_{20}H_8]^{4-}$ anion that is interconnected by indium atoms into a three-dimensional network structure. Indium(III) ions in the $[(InCl_2)(InCl_2)_{4/2}(C_{12}N_{20}H_8)]^-$ fragment are surrounded octahedrally in two different ways. One type of indium is centered within the $[C_{12}N_{20}H_8]^{4-}$ ion and four indium atoms surrounding the $[C_{12}N_{20}H_8]^{4-}$ ion having distorted octahedral $(-N)_4$-$InCl_2$ arrangements, displayed in Fig. 1. Indium in the center of the $(C_{12}N_{20}H_8)^{4-}$ anion is connected by dative bonding coming from the electron pairs of four nitrogen atoms, and two chloride ligands in the *trans* position. Four other indium atoms are showing *cis*-arrangements of their $(-N)_4InCl_2$ polyhedra, thereby inducing a tilted –N–In–N– connectivity between adjacent $(C_{12}N_{20}H_8)^{4-}$ moieties in the structure (Fig. 2).

The bridging connectivity of indium(III) ions in the structure involves In–N distances ranging between 204.2(2) pm and 228.1(6) pm. This connectivity leads to a complex structure, in which one central moiety connects to four adjacent $[C_{12}N_{20}H_8]^{4-}$ moieties and so on. The ammonium ions and $[InCl_3(NH_3)]$ molecules occupy voids in the arrangement of the

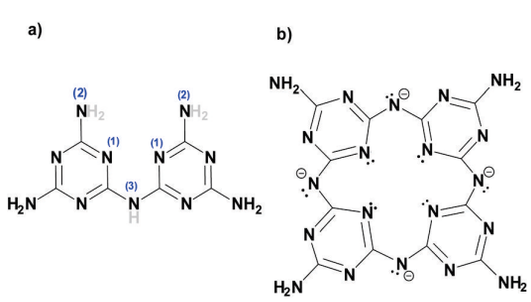

Scheme 1 (a) Structure of melam ($C_6N_{11}H_9$) with H atoms that are subjected to deprotonation drawn in grey and (b) the $[C_{12}N_{20}H_8]^{4-}$ anion centered and surrounded by indium atoms.

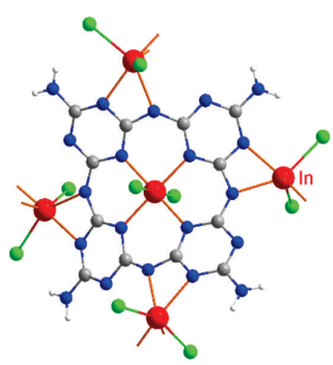

Fig. 1 Surrounding and connectivity of the $(C_{12}N_{20}H_8)^{4-}$ ion with indium(III) ions as $[(InCl_2)(InCl_2)_{4/2}(C_{12}N_{20}H_8)]^-$ (In is shown red, Cl green, C gray, and N in blue).

Table 1 Selected crystal and structure refinement data for $(NH_4)[(InCl_2)_3(C_{12}N_{20}H_8)]\cdot\frac{2}{3}[InCl_3(NH_3)]$, recorded at 150 K

Empirical formula	$C_{36}\ N_{71}H_{66}\ In_{11}Cl_{24}$
CCDC	2333063
Formula weight (g mol^{-1})	3607.41
Wavelength (Cu-K$_\alpha$) (Å)	1.54184
Crystal system	Cubic
Space group	$I\bar{4}3d$
Unit cell dimensions (Å)	28.1902(2)
Volume (Å^3)	22402.4(5)
Z	8
Density (calculated) (g cm^{-3})	2.139
Absorption coefficient (mm^{-1})	23.580
Final R indices ($I > 2\sigma(I)a$)	$R_1 = 0.0284$, w$R_2 = 0.0792$
R indices (all data)	$R_1 = 0.0296$, w$R_2 = 0.0798$
GOOF	1.058

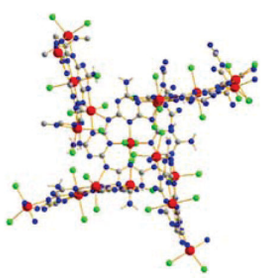

Fig. 2 Section of the structure showing the tilted connectivity pattern between one $(C_{12}N_{20}H_8)^{4-}$ unit with four adjacent ones *via* –N–In–N– bonding.

$(NH_4)[(InCl_2)_3(C_{12}N_{20}H_8)]^-$ network, as shown in Fig. 3 on the right. These molecules are very similar to those of the obtained side phase in the reaction, which is characterized as $(NH_4)_2[InCl_5(NH_3)]$, with its $[InCl_5(NH_3)]^{2-}$ ion displayed in Fig. 4, in comparison to the neutral $[InCl_3(NH_3)]$ in the title compound. The crystal structure of the side phase $(NH_4)_2[InCl_5(NH_3)]$ consists of indium, coordinated to five chloride ions and one ammonia molecule, arranged in a distorted octahedral geometry, with ammonium ions serving as counter ions to balance the charge. In the other side phase $((NH_4)_3InCl_6)$, indium is coordinated to six chloride ions and three ammonium ions act as counterions.

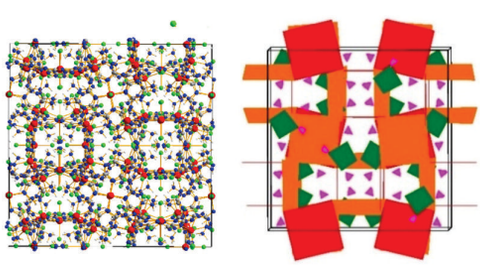

Fig. 3 Unit cell content in the cubic ($I\bar{4}3d$) structure of $(NH_4)[(InCl_2)_3(C_{12}N_{20}H_8)]\cdot\frac{2}{3}[InCl_3(NH_3)]$ (left) and a schematic polyhedra drawing in the structure (right), emphasizing NH_4^+ ions as tetrahedra (violet) and $[InCl_3(NH_3)]$ molecules as distorted octahedra (green).

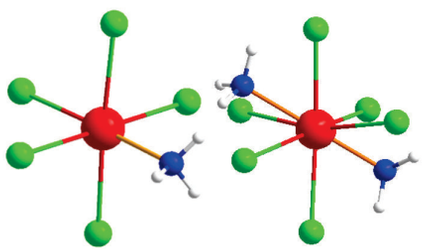

Fig. 4 The $[InCl_5(NH_3)]^{2-}$ ion in the structure of $(NH_4)_2[InCl_5(NH_3)]$ (left) and the neutral $[InCl_3(NH_3)]$ in $(NH_4)[(InCl_2)_3(C_{12}N_{20}H_8)]\cdot\frac{2}{3}[InCl_3(NH_3)]$ (right). Note that all ligands are occupied by 50% only in the latter.

Thermoanalytic studies

The reaction of a 1.2 : 1 molar mixture of $InCl_3$ and melamine was examined through differential scanning calorimetry (DSC) at a heating and cooling rate of 2 °C min^{-1} within the temperature range from room temperature to 500 °C (Fig. 5). The DSC curve revealed two distinct exothermic regions at 150 °C and a broad peak at around 217–265 °C, each indicative of a reaction between the reactants. To discern each reaction, we interrupted the process at each peak and studied the X-ray diffraction (XRD) patterns obtained from each experiment. The first peak at around 150 °C shows the formation of intermediate unknown phases. Multiple exothermic peaks in the range of 217–265 °C indicate the formation of the $(NH_4)[(InCl_2)_3(C_{12}N_{20}H_8)]\cdot\frac{2}{3}[InCl_3(NH_3)]$ compound, and the side phases of $(NH_4)_2[InCl_5(NH_3)]$ and $(NH_4)_3InCl_6$. It's important to note that there are also multiple peaks within this temperature range, which can be assigned to by-products produced at this temperature range. These side phases could be separated by temperature gradient. The decomposition of the product is evident at the endothermic peak (435 °C) and has been further analysed in the TGA and stability sections.

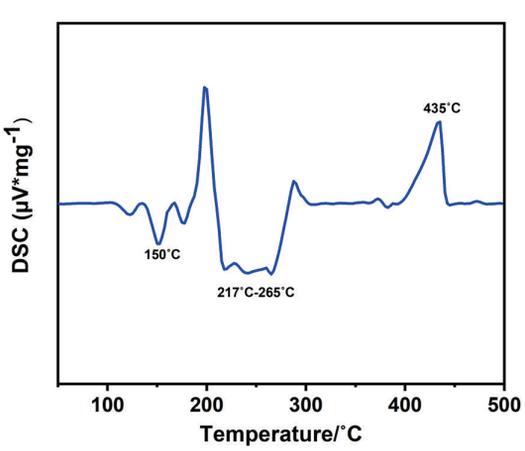

Fig. 5 DSC of the reaction of $InCl_3$ melamine in a stoichiometric ratio of 1.2 : 1.

X-ray powder diffraction

As part of the investigation into reaction products, we conducted a PXRD analysis. The XRD pattern for $(NH_4)[(InCl_2)_3(C_{12}N_{20}H_8)]\cdot\frac{2}{3}[InCl_3(NH_3)]$ is shown in Fig. S1† These recorded patterns were then compared with calculated counterparts obtained through structure refinement based on single-crystal data. The compound was successfully obtained with a yield of 58%. Since the by-products crystallized at the top of the ampule, characterization was also conducted through single-crystal diffraction, leading to the characterization of the yet unknown adducts of $(NH_4)_2[InCl_5(NH_3)]$, and $(NH_4)_3InCl_6$ (CCDC 2301094 and 2334831). The XRD taken from side-phases sublimated on the top of the ampule is depicted in Fig. S2† along with the crystal structures data provided in Table S1.†

Infrared spectroscopy (IR)

The experimental IR spectrum of the $(NH_4)[(InCl_2)_3(C_{12}N_{20}H_8)]\cdot\frac{2}{3}[InCl_3(NH_3)]$ compound has been compared with that of melamine and melem as shown in Fig. 6. Table S2† provides information on the frequencies linked to individual vibrational modes of these molecules, along with the corresponding assignments of bonds. This comparison helps us understand the $(NH_4)[(InCl_2)_3(C_{12}N_{20}H_8)]\cdot\frac{2}{3}[InCl_3(NH_3)]$ compound's spectral features by relating them to the well-known vibrational patterns of melamine, and melem.[17] As shown in Fig. 6, infrared spectra were recorded for three compounds in the range of 4000 to 500 cm^{-1}. Given that all the compounds contain NH_2 groups, it is not surprising that they exhibit similar patterns in the regions between 3500–3200 cm^{-1} and 1580–1600 cm^{-1}, ascribed to NH stretching and bending vibrations, respectively.[17,28] However, apart from slight variations in relative intensities and splitting, there is a distinctive difference in $(NH_4)[(InCl_2)_3(C_{12}N_{20}H_8)]\cdot\frac{2}{3}[InCl_3(NH_3)]$ compound compared to melem, and melamine in these regions. In fact, in the spectrum of the $(NH_4)[(InCl_2)_3(C_{12}N_{20}H_8)]\cdot\frac{2}{3}[InCl_3(NH_3)]$ compound, the band at around 3500–3200 cm^{-1} appears broader and slightly less intense compared to the two others, which can signify differences in structures, especially the number of NH_2 groups present in this structure. As expected, the compounds show a similar spectrum in the regions around 800 cm^{-1} and 1400–1550 cm^{-1}, which are related to ring out-of-plane bending and side chain C–N breathing, respectively.[28]

Stability of $(NH_4)[(InCl_2)_3(C_{12}N_{20}H_8)]\cdot\frac{2}{3}[InCl_3(NH_3)]$

The $(NH_4)[(InCl_2)_3(C_{12}N_{20}H_8)]\cdot\frac{2}{3}[InCl_3(NH_3)]$ compound has been kept for two months outside of the glove box inside an open container, and XRD measurements taken from the crystalline powder shown in Fig. S3† show the high stability of this compound in air. The thermal stability of this compound has also been studied with TGA analysis, as can be seen in Fig. 7. The decomposition starts at around 425 °C and continues to 700 °C until the compound is finally converted into indium carbodiimide, $In_{2.24}(NCN)_3$.[34] The XRD pattern taken from the final product which appears to be indium carbodiimide, is shown in Fig. S4.†

Photoluminescence measurements

Metal–organic complexes with indium metal centers were reported before to have photoluminescent properties.[35–38] In fact, complexes with a d^{10} metal center have been considered as luminescent materials.[39] Furthermore, the luminescence and photochemistry of porphyrin and phthalocyanine complexes with group 13 metals have been reported in several studies.[40,41] Therefore, the solid-state luminescence of the synthesized material was investigated at ambient temperature (Fig. 8). The emission spectra depicted two broad bands at 380 and 530 nm, while the corresponding excitation bands are at 350 and 460 nm, respectively. The 530 nm emission causes greenish luminescence as displayed in the inset in Fig. 8. To further analyse the photoluminescence behaviour, decay curves of the emission spectra excited at 350 nm were recorded (Fig. 9a and b). The decay curves indicated emission lifetimes

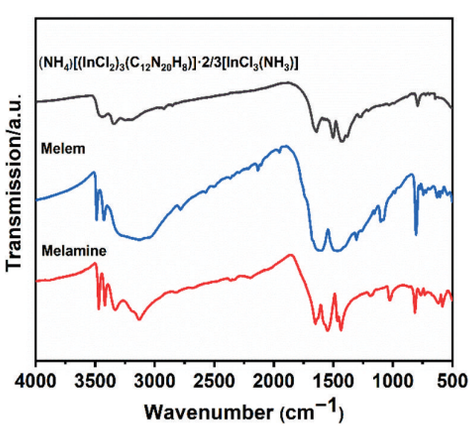

Fig. 6 IR comparison of $(NH_4)[(InCl_2)_3(C_{12}N_{20}H_8)]\cdot\frac{2}{3}[InCl_3(NH_3)]$ with melamine, and melem.

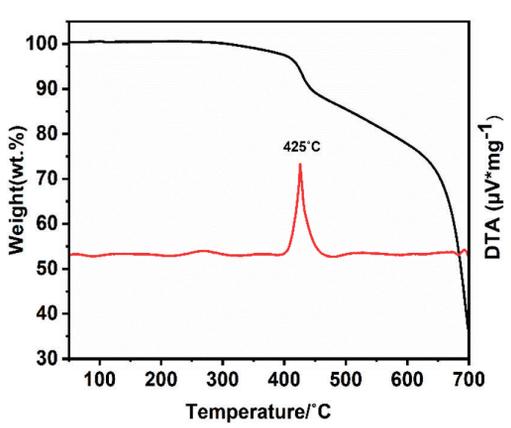

Fig. 7 TGA analysis and stability of $(NH_4)[(InCl_2)_3(C_{12}N_{20}H_8)]\cdot\frac{2}{3}[InCl_3(NH_3)]$.

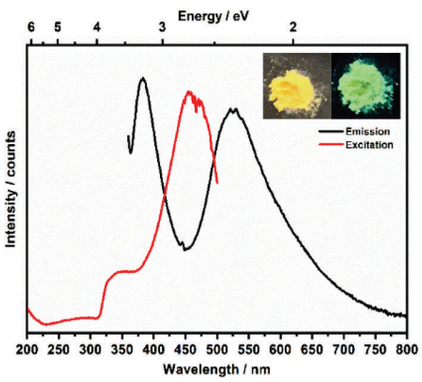

Fig. 8 Photoluminescence spectra of $(NH_4)[(InCl_2)_3(C_{12}N_{20}H_8)]\cdot\frac{2}{3}[InCl_3(NH_3)]$ in the solid-state at room temperature. The emission spectrum was recorded upon 350 nm excitation, while the excitation spectrum was monitored at 535 nm. The inset shows the crystalline yellow powder of the title compound and the green emission under UV excitation.

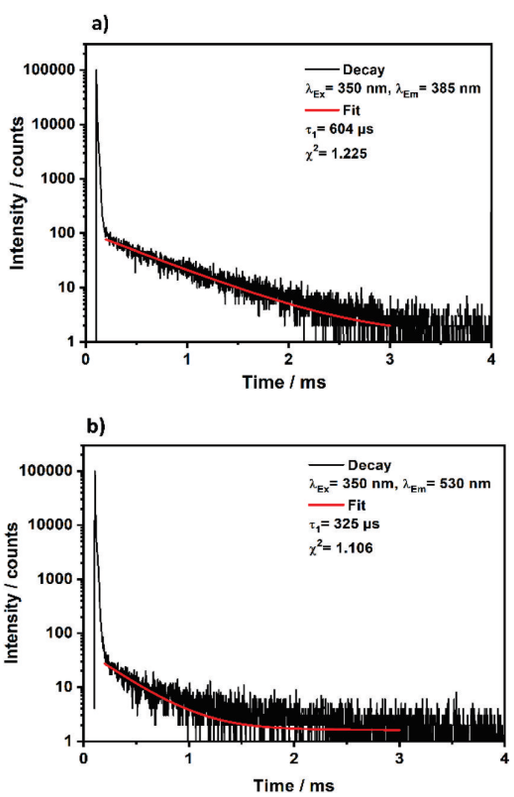

Fig. 9 Decay curves obtained for crystalline $(NH_4)[(InCl_2)_3(C_{12}N_{20}H_8)]\cdot\frac{2}{3}[InCl_3(NH_3)]$ upon excitation at 350 nm and monitoring the emission band at 358 nm (a) or monitoring the emission at 530 nm (b).

τ_1 = 604 µs and τ_1 = 325 µs for the emission bands at 358 nm and 530 nm, respectively. In some of indium metal–organic compounds, the ligands alone doesn't show any photoluminescent property meaning that rather the ligand-to-metal charge transfer is responsible for the observed photoluminescence.[38] In this study, the emission band of 530, and also the calculated decay times fall in the region of similar works on indium-based complexes.[35,37,42–44] The observed luminescence of this compound is most likely due to ligand-to-metal charge transfers (LMCT) or metal-centered transitions, as the decay times are in the microsecond range. This is inconsistent with ligand-centered processes such as π–π* transitions, which typically decay within the nanosecond range.[45] The transitions are most likely caused by an LMCT, since In^{3+} can easily take up one or two electrons, which yields the monovalent ion s^2 ion (In^+) as an excited state.[45] Additionally, metal-centered transitions in In^{3+} ($[Kr]4d^{10}$) comprising materials are known and could explain the observed emission spectrum.[36,37,45]

Conclusion

This research work introduces a novel, simple solid-state synthesis for creating supramolecular and porphyrin-like assemblies from the thermal condensation of melamine. The compound, denoted as $(NH_4)[(InCl_2)_3(C_{12}N_{20}H_8)]\cdot\frac{2}{3}[InCl_3(NH_3)]$ results from the reaction between indium(III) chloride and melamine, featuring a unique supramolecular assembly of deprotonated melamine or deprotonated melam interconnected with indium chloride centers. This study introduces the first compound made from four times deprotonation of melamine, with the $[C_{12}N_{20}H_8]^{4-}$ anion. Our findings highlight that this compound is also stable under ambient conditions, indicating its potential for further research and exploration. Infrared spectroscopy, X-ray diffraction analysis, thermal gravimetric analysis (TGA), and differential scanning calorimetry (DSC) analyses confirm its stability and reveal its structural characteristics. Analogous to porphyrins and metal–organic assemblies with d^{10} metal centres, this supramolecular arrangement has the potential to exhibit luminescence attributable to ligand-to-metal charge transfers (LMCT) or metal-centered transitions. The luminescent color under UV radiation originates from an interconnected structure binding to the metal core. Overall, the synthesized compound not only holds promise for advancing deprotonation ligands derived from melamine and its condensation products but also offers valuable insights into supramolecular C/H/N chemistry, and their properties.

Experimental section

Materials and methods

The starting substances, melamine (2,4,6-triamino-1,3,5-triazine, purchased from Sigma-Aldrich, 99%), and indium(III) chloride (Sigma-Aldrich, 99%), were utilized without additional purification. The reaction mixtures were prepared in a glovebox under an argon atmosphere with moisture and oxygen levels maintained below 1 ppm. Subsequently, the pre-

pared mixtures were transferred into handmade silica tubing (length: 6 cm, inner diameter: 7 mm) and sealed under a vacuum. The reactions were conducted in Simon–Müller furnaces.

Synthesis of $(NH_4)[(InCl_2)_3(C_{12}N_{20}H_8)]\cdot\frac{2}{3}[InCl_3(NH_3)]$

Indium(III) chloride and melamine in a molar ratio of 1.2 : 1, respectively were ground together in an agate mortar as precursors. The resulting mixture weighing approximately 50 is vacuum-sealed. This ampule was subsequently placed horizontally in a Simon–Müller furnace, heated to 250 °C for 20 h with a heating rate of 2 °C min^{-1}, and cooling at a rate of 0.5 °C min^{-1}. The reaction yielded a yellow crystalline product at the ampule's bottom, achieving a yield of 58% relative to the precursors. The separation of the product from by-products is primarily influenced by the temperature gradient.

Instrumentation

X-ray powder diffraction

The powder diffractometer (STOE Darmstadt, STADIP, Ge-monochromator) was utilized to record the X-ray diffraction patterns of the prepared powders. The radiation employed was Cu-Kα_1 (λ = 1.540598 Å), and data was collected within the 5 < 2θ < 100° range. Match$_3$! Software was used to compare these patterns with those of the relevant crystal structures.

Single-crystal X-ray diffraction

Single crystals of the product were chosen and positioned on a light-yellow single-crystal X-ray diffractometer (Rigaku XtaLab Synergy-S) utilizing Cu-K$_\alpha$ radiation (λ = 1.54184 Å) and a mirror monochromator at either 150 or 220 K. The crystal structures were determined through direct methods (SHELXT),[46] followed by full-matrix least-squares structure refinements (SHELXL-2014).[46] X-ray intensity absorption correction was carried out using numerical methods with the CrysAlisPro 1.171.41.92a software (Rigaku Oxford Diffraction). Hydrogen atoms were identified in the difference map and refined isotopically based on their positions.

Infrared spectra

The infrared (IR) spectra for the samples were obtained utilizing a Bruker VERTEX 70 FT-IR spectrometer, covering a spectral range from 400 to 4000 cm^{-1}. KBr tablets were employed as the background during the spectroscopic measurements.

Optical measurements

The fluorescence spectrometer FLS920 (Edinburgh Instruments) equipped with a 450 W xenon discharge lamp (OSRAM) was utilized to capture the emission and excitation spectra of $(NH_4)[(InCl_2)_3(C_{12}N_{20}H_8)]\cdot\frac{2}{3}[InCl_3(NH_3)]$. Inside the sample chamber, a mirror optic designed for powder samples was incorporated. For detection purposes, an R2658P single-photon-counting photomultiplier tube manufactured by Hamamatsu was utilized. Photoluminescence spectra were recorded with a spectral resolution of 1 nm, a dwell time of 0.5 seconds at 1 nm intervals, and 2 repetitions. The photoluminescence decay curves were recorded using the same spectrometer but with a 445 nm picosecond laser as a pulsed excitation source.

Thermoanalytic studies

Differential scanning calorimetry (DSC) experiments were conducted utilizing a DSC 204 F1 Phoenix instrument (Fa. Netzsch, Selb, Germany). The initial components were sealed in a glovebox under an argon atmosphere and placed in gold-plated (5 μm) steel autoclaves with a 100 μl volume (Bächler Feintech AG in Hölstein, Switzerland). The reaction between $InCl_3$ and melamine was investigated on 1.2 : 1 ratio, covering a temperature range from room temperature to 500 °C. The heating and cooling processes were performed at a rate of 2 °C min^{-1}.

The TGA experiments were conducted using a Netzsch Jupiter STA 449 F3 apparatus. The final product was transferred under argon into an open-ended custom silica container and exposed to gradual heating and cooling at a rate of 2 K min^{-1}. This enabled stability analysis of the product across the temperature spectrum from room temperature to 700 °C.

Data availability statement

The data that support the findings of this study are openly available in CCDC.

$(NH_4)_2[InCl_5(NH_3)]$: CCDC 2301094.

$(NH_4)_3InCl_6$: CCDC 2334831.

$(NH_4)[(InCl_2)_3(C_{12}N_{20}H_8)]\cdot\frac{2}{3}[InCl_3(NH_3)]$: CCDC 2333063.†

Data are available within the article or its ESI.†

The data that support the findings of this study are available on request from the corresponding author, H.-J. Meyer.

Author contributions

H.-J. M.: conceptualization, supervision, funding acquisition, review, and editing. E. B.: synthesis, PXRD, and IR, writing. M. S.: X-ray diffraction refinements and structure solutions. T. J. and D. E.: photoluminescence spectroscopy. All authors have read and agreed to the published version of the manuscript.

Conflicts of interest

The authors declare no conflict of interest.

Acknowledgements

We gratefully acknowledge the support provided by the Deutsche Forschungsgemeinschaft (DFG-Bonn) for this research project (ME 914/34-1) and Keno Kraut (Univ. Tübingen) for his preparative work within the framework of an

advanced lab course. Sincere thank you to Mike Healey Smith for his English revisions and proofreading of this article.

References

1 J. Liebig, *Ann. Pharm.*, 1834, **10**, 1–47.
2 G. M. Crews, W. Ripperger, D. B. Kersebohm, T. Güthner and B. Mertschenk, *Ullmann's Encyclopedia of Industrial Chemistry*, 2000.
3 F. K. Keßler, Ph.D. Thesis, Ludwig Maximilian University of Munich, 2019.
4 P. Klason, *J. Prakt. Chem.*, 1886, **33**, 285–289.
5 L. Gmelin, *Ann. Pharm.*, 1835, **15**, 252–258.
6 A. Schwarzer, T. Saplinova and E. Kroke, *Coord. Chem. Rev.*, 2013, **257**, 2032–2062.
7 E. C. Franklin, *J. Am. Chem. Soc.*, 1922, **44**, 486–509.
8 L. Pauling and J. Sturdivant, *Proc. Natl. Acad. Sci. U. S. A.*, 1937, **23**, 615–620.
9 T. Komatsu, *Macromol. Chem. Phys.*, 2001, **202**, 19–25.
10 H. Schroeder and E. Kober, *J. Org. Chem.*, 1962, **27**, 4262–4266.
11 B. V. Lotsch, M. Döblinger, J. Sehnert, L. Seyfarth, J. Senker, O. Oeckler and W. Schnick, *Chem. – Eur. J.*, 2007, **13**, 4969–4980.
12 H. May, *J. Appl. Chem.*, 1959, **9**, 340–344.
13 T. Saplinova, C. Lehnert, U. Böhme, J. Wagler and E. Kroke, *New J. Chem.*, 2010, **34**, 1893–1908.
14 A. Sattler, L. Seyfarth, J. Senker and W. Schnick, *Z. Anorg. Allg. Chem.*, 2005, **631**, 2545–2554.
15 A. Sattler and W. Schnick, *Z. Anorg. Allg. Chem.*, 2008, **634**, 457–460.
16 E. Wirnhier, M. B. Mesch, J. Senker and W. Schnick, *Chem. – Eur. J.*, 2013, **19**, 2041–2049.
17 V. L. Bettina and W. Schnick, *Chem. – Eur. J.*, 2007, **13**, 4956–4968.
18 B. V. Lotsch, Doctoral dissertation, Ludwig Maximilian University of Munich, 2006.
19 A. Sattler, S. Pagano, M. Zeuner, A. Zurawski, D. Gunzelmann, J. Senker, K. Müller-Buschbaum and W. Schnick, *Chem. – Eur. J.*, 2009, **15**, 13161–13170.
20 N. E. Braml, A. Sattler and W. Schnick, *Chem. – Eur. J.*, 2012, **18**, 1811–1819.
21 M. M. Zhao and P. P. Shi, *Acta Crystallogr., Sect. E: Struct. Rep. Online*, 2010, **66**, o1463–o1463.
22 F. K. Kessler, T. J. Koller and W. Schnick, *Z. Anorg. Allg. Chem.*, 2018, **644**, 186–192.
23 F. K. Kessler, A. M. Schuhbeck and W. Schnick, *Z. Anorg. Allg. Chem.*, 2019, **645**, 840–847.
24 P. Kallenbach, Master dissertation, Eberhard Karls Universität Tübingen, 2021.
25 Z. Bai, J. Lee, H. Kim, C. L. Hu and K. M. Ok, *Small*, 2023, 2301756.
26 L. Liu, Y. Wu, L. Ma, G. Fan, W. Gao, W. Wang and X. Ma, *J. Struct. Chem.*, 2022, **63**, 302–309.
27 P. Kallenbach, E. Bayat, M. Ströbele, C. P. Romao and H.-J. R. Meyer, *Inorg. Chem.*, 2021, **60**, 16303–16307.
28 E. Bayat, M. Ströbele and H.-J. Meyer, *Chemistry*, 2023, **5**, 1465–1476.
29 L. Zhang, J. Zhang, Z.-J. Li, J.-K. Cheng, P.-X. Yin and Y.-G. Yao, *Inorg. Chem.*, 2007, **46**, 5838–5840.
30 A. Rana, M. Bera, D. S. Chowdhuri, D. Hazari, S. K. Jana, E. Zangrando and S. Dalai, *J. Inorg. Organomet. Polym. Mater.*, 2012, **22**, 360–368.
31 K. Sivashankar, A. Ranganathan, V. Pedireddi and C. Rao, *J. Mol. Struct.*, 2001, **559**, 41–48.
32 A. L. Görne, T. Scholz, D. Kobertz and R. Dronskowski, *Inorg. Chem.*, 2021, **60**, 15069–15077.
33 W. Schnick and H. Huppertz, *Z. Anorg. Allg. Chem.*, 1995, **621**, 1703–1707.
34 R. Dronskowski, *Z. Naturforsch., B: J. Chem. Sci.*, 1995, **50**, 1245–1251.
35 S. Herrera, K. I. Rivero, A. Guzmán, J. Cedeño, J. Miksovska and R. G. Raptis, *Dalton Trans.*, 2022, **51**, 14277–14286.
36 S. H. Lee, N. Shin, S. W. Kwak, K. Hyun, W. H. Woo, J. H. Lee, H. Hwang, M. Kim, J. Lee and Y. Kim, *Inorg. Chem.*, 2017, **56**, 2621–2626.
37 C. H. Ryu, S. W. Kwak, H. W. Lee, J. H. Lee, H. Hwang, M. Kim, Y. Chung, Y. Kim, M. H. Park and K. M. Lee, *Inorg. Chem.*, 2019, **58**, 12358–12364.
38 Y.-Q. Zhang, W.-L. Ma, W.-Z. Li, Y.-L. Lan, Y. Liu, Y.-N. Zhao and J. Luan, *J. Mol. Struct.*, 2024, **1301**, 137380.
39 X. Du, R. Fan, X. Wang, L. Qiang, P. Wang, S. Gao, H. Zhang, Y. Yang and Y. Wang, *Cryst. Growth Des.*, 2015, **15**, 2402–2412.
40 V. S. Thoi, J. R. Stork, D. Magde and S. M. Cohen, *Inorg. Chem.*, 2006, **45**, 10688–10697.
41 S. Ito, M. Gon, K. Tanaka and Y. Chujo, *Natl. Sci. Rev.*, 2021, **8**, nwab049.
42 P. C. Teeuwen, Z. Melissari, M. O. Senge and R. M. Williams, *Molecules*, 2022, **27**, 6967.
43 O. T. Alexander, M. M. Duvenhage, R. E. Kroon, A. Brink and H. G. Visser, *New J. Chem.*, 2021, **45**, 2132–2140.
44 Q. Gao, F.-L. Jiang, M.-Y. Wu, Y.-G. Huang, L. Chen, W. Wei and M.-C. Hong, *J. Solid State Chem.*, 2009, **182**, 1499–1505.
45 G. Blasse, *Chem. Phys. Lett.*, 1990, **175**, 237–241.
46 G. Sheldrick, *Acta Crystallogr., Sect. A: Cryst. Phys., Diffr., Theor. Gen. Crystallogr.*, 1984, **40**, C440–C440.

Thermal Deprotonation and Condensation of Melamine in the Presence of Indium(III)chloride

Elaheh Bayat[a], Markus Ströbele[a], David Enseling[b], Thomas Jüstel[b] and H.-Jürgen Meyer*[a]

Supporting Information

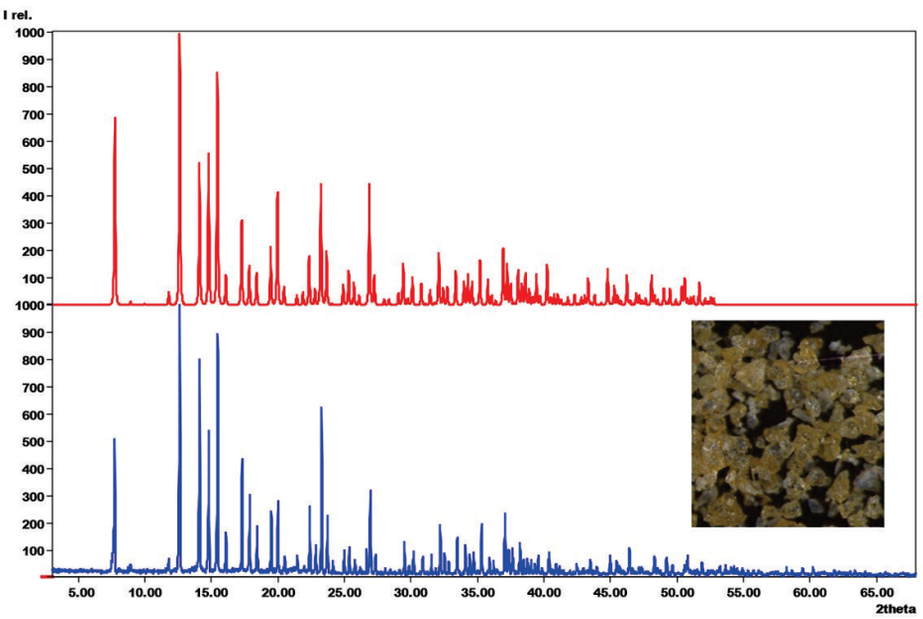

Figure SI 1. XRD pattern of the synthesized $(NH_4)[(InCl_2)_3\ (C_{12}N_{20}H_8)]\cdot\frac{2}{3}[InCl_3(NH_3)]$(bottom), Calculated pattern from single crystal measurement (top) (CCDC code: 2333063).

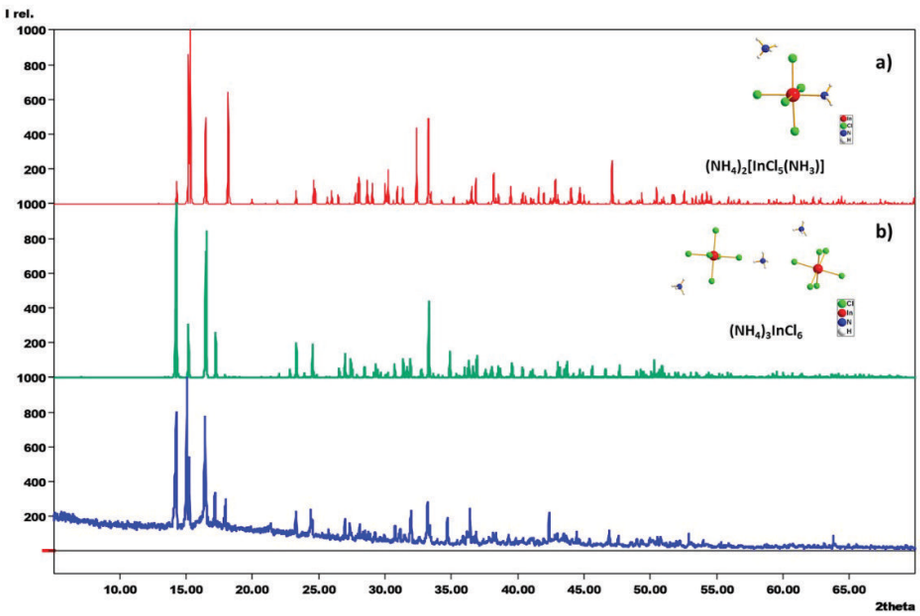

Figure SI.2. XRD pattern of the side-phases sublimated on the top part of ampule synthesized along with the main phase of $(NH_4)[(InCl_2)_3\ (C_{12}N_{20}H_8)]\cdot\frac{2}{3}[InCl_3(NH_3)]$(bottom). **(a)** Calculated pattern from single crystal measurement of $(NH_4)_2[InCl_5(NH_3)]$ (CCDC code: 2301094) **(b)** Calculated pattern from single crystal measurement of $(NH_4)_3\ InCl_6$ (CCDC code: 2334831).

Table S1. Crystal structure data of $(NH_4)_2[InCl_5(NH_3)]$, and $(NH_4)_3\ InCl_6$ as side phases of the reaction.

Empirical Formula	**$(NH_4)_2[InCl_5(NH_3)]$**	**$(NH_4)_3\ InCl_6$**
CCDC code	2301094	2334831
Formula weight (g/mol)	345.19	381.65
Wavelength (Cu-Kα) (Å)	1.54184	1.54184
Crystal system	orthorhombic	monoclinic
Space group	*Pnma*	$P2_1/c$
Unit cell dimensions (Å)	*a*/Å 13.7070(2) *b*/Å 10.76210(10) *c*/Å 6.93960(10)	*a*/Å 13.1270(3) *b*/Å 7.78800(10) *c*/Å 12.2894(2)
Volume (Å^3)	1023.70(2)	1192.96(4)
Z	4	4
Density (calculated) (g/cm^3)	2.240	2.125
Absorption coefficient (mm^{-1})	29.980	27.819
Final R indices (I>2σ(I)) a)	R_1 = 0.0133, wR_2 = 0.0364	R_1 = 0.0148, wR_2 =0.0371

R indices (all data)	R_1 = 0.0133, wR_2 = 0.0364	R_1 = 0.0149, wR_2 =0.0372
GOOF	1.264	1.211

Table S2. Vibrational frequencies (in cm^{-1}) for In-Ring compared to those of Melamine, Melem, and $(NH_4)[(InCl_2)_3\ (C_{12}N_{20}H_8)]\cdot⅔[InCl_3(NH_3)]$

	Melamine	**Melem**	**$(NH_4)[(InCl_2)_3(C_{12}N_{20}H_8)]\cdot⅔[InCl_3(NH_3)]$**
Ring-sextant out-of-plane bending	813	804	792
CNC bending	1193	1306	1284
Side-chain CN breathing	1434 1440 1550	1470	1380 1434 1504
NH_2 bending	1652	1612	1647
NH stretching	3128 3334 3421 3469	3119 3325 3424 3487	3200 3348 3452

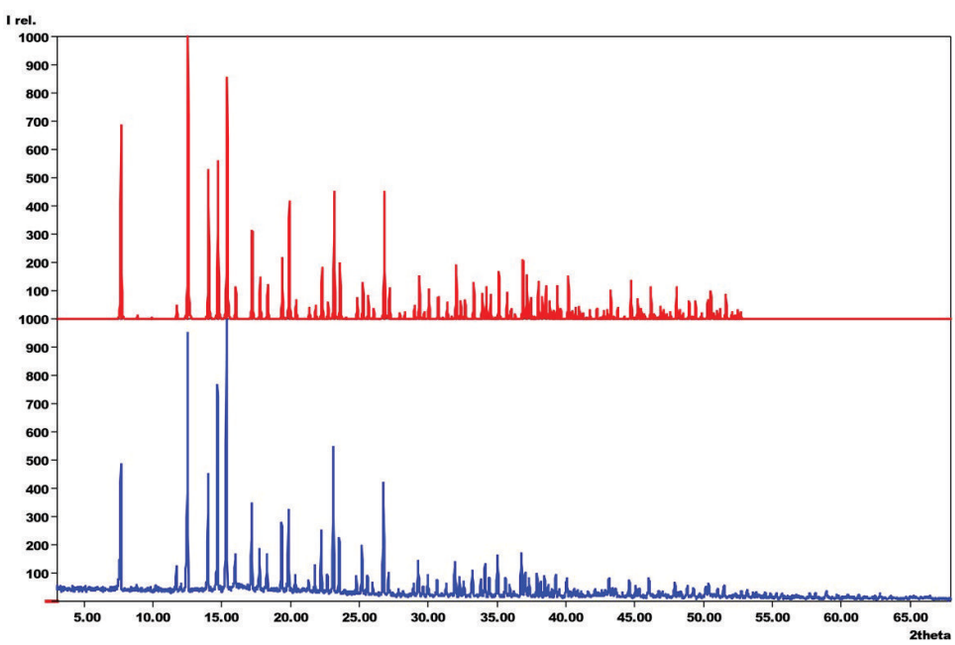

Figure SI 3. XRD pattern of the synthezied $(NH_4)[(InCl_2)_3\ (C_{12}N_{20}H_8)]\cdot⅔[InCl_3(NH_3)]$ after two month in ambient condition(bottom), Calculated pattern from single crystal measurement (top) (CCDC code: 2333063).

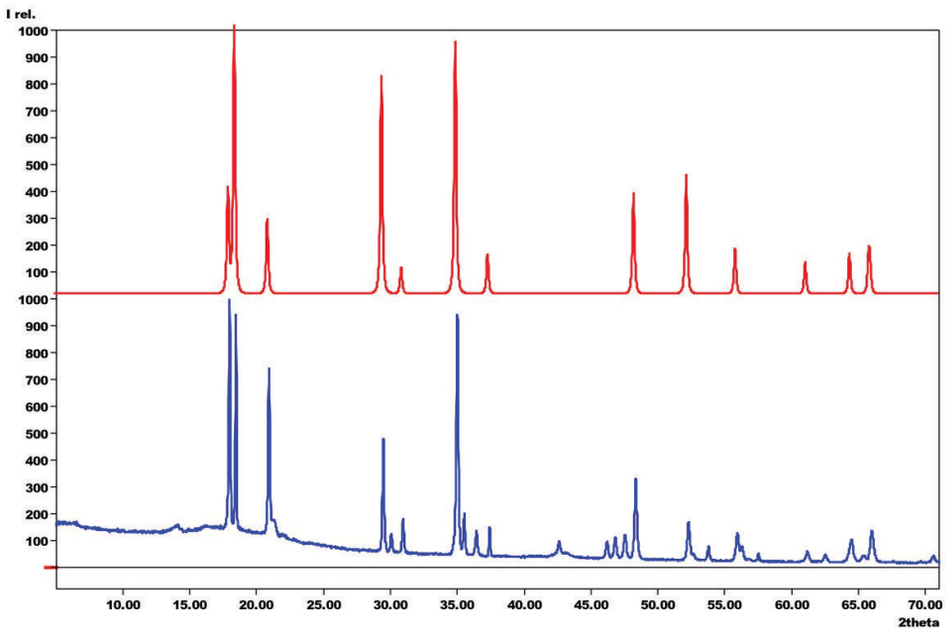

Figure SI 4. The XRD pattern taken from decomposed material at 700˚C in TGA analysis(bottom), Calculated pattern from single crystal measurement of $In_{2.24}(NCN)_3$(top)

Publication 5

A Systematic Study of the Solid-State Pathway from Melamine via Melaminate to Carbodiimide under Evolution of Hydrogen

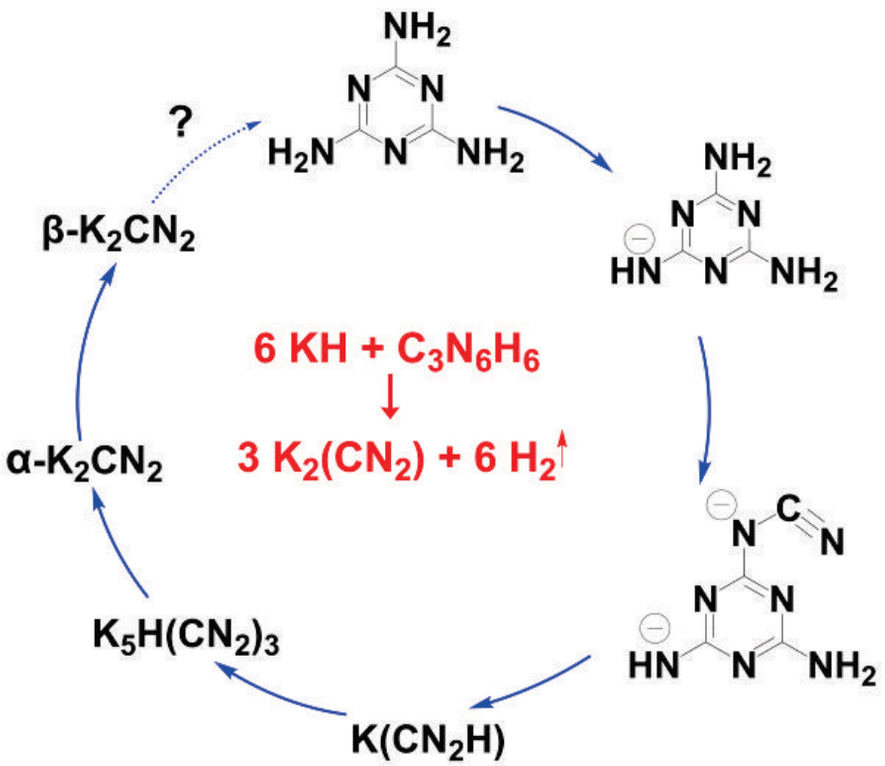

https://doi.org/10.1021/acs.inorgchem.4c02996

Reprinted with permission from

Inorg. Chem. 2024, 63, 16565−16572

Inorganic Chemistry

pubs.acs.org/IC Article

A Systematic Study of the Solid-State Pathway from Melamine via Melaminate to Carbodiimide under Evolution of Hydrogen

Markus Ströbele, Elaheh Bayat, and Hans-Jürgen Meyer*

Cite This: *Inorg. Chem.* 2024, 63, 16565−16572 Read Online

ACCESS | Metrics & More | Article Recommendations | Supporting Information

ABSTRACT: Thermal analysis techniques, such as differential scanning calorimetry (DSC) and thermogravimetric analysis (TGA), can provide valuable insights into thermal properties, intermediate phases, and phase transitions; sometimes even a whole series of compounds appears in a given system. The solid-state reaction pathway from melamine to carbodiimide, monitored by DSC, involves a sequence of chemical reactions and intermediate phases departing from the reaction of potassium hydride and melamine. The fully analyzed reaction cascade begins with the formation of potassium melaminate, $K(C_3N_6H_5)$, and progresses through several intermediate phases, each with distinct structures and properties, before ultimately yielding β-$K_2(CN_2)$. All crystalline compounds appearing in this reaction sequence are identified using X-ray diffraction analyses. With a 6:1 ratio of potassium hydride and melamine, equal numbers of protic and hydridic hydrogen atoms in the starting materials favor the release of H_2 until the formation of the final product $K_2(CN_2)$, which appears with two modifications.

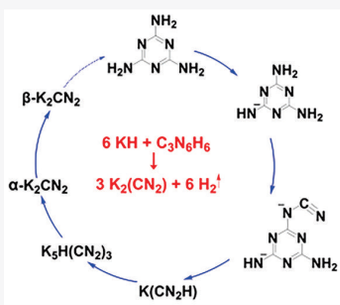

INTRODUCTION

Melamine-based materials are typically synthesized through the condensation reaction of melamine with formaldehyde or other aldehydes, resulting in a cross-linked polymer network.[1−3] These materials can be further modified by incorporating other functional groups or additives to tailor their properties for specific applications.[4−7] A new category of melamine materials, called melaminates, is currently being developed. These salts could potentially display distinctive properties and characteristics that have not yet been fully explored. The number of compounds containing deprotonated melamine is very small since the deprotonation of a weak base is challenging.[8]

Synthesis of melaminates has been attempted in liquid ammonia and solid-state reactions. The choice of the preparation method may depend on factors such as reaction conditions and ease of handling. Liquid ammonia can provide a solvent-like environment for the reaction under ammonothermal conditions, while the solid-state method may offer more control over the reaction kinetics. Both methods have been utilized to synthesize melaminates. Melaminates obtained from the ammonia route have been evidenced as ammonia adducts that are reported to turn amorphous upon removal of NH_3. Two compounds, potassium melaminate $K(C_3N_6H_5)\cdot nNH_3$ and tripotassium melaminate $K_3(C_3N_6H_3)$, have been proposed for the first time as melaminates.[8−10] However, some of these melaminate compounds were obtained as amorphous phases, and their compositions were only derived from elemental analysis. Later on, reactions of elemental potassium, sodium, and rubidium with melamine in liquid ammonia have yielded crystals of adducts of potassium and rubidium as $K(C_3N_6H_5)\cdot NH_3$ and $Rb(C_3N_6H_5)\cdot 1/2NH_3$, and amorphous $Na(C_3N_6H_5)\cdot NH_3$, under ammonothermal conditions.[8]

In our previous work, we were able to deprotonate melamine thrice in a solid-state metathesis reaction (SSM) with copper chloride (CuCl) to yield tricopper melaminate.[11] $Cu_3(C_3N_6H_3)$ represents a semiconducting MOF with Cu-to-Cu bonding and shows the applicability of melaminate as a building block in a supramolecular architecture.[11] An improved synthesis for this material was given very recently by a solid-state reaction of copper chloride with $Na(HCN_2)$ to obtain $Cu_3(C_3N_6H_3)$ via trimerization reaction of $(HNCN)^-$ ions.[12]

Corresponding SSM reactions of melamine with antimony chloride ($SbCl_3$) yielded a melaminate dianion in $SbCl(C_3N_6H_4)$.[13] Reactions with indium chloride ($InCl_3$) resulted in the formation of melaminate monoanions in a tetrameric arrangement of the $[C_{12}N_{20}H_8]^{4-}$ ion.[14]

In a new attempt, we have studied the effect of bases such as LiH, NaH and KH in the deprotonation process of melamine in the solid state. Thermoanalytical studies revealed a sharp exothermic reaction with LiH, a tight reaction sequence with NaH (Figure S1), and a well resolved reaction sequence for the reaction between KH and melamine, which is thoroughly analyzed and reported herein.

Received: July 16, 2024
Revised: August 12, 2024
Accepted: August 15, 2024
Published: August 23, 2024

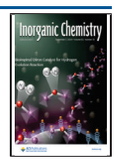

Previous studies in the system K−H−(NCN) were commonly performed in liquid ammonia and have led to the structural identification of several compounds in which hydrogen atoms act as a proton in $K_5H(CN_2)_3$,[15] as a protonic imide in K(HNCN),[16] and as a hydride in $K_5(CN_2)_2H$.[17]

$K_5H(CN_2)_3$ was obtained from K(HNCN) and metallic potassium in liquid ammonia, or alternatively from a solid-state reaction of KNH_2 with melamine at 320 °C.[15] Protons in this compound are only weakly bound to nitrogen atoms of $(NCN)^{2-}$ and are showing significant mobility as demonstrated by ^1H NMR and impedance measurements. The synthesis of K(HNCN) was achieved from the reaction of melamine and $K(NH_2)$ in liquid ammonia. $K_5(CN_2)_2H$ was prepared from $K(NH_2)$ and carbon in an autoclave reaction at 650 °C.[17] The synthesis of monoclinic (α-)$K_2(CN_2)$ was reported from a reaction of $KH(CN_2)$ with $K(NH_2)$ in liquid ammonia.[16]

All of these previously reported compounds have been prepared following their individual protocols. In this work, we show the formation of all of these compounds within one reaction sequence of a mixture of KH and melamine, as monitored by differential thermal scanning (DSC) analysis. All thermal effects in the DSC are analyzed, and the corresponding compounds are characterized by means of X-ray diffraction, including some new phases such as the new potassium melaminate and potassium cyanomelaminate. In spite of the formation of so many intermediate phases and the loss of a significant amount of molecular hydrogen, this method appears to be most useful for the preparation of potassium carbodiimide.

$Li_2(CN_2)$ is most common among alkali carbodiimides, thermally stable up to more than 700 °C, and has multiple reaction sites due to the existence of negative nitrogen atoms and carbon−nitrogen double bonds. It is easy to prepare from a reaction of Li_3N or LiH with melamine, as we show in our DSC study. Carbodiimides and cyanamides, commonly summarized as dinitridocarbonates, exhibit great prospects as versatile intermediates in various synthetic transformations, and are important compounds in organic synthesis, agriculture, and materials.[18]

RESULTS AND DISCUSSION

Differential Scanning Analyses. Solid-state reactions of melamine are analyzed by differential scanning calorimetry (DSC) using appropriate reaction mixtures encapsulated in gold-plated steel metal containers. Parallel reactions in fused silica ampules are used to grow single crystals for structure determination by means of single-crystal XRD to characterize intermediate phases at several stages of the reaction by means of powder X-ray diffraction (ex situ PXRD) and for the synthesis of pure phases.

Lithium carbodiimide, $Li_2(CN_2)$, is a well established reagent for the development of metal carbodiimide compounds.[19] Its synthesis is commonly achieved by reacting Li_3N with (excess of) melamine following eq 1.[15] This reaction is briefly evaluated and compared to an alternative reaction between LiH and melamine (eq 2).

The reaction between Li_3N and melamine requires an excess of melamine (relative to eq 1), due to the thermal mass loss of melamine resulting from the heat generation of the vigorous exothermic reaction, envisioned in Figure 1 (black line). These strongly exothermic reactions produce about −500 kJ/mol (calculated from DSC) in the reaction with Li_3N (eq 1) and ca. −350 kJ/mol (calculated from DSC) in the reaction with LiH (eq 2).

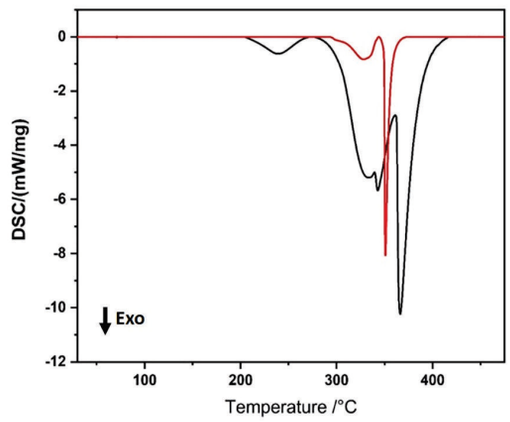

Figure 1. DSC plot of the reaction of Li_3N and melamine according to eq 1 (black line) and the reaction of LiH with melamine following eq 2 (red line) with a heating rate of 2°/min (corrected for the baseline).

$$2Li_3N + C_3N_6H_6 \rightarrow 3Li_2(CN_2) + 2NH_3\uparrow \quad (1)$$

$$6LiH + C_3N_6H_6 \rightarrow 3Li_2(CN_2) + 6H_2\uparrow \quad (2)$$

The parent reaction with LiH (eq 2) can serve as a beneficial alternative to the reaction reported previously (eq 1). The thermal study of the reaction with LiH reveals this reaction to be less exothermic, and for this reason, it does not require an excess of melamine.

The reaction of lithium hydride with melamine produces $Li_2(CN_2)$ under the release of hydrogen, originating from equal numbers of negatively and positively charged hydrogen species. This reaction was investigated for A = Li, Na, and K by differential scanning calorimetry (DSC) with samples encapsulated into gold-plated steel containers. The reaction with LiH (eq 2) reveals a sharp exothermic peak in the DSC (Figure 1). The reaction with Na revealed a DSC pattern, showing a relatively tight sequence of thermal events that were not well resolved (Figure S1).

In this study, we analyzed the reaction of KH with melamine in more detail, which reveals six exothermic and one endothermic effects (Figure 2). Compounds appearing in every single thermal event were separately prepared and subsequently characterized by single-crystal and powder X-ray diffraction (ex situ PXRD) techniques. We note here that the formation of intermediate phases depends very much on the chosen (6:1) ratio of KH to melamine in the DSC experiment, with the consequence that an increase or decrease of this ratio can lead into a different sequence of compounds.

The first broad exothermic effect in the reaction cascade between KH and melamine in Figure 2 is attributed to the formation of the new melaminate $K(C_3N_6H_5)$ at 170 °C (Figure S2) and to $K_2(C_4N_7H_3)$ at a slightly higher temperature (175 °C). The exothermic shoulder around 230 °C can be attributed to the decomposition of $K_2(C_4N_7H_3)$ into K(HNCN) (equals "$K_3(C_3N_6H_3)$") (Figure S3) and is part of the strong exothermic formation of $K_5H(CN_2)_3$ (Figure S4) near 250 °C. The weak exothermic effect observed at around 300 °C is assigned to the formation of $K_5(CN_2)_2H$, followed by an exothermic peak at approximately 340 °C, corresponding

https://doi.org/10.1021/acs.inorgchem.4c02996
Inorg. Chem. 2024, 63, 16565−16572

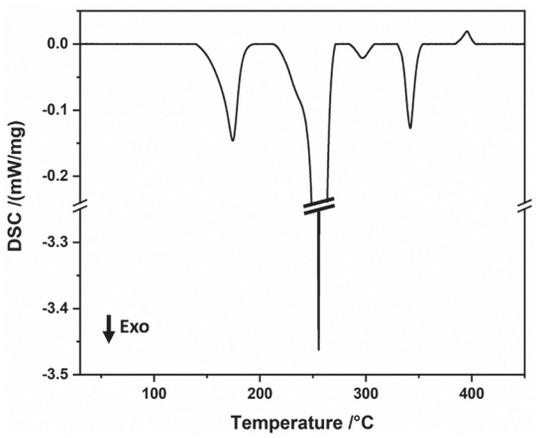

Figure 2. DSC plot of the reaction of 6KH + $C_3N_6H_6$ → $3K_2(CN_2)$ + $6H_2$ with a heating rate of 2°/min.

to the loss of hydrogen (Figure S5) and the formation of α-$K_2(CN_2)$ (Figure S6). The weak endothermic effect near 400 °C represents an irreversible phase transition of α-$K_2(CN_2)$ into the hitherto unknown tetragonal (β) modification.

Separate reactions at certain temperatures constitute a fundamental part of this study (Experimental Section) for the assignment of compounds being involved in thermal effects (conversions) in the recorded DSC (Figure 2). The reaction condition for every single intermediate compound appearing in the system was optimized to obtain single-phase samples for the identification of (already known and new) compounds (S1−S6). Finally, the complete reaction sequence determined for the reaction 6KH + $C_3N_6H_6$ is summarized in Figure 3.

The formation of phase-pure $K_5(CN_2)_2H$ (Figure S7) was obtained with a 7:1 ratio of KH to melamine and a heating rate of 3 °C/min and completes the series of known compounds in the K−H−(NCN) system represented as K(HNCN), $K_5H(CN_2)_3$, and $K_5(CN_2)_2H$ as well as the monoclinic (α) modification of $K_2(CN_2)$ that are discussed in the introduction part. Moreover, there are a number of new compounds appearing in the given reaction sequence (Figure 3).

The formation of potassium monocyanomelaminate $K_2(C_4N_7H_3)$ from potassium melaminate $K(C_3N_6H_5)$ can be explained by the decomposition of some melaminate rings at slightly higher temperatures. In fact, the melaminate ring is not stable and decomposes into cyanamide or dicyandiamide. The decomposition of melamine or melaminate may occur at low temperatures under specific conditions, and this can be proven with a similar reaction of melamine with metal chloride and the formation of protonated guanylmelamine (see Figure S8). Following this decomposition, the cyanamide reacts with deprotonated melamine, leading to the formation of potassium monocyanomelaminate $K_2(C_4N_7H_3)$ as shown in Figure 4.

The result of the given reaction sequence, compacted in eq 3, represents an efficient and easy-to-handle synthetic route for the preparation of phase-pure potassium carbodiimide (described in the Experimental Section). Moreover, this reaction involves the formation of a considerable amount of molecular hydrogen.

$$6KH + C_3N_3(NH_2)_3 \rightarrow 3K_2(CN_2) + 6H_2\uparrow \quad (3)$$

Hydrogen-containing compounds offer hydrogen storage capacities and can release hydrogen under controlled

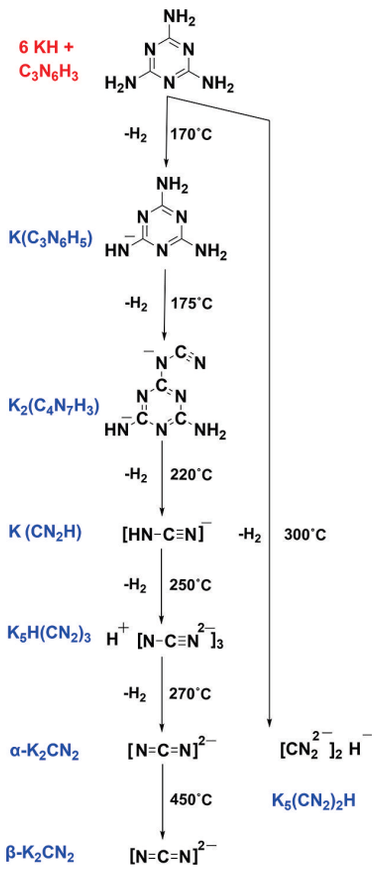

Figure 3. Summary of compounds as detected and identified at different temperatures during the course of the reaction of KH with melamine.

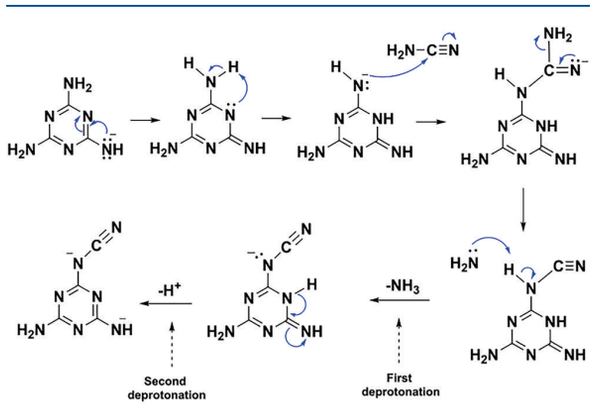

Figure 4. Possible reaction mechanism of the formation of monocyanomelaminate $K_2(C_4N_7H_3)$ from potassium melaminate $K(C_3N_6H_5)$.

conditions. Hydrogen storage in amides and borohydrides is a topic of interest in the field of hydrogen storage materials. Amides, such as ammonia borane, and borohydrides, such as sodium borohydride, have shown potential hydrogen storage capacities. Composite materials like $LiBH_4$−$LiNH_2$ resemble a combination of hydridic and protic hydrogen atoms that are considered favorable for hydrogen generation as they can

https://doi.org/10.1021/acs.inorgchem.4c02996
Inorg. Chem. 2024, 63, 16565−16572

efficiently release hydrogen gas through dehydrogenation reactions (eq 4).[20,21]

$$LiBH_4 + 2LiNH_2 \rightarrow Li_3(BN_2) + 4H_2\uparrow \quad (4)$$

The thermal decomposition of the $LiBH_4$−$LiNH_2$ composite system results in the formation of lithium dinitridoborate.[25] This reaction can be well correlated with reactions shown between hydride and amide in eqs 2 and 3, describing reactions of metal hydride with melamine. Aliphatic carbodiimides can rapidly absorb hydrogen during catalytic hydrogenation, resulting in the formation of formamidine.[22] Similarly, the hydrogenation of nitriles to primary amines is readily achievable by reacting them with hydrogen gas and specific catalysts.[23,24] Despite structural differences in $K_2(CN_2)$ from organic carbodiimides, this observation highlights the potential of the metal hydride−melamine system for further in-depth studies.

Crystal Structures. The crystal structures of intermediate compounds in the given system were solved and refined based on powder and single-crystal X-ray diffraction data, summarized in Table 1.

Table 1. Crystal and Structure Refinement Data of Selected Compounds Based on Single-Crystal and Powder X-ray Diffraction Measurements

formula	$K(C_3N_6H_5)$	$K_2(C_4N_7H_3)$	β-$K_2(CN_2)$
space group	*Pbcn* (no. 60)	$Pmc2_1$ (no. 26)	$I4_1/a$ (no. 88)
a (pm)	1227.077(6)	383.30(6)	1730.1(1)
b (pm)	1111.785(6)	966.1(1)	1730.1(1)
c (pm)	1881.829(9)	1117.7(2)	596.35(8)
cell volume (Å^3)	2567.28(2)	413.9(1)	1785.0(4)
formula units (Z)	16	2	20
goodness of fit	1.074	1.058	1.060
R-values [$I \geq 2\sigma(I)$]	-	R_1 = 0.0450; wR_2 = 0.0814	R_1 = 0.0230; wR_2 = 0.0562
R-values (all data)	-	R_1 = 0.0786; wR_2 = 0.0888	R_1 = 0.0264; wR_2 = 0.0574
$\Delta\rho_{min}, \Delta\rho_{max}$ (e·Å^3)	-	−0.313; 0.248	−0.223; 0.281
R_{Bragg}	3.1143	-	-
χ^2	1.1534	-	-
R_p	2.7975	-	-
R_{wp}	3.8228	-	-
CCDC no.	2332888	2350483	2270217

$K(C_3N_6H_5)$. The crystal structure of the monopotassium melaminate $K(C_3N_6H_5)$ represents a new member of melaminate compounds with the $(C_3N_3)(NH_2)_2(NH^-)$ monoanion. The crystal structure contains two crystallographically different potassium and two different melaminate ions. Both potassium ions are coordinated by the six nearest nitrogen atoms in a distorted trigonal-prismatic fashion with distances ranging between 280 and 301 pm (Figure 5).

The crystallographic unit cell of $K(C_3N_6H_5)$ contains 16 melaminate ions, forming an apparently complex distribution pattern which is dominated by the orientation of the melaminate ions with their negatively charged −NH group pointing toward potassium ions (Figure 6).

$K_2(C_4N_7H_3)$. The crystal structure of $K_2(C_4N_7H_3)$ is composed of monocyanomelaminate anions coordinated by two crystallographically different potassium anions. The (NCN) group of the cyanomelaminate is disordered with the terminal NH group, and the adjacent K2 is correspondingly disordered over two crystallographic positions. The crystal structure is shown for one of these patterns in Figure 7, with a layered arrangement of $(C_4N_7H_3)^{2-}$ anions within the *bc*-plane, covered by potassium ions from above and below.

$K(CN_2H)$. The compound was described by Schnick and Huppertz in 1995,[9] solved and refined from single-crystal X-ray data.

$K_5(CN_2)_2H$. The compound was described by Jacobs and coworkers in 2001,[17] solved and refined from single-crystal X-ray data.

$K_5H(CN_2)_3$. The compound was described by Schnick and coworkers in 1997,[15] solved and refined from single-crystal X-ray data.

K_2CN_2. The monoclinic (α-)modification of $K_2(CN_2)$ was described by Becker and Jansen in 2000, solved and refined from powder ex situ PXRD data with the space group $C2/m$.[16] The formation of the monoclinic phase is confirmed in our studies near 270 °C. α-$K_2(CN_2)$ shows a phase transition into its tetragonal (β-)modification at about 450 °C. β-$K_2(CN_2)$ crystallizes in the tetragonal space group $I4_1/a$ as clear colorless needle-shaped crystals that behave sensitively in moist air. The crystal structure contains one fully symmetric ($d_{N2-C2-N3}$ = 124.9(2) pm) and one nearly symmetric ($d_{N1-C1-N2}$ = 121.4(3) and 121.9(3) pm) $(NCN)^{2-}$ ion, that can be both safely addressed as carbodiimides. The fully symmetric carbodiimide is surrounded by 12 potassium ions (K1 and K2) in a double-square-antiprismatic arrangement. These columns are surrounded via the second type of carbodiimide ions N(1)−C(1)−N(2) (Figure 8). This arrangement allows for additional channels in the structure, which are occupied by disordered potassium ions (K3 and K4) occupying two adjacent positions (16f with 20(2)% and 30(2)% occupancy), as shown in Figure 9.

The comparison of C−N distances in the (N−C−N) groups of all six compounds is summarized in Table S1.

CONCLUSION

Thermal analysis has emerged as a very helpful tool in studying reactive systems. Recent examples have involved a comprehensive study of the binary tungsten iodide (W−I) system, where phase relations in the system with more than 20 binary phases are reported and characterized.[25] Additionally, thermal analyses have been utilized in the successive reduction cascades of metal halides using nonconventional reduction agents.[26] These studies have provided valuable insights into successive reduction steps and intermediate compounds, enabling a deeper understanding of the reduction mechanism. Finally, thermal analyses have been successfully applied to uncover intermediate phases and to monitor the ignition temperatures of exothermic solid-state metathesis (SSM) reactions.[19]

The study presented here explores the successive reaction steps involved in the reaction of potassium hydride with melamine. It is shown that phase equilibria in the given system are strongly influenced by the reaction conditions, simply induced by minor changes in the temperature and of course the composition.

In fact, some compounds in the presented K−H−(NCN) system have been previously reported, while others remained unknown and are now discovered and structurally characterized to finally complete a whole reaction sequence. Along that way, the new melaminate $K(C_3N_6H_5)$ is a subject of

https://doi.org/10.1021/acs.inorgchem.4c02996
Inorg. Chem. 2024, 63, 16565−16572

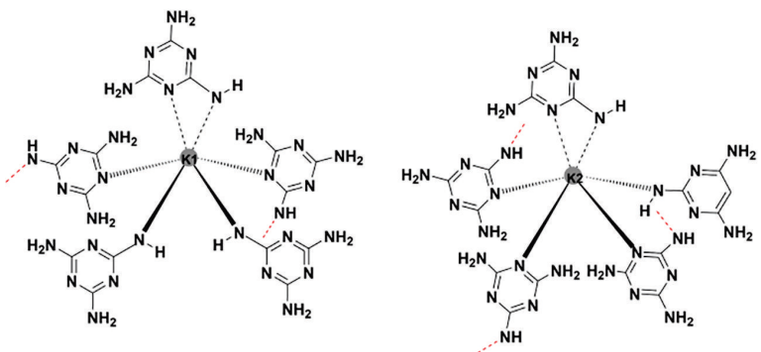

Figure 5. Environment of the two crystallographically distinct K ions in $K(C_3N_6H_5)$ with distances $d_{K1\text{-}Namid}$ = 290.6(6), 291.8(7), and 294.4(6) pm; $d_{K1\text{-}Nring}$ 279.5(6), 288.4(6), and 302.4(6) pm; $d_{K2\text{-}Namid}$ = 286.8(6) and 290.3(6) pm; and $d_{K\text{-}Nring}$ = 282.2(6), 287.9(6), 300.9(6), and 301.0(7) pm.

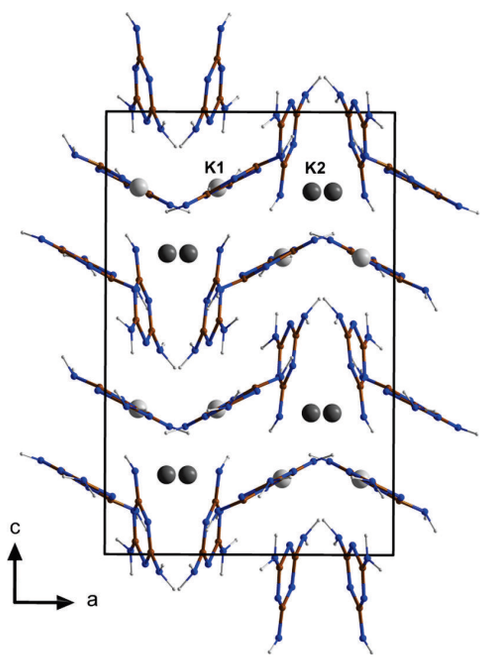

Figure 6. Projection of the unit cell content of the structure of $K(C_3N_6H_5)$. K atoms are shown in dark gray, carbon atoms in brown, nitrogen atoms in blue, and hydrogen atoms in white. Cell edges are drawn as black lines.

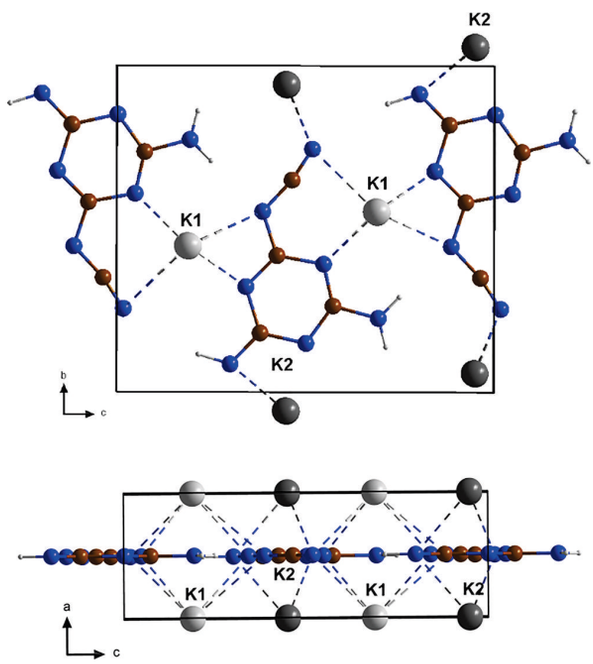

Figure 7. Two views of the unit cell of $K_2(C_4N_7H_3)$ with nearest neighbor distances $d_{K1\text{-}Nring}$ = 284.4(5) and 291.9(5) pm; $d_{K1\text{-}NCN}$ = 309.9(9) and 328.2(9) pm; $d_{K2\text{-}Nring}$ = 283.4(6) and 280(1) pm; $d_{K2\text{-}Namid}$ = 288.9(7) pm; and $d_{K2\text{-}NCN}$ = 280.9(8) pm.

interest for development of the emerging family of metal melaminates, together with a number of other compounds highlighting the dynamic nature of the chemical transformations occurring within the given reaction cascade.

The combination of equal amounts of oppositely polarized hydrogen atoms in the reaction of KH and $C_3N_3(NH_2)_3$ in a 6:1 ratio involves hydridic and protic hydrogen intermediates in the gradually advancing reaction sequence under the release of hydrogen. The system $KH-C_3N_3(NH_2)_3$ parallels the composite $LiBH_4-LiNH_2$ that is under discussion as a hydrogen storage material.[25] Both systems are capable of releasing significant amounts of hydrogen.

The reactions described herein between KH or LiH and melamine ultimately lead to the high-purity compounds $K_2(CN_2)$ and $Li_2(CN_2)$. Particularly $K_2(CN_2)$ can be considered as a feasible fertilizer, capable of delivering two key elements of the essential nitrogen, phosphorus, and potassium (N−P−K) nutrition supply[27] of plants.

In summary, this study demonstrates the complexity and intricacies of chemical reactions in reactive solid-state systems and the importance of thermal analysis for insight into such reactions.

EXPERIMENTAL SECTION

Syntheses of compounds were carried out in Schlenk tubes with a length of 40 cm and an inner diameter of 35 mm, closed with a GL45 cap with a silicon seal (Schott AG, Mainz, Germany). The starting materials (KH (Alfa Aesar, 95%) and melamine (Sigma-Aldrich, 99%)) were ground in an agate mortar in a glovebox under an argon atmosphere. The mixture was filled into an open screw neck vial (Chroma Globe, Kreuzau, Germany) and placed into the Schlenk tube (Figure S9). The tube was heated in a Simon−Müller furnace,

https://doi.org/10.1021/acs.inorgchem.4c02996
Inorg. Chem. 2024, 63, 16565−16572

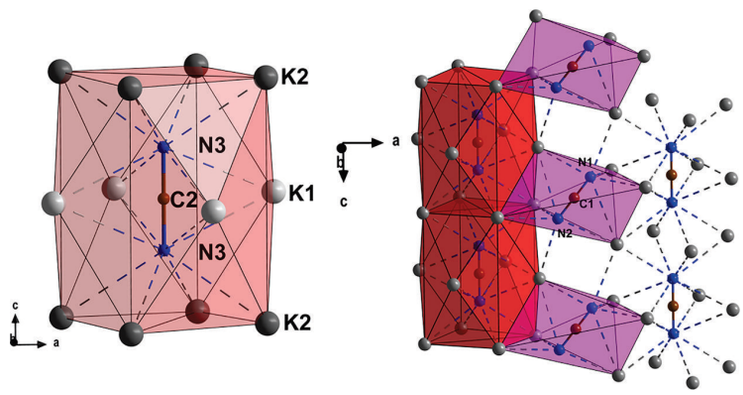

Figure 8. Environments of two types of $(NCN)^{2-}$ ions by 12 (left, red polyhedra) and six (right, violet polyhedral) potassium ions in the structure of (tetragonal) β-$K_2(CN_2)$.

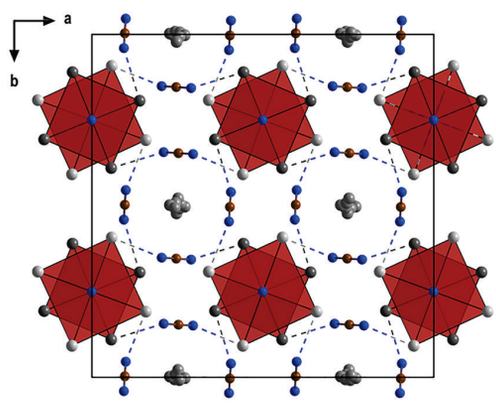

Figure 9. Unit cell of tetragonal β-$K_2(CN_2)$ showing disordered potassium atoms. K atoms are drawn in gray, carbon atoms in brown, and nitrogen atoms in blue.

with rates and holding times given below for each compound. The purity of the samples was examined by powder XRD measurements and full Rietveld refinements, which are given in the Figures S2–S7.

$K(C_3N_6H_5)$. Only the synthesis of $K(C_3N_6H_5)$ was performed in a classical way. A mixture of 75 mg of KH (1.9 mmol) and 214.41 mg of melamine ($C_3N_6H_6$) (1.7 mmol) were heated in a fused silica ampule at 225 °C for 40 h (heating rate 2 °C/min, cooling rate 1 °C/min). $K(C_3N_6H_5)$ was obtained as a white microcrystalline X-ray pure powder. $K(C_3N_6H_5)$ obtained from this reaction appears to be moisture-sensitive.

$K_2(C_4N_7H_3)$. A mixture of 75 mg of KH (1.9 mmol) and 147.4 mg of melamine ($C_3N_6H_6$) (1.17 mmol) was heated at 240 °C for 60 h (heating rate 2 °C/min, cooling rate 1 °C/min). $K_2(C_4N_7H_3)$ was obtained as a beige microcrystalline powder together with unreacted melamine which was carefully sublimed off in a temperature gradient of 215 to 25 °C in a sealed silica glass tube. $K_2(C_4N_7H_3)$ obtained from this reaction appears to be moisture-sensitive.

$K(CN_2H)$. A mixture of 100 mg of KH (2.5 mmol) and 104.8 mg of melamine ($C_3N_6H_6$) (0.83 mmol) was heated at 250 °C for 4 h (heating rate 3 °C/min, cooling rate 1 °C/min). The congealed molten mass was ground in an agate mortar in a glovebox under an argon atmosphere. $K(CN_2H)$ was obtained phase-pure and is moisture-sensitive.

$K_5H(CN_2)_3$. A mixture of 150 mg of KH (3.74 mmol) and 94.3 mg of melamine ($C_3N_6H_6$) (0.75 mmol) was heated at 250 °C for 16 h (heating rate 3 °C/min, cooling rate 2 °C/min). $K_5H(CN_2)_3$ was obtained phase-pure as a white microcrystalline powder and behaves moisture-sensitive.

$K_5(CN_2)_2H$. A mixture of 50 mg of KH (1.25 mmol) and 21 mg of melamine ($C_3N_6H_6$) (0.17 mmol) was heated at 300 °C for 16 h (heating rate 3 °C/min, cooling rate 2 °C/min). $K_5(CN_2)_2H$ was obtained as a phase-pure white microcrystalline powder and is moisture-sensitive.

α-$K_2(CN_2)$, Monoclinic Modification. A mixture of 150 mg of KH (3.74 mmol) and 78.6 mg of melamine ($C_3N_6H_6$) (0.62 mmol) was heated at 270 °C for 16 h (heating rate 3 °C/min, cooling rate 2 °C/min). Monoclinic $K_2(CN_2)_2$ was obtained in 70+ % purity as light gray powder and behaves moisture-sensitive. The side phases were identified as $K_5(CN_2)_2H$ and $K_5H(CN_2)_3$.

β-$K_2(CN_2)$, Tetragonal Modification. A mixture of 150 mg of KH (3.74 mmol) and 78.6 mg of melamine ($C_3N_6H_6$) (0.62 mmol) was heated at 450 °C for 2 h (heating rate 3 °C/min, cooling rate 2 °C/min). Phase-pure β-$K_2(CN_2)_2$ was obtained as light gray moisture-sensitive powder (yield, >98%).

Powder X-ray Diffraction. Compounds were investigated by powder X-ray diffraction (PXRD) on a Stadi-P (STOE, Darmstadt) diffractometer with germanium-monochromated Cu–$K_{\alpha 1}$ radiation. The PXRD pattern of $K(C_3N_6H_5)$ was indexed and solved with the program EXPO.[28] The structure solution was generated with a simulated annealing approach by using a melamine molecule and potassium atoms as starting points. The structure refinement was carried out with Winplotr (Fullprof),[29] with the final full refinement plot displayed in Figure S2. Relevant data for the structure refinements are given in Table S2.

Thermoanalytic Studies. DSC was performed with a DSC 204 F1 Phoenix instrument (Fa. Netzsch, Selb, Germany). The starting materials were enclosed in gold-plated (5 μm) steel autoclaves (volume 100 μL; BFT 94; Bächler Feintech AG, Hölstein, Switzerland) under a dry argon atmosphere (glovebox). The reactions of MH (M = Li, Na, and K) with melamine were analyzed between room temperature and 500 °C at a heating and cooling rate of 2 K/min.

Single-Crystal X-ray Diffraction. Colorless crystals were used as obtained. A suitable single crystal was selected and mounted on a XtaLAB Synergy, Dualflex, HyPix diffractometer. The crystals were kept at a steady temperature of 150.0(1) K during data collection. Structures were solved by the ShelXT 2018/2 (Sheldrick, 2018) structure solution program using dual methods and refined by full matrix least-squares minimization on F^2 using version 2018/3 of ShelXL 2018/3 (Sheldrick, 2015) with Olex2 1.5-ac5-024 (Dolomanov et al., 2009) as the graphical interface. All non-hydrogen atoms were refined anisotropically. Hydrogen atom positions were calculated geometrically and refined by using the riding model.

https://doi.org/10.1021/acs.inorgchem.4c02996
Inorg. Chem. 2024, 63, 16565–16572

■ ASSOCIATED CONTENT

Data Availability Statement

Data is contained within the article and Supporting Information.

Supporting Information

The Supporting Information is available free of charge at https://pubs.acs.org/doi/10.1021/acs.inorgchem.4c02996.

Calculated XRD patterns (PDF)

Accession Codes

CCDC 2270217, 2332888, and 2350483 contain the supplementary crystallographic data for this paper. These data can be obtained free of charge via www.ccdc.cam.ac.uk/data_request/cif, or by emailing data_request@ccdc.cam.ac.uk, or by contacting The Cambridge Crystallographic Data Centre, 12 Union Road, Cambridge CB2 1EZ, UK; fax: +44 1223 336033.

■ AUTHOR INFORMATION

Corresponding Author

Hans-Jürgen Meyer − *Section for Solid State and Theoretical, Inorganic Chemistry, Institute of Inorganic Chemistry, Eberhard Karls Universität Tübingen, 72076 Tübingen, Germany*; orcid.org/0000-0003-2450-4011; Email: juergen.meyer@uni-tuebingen.de

Authors

Markus Ströbele − *Section for Solid State and Theoretical, Inorganic Chemistry, Institute of Inorganic Chemistry, Eberhard Karls Universität Tübingen, 72076 Tübingen, Germany*; orcid.org/0000-0002-5147-5677

Elaheh Bayat − *Section for Solid State and Theoretical, Inorganic Chemistry, Institute of Inorganic Chemistry, Eberhard Karls Universität Tübingen, 72076 Tübingen, Germany*

Complete contact information is available at: https://pubs.acs.org/10.1021/acs.inorgchem.4c02996

Author Contributions

Conception, supervision, funding acquisition, and review and editing: H.-J.M. X-ray diffraction and modeling, synthesis, and preparation: M.S. Writing, artwork, and preparation: E.B.

Funding

This research is supported by the Deutsche Forschungsgemeinschaft (DFG) through Grant ME 914/34-1.

Notes

The authors declare no competing financial interest.

■ ACKNOWLEDGMENTS

Funding by the Deutsche Forschungsgemeinschaft through Grant ME 914/34-1 is gratefully acknowledged.

■ REFERENCES

(1) Wohnsiedler, H. Urea-formaldehyde and melamine-formaldehyde condensations. *Industrial & engineering chemistry* **1952**, *44* (11), 2679−2686.

(2) Wohnsiedler, H. Polymerization in melamine-formaldehyde molded resins. *Industrial & Engineering Chemistry* **1953**, *45* (10), 2307−2311.

(3) Hodgins, T.; Hovey, A.; Hewett, S.; Barrett, W.; Meeske, C. Melamine-Formaldehyde Film-Forming Compositions. *Industrial & Engineering Chemistry* **1941**, *33* (6), 769−779.

(4) Pizzi, A. Melamine-formaldehyde adhesives. In *Handbook of adhesive technology*; Pizzi, A., Mittal, K. L., Eds.; Marcel Dekker, Inc., 2003. DOI: 10.1201/9780203912225.ch32

(5) Parameswaran, P.; Eby Thomas, T. *Modification of phenol formaldehyde resin for improved mechanical properties*; Cochin University of Science and Technology, 2009.

(6) Oribayo, O.; Feng, X.; Rempel, G. L.; Pan, Q. Modification of formaldehyde-melamine-sodium bisulfite copolymer foam and its application as effective sorbents for clean up of oil spills. *Chem. Eng. Sci.* **2017**, *160*, 384−395.

(7) Song, B.; Zhu, X.; Wang, W.; Wang, L.; Pei, X.; Qian, X.; Liu, L.; Xu, Z. Toughening of melamine−formaldehyde foams and advanced applications based on functional design. *Journal of Industrial and Engineering Chemistry* **2023**, *119*, 130−152.

(8) Görne, A. L.; Scholz, T.; Kobertz, D.; Dronskowski, R. Deprotonating melamine to gain highly interconnected materials: Melaminate salts of potassium and rubidium. *Inorg. Chem.* **2021**, *60* (20), 15069−15077.

(9) Schnick, W.; Huppertz, H. Darstellung, Kristallstruktur und Eigenschaften von Kaliumhydrogencyanamid. *Zeitschrift für anorganische und allgemeine Chemie* **1995**, *621* (10), 1703−1707.

(10) Franklin, E. C. The ammono carbonic acids. *J. Am. Chem. Soc.* **1922**, *44* (3), 486−509.

(11) Kallenbach, P.; Bayat, E.; Ströbele, M.; Romao, C. P.; Meyer, H.-J. Tricopper melaminate, a metal−organic framework containing dehydrogenated melamine and Cu−Cu bonding. *Inorg. Chem.* **2021**, *60* (21), 16303−16307.

(12) Bayat, E.; Ströbele, M.; Abbasi, M.; Kroeker, S.; Valenta, J.; Enseling, D.; Jüstel, T.; Meyer, H.-J. High-Yield Synthesis Route, Post-Synthesis Treatment, and Insights into the Photoluminescence and Magnetic Properties of Tricopper(I) Melaminate $Cu_3(C_3N_6H_3)$. *Inorganic Chemistry* **2024**, n/a.

(13) Bayat, E.; Ströbele, M.; Meyer, H.-J. Unraveling the Synthesis of $SbCl(C_3N_6H_4)$: A Metal-Melaminate Obtained through Deprotonation of Melamine with Antimony (III) Chloride. *Chemistry* **2023**, *5* (2), 1465−1476.

(14) Bayat, E.; Ströbele, M.; Enseling, D.; Jüstel, T.; Meyer, H.-J. Thermal deprotonation and condensation of melamine in the presence of indium (III) chloride. *Dalton transactions (Cambridge, England: 2003)* **2024**, *53*, 10912−10918.

(15) Becker, M.; Jansen, M.; Lieb, A.; Milius, W.; Schnick, W. Synthese, Kristallstruktur und Festkörper-NMR-spektroskopische Untersuchungen von $K_5H(CN_2)_3$. *Zeitschrift für anorganische und allgemeine Chemie* **1998**, *624* (1), 113−118.

(16) Becker, M.; Jansen, M. Synthesis of potassium cyanamide, and crystal structure determination by pareto optimization of the cost functions 'lattice energy'and 'powder intensities'. *Solid state sciences* **2000**, *2* (7), 711−715.

(17) Niewa, R.; Höhn, P.; Kniep, R.; Weiske, A.; Jacobs, H. Crystal structure of pentapotassium dicarbodiimide monohydride, $K_5[CN_2]_2H$. *Zeitschrift für Kristallographie-New Crystal Structures* **2001**, *216* (1−4), 357−358.

(18) Kurzer, F.; Douraghi-Zadeh, K. Advances in the chemistry of carbodiimides. *Chem. Rev.* **1967**, *67* (2), 107−152.

(19) Meyer, H.-J. Solid state metathesis reactions as a conceptual tool in the synthesis of new materials. *Dalton Transactions* **2010**, *39* (26), 5973−5982.

(20) Singer, J. P.; Meyer, M. S.; Speer, R. M., Jr; Fischer, J. E.; Pinkerton, F. E. Determination of the phase behavior of $(LiNH_2)_c(LiBH_4)_{1-c}$ quaternary hydrides through in situ X-ray diffraction. *J. Phys. Chem. C* **2009**, *113* (43), 18927−18934.

(21) Meisner, G. P.; Scullin, M. L.; Balogh, M. P.; Pinkerton, F. E.; Meyer, M. S. Hydrogen release from mixtures of lithium borohydride and lithium amide: a phase diagram study. *J. Phys. Chem. B* **2006**, *110* (9), 4186−4192.

(22) Jochims, J. C. Hydrierung von Carbodiimiden. *Chem. Ber.* **1965**, *98* (7), 2128−2133.

(23) Feller, M. Hydrogenation of nitriles and imines for hydrogen storage. *Physical sciences reviews* **2019**, *4* (3), No. 20180033.

(24) Lu, Q.; Liu, J.; Ma, L. Recent advances in selective catalytic hydrogenation of nitriles to primary amines. *J. Catal.* **2021**, *404*, 475−492.
(25) Ströbele, M.; Meyer, H.-J. Pandora's box of binary tungsten iodides. *Dalton Transactions* **2019**, *48* (5), 1547−1561.
(26) Ströbele, M.; Mos, A.; Meyer, H.-J. r. Cluster harvesting by successive reduction of a metal halide with a nonconventional reduction agent: A benefit for the exploration of metal-rich halide systems. *Inorg. Chem.* **2013**, *52* (12), 6951−6956.
(27) Boroomand, N. Macro elements nutrition (NPK) of medicinal plants. *Journal of Medicinal Plant Research* **2012**, *6* (12), 2249−2255.
(28) Altomare, A.; Camalli, M.; Cuocci, C.; Giacovazzo, C.; Moliterni, A.; Rizzi, R. EXPO2009: structure solution by powder data in direct and reciprocal space. *J. Appl. Crystallogr.* **2009**, *42* (6), 1197−1202.
(29) Roisnel, T.; Rodriguez-Carvajal, J. WinPLOTR: A windows tool for powder diffraction patterns analysis. *Proceedings of the Seventh European Powder Diffraction Conference (EPDIC 7)* **2001**, 118−123.

https://doi.org/10.1021/acs.inorgchem.4c02996
Inorg. Chem. 2024, 63, 16565−16572

Supporting Information

A systematic Study of the Solid-State Pathway from Melamine via Melaminate to Carbodiimide under evolution of Hydrogen

Markus Ströbele [a], *Elaheh Bayat* [a], *and Hans-Juergen Meyer* *[a]

Section for Solid State and Theoretical, Inorganic Chemistry, Institute of Inorganic Chemistry, Eberhard Karls Universität Tübingen, Auf der Morgenstelle 18, 72076 Tübingen (Germany), E-mail: juergen.meyer@uni-tuebingen.de

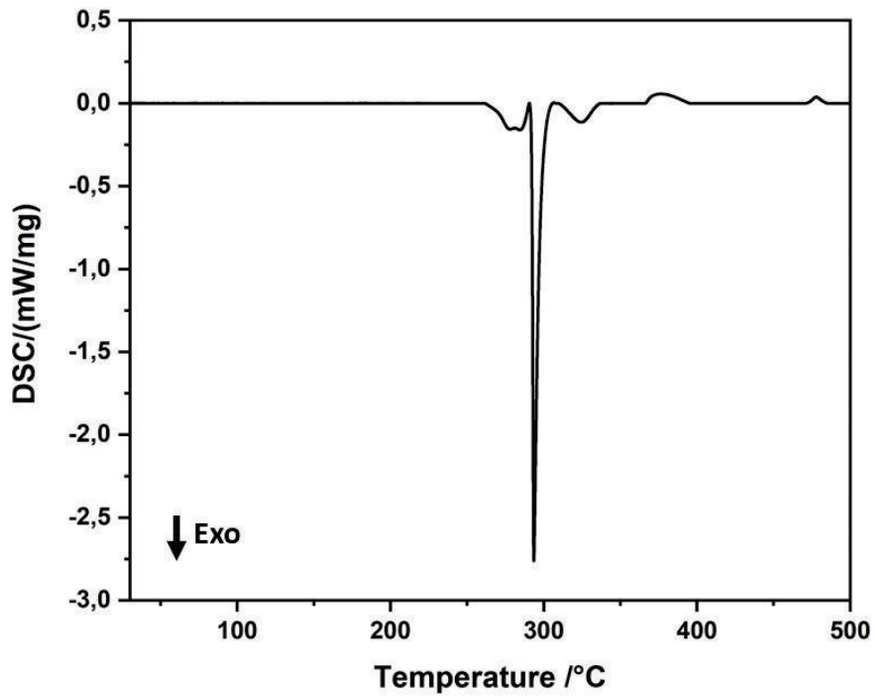

Figure S1. DSC plot of the reaction 6 NaH + $C_3N_6H_6$ → 3 $Na_2(CN_2)$ + 6 H_2 with a heating rate of 2˚/min.

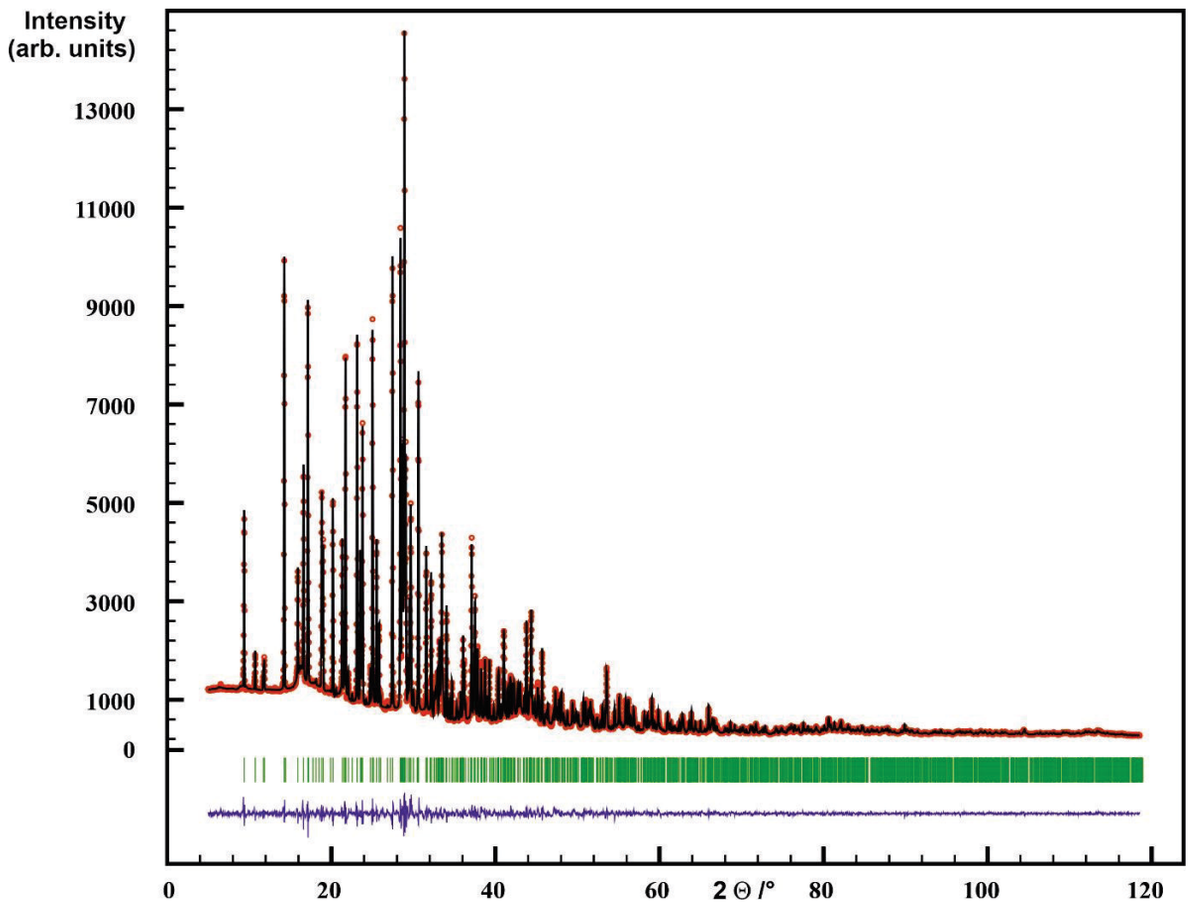

Figure S2. Rietveld refinement of $K(C_3N_6H_5)$. Observed intensities are marked as red circles, calculated intensities as black line. Bragg positions are marked as green lines, the difference curve $I_{observed} - I_{calculated}$ as blue line.

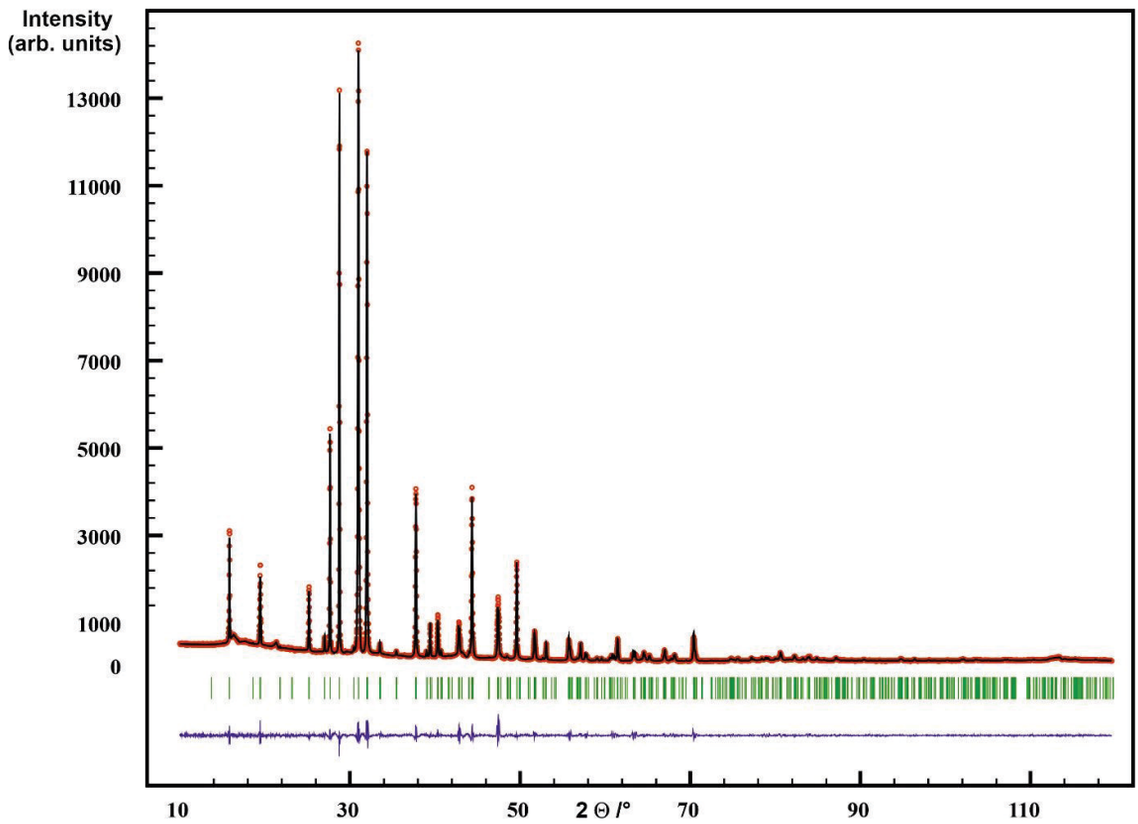

Figure S3. Rietveld refinement of $K(CN_2H)$. Observed intensities are marked as red circles, calculated intensities as black line. Bragg positions are marked as green lines, the difference curve $I_{observed} - I_{calculated}$ as blue line.

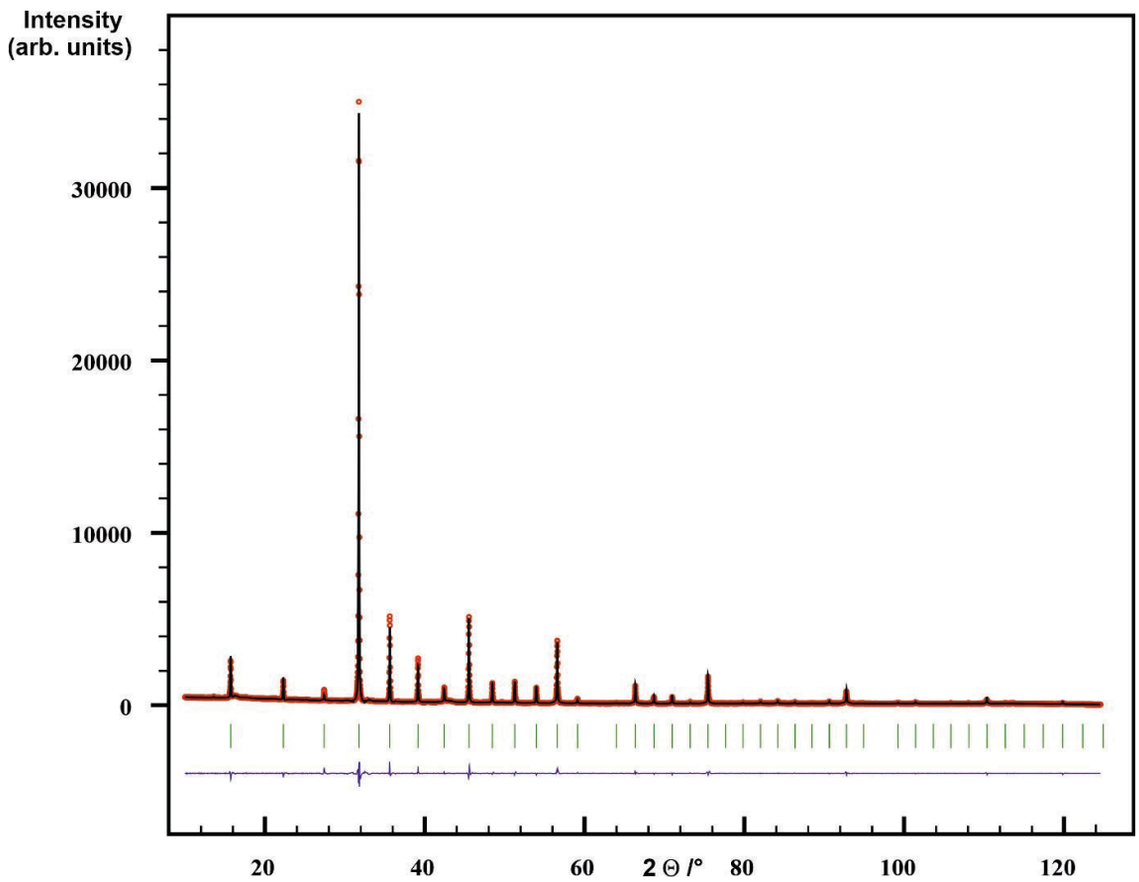

Figure S4. Rietveld refinement of $K_5H(CN_2)_3$. Observed intensities are marked as red circles, calculated intensities as black line. Bragg positions are marked as green lines, the difference curve $I_{observed} - I_{calculated}$ as blue line.

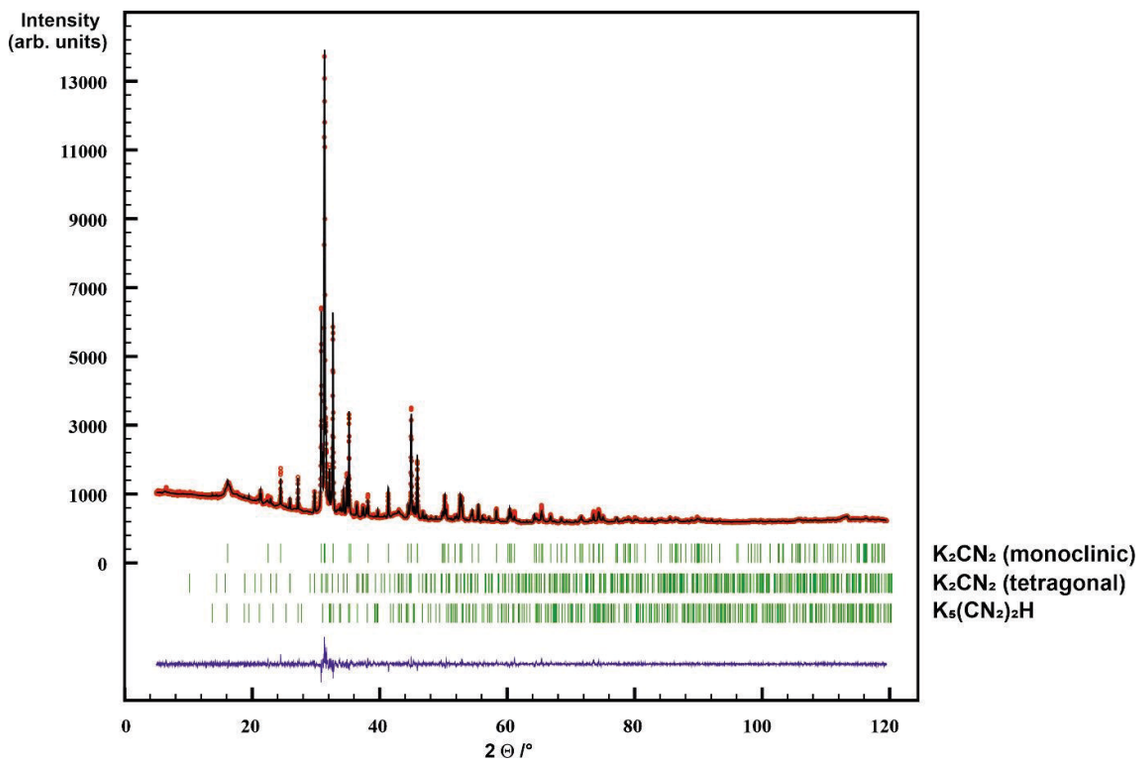

Figure S5. Rietveld refinement of $K_2(CN_2)$ (monoclinic modification). Observed intensities are marked as red circles, calculated intensities as black line. Bragg positions are marked as green lines, the difference curve $I_{observed} - I_{calculated}$ as blue line. Purity around 75 %.

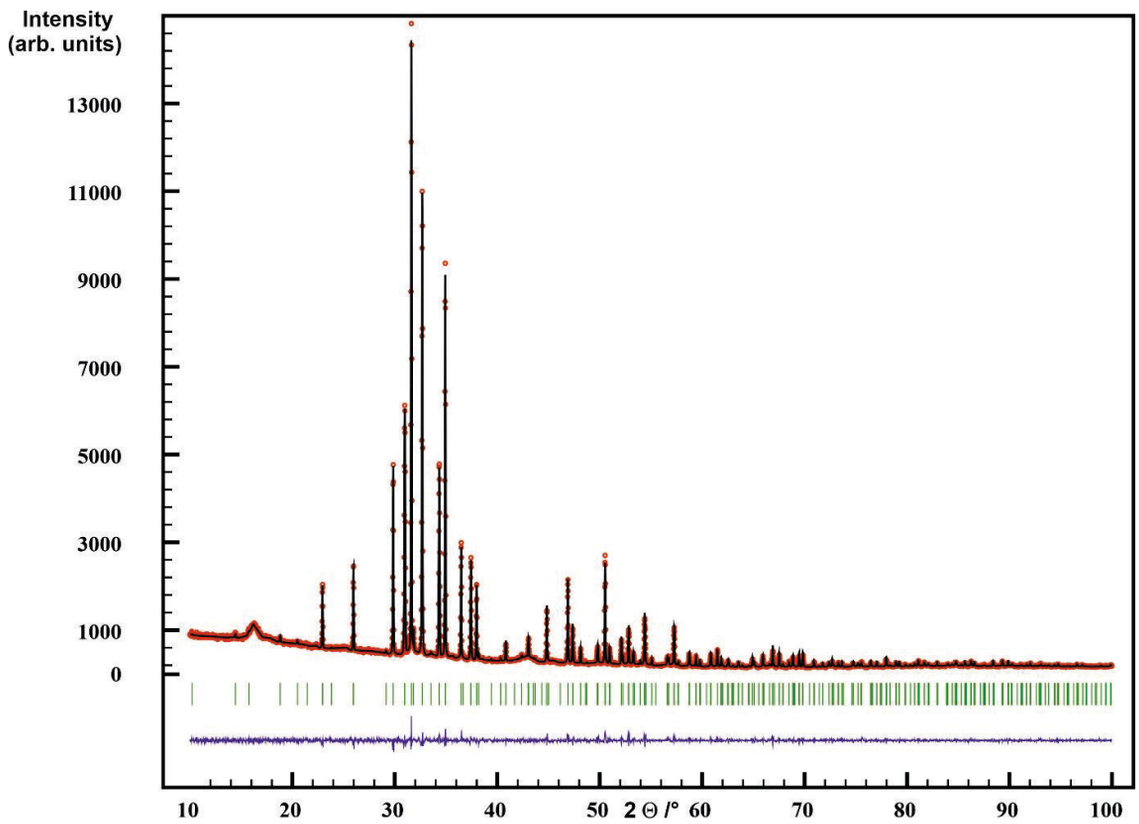

Figure S6. Rietveld refinement of $K_2(CN_2)$ (tetragonal modification). Observed intensities are marked as red circles, calculated intensities as black line. Bragg positions are marked as green lines, the difference curve $I_{observed} - I_{calculated}$ as blue line.

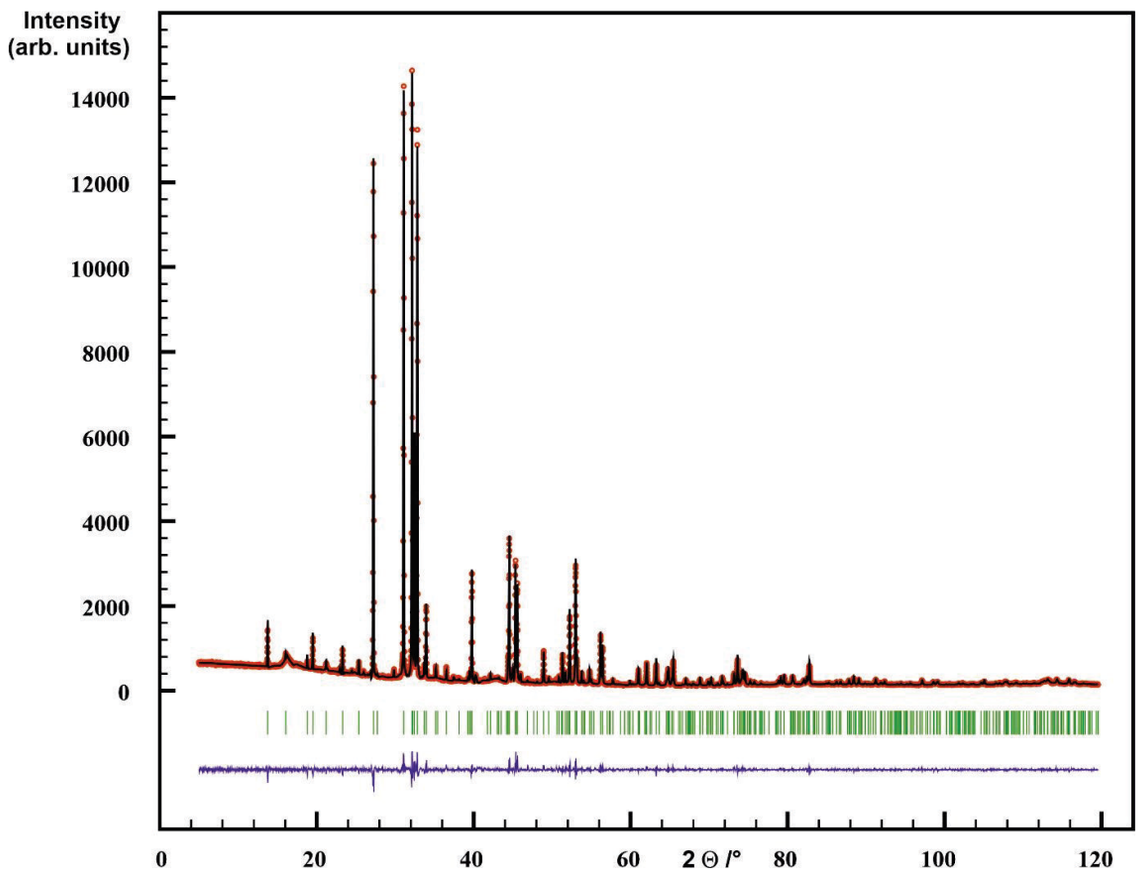

Figure S7. Rietveld refinement of $K_5H(CN_2)_2$. Observed intensities are marked as red circles, calculated intensities as black line. Bragg positions are marked as green lines, the difference curve $I_{observed} - I_{calculated}$ as blue line.

Table S1. Comparison of C-N distances of the (N-C-N) groups.

Formula	Label	/pm
$K_2(C_4N_7H_3)$**	C(4) – N(6)	127(2)
	C(4) – N(7)	110(2)
	C(4A) – N(5)	119(2)
	C(4A) – N(7A)	137(3)
$K(CN_2H)$*	C(1) – N(1)	128.4(4)
	C(1) – N(2)	117.2(4)
	C(2) – N(3)	128.9(5)
	C(2) – N(4)	117.4(5)
$K_5H(CN_2)_3$*	C(1) – N(1)	122.5(4) 2x
$K_5H(CN_2)_2$*	C(1) – N(1)	122.6(5) 2x
$K_2(CN_2)$ monoclinic modification*	C(1) – N(1)	123.4(2) 2x
$K_2(CN_2)$ tetragonal modification	C(1) – N(1)	121.4(3)
	C(1) – N(2)	121.9(2)
	C(2) – N(3) 2x	124.9(2)

*Data given in the literature; ** the N-C-N group in $K_2(C_4N_7H_3)$ is disordered with a ⅔:⅓ ratio.

Table S2. Structure refinement data of powder X-ray diffraction measurements.

Formula	$K(C_3N_6H_5)$	$K(CN_2H)$	$K_5H(CN_2)_3$	$K_5H(CN_2)_2$
Space group	*Pbcn* (no. 60)	$P2_12_12_1$ (no. 19)	$Im\bar{3}m$ (no. 229)	*P4/ncc* (no. 130)
a/pm	1227.077(6)	707.236(6)	796.110(3)	908.918(5)
b/pm	1111.785(6)	909.605(7)	796.110(3)	908.918(5)
c/pm	1881.829(9)	912.788(6)	796.110(3)	1102.499(6)
Cell volume / Å^3	2567.28(2)	587.201(7)	504.568(4)	910.810(8)
Formula units, Z	16	8	2	4
R_{Bragg}	3.1143	2.6753	2.6540	3.4737
χ^2	1.1534	1.0901	1.0647	1.2117
R_p	2.7975	3.9127	4.0937	4.1332
R_{wp}	3.8228	5.8888	6.6826	5.8930
CCDC No.	2332888	-	-	-
ICSD No.	-	401784	407310	409559

Formula	$K_2(CN_2)$	$K_2(CN_2)$
Space group	*C2/m* (no. 12)	$I4_1/a$ (no. 88)
a/pm	578.730(5)	1731.514(5)
b/pm	570.351(5)	1731.514(5)
c/pm	578.937(5)	593.457(3)
β/°	108.9835(5)	-
Cell volume / Å^3	180.702(3)	1779.27(1)
Formula units, Z	2	20
R_{Bragg}	4.7018	3.3286
χ^2	1.3632	1.1499
R_p	3.8640	3.6198
R_{wp}	5.3590	5.1700
CCDC No.	-	2270217
ICSD No.	411094	-

In a reaction of $NiCl_2$ with melamine (1:2.5) at 300˚C, we identified the formation of a protonated guanylmelamine chloride crystals adduct with melem (CCDC: 2171178). This suggests that the metal chloride deprotonates melamine, producing HCl in the process. Previous studies have demonstrated that guanylmelamine can be synthesized from dicyandiamide in the presence of hydrogen chlorides[1]. Thus, it is likely that melamine undergoes a similar decomposition, forming cyanamide or dicyandiamide as intermediate products, and then reacting with melaminate anion forming extraordinary structures such as guanylmelamine or monocyanomelamine.

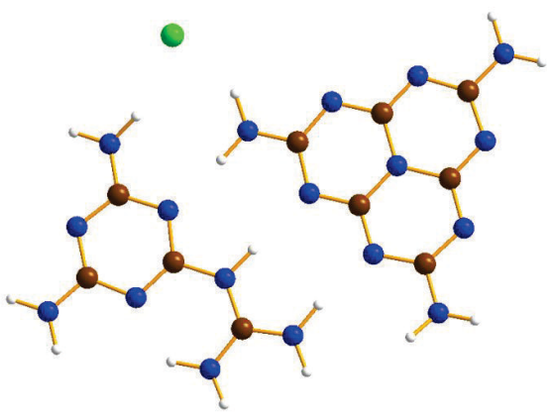

Figure S8. An adduct of protonated guanylmelamine chloride with Melem ($C_{10}H_{15}ClN_{18}$) (CCDC: 2171178)

Figure S9. Reaction vessel, based on a 4 ml screw neck vial (Chroma Globe, Kreuzau, Germany) and Schlenk-type tube.

References:

1. MacLean, A. F. **Guanymelamines and Method of Preparing**. U.S. Patent 2,537,840, January 9, 1951.

Publication 6

$MnCl_2(C_6N_{10}H_6)$: Insights into a Luminescent Transition Metal–Melem Complex

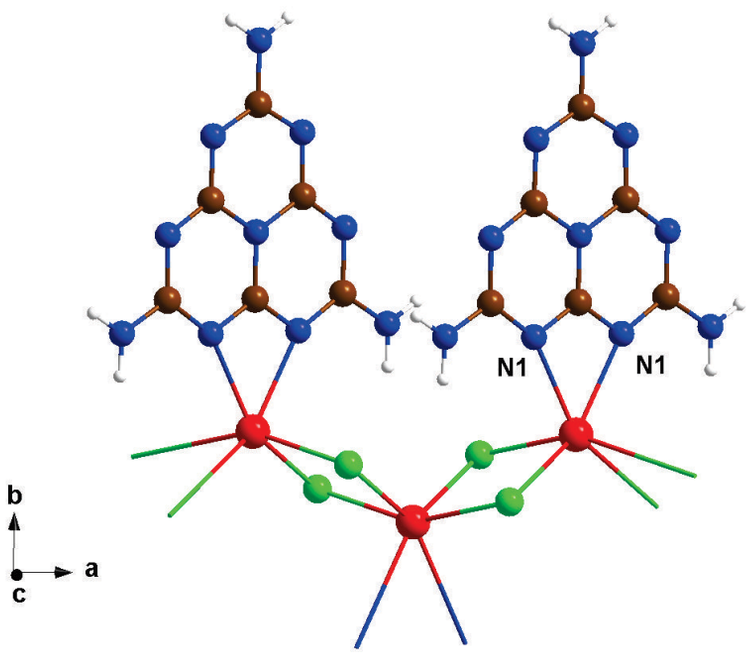

]

https://doi.org/10.3390/molecules29235598

Reprinted with permission from

Molecules ***2024***, *29(23), 5598*

molecules

MDPI

Article

$MnCl_2(C_6N_{10}H_6)$: Insights into a Luminescent Transition Metal–Melem Complex

Elaheh Bayat [1], Markus Ströbele [1], David Enseling [2], Thomas Jüstel [2] and Hans-Jürgen Meyer [1,*]

[1] Section for Solid State and Theoretical Inorganic Chemistry, Institute of Inorganic Chemistry, University of Tübingen, Auf der Morgenstelle 18, 72076 Tübingen, Germany; elaheh.bayat@anorg.uni-tuebingen.de (E.B.); markus.stroebele@uni-tuebingen.de (M.S.)
[2] Department of Chemical Engineering, FH Münster University of Applied Sciences, Stegerwaldstraße 39, 48565 Steinfurt, Germany; david.enseling@fh-muenster.de (D.E.); juestel@fh-muenster.de (T.J.)
* Correspondence: juergen.meyer@uni-tuebingen.de

Abstract: In this work, the ($MnCl_2(C_6N_{10}H_6)$) complex has been synthesized via solid-state reaction between manganese (II) chloride and melamine in the molar ratio of 1:2. A similar synthesis has been repeated with $CoCl_2$, and $FeCl_2$, resulting in two new metal–melam complexes ($FeCl_2(C_6N_{11}H_9)$ and $CoCl_2(C_6N_{11}H_9)$). $MnCl_2(C_6N_{10}H_6)$ crystallizes in the monoclinic crystal system with the space group *I*2/*a*. The crystalline powder of $MnCl_2(C_6N_{10}H_6)$ was studied by X-ray diffraction, infrared spectroscopy, and thermogravimetric analysis to examine its structure and properties. $MnCl_2(C_6N_{10}H_6)$ also shows good thermal stability up to 370 °C; however, the complete decomposition occurred at 900 °C, yielding Mn_7C_3. This paper presents an easy synthesis of the first luminescent transition metal–melem complex, providing new insights into the reactivity of melamine at elevated temperatures in the presence of transition metal chlorides.

Keywords: melem; melamine; coordination sites of melem; manganese chloride; photoluminescence; transition metal carbide

Citation: Bayat, E.; Ströbele, M.; Enseling, D.; Jüstel, T.; Meyer, H.-J. $MnCl_2(C_6N_{10}H_6)$: Insights into a Luminescent Transition Metal–Melem Complex. *Molecules* **2024**, *29*, 5598. https://doi.org/10.3390/molecules29235598

Academic Editor: Shengjie Wang

Received: 1 October 2024
Revised: 21 November 2024
Accepted: 25 November 2024
Published: 27 November 2024

1. Introduction

The first synthesis of melamine (1,3,5-triazine-2,4,6-triamine) dates back to a century ago with the reaction of thiocyanate with ammonium chloride [1]. Later on, there were more synthetic methods suggested by many researchers to yield melamine based on heating thiourea, guanidine carbonate, cyanamide, or dicyandiamide [1,2]. Nowadays, urea is a precursor for the industrial production of melamine, which has increased the production of melamine to millions of tons per year, making this material widely available.

When pure melamine ($C_3N_6H_6$) is heated up, it will form different condensation products such as melam ($C_6N_{11}H_9$) at around 360 °C [3] (340 °C [4]), and subsequently melem ($C_6N_{10}H_6$) at approximately 400 °C [3] (380 °C [4]) (Figure 1). This process is accompanied by the release of ammonia during the condensation. Interestingly, during this transformation process, the characteristic rings of triazine (cyanuric nuclei) and heptazine (cyameluric nuclei) are retained or restructured. Triazine rings are composed of a single six-membered ring with alternating carbon and nitrogen atoms, as can be found in melamine. Heptazine rings, on the other hand, consist of three fused triazine rings which create a larger and more complex structure of melem and melon [5].

The formation of extended supramolecular structures based on the molecular entities of melem and melon through the thermal condensation of melamine is a conventional way to form metal-free molecules and polymers [6]. Derivatives of s-heptazine are particularly interesting due to their intriguing thermal stability and unique electronic structures. The formation of ionic and polymeric carbon nitride compounds [7–9] based on aromatic tricyclic units (tri-s-triazine, C_6N_7) typically involves an ordered self-assembly with bonding via covalent and noncovalent interactions [2]. These polymeric materials are represented

by an extended network of melem, connected by hydrogen bonding and π-π stacking, featuring surprisingly high thermal stabilities. The research on carbon nitride compounds is extensive, covering a wide range of materials. Depending on the bonding arrangement and ratio of carbon to nitrogen atoms, these compounds are classified with their very own nomenclature, such as triazine-based polymers [10], graphitic carbon nitride, carbon nitride nanotubes, boron carbon nitrides, and so on. Melem and carbon nitride (C_3N_4) were reported for their potential applications in flame retardance [11], photocatalysis [12,13], heterogeneous catalysis [14], as nanosheets for bioimaging [15], luminescence devices [16], the anode material of lithium-ion battery [17], and as an adsorbent of heavy metals and dyes [18,19], etc.

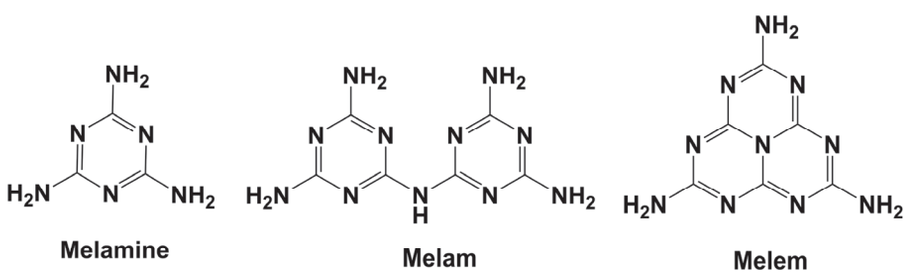

Figure 1. Structures of melamine ($C_3N_6H_6$), melam ($C_6N_{11}H_9$) and melem ($C_6N_{10}H_6$).

Carbon-nitride materials have significant and various applications; however, there are few studies on the reactivity of melem up to now [12,20]. Early studies on s-heptazine derivatives faced challenges because of the insolubility (in water and any organic solvents) and low reactivity of melem [21]. S-heptazine and s-triazine are considered electron-deficient aromatic compounds due to the existence of nitrogen atoms in the ring, which makes them able to undergo nucleophilic substitution under specific conditions [20]. Yet, the chemical behavior of melem remains less explored when compared to the triazine analog. There are only limited examples of the reactivity of NH_2-groups of melem reported up to now [12,20]. Examples of such studies include those on 2,5,8-triphthalimido-tri-s-triazine [22], 2,5,8-tri(2,3,4,5-tetrafluorophthalimido)-tri-s-triazine [23]. Furthermore, by treating melem with mineral acids, several melemium salts were obtained such as phosphate salt $C_6N_7(NH_2)_3 \cdot H_3PO_4$, sulfate salt $H_2C_6N_7(NH_2)_3SO_4 \cdot 2H_2O$, melemium melem perchlorate $HC_6N_7(NH_2)_3ClO_4 \cdot C_6N_7(NH_2)_3$, etc. [24,25].

Recent research by Xu et al. has explored the reactivity of melem with various metals. Their study involved the interactions of melem in an aqueous suspension with $AgNO_3$, $Zn(NO_3)_2$, $Cu(NO_3)_2$, $Co(NO_3)_2$, and $Ni(NO_3)_2$. Among these, the only compound obtained was an infinite Ag-N nanocage coordinated with melem [26]. Simultaneously, our research group investigated the formation of complex metal-halide–melem compounds by reacting binary metal halides with melem, which introduces compounds of $CaBr_2$, $SrBr_2$, SrI_2, BaI_2, and $PbBr_2$ with melem [27].

In this study, we explored the solid-state reactivity of melamine in the presence of transition metal chlorides at higher temperatures, where melam and melem can form new complexes of $FeCl_2(C_6N_{11}H_9)$, $CoCl_2(C_6N_{11}H_9)$, and more importantly $MnCl_2(C_6N_{10}H_6)$. $MnCl_2(C_6N_{10}H_6)$ has been characterized by powder X-ray diffraction (PXRD), single-crystal diffraction, and infrared (IR) spectroscopy. Additionally, thermogravimetric analyses (TGA) were conducted to evaluate the stability of $MnCl_2(C_6N_{10}H_6)$ and to determine its decomposition products. The TGA analysis indicates that manganese carbodiimide [28] is formed as an intermediate compound at 700 °C, and at higher temperatures, the decomposition product is manganese carbide, Mn_7C_3 (ICSD 69534).

This transition metal carbide has been previously synthesized in the carbothermal reduction of manganese oxide in two steps, forming MnO at 1050 °C and Mn_7C_3 at 1300 °C. Alternatively, Mn_7C_3 can also be obtained from the reaction of manganese dust with n-pentane at 850 °C at reduced pressure [29]. Additionally, various researchers have proposed

other methods for synthesizing this carbide [30]. Due to the wide range of applications of transition metal carbides in the heat-resistance and hard material industry, Mn_7C_3 is valued [31]. Furthermore, manganese carbodiimide and manganese carbide can exhibit various applications due to the position of manganese in the middle of the 3d series [30].

Finally, the photoluminescence properties of $MnCl_2(C_6N_{10}H_6)$ are discussed, providing comprehensive insight into its remarkable photochemical behavior

2. Results and Discussion

2.1. Crystal Structure of $MnCl_2(C_6N_{10}H_6)$, and $FeCl_2(C_6N_{11}H_9)$

The $MnCl_2(C_6N_{10}H_6)$ crystallizes in a monoclinic crystal system and the space group of $I2/a$ with crystallographic details summarized in Table 1. The crystal structure is composed of $MnCl_{4/4}$ chains along the *a*-axis that are interconnected by melem units to form a layered arrangement (Figure 2). The melem units are connected to the manganese atom through the two inner nitrogen atoms of N1, with a bond distance of 2.331 (5) Å, thereby completing the coordination number six of manganese. These melem units are situated between the $MnCl_4/_4$ layers, as shown in Figure 2b. $FeCl_2(C_6N_{11}H_9)$ crystallizes in a monoclinic crystal system, in the space group P21/c. The iron chloride is coordinated through N1 and N7 to the bidentate melamine ligand binding a melam unit. The steric demand and tetrahedral environment of the central atom force the melamine ligand to protrude from the plane, disrupting the planarity of the triazine rings. The crystal structure of $FeCl_2(C_6N_{11}H_9)$, along with the crystallographic details, is presented in Figure S1 and Table S1, respectively.

Table 1. Crystallographic details of the crystal structure refinement of $MnCl_2(C_6N_{10}H_6)$.

Empirical Formula	**$MnCl_2(C_6N_{10}H_6)$**	
CCDC code	2141509	
Formula weight (g/mol)	344.05	
Wavelength (Å)	1.54184	
Crystal system	Monoclinic	
Space group	*I* 1 2/*a* 1	
Unit cell dimensions (Å)	*a*/Å	6.6697 (4)
	b/Å	21.926 (1)
	c/Å	7.718 (2)
Volume ($Å^3$)	1128.61	
Z	4	
Density (calculated) (g/cm^3)	2.025	
Absorption coefficient (mm^{-1})	13.947	
Final R indices (I > 2σ(I))	*R*1 = 0.0288, wR2 = 0.0581	
R indices (all data)	*R*1 = 0.0333, wR2 = 0.0594	
GOOF	1.070	

Crystals of $CoCl_2(C_6N_{11}H_9)$ were obtained under the same reaction conditions. The PXRD pattern closely matches the calculated pattern based on the single-crystal refinement of $FeCl_2(C_6N_{11}H_9)$, indicating both structures to be isotypic.

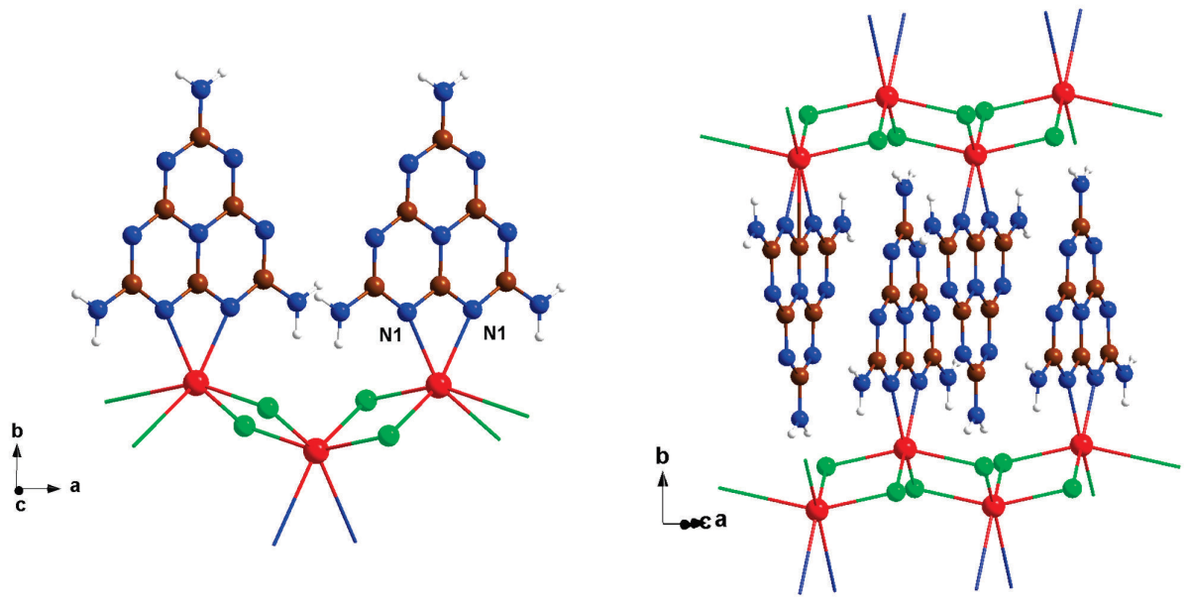

(**a**) (**b**)

Figure 2. (**a**) A perspective view of the crystal structure of $MnCl_2(C_6N_{10}H_6)$ of the *ab*-plane and (**b**) the stacking along the *b*-axis (with the color code for N: blue, C: brown, H: white, Cl: green, and Mn: red).

2.2. Thermoanalytic Studies

A valuable technique that can provide insights into the formation or decomposition of new phases is combining differential scanning calorimetry (DSC) with X-ray diffraction (XRD). In the DSC analysis of a 1:2 molar mixture of manganese (II) chloride and melamine, as shown in Figure 3a, there are three notable thermal effects: two endothermic peaks centered at 300 °C and 370 °C, and an exothermic peak at 306 °C. The endothermic peak at 300 °C is followed by an exothermic peak at 306 °C, which is attributed to the formation of an unknown intermediate phase (see Figure S2), which subsequently decomposes around 370 °C, resulting in the formation of $MnCl_2(C_6N_{10}H_6)$. The stability of $MnCl_2(C_6N_{10}H_6)$ has been further investigated using thermogravimetric analysis (TGA).

The compound demonstrates good thermal stability up to 400 °C, with only a 2.6% weight loss. This reduction in weight may be attributed to a small amount of an amorphous side phase from the reaction, which will be further explained in the next section. The TGA results, presented in Figure 3b, indicate that the complex gradually decomposes into different compounds when it is heated to 900 °C. To better understand the decomposition process, the TGA was repeated, with the analysis stopped at specific temperature intervals (approximately 500 °C, 700 °C, and 900 °C) to identify the decomposition products. At around 500 °C, an ex situ powder X-ray diffraction (PXRD) analysis revealed that $MnCl_2(C_6N_{10}H_6)$ had decomposed into an amorphous intermediate phase. By 700 °C, the complex forms manganese carbodiimide [28] (Figure S3a). Finally, at 900 °C, the complex underwent complete decomposition, resulting in the formation of the transition metal carbide Mn_7C_3, as confirmed by the XRD pattern shown in Figure S3b.

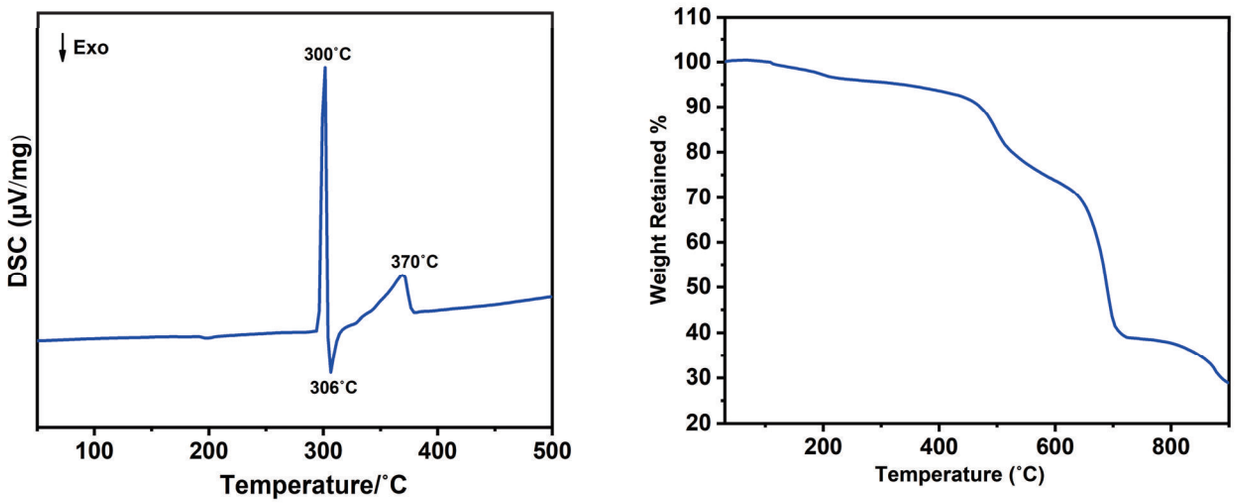

(**a**) (**b**)

Figure 3. (**a**) DSC of the reaction of $MnCl_2$ and melamine in a molar ratio of 1:2 and (**b**) TGA of $MnCl_2(C_6N_{10}H_6)$.

2.3. X-Ray Powder Diffraction

The reaction between $MnCl_2$ and melamine in the ratio of 1:2 at 400 °C for 100 h yields a product where $MnCl_2(C_6N_{10}H_6)$ can be isolated as a separate phase. From the theoretical Equation (1), we would have expected that this product is formed by the release of NH_3 and can be obtained as a pure phase (Figure 4). However, the XRD powder pattern showed a high background after the first synthesis, implying that there might be an amorphous phase. Therefore, in order to purify the $MnCl_2(C_6N_{10}H_6)$, a double chamber ampule with a temperature gradient (Figure S4) was utilized. Subsequently, the product (orange powder, Figure S4) is subjected to analysis via powder X-ray diffraction (PXRD), with the resulting diffractogram then compared with the calculated pattern derived from structure refinement based on single-crystal data (Figure 3). The white residue on the colder side of the ampule has been also analyzed, which shows that the amorphous phase is crystallized into melamine and ammonium chloride (Figure S4a,b).

$$MnCl_2 + 2C_3N_6H_6 \rightarrow MnCl_2(C_6N_{10}H_6) + 2NH_3 \quad (1)$$

Figure S5 presents the PXRD patterns of two complexes of $FeCl_2(C_6N_{11}H_9)$ and $CoCl_2(C_6N_{11}H_9)$. Similarly, the high background of the XRD pattern can be attributed to either the fluorescence effect of Fe and Co or the presence of an amorphous phase. These complexes were also prepared from a molar ratio of 1:2 of $FeCl_2$, and $CoCl_2$ with melamine, in the same condition as a synthesis of $MnCl_2(C_6N_{10}H_6)$. The theoretical reaction equation is shown in Equations (2), and (3). These complexes closely resemble those previously introduced by our group, including $LiBr(C_6N_{11}H_9)$ (CCDC: 2039843), $CuX(Cl,Br,I)(C_6N_{11}H_9)$ (CCDC: 2057533, 2059117, 2041008, respectively), and $ZnI_2(C_6N_{11}H_9)$ (CCDC: 2056462).

$$FeCl_2 + 2C_3N_6H_6 \rightarrow FeCl_2(C_6N_{11}H_9) + NH_3 \quad (2)$$

$$CoCl_2 + 2C_3N_6H_6 \rightarrow CoCl_2(C_6N_{11}H_9) + NH_3 \quad (3)$$

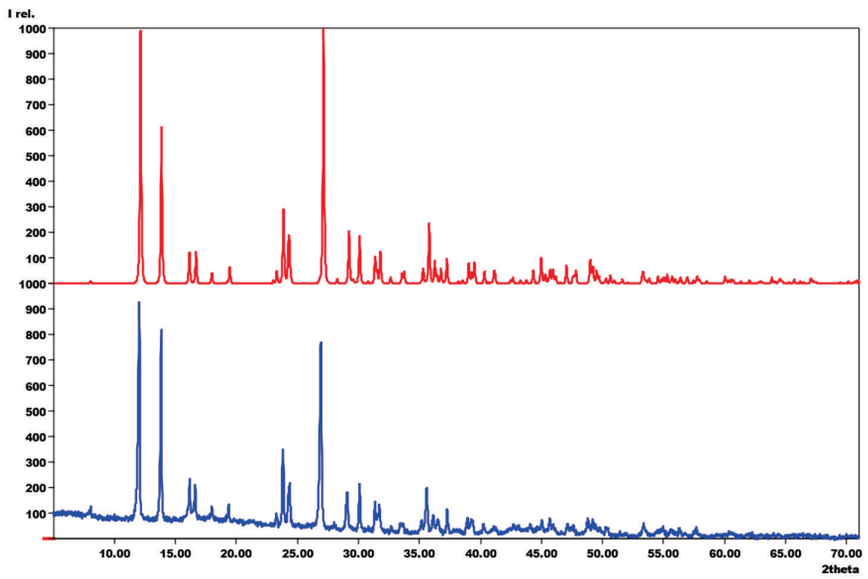

Figure 4. XRD powder pattern of the synthesized $MnCl_2(C_6N_{10}H_6)$ (bottom), compared with the calculated pattern based on the single-crystal refinement (top) (CCDC code: 2141509).

2.4. Infrared (IR) Spectroscopy

The IR spectrum of the $MnCl_2(C_6N_{10}H_6)$ complex was compared with the spectra of melamine and melem as shown in Figure 5. Table S2 shows details of the frequencies related to the different vibrational modes of these compounds and the corresponding bond assignments. As illustrated in Figure 5, infrared spectra for all three compounds were recorded in the range from 4000 to 500 cm^{-1}. This comparison aids in visualizing the similarity and difference of the $MnCl_2(C_6N_{10}H_6)$ with that of melem and linking them to the established vibrational modes. As expected, because all the compounds contain NH_2 groups, similar spectral patterns in the 3500–3100 cm^{-1} and 1580–1600 cm^{-1} regions are related to NH stretching and bending vibrations. However, $MnCl_2(C_6N_{10}H_6)$ reveals notable differences from melamine in these areas. Despite some minor changes in intensity and splitting, the vibrational features of $MnCl_2(C_6N_{10}H_6)$ are similar to those of melem.

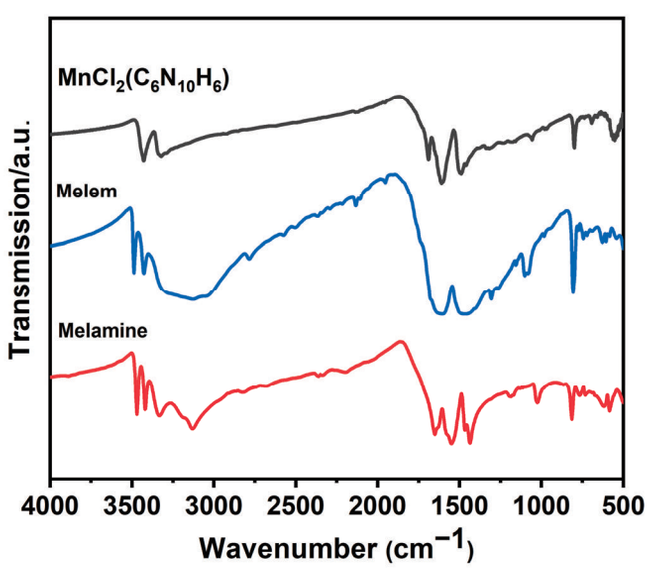

Figure 5. FT-IR-spectrum of $MnCl_2(C_6N_{10}H_6)$ compared to melamine and melem.

2.5. Photoluminescence Measurements

The photoluminescence (PL) properties of Mn(II) complexes, whether in inorganic compounds [32] or organic–inorganic complexes [33–35], are particularly captivating. These complexes exhibit intriguing optical properties and have potential applications in sensors, optical devices, optical markers, and cost-effective OLEDs [33]. The PL of Mn^{2+} is primarily associated with 3d-3d transitions [36,37]. However, its photoluminescence can be significantly affected by both the local coordination environment of the manganese ions and the overall crystal structure. Mn^{2+} comprising luminescent materials with multiple 3d-3d transitions (see Figure S6, Tanabe-Sugano-Diagram for d^5 ions) have been known since the forties of the last century [38], while the Mn-centered absorption lines are rather weak due to the spin and Laporte forbidden character of these 3d-3d transitions. Therefore, applied Mn^{2+} luminophores are sensitized, either by the band-to-band transition of the host, e.g., in the widely applied EL and display phosphors ZnS:Mn or Zn_2SiO_4:Mn [39,40]. Alternatively, sensitization is achieved by a co-activator, as in the fluorescent lamp phosphors $Ca_5(PO_4)_3$(F,Cl):Sb,Mn and $BaMgAl_{10}O_{17}$:Eu,Mn [41,42], or by ligand-centered transitions as in coordination compounds. In its pure phase, $MnCl_2$ displays different emission characteristics under varying pressures [43]. At ambient pressure, the emission occurs at 642 nm (15,580 cm^{-1}), attributed to the spin-forbidden $^4T_{1g}(G) \rightarrow {}^6A_{1g}(^6S)$ transition [36,37,43]. As pressure increases, a red-shift of the emission band is observed as the ligand to metal distances decline and the crystal field strength increases. Moreover, the color of the emission from Mn(II) complexes and phosphors is dependent on the coordination geometry. In a tetrahedral field, the emission is typically green, while in an octahedral crystal field, it is observed from the red to the orange range [43].

In this study, $MnCl_2(C_6N_{10}H_6)$ exhibits red photoluminescence upon excitation with a UV radiation source. The emission spectrum reveals a broad band centered at 620 nm (16,130 cm^{-1}), while the FWHM is 2460 cm^{-1}. Weak excitation bands are observed between 350 and 500 nm (Figure 6), which are attributed to the Mn^{2+}-centered transitions between the ground state term $^6A_{1g}$ and the excited state terms $4T_{1g}$, $4T_{2g}$, $4A_{1g}$, and ^4E_g [41]. The strong excitation band at 325 nm is caused by the coordinated ligand melem, which sensitizes the Mn^{2+} luminescence.

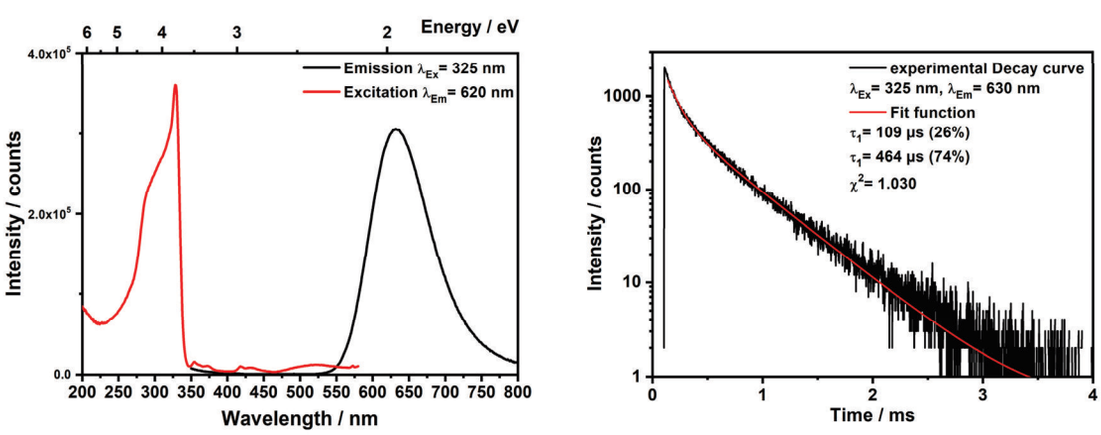

(**a**) (**b**)

Figure 6. (**a**) Photoluminescence spectra of $MnCl_2(C_6N_{10}H_6)$ in the solid-state at room temperature. (**b**) Decay curve obtained for $MnCl_2(C_6H_6N_{10})$ upon 325 nm excitation at room temperature.

The decay measurement after a 325 nm excitation delivers a biexponential decay curve with an emission lifetime τ_1 of 109 µs (26%) and a longer component with τ_2 of 464 µs (74%). The decay time of Mn^{2+}-activated phosphors with a high quantum yield close to unity is in the range of 8 to 40 ms [44], while the decay time of Mn^{2+} in coordination compounds is in the range from 0.1 to 25 ms [33]. However, the decay time can be strongly

reduced by concentration quenching, by Mn^{2+} ions at the particle surface [45], and/or by magnetic interaction (superexchange) between ligand-bridged Mn^{2+} ions [46]. We observed a low quantum yield < 10%, which is in line with a rather short decay time. Upon comparing the qualitative absorption spectrum of $MnCl_2(C_6N_{10}H_6)$ (Figure S7) with the UV/Vis absorption spectra of melem [6,47], it is evident that while the absorption in pure melem completely diminishes in the visible-light region, the absorption in $MnCl_2(C_6N_{10}H_6)$ shows a similar initial decline but persists slightly longer, though only at a very low intensity (approximately 2% of the absorption), before fully fading away at a wavelength of 600 nm. Melem has also been previously coupled with other organic monomers to construct extended conjugated networks, thereby enhancing visible-light absorption and improving photocatalytic performance [6].

3. Materials and Methods

The starting materials, $MnCl_2$ (ABCR, Nagano, Japan, 97%), $FeCl_2$ (ABCR, 98%) and $CoCl_2$ (ABCR, 97%), and melamine (Sigma-Aldrich, St. Louis, MO, USA, 99%), were used as received without additional purification. All the handling and storage of these materials were conducted within a glovebox, maintaining an argon atmosphere with moisture and oxygen levels below 1 ppm.

For the synthesis of $MnCl_2(C_6N_{10}H_6)$, the reaction mixture was prepared with a molar ratio of 1:2 for $MnCl_2$ to melamine. This mixture was then transferred into a hand-made silica tube with a length of 6 cm, an outer diameter of 10 mm, and an inner diameter of 7 mm. The resulting mixture, weighing approximately 50 g, was vacuum-sealed. This ampule was then placed in a Carbolite furnace, where it was heated at a rate of 1 °C min^{-1} to 400 °C and remained at this temperature for 100 h, followed by cooling at a rate of 0.1 °C min^{-1} to room temperature. The crystals of $MnCl_2(C_6N_{10}H_6)$ appeared on the wall of the ampule slightly above the crystalline powder. To prepare the crystalline powder of $MnCl_2(C_6N_{10}H_6)$, the reaction time can be reduced to 20 h with a heating and cooling rate of 1 °C min^{-1}. The obtained XRD powder pattern revealed the presence of small unidentified peaks and a high background, suggesting the presence of an unknown amorphous phase. To purify the sample, a double chamber ampule, as shown in Figure S4, was used. One chamber of ampule was placed in a glass oven at 350 °C for 72 h, while the other chamber was outside of the furnace at room temperature. The pure phase remained on the hot side of the ampule, while the side phase, consisting of ammonium chloride and melamine, was separated. The yield of the reaction is estimated to be around 64%.

$FeCl_2(C_6N_{11}H_9)$ and $CoCl_2(C_6N_{11}H_9)$ were synthesized in a similar route by mixing one molar ratio of $FeCl_2$, or $CoCl_2$ with 2 molar ratios of melamine (Sigma-Aldrich, 99%). A total of 50 mg of each mixture was transferred into a 6 cm ampule and heated to 400 °C in the Carbolite furnace for 100 h (with a ramp of 1 and 0.1 °C min^{-1}). To obtain crystals of these complexes, the same mixture was subjected to the same conditions except in a Simon furnace with a very small temperature gradient. At the bottom of the ampule, we could see a few crystals of $FeCl_2(C_6N_{11}H_9)$ and $CoCl_2(C_6N_{11}H_9)$. (If the temperature gradient is too high, the formation of ammonium melem chloride hinders the formation of main phases). The reaction scheme of all three compounds is shown in Figure S8.

X-ray diffraction patterns of the prepared powders were recorded using a powder diffractometer (STOE, Darmstadt, Germany, STADIP, Ge-monochromator) with Cu-Kα_1 radiation (λ = 1.540598 Å). Data were collected in the range of $5 < 2\theta < 70°$. The patterns were then compared to those of the relevant crystal structures using Match3! Software [48].

Single crystals of $MnCl_2(C_6N_{10}H_6)$ were selected and mounted on a Rigaku XtaLab Synergy-S single-crystal X-ray diffractometer [49]. X-ray diffraction data were collected using Cu-Kα radiation (λ = 1.54184 Å) and a mirror monochromator, with measurements taken at a temperature of 180 K. Crystal structures were determined using direct methods (SHELXT), followed by full-matrix least-squares refinement (SHELXL-2014) [50,51]. X-ray intensity absorption corrections were applied using numerical methods with CrysAlisPro 1.171.41.92a software (Rigaku Oxford Diffraction, Neu-Isenburg, Germany) [49]. Hydrogen

atoms were identified in the difference maps and refined isotropically based on their positions. The crystal structure of $FeCl_2(C_6N_{11}H_9)$ was also solved and refined on the basis of single-crystal X-ray diffraction data (Table S1).

Differential scanning calorimetry (DSC) was performed using a DSC 204 F1 Phoenix instrument (Netzsch, Selb, Germany). In a glovebox, under an argon atmosphere, the starting materials were sealed in 100 µL gold-plated (5 µm) steel autoclaves (Bächler Feintech AG, Hölstein, Switzerland). The reaction between $MnCl_2$ and melamine, with a 1:2 ratio, was investigated over a temperature range from room temperature to 500 °C, applying heating and cooling rates of 2 and 0.5 °C/min.

For thermogravimetric analysis (TGA), a Netzsch Jupiter STA 449 F3 apparatus was employed. The final product was placed in a hand-made open-ended silica container under argon and underwent gradual heating and cooling at a rate of 2 K/min. This approach allowed for the evaluation of the product's thermal stability across a temperature range from room temperature to 900 °C.

Infrared (IR) spectra of the samples were acquired using a Bruker (Frankfurt, Germany) VERTEX 70 FT-IR spectrometer, covering the spectral range from 400 to 4000 cm^{-1}. KBr tablets were utilized as a background reference.

For optical measurements the emission and excitation spectra of $MnCl_2(C_6N_{10}H_6)$ were recorded optically using the fluorescence spectrometer FLS920 (Edinburgh Instruments, Livingston, UK) equipped with a 450 W xenon discharge lamp (Osram, Munich, Germany). A mirror optic designed for powder samples was also utilized. An R2658P single-photon-counting photomultiplier tube manufactured by Hamamatsu was used for detection. Photoluminescence spectra were recorded with a spectral resolution of 1 nm, a dwell time of 0.5 s at 1 nm intervals, and 2 repetitions. Photoluminescence decay curves were measured using the same spectrometer, with a 445 nm picosecond laser serving as the pulsed excitation source.

4. Conclusions

In conclusion, the successful synthesis of $MnCl_2(C_6N_{10}H_6)$ is a very important step toward understanding the coordination chemistry of melem. We attempted to extend this work by investigating the solid-state reactivity of melamine with transition metal chlorides at elevated temperatures. This approach led to the successful synthesis of several new coordination complexes with melam, such as $FeCl_2(C_6N_{11}H_9)$, and $CoCl_2(C_6N_{11}H_9)$.

It is noteworthy to mention that our primary focus is on synthesizing $MnCl_2(C_6N_{10}H_6)$ since it is the first luminescent transition metal–melem complex. Infrared (IR) spectroscopy, powder X-ray diffraction (PXRD), and single-crystal X-ray diffraction were used to characterize the structure of $MnCl_2(C_6N_{10}H_6)$. Thermal gravimetric analysis (TGA) also provided insights into the thermal stability and decomposition of this compound, showing that $MnCl_2(C_6N_{10}H_6)$ is first decomposed into manganese carbodiimide [28] at 700 °C and then at 900 °C to manganese carbide (Mn_7C_3). The synthesis of manganese carbide, which is typically produced via carbothermal reduction processes, has applications in heat-resistant and hard materials. Proposing a new synthetic route for manganese carbodiimide and Mn_7C_3 is also another aspect of this work. Finally, the photoluminescence properties of $MnCl_2(C_6N_{10}H_6)$ were studied which shows red-to-orange fluorescence with an emission peak at 620 nm and a biexponential decay with a lifetime in the 100 µs range.

Supplementary Materials: The following supporting information can be downloaded at: https://www.mdpi.com/article/10.3390/molecules29235598/s1, Figure S1: Section of the crystal structure of $FeCl_2(C_6N_{11}H_9)$ projected on *bc*-plane (top) and the unit cell content of the structure (bottom). Table S1: Crystallographic details of the crystal structure refinement on $FeCl_2(C_6N_{11}H_9)$.; Figure S2: Ex-situ powder XRD pattern of an unknown phase formed by heating a mixture of $MnCl_2$ and melamine in a 1:2 ratio to the first exothermic DSC peak, observed at 306 °C. Figure S3: a. XRD pattern of manganese carbodiimide ($MnCN_2$) obtained by heating $MnCl_2(C_6H_6N_{10})$ to 700 °C, along with reflections of unknown side-phase (shown with black stars) compared with the calculated pattern based on the single-crystal structure refinement (top) (CCDC code: 272236). b. XRD pat-

tern of manganese carbide (Mn_7C_3) obtained from heating $MnCl_2(C_6N_{10}H_6)$ to 900 °C (bottom), compared with the calculated pattern based on the single-crystal refinement (top) (CCDC code: 2141509). Figure S4: a. Photograph of a two-chamber ampule used for separation of side-phase from $MnCl_2(C_6N_{10}H_6)$ under daylight (top) and under UV irradiation (bottom). (The observed blue light observed in the Figure originates from the reflectance of the blue light (366 nm) on the white powder. b. XRD pattern of side phase on the left side of two-sided chamber. Figure S5: Recorded XRD patterns of $FeCl_2(C_6N_{11}H_9)$, $CoCl_2(C_6N_{11}H_9)$ with the calculated pattern from the structure refinement of $FeCl_2(C_6N_{11}H_9)$ (top). Table S2: Vibrational frequencies (in cm^{-1}) for $MnCl_2(C_6N_{10}H_6)$ compared to those of melamine and melem. Figure S6: Tanabe-Sugano-Diagram for a d^5 ion with the most prominent emission transition between $^4T_1(^4G)$ and $^6A_1(^6S)$. Figure S7: A qualitative absorption spectrum by the aid of the Kubelk-Munk function from the reflection spectrum of $MnCl_2(C_6N_{10}H_6)$. Figure S8: A reaction scheme of melamine with some transition metal chlorides to obtain $FeCl_2(C_6N_{11}H_9)$, $CoCl_2(C_6N_{11}H_9)$, and $MnCl_2(C_6N_{10}H_6)$ compounds.

Author Contributions: Conceptualization, supervision, funding acquisition, review, and editing, H.-J.M.; Synthesis, TGA, DTA, PXRD, and IR, writing, E.B.; structure refinements, M.S.; photoluminescence spectroscopy, T.J. and D.E. All authors have read and agreed to the published version of the manuscript.

Funding: This research is supported by the Deutsch Forschungsgemeinschaft (DFG) through grant ME 914/34-1.

Data Availability Statement: Data are contained within the article and Supplementary Materials.

Conflicts of Interest: The authors declare no conflicts of interest.

References

1. Bann, B.; Miller, S.A. Melamine and derivatives of melamine. *Chem. Rev.* **1958**, *58*, 131–172. [CrossRef]
2. Schwarzer, A.; Saplinova, T.; Kroke, E. Tri-s-triazines (s-heptazines)—From a "mystery molecule" to industrially relevant carbon nitride materials. *Coord. Chem. Rev.* **2013**, *257*, 2032–2062. [CrossRef]
3. May, H. Pyrolysis of melamine. *J. Appl. Chem.* **1959**, *9*, 340–344. [CrossRef]
4. Lotsch, B.V.; Schnick, W. New light on an old story: Formation of melam during thermal condensation of melamine. *Chem. Eur. J.* **2007**, *13*, 4956–4968. [CrossRef]
5. Keßler, F.K. Structure and Reactivity of s-Triazine-Based Compounds in C/N/H Chemistry. Ph.D. Thesis, Ludwig Maximilian University of Munich, Munich, Germany, 2019.
6. Chu, S.; Wang, C.; Feng, J.; Wang, Y.; Zou, Z. Melem: A metal-free unit for photocatalytic hydrogen evolution. *Int. J. Hydrogen Energy* **2014**, *39*, 13519–13526. [CrossRef]
7. Humayun, M.; Ullah, H.; Tahir, A.A.; bin Mohd Yusoff, A.R.; Mat Teridi, M.A.; Nazeeruddin, M.K.; Luo, W. An overview of the recent progress in polymeric carbon nitride based photocatalysis. *Chem. Rec.* **2021**, *21*, 1811–1844. [CrossRef] [PubMed]
8. Savateev, A.; Antonietti, M. Ionic carbon nitrides in solar hydrogen production and organic synthesis: Exciting chemistry and economic advantages. *ChemCatChem* **2019**, *11*, 6166–6176. [CrossRef]
9. Fang, Y.; Fu, X.; Wang, X. Diverse polymeric carbon nitride-based semiconductors for photocatalysis and variations. *ACS Mater. Lett.* **2020**, *2*, 975–980. [CrossRef]
10. Butchosa, C.; McDonald, T.O.; Cooper, A.I.; Adams, D.J.; Zwijnenburg, M.A. Shining a light on s-triazine-based polymers. *J. Phys. Chem. C* **2014**, *118*, 4314–4324. [CrossRef]
11. Shi, Y.; Long, Z.; Yu, B.; Zhou, K.; Gui, Z.; Yuen, R.K.; Hu, Y. Tunable thermal, flame retardant and toxic effluent suppression properties of polystyrene based on alternating graphitic carbon nitride and multi-walled carbon nanotubes. *J. Mater. Chem. A* **2015**, *3*, 17064–17073. [CrossRef]
12. Li, Y.; Jiang, Z.; Dong, G.; Ho, W. Construction and Activity of an All-Organic Heterojunction Photocatalyst Based on Melem and Pyromellitic Dianhydride. *ChemSusChem* **2022**, *15*, e202200477. [CrossRef] [PubMed]
13. Nikookar, M.; Rezaeifard, A.; Grzhegorzhevskii, K.V.; Jafarpour, M.; Khani, R. Melem Nanorectangular Prism-Modified $\{Mo_{72}Fe_{30}\}$ Nanocapsule as a Visible-Light-Assisted Photocatalyst for Catalase-like Activity. *ACS Appl. Nano Mater.* **2022**, *5*, 7917–7931. [CrossRef]
14. Thomas, A.; Fischer, A.; Goettmann, F.; Antonietti, M.; Müller, J.-O.; Schlögl, R.; Carlsson, J.M. Graphitic carbon nitride materials: Variation of structure and morphology and their use as metal-free catalysts. *J. Mater. Chem.* **2008**, *18*, 4893–4908. [CrossRef]
15. Zheng, H.; Zhao, Z.; Phan, J.B.; Ning, H.; Huang, Q.; Wang, R.; Zhang, J.; Chen, W. Highly efficient metal-free two-dimensional luminescent melem nanosheets for bioimaging. *ACS Appl. Mater. Interfaces* **2019**, *12*, 2145–2151. [CrossRef] [PubMed]
16. Guo, Q.; Wei, M.; Zheng, Z.; Huang, X.; Song, X.; Qiu, S.B.; Yang, X.b.; Liu, X.; Qiu, J.; Dong, G. Full-color chemically modulated g-C_3N_4 for white-light-emitting device. *Adv. Opt. Mater.* **2019**, *7*, 1900775. [CrossRef]

17. Yu, Y.; Jin, Q.; Zhu, D.; Ren, Y. Exceptional Lithium-Ion Storage Performance on an Azo-Bridged Covalent Heptazine Framework. *Adv. Funct. Mater.* **2024**, *34*, 2308706. [CrossRef]
18. Rani, B.; Nayak, A.K.; Sahu, N.K. Degradation of mixed cationic dye pollutant by metal free melem derivatives and graphitic carbon nitride. *Chemosphere* **2022**, *298*, 134249. [CrossRef]
19. Liu, S.; Sun, H.; O'Donnell, K.; Ang, H.; Tade, M.O.; Wang, S. Metal-free melem/g-C_3N_4 hybrid photocatalysts for water treatment. *J. Colloid Interface Sci.* **2016**, *464*, 10–17. [CrossRef]
20. Kroke, E.; Saplinova, T.; Bakumov, V.; Gmeiner, T.; Wagler, J.; Schwarz, M. 2,5,8-Trihydrazino-s-heptazine: A precursor for heptazine-based iminophosphoranes. *Z. Anorg. Allg. Chem.* **2009**, *635*, 2480–2487. [CrossRef]
21. Audebert, P.; Kroke, E.; Posern, C.; Lee, S.-H. State of the art in the preparation and properties of molecular monomeric s-heptazines: Syntheses, characteristics, and functional applications. *Chem. Rev.* **2021**, *121*, 2515–2544. [CrossRef]
22. Schwarzer, A.; Böhme, U.; Kroke, E. Use of melem as a nucleophilic reagent to form the triphthalimide C_6N_7 (phthal)$_3$-new targets and prospects. *Chem. Eur. J.* **2012**, *18*, 12052–12058. [CrossRef] [PubMed]
23. Schwarzer, A.; Kroke, E. Imido-s-Heptazinderivate-Verfahren zu Deren Herstellung und Anwendungen. DE102012007529A1, 17 October 2013.
24. Sattler, A.; Seyfarth, L.; Senker, J.; Schnick, W. Synthesen, Kristallstrukturen und spektroskopische Eigenschaften des Melem-Adduktes $C_6N_7(NH_2)_3 \cdot H_3PO_4$ sowie der Melemium-Salze $(H_2C_6N_7(NH_2)_3)SO_4 \cdot 2H_2O$ und $(HC_6N_7(NH_2)_3)ClO_4 \cdot H_2O$. *Z. Anorg. Allg. Chem.* **2005**, *631*, 2545–2554. [CrossRef]
25. Sattler, A. Investigations into s-Heptazine-Based Carbon Nitride Precursors. Ph.D. Thesis, Ludwig Maximilian University of Munich, Munich, Germany, 2010.
26. Meng, H.; Meng, P.; Liu, Z.; McMurtrie, J.; Xu, J. Exclusive Coordination between Melem and Silver (I) Ions: From Irregular Aggregates to Nanofibers to Crystal Cubes. *Inorg. Chem.* **2024**, *63*, 6980–6987. [CrossRef] [PubMed]
27. Meyer, H.J.; Ströbele, M.; Enseling, D.; Jüstel, T.; Abbasi, M.; Kroeker, S. Metal-Halide–Melem Compound based on M6-, M9-and M12-Clusters. *Eur. J. Inorg. Chem.* **2024**, e202400434. [CrossRef]
28. Liu, X.; Krott, M.; Müller, P.; Hu, C.; Lueken, H.; Dronskowski, R. Synthesis, crystal structure, and properties of MnNCN, the first carbodiimide of a magnetic transition metal. *Inorg. Chem.* **2005**, *44*, 3001–3003. [CrossRef]
29. Hájek, B.; Karen, P.; Brožek, V. Heptamanganese tricarbide Mn_7C_3. *Collect. Czechoslov. Chem. Commun.* **1983**, *48*, 2740–2750. [CrossRef]
30. Karen, P.; Fjellvåg, H.; Kjekshus, A.; Andresen, P. On phase relations, structural and magnetic properties of the stable manganese carbides $Mn_{23}C_6$, Mn_5C_2 and Mn_7C_3. *Acta Chem. Scand.* **1991**, *45*, 549–557. [CrossRef]
31. Xie, J.-Y.; Chen, N.-X.; Shen, J.; Teng, L.; Seetharaman, S. Atomistic study on the structure and thermodynamic properties of Cr_7C_3, Mn_7C_3, Fe_7C_3. *Acta Mater.* **2005**, *53*, 2727–2732. [CrossRef]
32. Hernández, I.; Rodríguez, F. Intrinsic and extrinsic photoluminescence in the NH_4MnCl_3 cubic perovskite: A spectroscopic study. *J. Condens. Matter Phys.* **2003**, *15*, 2183. [CrossRef]
33. Qin, Y.; She, P.; Huang, X.; Huang, W.; Zhao, Q. Luminescent manganese (II) complexes: Synthesis, properties and optoelectronic applications. *Coord. Chem. Rev.* **2020**, *416*, 213331. [CrossRef]
34. Berezin, A.S.; Samsonenko, D.G.; Brel, V.K.; Artem'Ev, A.V. "Two-in-one" organic–inorganic hybrid Mn (II) complexes exhibiting dual-emissive phosphorescence. *Dalton Trans.* **2018**, *47*, 7306–7315. [CrossRef] [PubMed]
35. Tao, P.; Liu, S.J.; Wong, W.Y. Phosphorescent manganese (II) complexes and their emerging applications. *Adv. Opt. Mater.* **2020**, *8*, 2000985. [CrossRef]
36. Duan, C.; Delsing, A.; Hintzen, H. Photoluminescence properties of novel red-emitting Mn^{2+}-activated MZnOS (M = Ca, Ba) phosphors. *Chem. Mat.* **2009**, *21*, 1010–1016. [CrossRef]
37. Bortoluzzi, M.; Ferraro, V.; Castro, J. Synthesis and photoluminescence of manganese (II) naphtylphosphonic diamide complexes. *Dalton Trans.* **2021**, *50*, 3132–3136. [CrossRef] [PubMed]
38. Jenkins, H.; McKeag, A.; Ranby, P. Alkaline earth halophosphates and related phosphors. *J. Electrochem. Soc.* **1949**, *96*, 1–12. [CrossRef]
39. Bol, A.A.; Meijerink, A. Luminescence quantum efficiency of nanocrystalline ZnS: Mn^{2+}. 1. Surface passivation and Mn^{2+} concentration. *J. Phys. Chem. B* **2001**, *105*, 10197–10202. [CrossRef]
40. Feldmann, C.; Jüstel, T.; Ronda, C.R.; Schmidt, P.J. Inorganic luminescent materials: 100 years of research and application. *Adv. Funct. Mater.* **2003**, *13*, 511–516. [CrossRef]
41. Blasse, G.; Grabmaier, B.C. *Luminescent Materials*, 1st ed.; Springer: New York, NY, USA, 1994.
42. Singh, V.; Sivaramaiah, G.; Rao, J.; Singh, N.; Srivastava, A.K.; Jirimali, H.; Li, J.; Gao, H.; Kumaran, R.S.; Singh, P.K. Eu^{2+} and Mn^{2+} co-doped $BaMgAl_{10}O_{17}$ blue-and green-emitting phosphor: A luminescence and EPR study. *J. Electron. Mater.* **2016**, *45*, 2776–2783. [CrossRef]
43. Yan, Z.; Li, N.; Wang, L.; Yu, Z.; Li, M.; Zhang, J.; Li, X.; Yang, K.; Gao, G.; Wang, L. Pressure-Induced Two-Color Photoluminescence and Phase Transition of Two-Dimensional Layered $MnCl_2$. *J. Phys. Chem. C* **2020**, *124*, 23317–23323. [CrossRef]
44. Jüstel, T.; Feldmann, C.; Ronda, C.R. Leuchtstoffe für aktive Displays: Neue Konzepte für flache Bildschirme erfordern speziell entwickelte Leuchtstoffe. *Phys. Blätter* **2000**, *56*, 55–58. [CrossRef]
45. Bechtel, H.; Jüstel, T.; Nikol, H.; Ronda, C.; Wiechert, D.; vd Kolk, E.; Dorenbos, P.; van Eijk, C. Optimised Co-activated Willemite Phosphors for Application in Plasma Display Panels. *J. Lumin.* **2000**, *87*, 1246. [CrossRef]

46. Romeiro, F.C.; Marinho, J.Z.; Silva, A.C.A.; Cano, N.F.; Dantas, N.O.; Lima, R.C. Photoluminescence and magnetism in Mn^{2+}-doped ZnO nanostructures grown rapidly by the microwave hydrothermal method. *J. Phys. Chem. C* **2013**, *117*, 26222–26227. [CrossRef]
47. Miyake, Y.; Seo, G.; Matsuhashi, K.; Takada, N.; Kanai, K. Synthesis of carbon nitride oligomer as a precursor of melon with improved fluorescence quantum yield. *Mater. Adv.* **2021**, *2*, 6083–6093. [CrossRef]
48. Putz, H.; Brandenburg, K. *Match!-Phase Analysis Using Powder Diffraction*, version 3.15.x; Crystal Impact: Bonn, Germany, 2023; Volume 102, p. 53227.
49. Rigaku, O.D. *CrysAlisPro Software System*, version 1.171.41.92a; Rigaku Corporation: Oxford, UK, 2018; Volume 1, p. l.
50. Dolomanov, O.V.; Bourhis, L.J.; Gildea, R.J.; Howard, J.A.; Puschmann, H. OLEX2: A complete structure solution, refinement and analysis program. *J. Appl. Crystallogr.* **2009**, *42*, 339–341. [CrossRef]
51. Sheldrick, G.M. SHELXT–Integrated space-group and crystal-structure determination. *Acta Crystallogr. Sect. A Found. Adv.* **2015**, *71*, 3–8. [CrossRef]

$MnCl_2(C_6N_{10}H_6)$: Insights into a Luminescent Transition Metal–Melem Complex

Elaheh Bayat [1], Markus Ströbele [1], David Enseling [2], Thomas Jüstel [2] and Hans-Jürgen Meyer [1,*]

[1] Section for Solid State and Theoretical Inorganic Chemistry, Institute of Inorganic Chemistry, University of Tübingen, Auf der Morgenstelle 18, 72076 Tübingen, Germany

[2] Department of Chemical Engineering, FH Münster University of Applied Sciences, Stegerwaldstraße 39, 48565 Steinfurt, Germany

* Correspondence: juergen.meyer@uni-tuebingen.de

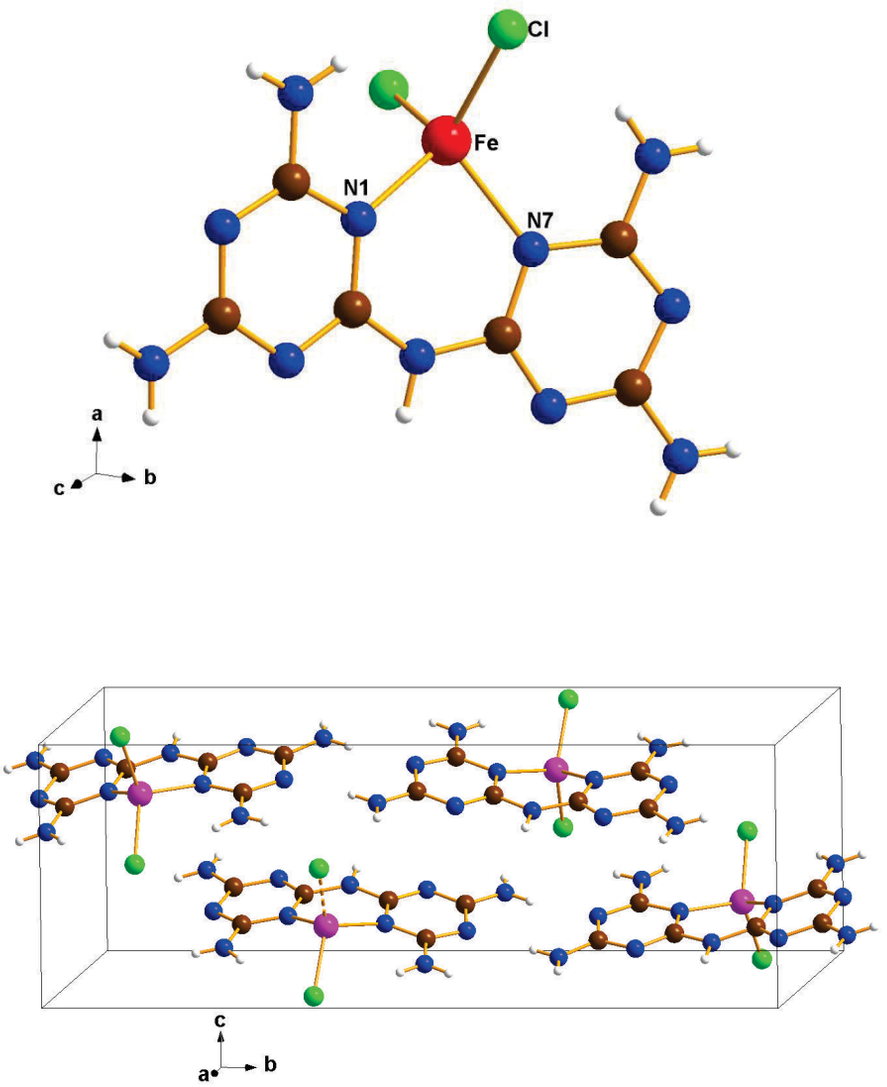

Figure S1. Section of the crystal structure of $FeCl_2(C_6N_{11}H_9)$ projected on *bc*-plane (top) and the unit cell content of the structure (bottom).

Table S1. Crystallographic details of the crystal structure refinement on $FeCl_2(C_6N_{11}H_9)$.

Empirical Formula		**$FeCl_2(C_6N_{11}H_9)$**
CCDC code		2159999
Formula weight (g/mol)		361.99
Wavelength (Å)		1.54184
Crystal system		Monoclinic
Space group		*P* 1 2_1/*c* 1
Unit cell dimensions (Å)	*a*/Å	7.472(6)
	b/Å	22.29(3)
	c/Å	7.693(1)
Volume ($Å^3$)		1261.40(3)
Z		4
Density (calculated) (g/cm^3)		1.906
Absorption coefficient (mm^{-1})		13.613
Final R indices (I>2σ(I)) a)		*R*1 = 0.0208, wR2 = 0.0584
R indices (all data)		*R*1 = 0.0217, wR2 = 0.0589
GOOF		1.083

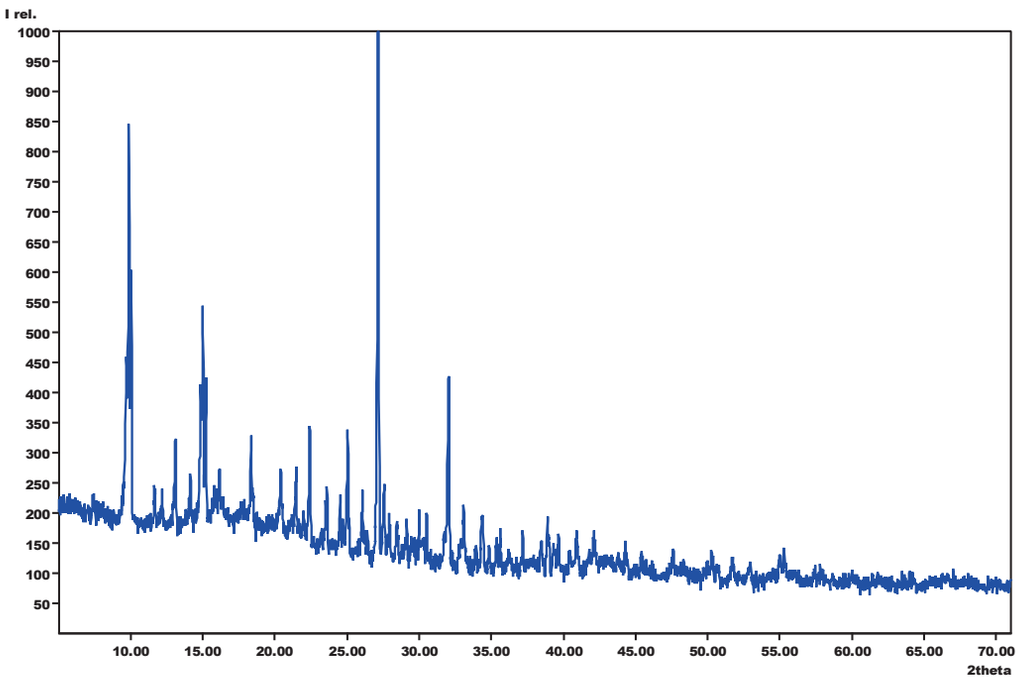

Figure S2. Ex-situ powder XRD pattern of an unknown phase formed by heating a mixture of $MnCl_2$ and melamine in a 1:2 ratio to the first exothermic DSC peak, observed at 306 °C.

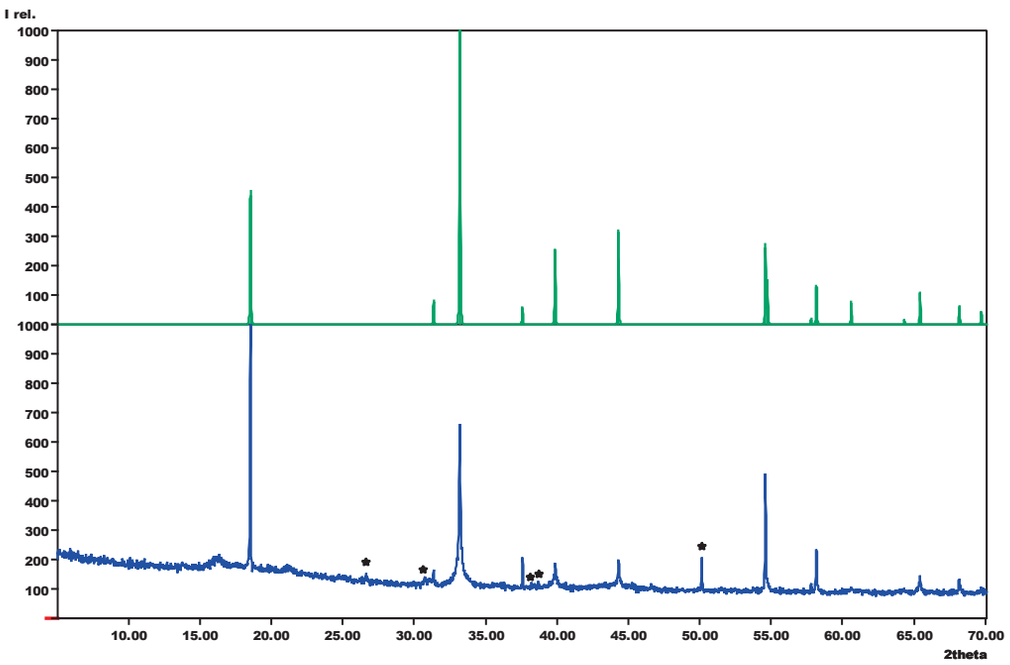

Figure S3. a. XRD pattern of manganese carbodiimide ($MnCN_2$) obtained by heating $MnCl_2(C_6H_6N_{10})$ to 700 °C, along with reflections of unknown side-phase (shown with black stars) compared with the calculated pattern based on the single-crystal structure refinement (top) (CCDC code: 272236). (Please note that the XRD patterns were obtained without annealing the product and only by stopping the decomposition process at 700 ˚C. The high background observed in the patterns can likely be attributed to the fluorescence effect of manganese-containing compounds when using Cu-K_α radiation.)

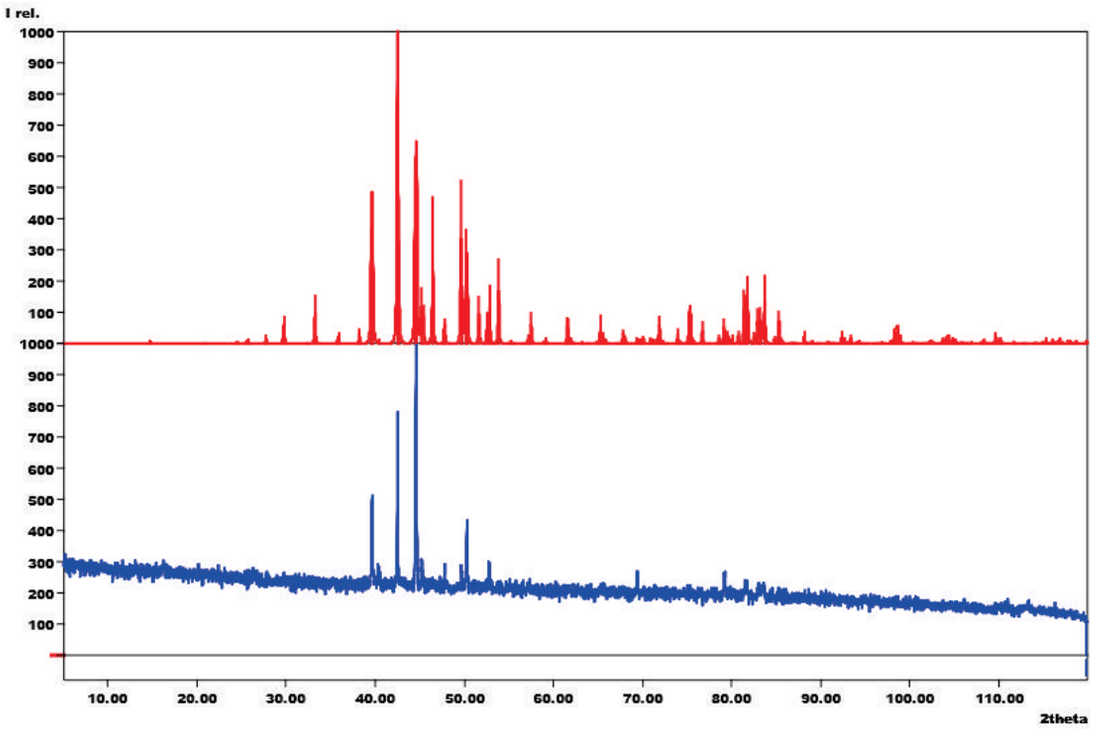

Figure S3.b. XRD pattern of manganese carbide (Mn_7C_3) obtained from heating $MnCl_2(C_6N_{10}H_6)$ to 900 °C (bottom), compared with the calculated pattern based on the single-crystal refinement (top) (CCDC code: 2141509). (Please note that the XRD patterns were obtained without annealing the product and only by stopping the decomposition process at 900 ˚C. The high background observed in the patterns can likely be attributed to the fluorescence effect of manganese-containing compounds when using Cu-K_α radiation.)

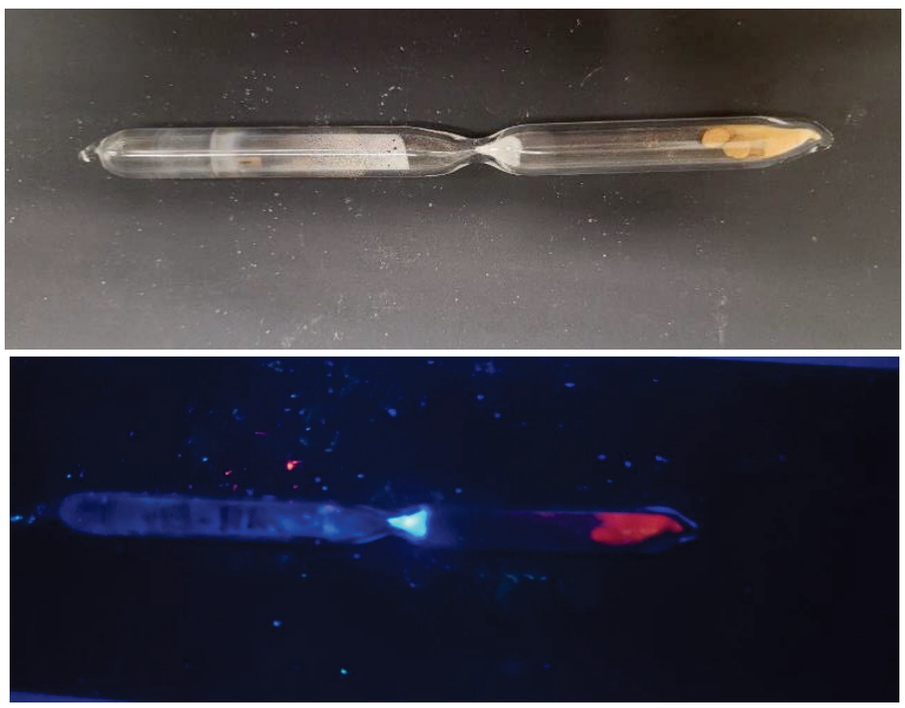

Figure S4a. Photograph of a two-chamber ampule used for separation of side-phase from $MnCl_2(C_6N_{10}H_6)$ under daylight (top) and under UV irradiation (bottom). (The observed blue light observed in the Figure originates from the reflectance of the blue light (366 nm) on the white powder

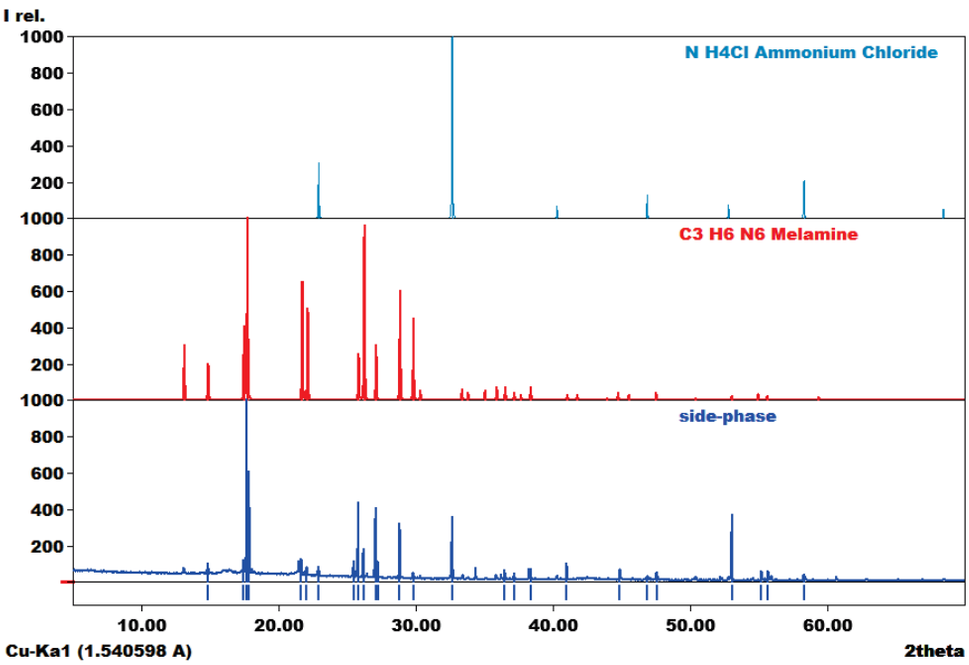

Figure S4b. XRD pattern of side phase on the left side of two-sided chamber.

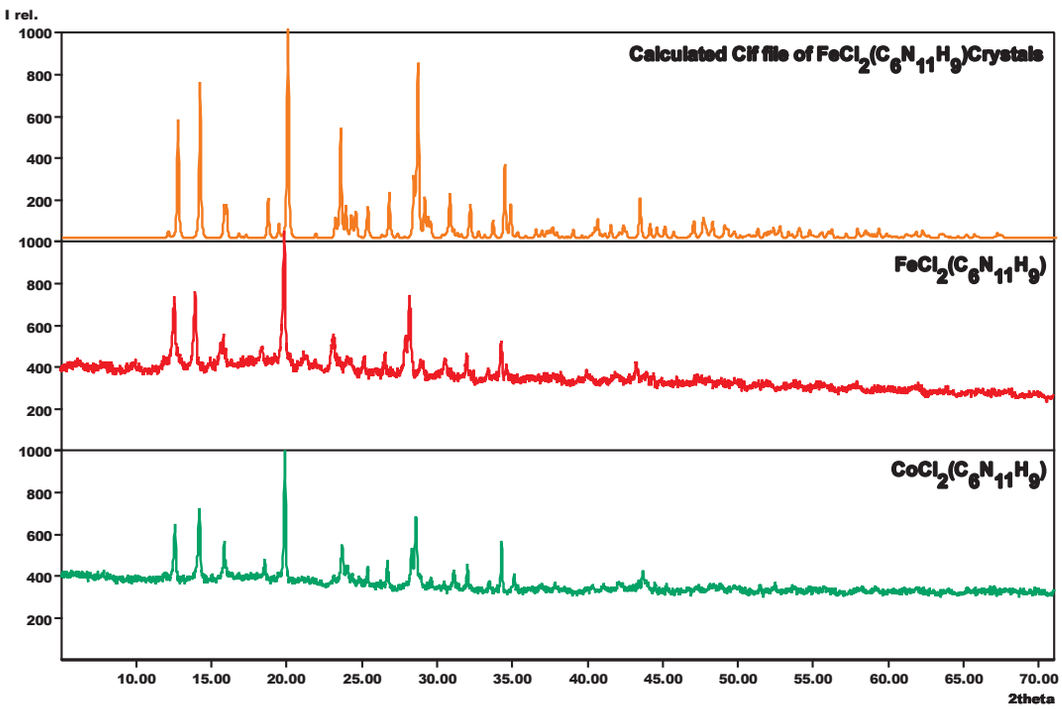

Figure S5. Recorded XRD patterns of $FeCl_2(C_6N_{11}H_9)$, $CoCl_2(C_6N_{11}H_9)$ with the calculated pattern from the structure refinement of $FeCl_2(C_6N_{11}H_9)$ (top).

Table S2. Vibrational frequencies (in cm^{-1}) for $MnCl_2(C_6N_{10}H_6)$ compared to those of melamine and melem.

Vibrational Modes	Melamine	Melem	$MnCl_2(C_6N_{10}H_6)$
Ring-sextant out-of-plane bending	813	804	800
CNC bending	1193	1306	1313
Side-chain CN breathing	1434 1440 1550	1470	1498
NH_2 bending	1652	1612	1610 1689
NH stretching	3128 3334 3421 3469	3119 3325 3424 3487	3323 3431

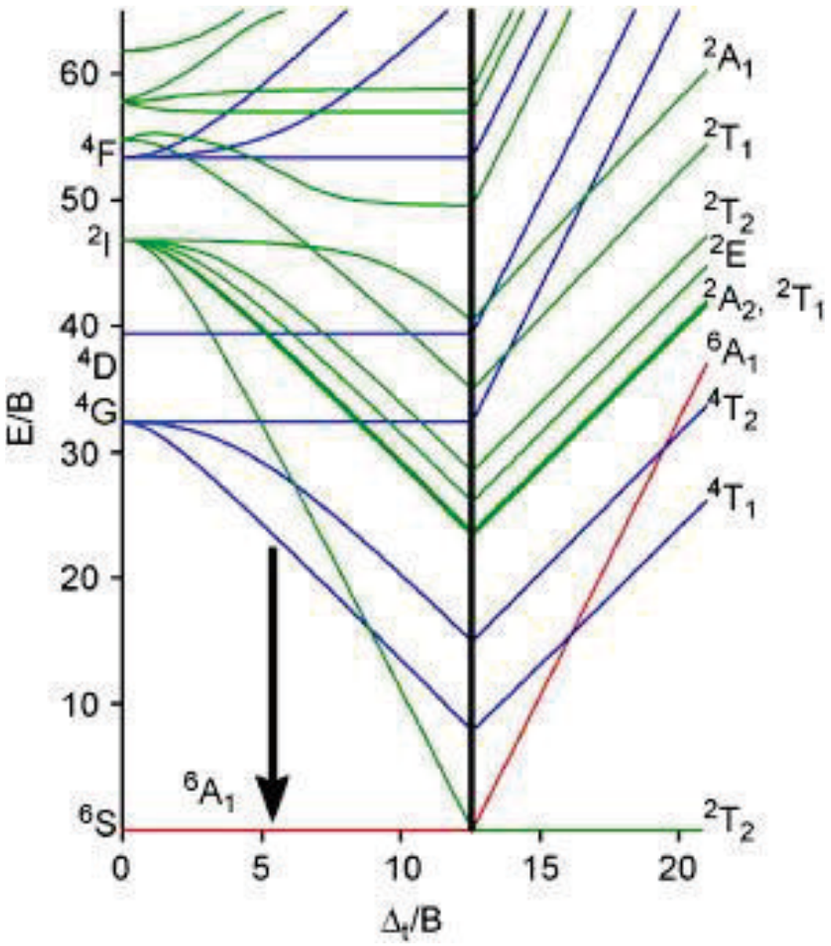

Figure S6. Tanabe-Sugano-Diagram for a d^5 ion with the most prominent emission transition between $^4T_1(^4G)$ and $^6A_1(^6S)$.

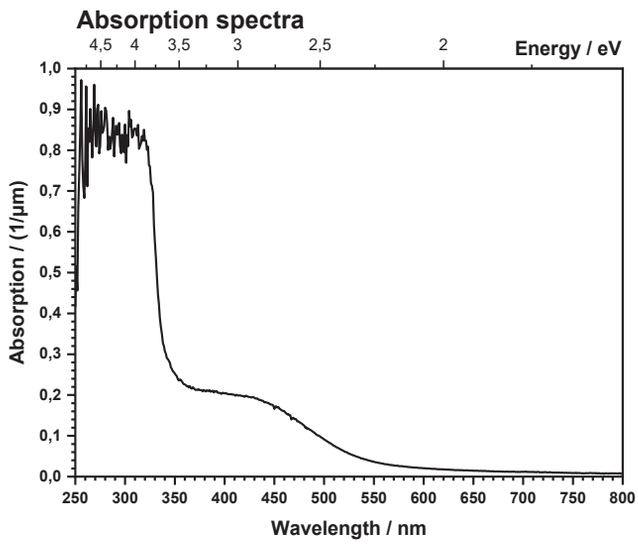

Figure S7. A qualitative absorption spectrum by the aid of the Kubelk-Munk function from the reflection spectrum of $MnCl_2(C_6N_{10}H_6)$.

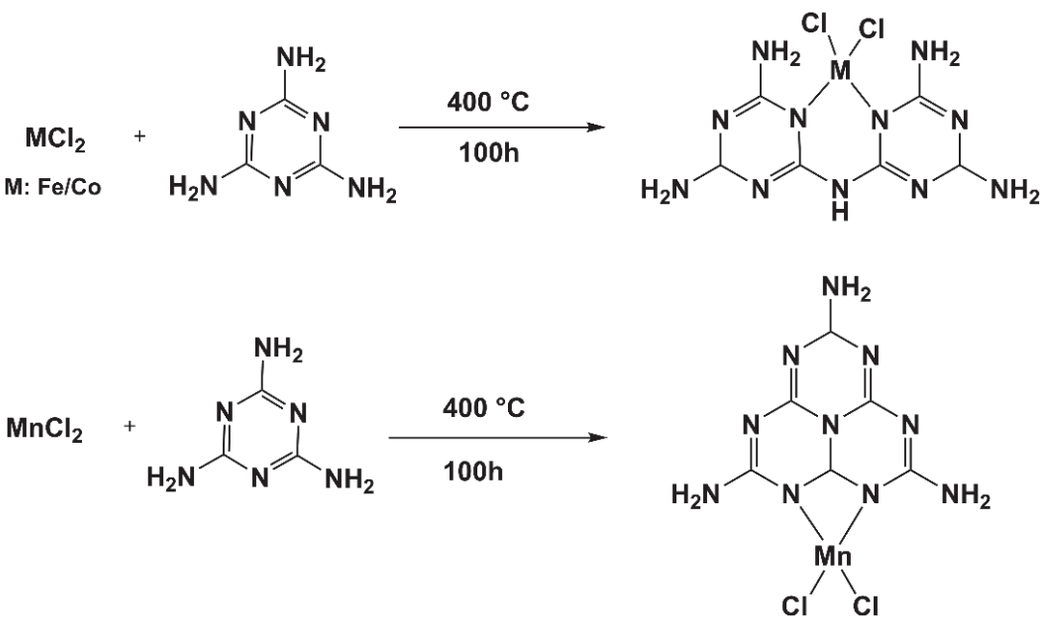

Figure S8. A reaction scheme of melamine with some transition metal chlorides to obtain $FeCl_2(C_6N_{11}H_9)$, $CoCl_2(C_6N_{11}H_9)$, and $MnCl_2(C_6N_{10}H_6)$ compounds

Publication 7

$La_2(CN_2)_3$ – the missing link of rare-earth carbodiimides, prepared through an efficient synthetic route and its Ce^{3+} activated photoluminescence

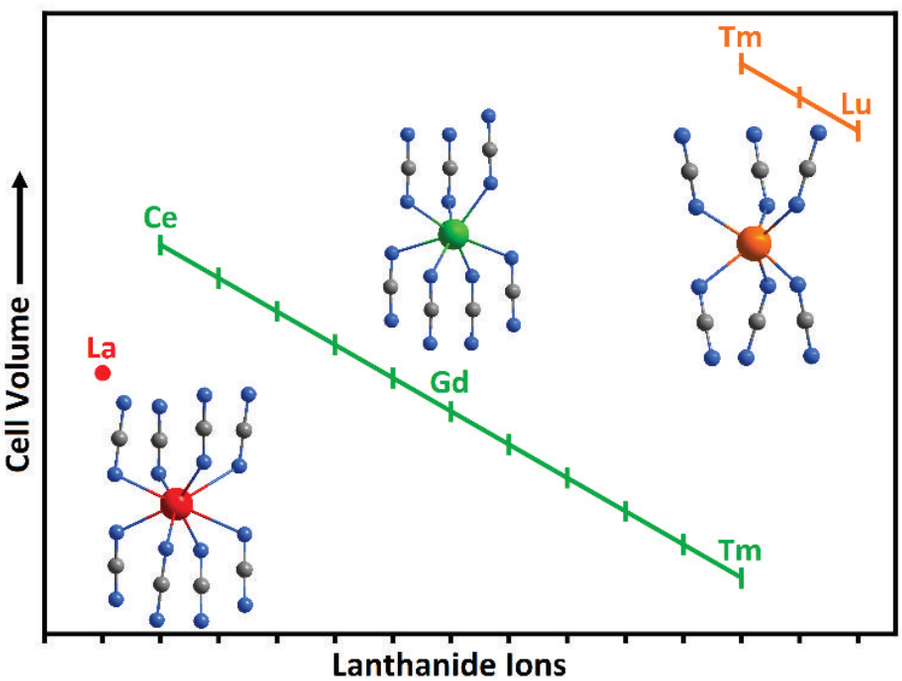

https://doi.org/10.1039/D5DT00060B

Reprinted with permission from

Dalton Trans., 2025, 1477-9226

Dalton Transactions

ROYAL SOCIETY OF CHEMISTRY

PAPER

View Article Online
View Journal | View Issue

Cite this: *Dalton Trans.*, 2025, **54**, 4909

$La_2(CN_2)_3$ – the missing link of rare-earth carbodiimides, prepared through an efficient synthetic route and its Ce^{3+} activated photoluminescence†

Philipp Schneiderhan,[a] Elaheh Bayat,[a] Markus Ströbele,[a] David Enseling,[b] Thomas Jüstel[b] and H.-Jürgen Meyer*[a]

Received 9th January 2025,
Accepted 14th February 2025

DOI: 10.1039/d5dt00060b

rsc.li/dalton

Rare-earth (RE) carbodiimides according to the composition $RE_2(CN_2)_3$ have been reported for the whole series of RE elements, all prepared by solid-state metathesis (SSM) reactions. Only one compound, $La_2(CN_2)_3$, could not be made by this way of synthesis. Herein, we report the preparation of $La_2(CN_2)_3$ by using lanthanum cyanurate as a single-source precursor. The conversion of the precursor is analyzed by thermoanalytical studies. The crystal structure of the precursor and the novel $La_2(CN_2)_3$ are characterized by X-ray diffraction techniques. $La_2(CN_2)_3$ is represented by a distinct crystal structure with a dodecahedral environment of the La^{3+} ion. Having the knowledge of the last missing rare-earth carbodiimide, we herein present a summary of all existing $RE_2(CN_2)_3$ compounds, including their structural relationships. Doping with Ce^{3+} leads to the $La_2(CN_2)_3{:}Ce^{3+}$ phosphor, which is reported with its photoluminescence properties.

Introduction

Metal dinitridocarbonates, commonly denoted as metal cyanamides ($N{\equiv}C{-}N^{2-}$) and metal carbodiimides ($^{-}N{=}C{=}N^{-}$), have been reported by different ways of synthesis. The first method for synthesizing a carbodiimide involves reacting calcium carbide (CaC_2) with nitrogen gas (N_2) at elevated temperatures, approximately 1000 °C, in a process known as the Frank-Caro method.[1]

Following the discovery of calcium carbodiimide, numerous metal carbodiimide or metal cyanamide compounds were developed. An early synthetic approach to lithium carbodiimide ($Li_2(CN_2)$) was achieved in the 1970s by heating Li_3N and Li_2C_2 together at about 600 °C.[2] Another proposed method for the synthesis of $Li_2(CN_2)$ is ammonolysis, which involves the reaction of lithium carbonates (Li_2CO_3) with ammonia (NH_3).[3] Alternatively, lithium carbodiimide ($Li_2(CN_2)$) can be synthesized using lithium nitride (Li_3N)[4] (eqn (1)) or hydride (LiH)[5] and melamine. For synthesizing other alkali metal carbodiimides such as sodium[6] and potassium[7] carbodiimides an alternative route was employed. Alkaline-earth metal carbodiimides such as $Mg(CN_2)$, $Sr(CN_2)$, and $Ba(CN_2)$ can be produced similarly utilizing the reaction of alkaline-earth metal nitrides with melamine at temperatures ranging from 740 to 850 °C.[8]

One of the most effective approaches for synthesizing many other metal carbodiimides is the solid-state metathesis (SSM), which allows for the production of relatively pure carbodiimides under moderate heating conditions, typically at 450–600 °C.[9,10] Within this process, a metal halide (MX_2 or MX_3) is converted with lithium carbodiimide in a salt-balanced reaction (eqn (2)) to yield a metal carbodiimide.

$$2Li_3N + C_3H_6N_6 \rightarrow 3Li_2(CN_2) + 2NH_3 \quad (1)$$

$$2MX_3 + 3Li_2(CN_2) \rightarrow M_2(CN_2)_3 + 6LiX \quad (2)$$

To produce calcium carbodiimide of high purity, another synthetic route was developed as shown in eqn (3). This methodology was first proposed by Seifer[11] and then further refined in 2023.[12] The study done by Seifer suggests briefly the preparation of lead, barium, and strontium carbodiimide in addition to calcium carbodiimide. These carbodiimides are prepared by the reaction of cyanuric acid with metal chlorides in the presence of sodium hydroxide in water to produce the corresponding cyanurate salts which are subsequently pyrolyzed to give the desired carbodiimides. This synthetic route shows the promising route of using triazine-derived precur-

[a]*Section for Solid State and Theoretical Inorganic Chemistry, Institute of Inorganic Chemistry, University of Tübingen, Auf der Morgenstelle 18, 72076 Tübingen, Germany. E-mail: juergen.meyer@uni-tuebingen.de*
[b]*FH Münster, University of Applied Science, Stegerwaldstraße 39, 48565 Steinfurt, Germany*

† Electronic supplementary information (ESI) available. CCDC 2403637, 2409323 and 2393819. For ESI and crystallographic data in CIF or other electronic format see DOI: **https://doi.org/10.1039/d5dt00060b**

sors, for example, melamine,[5,13] and derivatives of cyanuric acid in the production of carbodiimides.

$$Ca(HO_3C_3N_3) \rightarrow Ca(CN_2) + HOCN + CO_2 \uparrow \quad (3)$$

It is noteworthy to mention that some transition metal carbodiimides were also synthesized using aqueous solution-based methods for instance, $Zn(CN_2)$,[14] $Co(CN_2)$,[15] $Ni(CN_2)$,[15] $Cu(CN_2)$,[16] $Cd(CN_2)$,[17] $Ag_2(CN_2)$,[18] $Hg(CN_2)$.[19] Other transition metal carbodiimides, such as $Mn(CN_2)$,[20] $Cr_2(CN_2)_3$,[21] $Zr(CN_2)_2$,[22] and $Hf(CN_2)_2$,[22] can be synthesized using the similar solid-state metathesis (SSM) reactions between a metal halide with $Li_2(CN_2)$ or $Zn(CN_2)$.[14] p-Block metal carbodiimides, like $Pb(CN_2)$,[23] $Bi_2(CN_2)_3$,[24] $Tl_2(CN_2)$,[25] and $In_{2.24}(CN_2)_3$,[13,26] are synthesized by reacting metal salts with cyanamide or cyanide compounds. For tin carbodiimides, the conventional SSM reaction of $Li_2(CN_2)$ with metal halides such as $SnCl_2$ or SnF_2, yields $Sn(CN_2)$ and $Sn_4Cl_2(CN_2)_3$.[3,27]

SSM reactions have been extensively utilized by our research group to synthesize rare-earth (RE) carbodiimides, essentially by reacting lithium carbodiimide with a rare-earth metal chloride.[28,29] Most prominent is the series of $RE_2(CN_2)_3$ compounds that have been reported for RE elements from Sc to Lu, except for RE = La (and the radioactive element Pm).[28–30] Lanthanum carbodiimide was first reported 76 years ago from reactions of La_2O_3 with HCN.[31] However, the products were poorly characterized, with no structural or spectroscopic data available.[31] It is worth mentioning that compounds of smaller rare-earth ions like RE = Sc,[32] Tm, Yb, and Lu[28,33] crystallize with the trigonal rhombohedral space group $R\bar{3}c$ (Z = 6), and the coordination number (CN) six of the RE^{3+} ion.[28] Corresponding compounds with RE = Y and Ce–Er (except Pm) crystallize monoclinically with the space group $C2/m$ (Z = 2) and the CN of the RE^{3+} being seven.[28,33,34] $Tm_2(CN_2)_3$ has been shown to undergo a pressure transformation from $R\bar{3}c$ into $C2/m$ with a significant volume reduction.[28]

Through this route, not only pseudobinary but also pseudoternary, rare-earth (RE) compounds have been synthesized. These compounds cover a wide range of mixed cation and mixed anion carbodiimides such as $RE_2O_2(CN_2)$ (RE = Ce, Pr, Nd, Sm, Eu, Gd, Dy–Yb),[35,36] $RECl(CN_2)$ (RE = La–Pr),[37] $Sc_2O(CN_2)$,[32] $RE_2Cl(CN_2)N$ (RE = La, Ce),[38] $RE_2Br(CN_2)N$ (RE = La, Pr),[39] $REI(CN_2)N$ (RE = La, Gd),[40] and $Eu_2I_2(CN_2)$,[41] $Eu_4F_5(CN_2)_2$.[42] Furthermore, some pseudoquaternary NCN rare-earth (RE) compounds containing three different cations have been also developed by adding the third reactant to the conventional SSM reactions. Examples of these compounds are rare-earth carbidonitridosilicates,[34,43,44] and tetracyanamidogermanates.[45,46] For lanthanum, mixed anion compounds $La_2O_2(CN_2)$,[47] $La_2S_2(CN_2)$,[48] $La_2O(CN_2)_2$,[37] $La_3(CN_2)_3N$[49] or $LaCl(CN_2)$[50] have been so far reported.

The photoluminescence properties of lanthanide (Ln) doped $RE_2(CN_2)_3$[29] such as $Gd_2(CN_2)_3$:Ce or Tb, Ce, and Tb[29] have been thoroughly studied, leading to the development of a pc-LED prototype-based on $Y_2(CN_2)_3$:Ce.[51] In Ce^{3+} doped materials luminescence usually occurs due to electronic transition from ground state levels of ($^2F_{5/2}$ and $^2F_{7/2}$) of the [Xe]4f^1 configuration to lowest crystal-field components of the [Xe]5d^1. By tuning the crystal-field strength and covalent character of Ce^{3+}, the material's luminescence properties can be adjusted.[29]

Herein we explore the preparation of lanthanum carbodiimides through this efficient way of synthesis. We describe the formation and structural characterization of intermediate lanthanum cyanurates obtained from aqueous solution and the thermal conversion into the novel $La_2(CN_2)_3$. The $La_2(CN_2)_3$ represents the missing compound among the series of $RE_2(CN_2)_3$ compounds with a new crystal structure. The dodecahedral coordination of the lanthanum ion in $La_2(CN_2)_3$ parallels the coordination pattern of yttrium in the structure of yttrium aluminum garnet (YAG), which resembles the host structure for the most prominent YAG:Ce phosphor in today's phosphor converted light-emitting diodes (pc-LED).

Results and discussion

Preparation

Rare-earth carbodiimides were successfully prepared by means of solid-state metathesis reaction (see eqn (2)). However, this way of synthesis has been unsuccessful for $La_2(CN_2)_3$, because all reactions have led to the formation of $LaCl(CN_2)$.[37]

Herein, we report the preparation of $La_2(CN_2)_3$ *via* a precursor route. The compound was synthesized through the thermal decomposition of a lanthanum cyanurate precursor. This precursor was obtained by reacting lanthanum chloride with cyanuric acid and sodium hydroxide in an aqueous solution, yielding an insoluble precipitate eqn (4).

$$LaCl_3 + 2H_3C_3N_3O_3 + 3NaOH \rightarrow La(H_2O_3C_3N_3)(HO_3C_3N_3)(H_2O)_3 \downarrow + 3NaCl \quad (4)$$

It is noteworthy that two distinct phases of lanthanum cyanurates were obtained as insoluble precipitates. We found out that the formation of these two phases was dependent on the pH of the solution which can be controlled by varying the amount of water content. Lower amounts of water and thus higher pH values led to the formation of a lanthanum cyanurate composed of a single deprotonated and a double deprotonated cyanurate ($La(HC_3N_3O_3)(H_2C_3N_3O_3)(H_2O)_3$). In contrast, higher amounts of water and thus lower pH values led to the formation of a lanthanum cyanurate with two single deprotonated cyanurates along with a hydroxide ion ($La(H_2C_3N_3O_3)_2(OH)(H_2O)_4{\cdot}H_2O$). These results can be explained by the pK_a values of the first two deprotonation steps of cyanuric acid (pK_{a1} = 6.88 and pK_{a2} = 11.40).[52] Only at higher pH values, the solution becomes sufficiently basic to allow the second deprotonation of the cyanuric acid and thus the formation of the lanthanum cyanurate, whereby the cyanuric acid unit is present in its double deprotonated form. However, thermoanalytical studies in the next section, will demonstrate that both lanthanum cyanurate phases could be converted to

lanthanum carbodiimide at 770 °C under a flow of argon. The lanthanum carbodiimide demonstrated air and water stability over a period of four weeks, as confirmed by X-ray powder diffraction.

Thermoanalytic studies

The thermal decomposition of lanthanum cyanurates was investigated using thermal analysis methods such as thermogravimetric analysis (TGA) combined with differential thermal analysis (DTA). The measurements were made in an argon flow within a temperature range from room temperature up to 770 °C at a rate of 2 K min^{-1} for both heating and cooling. Fig. 1 represents the TGA of $La(HC_3N_3O_3)(H_2C_3N_3O_3)(H_2O)_3$ which shows that this material undergoes a decomposition in three steps, ultimately leading to the formation of lanthanum carbodiimide. Based on the measured and theoretical mass losses at each stage, the first step at 187 °C, with a mass loss of −12.04% (theory: −12.15%), is attributed to the loss of water (eqn (5)). The second step at 405 °C, with a mass loss of −28.38% (theoretical: −29.03%), can be corresponded to the decomposition of $La(HC_3N_3O_3)(H_2C_3N_3O_3)$ to $La(C_3N_3O_3)$ which is a completely deprotonated unit (eqn (6)). The final step, occurring at 737 °C with a mass loss of −14.82% (theory: −14.85%), is associated with the release of carbon dioxide, resulting in the formation of lanthanum carbodiimide, $La_2(CN_2)_3$ (eqn (7)). Heating the lanthanum carbodiimide to even higher temperatures (1000 °C), resulted in the formation of lanthanum nitride (LaN). This sequence can be summarized in the following reactions:

$$2La(HC_3N_3O_3)(H_2C_3N_3O_3)(H_2O)_3 \rightarrow 2La(HC_3N_3O_3)(H_2C_3N_3O_3) + 6H_2O\uparrow \quad (5)$$

$$2La(HC_3N_3O_3)(H_2C_3N_3O_3) \rightarrow 2La(C_3N_3O_3) + 2H_3C_3N_3O_3\uparrow \quad (6)$$

$$2La(C_3N_3O_3) \rightarrow La_2(CN_2)_3 + 3CO_2\uparrow \quad (7)$$

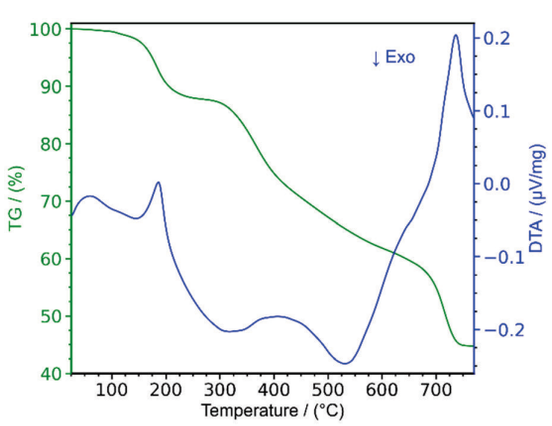

Fig. 1 Thermogravimetric analysis (TGA) combined with differential thermal analysis (DTA) of $La(HC_3N_3O_3)(H_2C_3N_3O_3)(H_2O)_3$.

Crystal structures

The synthesis of $La_2(CN_2)_3$ can be achieved by the decomposition of a single source precursor, which can be either $La(HC_3N_3O_3)(H_2C_3N_3O_3)(H_2O)_3$ **(1)** or $La(H_2C_3N_3O_3)_2(OH)(H_2O)_4{\cdot}H_2O$ **(2)**. Crystal structures of both precursors were refined based on single-crystal X-ray diffraction, with relevant data summarized in Table 1. Both compounds contain one type of La^{3+} in the structure. The first compound **(1)** contains mono- and divalent cyanurate anions and three water molecules in the coordination environment of the La^{3+}, the latter **(2)** monovalent cyanurate anions, bridging hydroxide and four water molecules as shown in Fig. 2 and 3. There are at least two more lanthanum cyanurate structures being reported in the literature. The crystal structure of $La[H_2N_3C_3O_3]_3{\cdot}8.5\ H_2O$ [53] was refined with the space group *P*1, containing monovalent cyanurate anions. Another structure, described as $La(H_2C_3N_3O_3)_2{\cdot}OH{\cdot}2H_2O$,[54] leaves a precise assignment of hydrogen atoms behind.

The appearance of a number of different lanthanum cyanurate compounds emphasizes the influence of pH conditions during precipitation in aqueous solution and by a varying extent of hydration. However, so far there is no indication that the decomposition of any of these precursors would not lead to $La_2(CN_2)_3$.

The crystal structure of $La(HC_3N_3O_3)(H_2C_3N_3O_3)(H_2O)_3$ **(1)** is characterized by one type of lanthanum, being surrounded by three coordinated water molecules and five cyanurate ions showing a bridging functionality (Fig. 2).

The crystal structure of $La_2(CN_2)_3$ was solved and refined on the basis of X-ray powder diffraction data by Rietveld refine-

Table 1 Crystallographic data of cyanurate precursor compounds $La(HC_3N_3O_3)(H_2C_3N_3O_3)(H_2O)_3$ **(1)**, $La(H_2C_3N_3O_3)_2(OH)(H_2O)_4{\cdot}H_2O$ **(2)** and of $La_2(CN_2)_3$

	(1)	(2)	$La_2(CN_2)_3$
CCDC code	2403637	2409323	2393819
Empirical formula	$C_6H_9LaN_6O_9$	$C_6H_{15}LaN_6O_{12}$	$C_3La_2N_6$
Formula weight (g mol^{-1})	448.10	502.15	397.88
Crystal system	Monoclinic	Triclinic	Monoclinic
Space group	$P2_1/c$	$P\bar{1}$	$I2/a$
a/Å	8.0793(4)	6.3215(3)	8.69003(6)
b/Å	17.1808(7)	11.0993(6)	6.88968(5)
c/Å	8.5107(4)	11.8544(5)	10.30517(9)
α/°		66.312(5)	
β/°	99.223(5)	88.178(3)	105.0711(6)
γ/°		75.768(4)	
V/Å^3	1166.09(9)	736.20(7)	595.764(8)
Z	4	2	4
μ/mm^{-1}	29.027	23.237	108.706
D_c/g cm^{-3}	2.552	2.265	4.436
Crystal size	0.05 × 0.03 × 0.01	0.04 × 0.04 × 0.01	Powder
Θ range/°	5.149 to 74.464	4.084 to 72.102	2.5 to 60
Reflections collected	41 457	22 199	488
Parameters	235	251	45
R_{Bragg}	—	—	4.0955
χ^2	—	—	1.0244
Wavelength (Cu-K_α) (Å)	1.54184	1.54184	1.54184
R_1, wR_2 ($I > 2\sigma(I)$)	0.0162, 0.0385	0.0333, 0.0837	—
R indices (all data)	0.0175, 0.0389	0.0360, 0.0854	—
GOOF	1.041	1.076	1.012

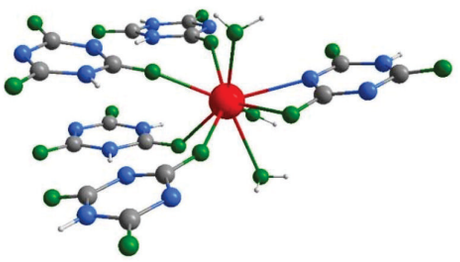

Fig. 2 Coordination environment of the La^{3+} in the structure of La $(HC_3N_3O_3)(H_2C_3N_3O_3)(H_2O)_3$ **(1)** (gray: C, blue: N, green: O, red: La, white: H).

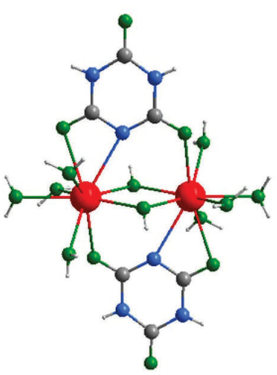

Fig. 3 Coordination environment of the La^{3+} ion in the structure of La $(H_2C_3N_3O_3)_2(OH)(H_2O)_4{\cdot}H_2O$ **(2)** (gray: C, blue: N, green: O, red: La, white: H).

ment with the space group *I*2/*a* (Table 1 and Fig. 4). Crystal structures of RE carbodiimides follow a characteristic structure pattern in which the $[N{=}C{=}N]^{2-}$ ions are arranged in layers, following the motif of a hexagonal closed packing of sticks. Cations are situated in between these layers to form an alternating arrangement.

This pattern is apparent also in the structure of $La_2(CN_2)_3$, displayed in Fig. 5. Major differences among the structures of $RE_2(CN_2)_3$ compounds are the tilting of N=C=N ions within layers relative to each other, and the exact position of RE ions in structures. The crystal structure of $La_2(CN_2)_3$ contains one type of lanthanum in the structure and two distinct carbodiimides ions. Lanthanum ions in the structure have the coordination number eight, shown in Fig. 6, together with the pattern of the corresponding dodecahedron.

The characterization of $La_2(CN_2)_3$ completes the series of binary rare-earth carbodiimides, which is represented by three distinct structures, respectively, coordination patterns (Fig. 7), with their unit volumes displayed in Fig. 8. The general trend of molar unit cell volumes represents the lanthanide contraction for the series from Ce to Tm with the space group *C*2/*m* (*Z* = 2) with the coordination number (CN) of the RE^{3+} being seven. Compounds of Tm, Yb, and Lu follow the same trend,

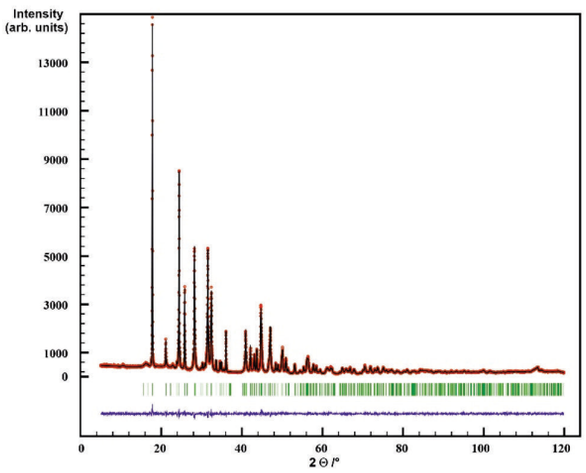

Fig. 4 Rietveld refinement of the XRD powder pattern of $La_2(CN_2)_3$. Observed intensities are marked as red circles, and calculated intensities as black lines. Bragg positions are marked as green lines, the difference curve $I_{observed} - I_{calculated}$ as blue line.

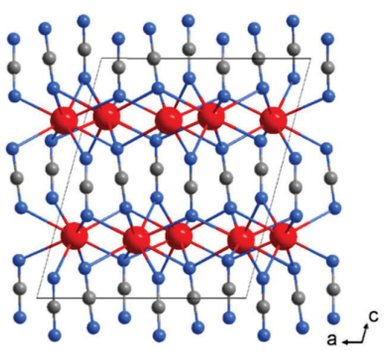

Fig. 5 The layered appearance of the crystal structure of $La_2(CN_2)_3$ with lanthanum ions is shown in red.

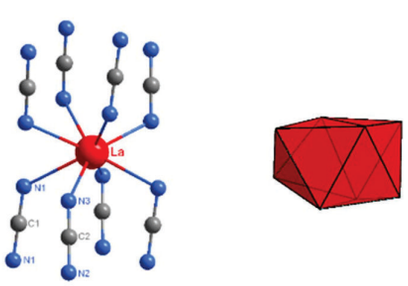

Fig. 6 The environment of lanthanum with two crystallographically distinct $[N{=}C{=}N]^{2-}$ ions (distances: C1–N1 = 124.41(6) pm, ∠N1–C1–N1 = 177.82(4)°; C2–N2 = 123.95(9) pm, C2–N3 = 124.17(9) pm, ∠N2–C2–N3 = 178.55(7)°) and a dodecahedron representing the coordination environment of La^{3+} in the structure of $La_2(CN_2)_3$.

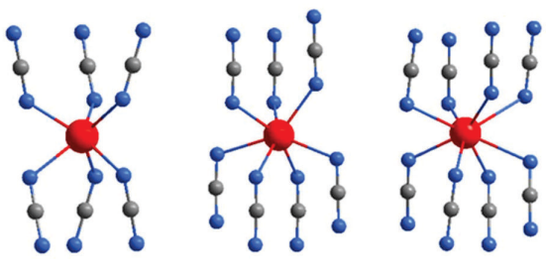

Fig. 7 Coordination environments of rare-earth ions (red) in the trigonal ($R\bar{3}c$), monoclinic ($C2/m$), and ($I2/a$) structures, from left to right.

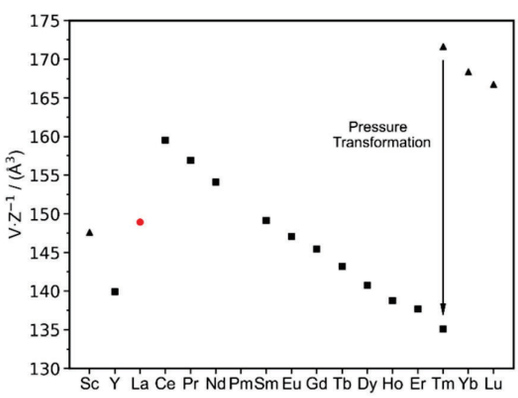

Fig. 8 Molar volume (V/Z) of rare-earth carbodiimides, $RE_2(CN_2)_3$, with the monoclinic ($C2/m$) structure for the series RE = Y, and Ce–Tm (displayed as squares), the trigonal ($R\bar{3}c$) structure for RE = Sc (displayed as triangles) and Tm–Lu, and monoclinic ($I2/a$) $La_2(CN_2)_3$ (displayed as a red dot). $Tm_2(CN_2)_3$ has been shown to be dimorphic with the monoclinic ($C2/m$) structure and the trigonal ($R\bar{3}c$) structure of the high-pressure phase.

however with a trigonal structure with the CN of the RE being six. $Tm_2(CN_2)_3$ is dimorphic and undergoes a pressure transformation from $R\bar{3}c$ into $C2/m$. Thereby, the coordination number of the Tm^{3+} ion increases from six to seven. Lanthanum, as the largest lanthanide ion, appears with the coordination number eight.

The lanthanum site with its dodecahedral environment in $La_2(CN_2)_3$ appears to be an interesting site for doping with a photoluminescence activator. A most prominent example of such a dodecahedral environment is apparent in the pc-LED phosphor $Y_3Al_5O_{12}$:Ce. Consequently, we conducted photoluminescence studies on $La_2(CN_2)_3$:Ce, discussed later in this work.

Infrared spectroscopy

The infrared (IR) spectrum of $La_2(CN_2)_3$ has also been reported to support its carbodiimide character (see Fig. 6 for distances and angles). As can be observed in Fig. 9 the characteristic vibrational bands of the $[NCN]^{2-}$ ion at 2029 and 1929 cm^{-1} can be ascribed to the asymmetric stretching vibrations (ν_{as}).

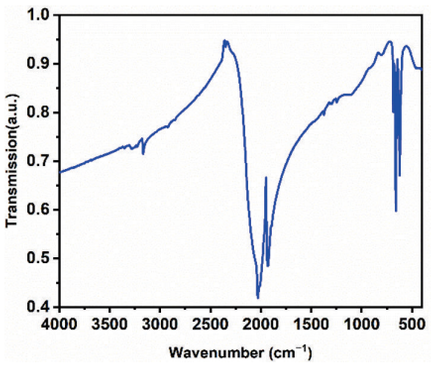

Fig. 9 FT-IR spectrum of $La_2(CN_2)_3$.

Furthermore, the corresponding bending vibrations (δ) are observed at 685, 660, and 621 cm^{-1}. The absence of a symmetric vibration (ν_s) in the IR spectrum supports the identification of the compound as a carbodiimide rather than a cyanamide.[37] Furthermore, the results align well with previously reported data on Table 2 for two other rare-earth metal carbodiimide modifications.[55]

Photoluminescence spectroscopy

The photoluminescence (PL) spectrum of $La_2(CN_2)_3$ doped with Ce^{3+} (5 atom% w.r.t La) has been studied to evaluate the potential of this novel material for application in a luminescent screen. Ce^{3+} is already well-known as an efficient emitter in various applications of luminescent materials.[56–59] For instance, Ce^{3+} is one of the most important emitters in LED phosphors, such as $Ln_3(Al,Ga,Sc)_5O_{12}$:Ce (Ln = Y, Gd, Tb, Lu), or acts as a primary activator ion in scintillators, including Lu_2SiO_5:Ce, $LuAlO_3$:Ce, and $Lu_3Al_5O_{12}$:Ce (LuAG:Ce^{3+}) (see Table 3). Ce^{3+}-activated materials also play an important role

Table 2 Vibrational frequencies (cm^{-1}) from lanthanum and selected rare-earth carbodiimides[55]

	ν_{as} $(CN_2)^{2-}$			δ $(CN_2)^{2-}$		
$Lu_2(CN_2)_3$	2080	2009	—	680	640	—
$Sm_2(CN_2)_3$	2023	1955	705	668	634	616
$La_2(CN_2)_3$	2029	1929	685	660	621	—

Table 3 Emission maxima, density, and decay time of some Ce^{3+} activated phosphors and scintillators[61,62]

Ce^{3+} phosphor or scintillator	Emission max. nm	Density g cm^{-3}	Decay time ns
$LaBr_3$:Ce	358	5.3	35
$YAlO_3$:Ce	360	5.6	20–30
$LuAlO_3$:Ce	365	8.3	18
Lu_2SiO_5:Ce	390	7.4	30
Gd_2SiO_5:Ce	420	6.7	60
$Lu_3Al_5O_{12}$:Ce	525	6.7	54

in UV lamps, such as YPO_4:Ce, $LaPO_4$:Ce, $LaMgAl_{11}O_{19}$:Ce, and $YMgB_5O_{10}$:Ce.[60]

The photoluminescence of materials doped with Ce^{3+} ions originates from interconfigurational transitions, *i.e.* of transitions between different electronic configurations. In the ground state, Ce^{3+} has the configuration $[Xe]4f^1$ which, upon excitation is promoted to the configuration $[Xe]5d^1$. The energy required for this transition depends on the crystal field splitting of the 5d levels, which is influenced by the surrounding coordinated anions and centroid shift caused by the local environment. The emission process caused by the relaxation of the $5d^1$ to the $4f^1$ configuration yields two broad emission bands due to the ground state term spin-orbit splitting yielding the terms $^2F_{5/2}$ and $^2F_{7/2}$. This kind of transition is spin and parity allowed, therefore, resulting in a high oscillator strength and a short decay constant. Since a 5d orbital is involved, cerium-activated materials may show UV, blue, green, or yellow emission depending on the crystal-field-determined energetic position of absorption and emission bands. The 5d orbitals are more spatially extended and thus strongly interact with the crystal field around the atom, therefore, splitting into different levels.

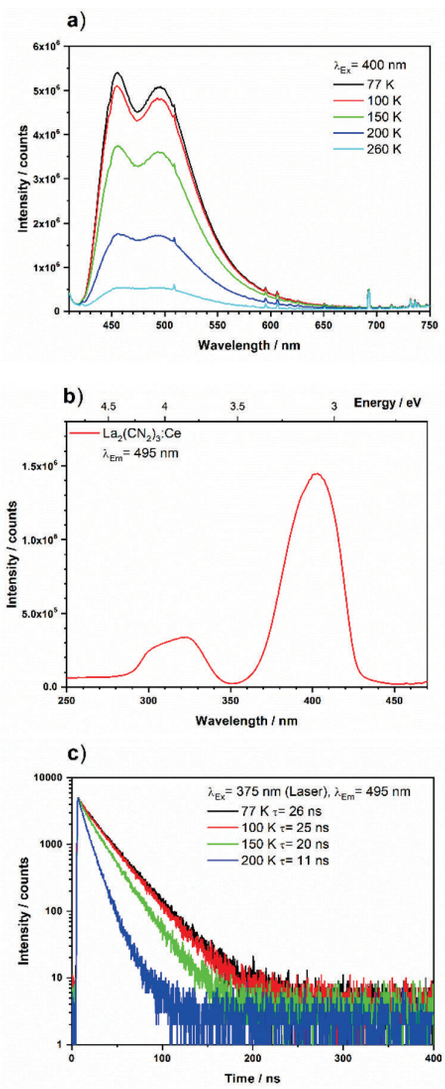

Fig. 10 (a) Emission spectra at several temperatures and (b) excitation spectra, and (c) decay curve upon 375 nm excitation of $La_2(CN_2)_3$:Ce^{3+}(5%).

Fig. 10a shows the broad emission band of $La_2(CN_2)_3$ doped with 5% of Ce^{3+}, with two maxima at 450 nm (2222 cm^{-1}) and 500 nm (20 000 cm^{-1}) upon 400 nm excitation, at various temperatures. The excitation spectrum monitored for 495 nm is also shown in Fig. 10b and exhibits a strong excitation band at 400 nm (25 000 cm^{-1}), thus the Stokes shift is just 2800 cm^{-1}, which points to little relaxation in the excited state. As mentioned above, the crystal field strength and thus chemical environment such as ligand type, symmetry, and metal-to-ligand distance determines the energy gap between the $[Xe]4f^1$ and $[Xe]5d^1$ configuration. Therefore, the PL spectra will change if Ce^{3+} is located onto different crystallographic sites. A weaker crystal field increases the energy gap and results in a shift of the PL spectra towards higher energy such as UV or blue light. A comparison with the earlier published $Gd_2(CN_2)_3$:Ce^{3+} with a broad emission band at 575 nm (17 391 cm^{-1}) under 415 nm excitation,[29] and $Y_2(CN_2)_3$:Ce^{3+} [51] with a emission band range of 570–577 nm under 415 nm excitation, confirms that the emission bands in $La_2(CN_2)_3$:Ce^{3+} are strongly blue-shifted. This can be explained by the weaker crystal field in $La_2(CN_2)_3$ than $Gd_2(CN_2)_3$, and $Y_2(CN_2)_3$ due to the larger metal-to-ligand distances onto the La^{3+} site. The material shows at low temperature a single exponential decay curve, while the calculated decay time of 26 ns at 77 K (Fig. 10c) is typical for blue-emitting Ce^{3+} activated luminescent materials or scintillators.

Conclusions

The vast majority of rare-earth carbodiimide compounds have been prepared by solid-state metathesis (SSM) reactions. However, the preparation of $La_2(CN_2)_3$ has yet failed by SSM, because its formation is hindered in favour of the formation of $La_2Cl(CN_2)$. An alternative way of preparation of metal carbodiimides is the employment of metal cyanurate precursors, showing the formation of pure $La_2(CN_2)_3$ by decomposition of lanthanum cyanurate hydrate as a single-source precursor.

Lanthanum cyanurate compounds can appear with mono- or divalent cyanurate anions and with different amounts of water molecules. The thermal conversion into lanthanum carbodiimide appears in three basic steps, by release of water, the loss of cyanuric acid, and finally the loss of CO_2.

The crystal structure of lanthanum carbodiimide completes the series of rare-earth carbodiimides that is represented by three distinct structure types and coordination numbers of the rare-earth ions. The structure of $La_2(CN_2)_3$ contains La^{3+} with the coordination number eight and represents an attractive

host lattice for doping with rare-earth activators. Doping with Ce^{3+} leads to the luminescent material $La_2(CN_2)_3$:Ce which shows a blue photoluminescence on excitation with 375 nm. Due to its high density and short decay time, this phosphor can be considered as a perspective szintillator material.

Experimental section

Materials and methods

The following starting materials cyanuric acid (Sigma-Aldrich, 98%), lanthanum(III) chloride heptahydrate (Fluka AG, 99.9%), sodium hydroxide (Chemsolute, 98.8%), and cerium(III) chloride heptahydrate (Merck, 98.5%) were used without further purification and were handled under air and standard conditions.

The thermal decomposition was carried out in a Carbolite HST 12/300 furnace equipped with a 1 m long quartz glass furnace tube. The decomposition product was handled under an inert argon atmosphere and transferred into a glovebox with maintained moisture and oxygen levels below 1 ppm.

Synthesis

$La(HC_3N_3O_3)(H_2C_3N_3O_3)(H_2O)_3$ (1). 69.5 mg (538.6 mmol) cyanuric acid and 100.0 mg (269.3 mmol) lanthanum(III) chloride heptahydrate were combined in a beaker equipped with a magnetic stirrer. 10 mL deionized water was then introduced at room temperature and the mixture was subsequently heated to 100 °C. Upon complete dissolution of the cyanuric acid, 32.3 mg (807.8 mmol) sodium hydroxide was added to the reaction. The mixture was then stirred for 1 h.

The resulting precipitate was collected by filtration (yield w.r.t. La 64%), washed three times with 20 mL of deionized water to remove sodium chloride and dried in an oven at 87.5 °C.

$La(H_2C_3N_3O_3)_2(OH)(H_2O)_4{\cdot}H_2O$ (2). 69.5 mg (538.6 mmol) cyanuric acid and 32.3 mg (807.8 mmol) sodium hydroxide were combined in a beaker equipped with a magnetic stirrer. Then 30 mL deionized water was introduced at room temperature and the mixture was subsequently heated to 100 °C. Upon complete dissolution of the cyanuric acid, 100.0 mg (269.3 mmol) lanthanum(III) chloride heptahydrate in 10 mL deionized water was added dropwise to the reaction. The mixture was then stirred for 3 h. The resulting precipitate was collected by filtration (yield w.r.t. La 27%), washed three times with 20 mL of deionized water and dried in an oven at 87.5 °C.

$La_2(CN_2)_3$. 100 mg (223.2 mmol) lanthanum cyanurate (2) was placed in a tube furnace and then heat-treated under flowing Ar at 770 °C for 30 min with a ramping rate of 2 K min^{-1}. Following the holding time, the furnace was cooled to room temperature with the same ramping rate of 2 K min^{-1}, yielding the final product (yield w.r.t. La >99%).

$La_2(CN_2)_3$:Ce. The synthesis for the doped lanthanum carbodiimide was performed similarly to the already established synthesis route. Hereby 200.0 mg (446.4 mmol) La $(H_2O_3C_3N_3)(HO_3C_3N_3)(H_2O)_3$ was mixed and subsequently mortared with 8.3 mg (22.3 mmol) cerium(III) chloride heptahydrate ($CeCl_3{\cdot}7H_2O$) and then placed into the oven.

Thermoanalytic studies

Thermogravimetric analysis and differential thermal analysis were performed using a Netzsch Jupiter STA 449 F3 thermal analyzer. The synthesized samples were measured in an open corundum crucible under a continuous argon flow.

X-ray powder diffraction

Compounds were investigated by powder X-ray diffraction (XRD) on a Stadi-P (STOE, Darmstadt) diffractometer with germanium monochromated Cu-$K_{\alpha1}$ radiation. The powder XRD pattern of $La_2(CN_2)_3$ was indexed in the space group *I*2/*a* (No. 15) using N-Treor09 [63] and the structure was solved by direct methods (both included in the program EXPO[64]). Other possible candidate space groups suggested by EXPO were lower in symmetry (structure solutions with space groups *Ia* or *I*2 were discarded by using the progam missym included in the program package PLATON[65]) or gave no reasonable structure solution (*I*2/*m*, *Im*). The crystal structure refinement was carried out with Winplotr (Fullprof), with the final full refinement plot displayed in Fig. 4.

Single-crystal X-ray diffraction

Suitable crystals were selected and mounted on XtaLAB Synergy, Dualflex, HyPix diffractometer. The crystals were kept at a steady T = 150.0(2) K during data collection. The structure was solved, and the space group was determined with the ShelXT 2018/2 (Sheldrick, 2018) solution program using dual methods and by using Olex2 1.5-ac5-024 [66] as the graphical interface. The model was refined with ShelXL 2018/3 [67] using full matrix least squares minimization on F^2. All non-hydrogen atoms were refined anisotropically. Hydrogen atom positions were found in the electron difference map and refined.

Infrared spectroscopy

The infrared spectroscopy was performed using a Bruker VERTEX 70 Fourier-transform infrared (FT-IR) spectrometer, with the measurement recorded in the spectral range of 400–4000 cm^{-1}. The samples were prepared as potassium bromide (KBr) pellets, with a pure KBr pellet serving as the reference for baseline correction.

Photoluminescence spectroscopy

Emission and excitation spectra of $La_2(CN_2)_3$:Ce^{3+} were measured using an FLS920 fluorescence spectrometer, Edinburgh Instruments, equipped with a 450 W xenon arc lamp OSRAM. The sample chamber was fitted with a mirror optic, specifically designed for powder samples. Detection was carried out with a R2658P single-photon counting photomultiplier tube Hamamatsu. The luminescence spectra were recorded at a spectral resolution of 1 nm, dwell time 0.5 seconds per 1 nm step, and the measurement was repeated three times. The correction file for the emission spectra was obtained from calibration with a tungsten incandescent lamp

certified by NPL (National Physics Laboratory, UK). For recording temperature dependent emission spectra, a cryostat "MicrostatN" from Oxford Instruments was introduced in the above described spectrometer. The decay curves were measured using an Edinburgh Instruments FLS920 fluorescence spectrometer with a photomultiplier from Hamamatsu H74422-40. The samples were excited with an Edinburgh EPL655 pulsed diode laser (65 ps pulse width).

Author contributions

H.-J. M.: conceptualization, supervision, funding acquisition, writing, review, and editing. P. S.: synthesis, PXRD, IR, TGA, writing. E. B.: writing, preparation, experimental analysis. M. S.: X-ray diffraction refinements and structure solutions. T. J. and D. E.: photoluminescence spectroscopy. All authors have read and agreed to the published version of the manuscript.

Data availability

Crystallographic data have been deposited at the CCDC under 2403637 (**1**), 2409323 (**2**), and 2393819 ($La_2(CN_2)_3$).†

Data are available within the article.

The data that support the findings of this study are available on request from the corresponding author, H.-J. Meyer.

Conflicts of interest

The authors declare no conflict of interest.

Acknowledgements

We gratefully acknowledge the support provided by the Deutsche Forschungsgemeinschaft (DFG-Bonn) for this research project (ME 914/34-1).

References

1 M. Kastens and W. McBurney, *Ind. Eng. Chem.*, 1951, **43**, 1020–1033.
2 M. G. Down, M. J. Haley, P. Hubberstey, R. J. Pulham and A. E. Thunder, *J. Chem. Soc., Dalton Trans.*, 1978, 1407–1411.
3 M. Löber, Doctoral dissertation, Universität Tübingen, 2022.
4 M. Becker, M. Jansen, A. Lieb, W. Milius and W. Schnick, *Z. Anorg. Allg. Chem.*, 1998, **624**, 113–118.
5 M. Ströbele, E. Bayat and H.-J. Meyer, *Inorg. Chem.*, 2024, **63**, 16565–16572.
6 M. Becker, J. Nuss and M. Jansen, *Z. Anorg. Allg. Chem.*, 2000, **626**, 2505–2508.
7 M. Becker and M. Jansen, *Solid State Sci.*, 2000, **2**, 711–715.
8 U. Berger and W. Schnick, *J. Alloys Compd.*, 1994, **206**, 179–184.
9 H.-J. Meyer, *Dalton Trans.*, 2010, **39**, 5973–5982.
10 K. Gibson, M. Ströbele, B. Blaschkowski, J. Glaser, M. Weisser, R. Srinivasan, H. J. Kolb and H.-J. Meyer, *Z. Anorg. Allg. Chem.*, 2003, **629**, 1863–1870.
11 G. Seifer, *Russ. J. Coord. Chem.*, 2002, **28**, 301–324.
12 A. Klimek, J. Yount, D. Wozniak, M. Zeller and D. G. Piercey, *Inorg. Chem.*, 2023, **62**, 16280–16282.
13 E. Bayat, M. Ströbele, D. Enseling, T. Jüstel and H.-J. Meyer, *Dalton Trans.*, 2024, **53**, 10912–10918.
14 M. Becker and M. Jansen, *Acta Crystallogr., Sect. C: Cryst. Struct. Commun.*, 2001, **57**, 347–348.
15 M. Krott, X. Liu, B. P. Fokwa, M. Speldrich, H. Lueken and R. Dronskowski, *Inorg. Chem.*, 2007, **46**, 2204–2207.
16 X. Liu, M. A. Wankeu, H. Lueken and R. Dronskowski, *Z. Naturforsch., B:J. Chem. Sci.*, 2005, **60**, 593–596.
17 G. Baldinozzi, B. Malinowska, M. Rakib and G. Durand, *J. Mater. Chem.*, 2002, **12**, 268–272.
18 M. Becker, J. Nuss and M. Jansen, *Z. Naturforsch., B:J. Chem. Sci.*, 2000, **55**, 383–385.
19 J. Peng, Y. Wang, M. Fecčík, L. Bayarjargal and R. Dronskowski, *ACS Appl. Mater. Interfaces*, 2024, 61946–61956.
20 X. Liu, M. Krott, P. Müller, C. Hu, H. Lueken and R. Dronskowski, *Inorg. Chem.*, 2005, **44**, 3001–3003.
21 X. Tang, H. Xiang, X. Liu, M. Speldrich and R. Dronskowski, *Angew. Chem., Int. Ed.*, 2010, **49**, 4738–4742.
22 K. Dolabdjian, A. Kobald, C. P. Romao and H.-J. Meyer, *Dalton Trans.*, 2018, **47**, 10249–10255.
23 X. Liu, A. Decker, D. Schmitz and R. Dronskowski, *Z. Anorg. Allg. Chem.*, 2000, **626**, 103–105.
24 X. Qiao, K. Chen, A. J. Corkett, D. Mroz, X. Huang, R. Wang, R. Nelson and R. Dronskowski, *Inorg. Chem.*, 2021, **60**, 12664–12670.
25 L. Stork, X. Liu, B. P. Fokwa and R. Dronskowski, *Z. Anorg. Allg. Chem.*, 2007, **633**, 1339–1342.
26 R. Dronskowski, *Z. Naturforsch., B:J. Chem. Sci.*, 1995, **50**, 1245–1251.
27 M. Löber, K. Dolabdjian, M. Ströbele, C. P. Romao and H.-J. Meyer, *Inorg. Chem.*, 2019, **58**, 7845–7851.
28 M. Neukirch, S. Tragl and H.-J. Meyer, *Inorg. Chem.*, 2006, **45**, 8188–8193.
29 J. Glaser, L. Unverfehrt, H. Bettentrup, G. Heymann, H. Huppertz, T. Jüstel and H.-J. Meyer, *Inorg. Chem.*, 2008, **47**, 10455–10460.
30 O. Reckeweg and F. J. DiSalvo, *Z. Anorg. Allg. Chem.*, 2003, **629**, 177–179.
31 H. Hartmann and W. Eckelmann, *Z. Anorg. Allg. Chem.*, 1948, **257**, 183–194.
32 P. Kallenbach, M. Ströbele and H.-J. Meyer, *Z. Anorg. Allg. Chem.*, 2020, **646**, 1281–1284.
33 O. Reckeweg, T. Schleid and F. J. DiSalvo, *Z. Naturforsch., B: J. Chem. Sci.*, 2007, **62**, 658–662.
34 D. Dutczak, M. Ströbele, D. Enseling, T. Jüstel and H.-J. Meyer, *Eur. J. Inorg. Chem.*, 2016, **2016**, 4011–4016.

35 Y. Hashimoto, M. Takahashi, S. Kikkawa and F. Kanamaru, *J. Solid State Chem.*, 1996, **125**, 37–42.
36 M. Li, W. Yuan, J. Wang, C. Gu and H. Zhao, *Powder Diffr.*, 2007, **22**, 59–63.
37 R. Srinivasan, J. Glaser, S. Tragl and H.-J. Meyer, *Z. Anorg. Allg. Chem.*, 2005, **631**, 479–483.
38 R. Srinivasan, M. Ströbele and H.-J. Meyer, *Inorg. Chem.*, 2003, **42**, 3406–3411.
39 R. Srinivasan, Doctoral dissertation, Universität Tübingen, 2004.
40 D. Dutczak, A. Siai, M. Ströbele, D. Enseling, T. Jüstel and H.-J. Meyer, *Eur. J. Inorg. Chem.*, 2020, **2020**, 3954–3958.
41 W. Liao, U. Englert and R. Dronskowski, *Eur. J. Inorg. Chem.*, 2006, **2006**, 4233–4236.
42 L. Unverfehrt, M. Ströbele, J. Glaser, T. Langer, R.-D. Hoffmann, R. Pöttgen and H.-J. Meyer, *Inorg. Chem.*, 2011, **50**, 6010–6018.
43 J. Glaser and H.-J. Meyer, *Angew. Chem., Int. Ed.*, 2008, **47**, 7547–7550.
44 J. Glaser, H. Bettentrup, T. Jüstel and H.-J. Meyer, *Inorg. Chem.*, 2010, **49**, 2954–2959.
45 M. Kalmutzki, D. Enseling, J. E. Wren, S. Kroeker, V. V. Terskikh, T. Jüstel and H.-J. Meyer, *Inorg. Chem.*, 2013, **52**, 12372–12382.
46 K. Dolabdjian, C. Schedel, D. Enseling, T. Jüstel and H.-J. Meyer, *Z. Anorg. Allg. Chem.*, 2017, **643**, 488–494.
47 Y. Hashimoto, M. Takahashi, S. Kikkawa and F. Kanamaru, *J. Solid State Chem.*, 1995, **114**, 592–594.
48 A. T. Schwarz, M. Ströbele and H.-J. Meyer, *Z. Anorg. Allg. Chem.*, 2024, **650**, e202400038.
49 L. Unverfehrt, Doctoral dissertation, Universität Tübingen, 2011.
50 N. Asakuma, M. Iijima, T. Tamura, S. Honda, D. Urushihara, T. Asaka, S. Bernard and Y. Iwamoto, *Inorg. Chem.*, 2024, **63**(43), 20380–20387.
51 Y.-C. Wu, T.-M. Chen, C.-H. Chiu and C.-N. Mo, *J. Electrochem. Soc.*, 2010, **157**, J342.
52 W. Haynes, T. Bruno and D. Lide, *CRC handbook of chemistry and physics*, CRC Press, Boca Raton, 95th edn, 2014, pp. 5–94.
53 O. Reckeweg, F. Lissner and T. Schleid, *Z. Naturforsch., B:J. Chem. Sci.*, 2021, **76**, 733–738.
54 X. Hao, M. Luo, C. Lin, D. Lin, L. Cao and N. Ye, *Dalton Trans.*, 2019, **48**, 12296–12302.
55 M. Neukirch, Doctoral dissertation, Universität Tübingen, 2007.
56 P. Dorenbos, *J. Lumin.*, 2002, **99**, 283–299.
57 Z. Xia and A. Meijerink, *Chem. Soc. Rev.*, 2017, **46**, 275–299.
58 A. C. Berends, M. A. van de Haar and M. R. Krames, *Chem. Rev.*, 2020, **120**, 13461–13479.
59 S. Wang, Z. Song and Q. Liu, *J. Mater. Chem. C*, 2023, **11**, 48–96.
60 A. Zukauskas, M. Shur and R. Gaska, *Solid state lighting*, John Wiley & Sons, 2002.
61 C. W. Van Eijk, *Phys. Med. Biol.*, 2002, **47**, R85.
62 P. A. Rodnyi, *Physical processes in inorganic scintillators*, CRC, New York, 1997.
63 A. Altomare, G. Campi, C. Cuocci, L. Eriksson, C. Giacovazzo, A. Moliterni, R. Rizzi and P.-E. Werner, *J. Appl. Crystallogr.*, 2009, **42**, 768–775.
64 A. Altomare, C. Cuocci, C. Giacovazzo, A. Moliterni, R. Rizzi, N. Corriero and A. Falcicchio, *J. Appl. Crystallogr.*, 2013, **46**, 1231–1235.
65 A. L. Spek, *Acta Crystallogr., Sect. D:Biol. Crystallogr.*, 2009, **65**, 148–155.
66 O. V. Dolomanov, L. J. Bourhis, R. J. Gildea, J. A. K. Howard and H. Puschmann, *J. Appl. Crystallogr.*, 2009, **42**, 339–341.
67 G. Sheldrick, *Acta Crystallogr., Sect. C:Struct. Chem.*, 2015, **71**, 3–8.